

NOTES ON NUMERICAL ANALYSIS AND SOLITARY WAVE SOLUTIONS OF BOUSSINESQ/BOUSSINESQ SYSTEMS FOR INTERNAL WAVES

VASSILIOS A. DOUGALIS, ANGEL DURAN, AND LEETHA SARIDAKI

ABSTRACT. In this paper a three-parameter family of Boussinesq systems is studied. The systems have been proposed as models of the propagation of long internal waves along the interface of a two-layer system of fluids with rigid-lid condition for the upper layer and under a Boussinesq regime for the flow in both layers. The contents of the paper are as follows. We first present some theoretical properties of well-posedness, conservation laws and Hamiltonian structure of the systems, using the results for analogous models for surface wave propagation. Then the corresponding periodic initial-value problem is discretized in space by the spectral Fourier Galerkin method and for each well posed system, error estimates for the semidiscrete approximation are proved. The rest of the paper is concerned with the study of existence and the numerical simulation of some issues of the dynamics of solitary-wave solutions. Standard theories are used to derive several results of existence of classical and generalized solitary waves, depending on the parameters of the models. A numerical procedure based on a Fourier collocation approximation for the ode system of the solitary wave profiles with periodic boundary conditions, and on the iterative solution of the resulting fixed-point systems with the Petviashvili scheme combined with vector extrapolation techniques, is used to generate numerically approximations of solitary waves. These are taken as initial conditions in a computational study of the dynamics of the solitary waves, both classical and generalized. To this end, the spectral semidiscretizations of the periodic initial-value problem for the systems are numerically integrated by a fourth-order Runge-Kutta-composition method based on the implicit midpoint rule. The fully discrete scheme is then used to approximate the evolution of small and large perturbations of computed solitary wave profiles, and to study computationally the collisions of solitary waves as well as the resolution of initial data into trains of solitary waves.

CONTENTS

1. Introduction	2
2. Derivation and well-posedness	5
2.1. Alternative derivation	5
2.2. Well-posedness theory	6
2.3. Conserved quantities	8
3. Error estimates for a spectral semidiscretization of the periodic initial-value problem	9
4. Solitary waves	20

2010 *Mathematics Subject Classification.* 76B15 (primary), 76B25, 65M70 (secondary).

Key words and phrases. Internal waves, Boussinesq/Boussinesq systems, solitary waves, spectral methods.

4.1. Some existence results	20
4.2. Numerical generation of solitary waves	36
5. Computational study of solitary wave dynamics	48
5.1. Numerical approximation of the periodic ivp for the B/B system	49
5.2. Validation of the codes	54
5.3. CSW dynamics. Numerical experiments	59
5.4. GSW dynamics. Numerical experiments	78
5.5. Dynamics of classical solitary wave solutions with non monotone decay	88
6. Concluding remarks	98
Acknowledgements	112
References	112

1. INTRODUCTION

The following three-parameter family of Boussinesq/Boussinesq (B/B) systems for internal waves was derived by Bona, Lannes and Saut, [21]:

$$\begin{aligned} (1 - b\Delta)\zeta_t + \frac{1}{\gamma + \delta}\nabla \cdot \mathbf{v}_\beta + \left(\frac{\delta^2 - \gamma}{(\delta + \gamma)^2}\right)\nabla \cdot (\zeta\mathbf{v}_\beta) + a\nabla \cdot \Delta\mathbf{v}_\beta &= 0, \\ (1 - d\Delta)(\mathbf{v}_\beta)_t + (1 - \gamma)\nabla\zeta + \left(\frac{\delta^2 - \gamma}{2(\delta + \gamma)^2}\right)\nabla|\mathbf{v}_\beta|^2 + (1 - \gamma)c\Delta\nabla\zeta &= 0. \end{aligned} \quad (1.1)$$

The system (1.1) is a model (in nondimensional, unscaled form) for the propagation of internal waves along the interface of an inviscid, homogeneous two-layer system of fluids, the upper of which is labelled 1 and the lower 2. The layers have depths d_1, d_2 and densities ρ_1, ρ_2 with $\rho_2 > \rho_1$. The upper layer is restricted by the rigid-lid assumption, at depth $z = 0$, while the rigid, horizontal bottom lies at depth $z = -(d_1 + d_2)$. In (1.1) $\zeta = \zeta(x, y, t)$ represents the deviation of the interface from the rest position at (x, y) at time t , while $\mathbf{v}_\beta = (I - \beta\Delta)^{-1}\mathbf{v}$, where $\beta \geq 0$ is a modelling parameter, Δ denotes the Laplace operator and \mathbf{v} is a ‘velocity’ variable defined in [21] in terms of the horizontal components of the velocities of the two layers of fluids $\mathbf{v}^{(1)}$ and $\mathbf{v}^{(2)}$ as the difference $\mathbf{v}^{(2)} - \gamma\mathbf{v}^{(1)}$ evaluated at the interface. The constants

$$\gamma = \frac{\rho_1}{\rho_2} < 1, \quad \delta = \frac{d_1}{d_2},$$

denote the density and depth ratios, respectively. The parameters a, b, c, d depend on the physical parameters δ, γ and the modelling parameters $\alpha_1 \geq 0, \beta \geq 0$ and $\alpha_2 \leq 1$, [21], and are given by

$$\begin{aligned} a &= \frac{(1 - \alpha_1)(1 + \gamma\delta) - 3\delta\beta(\delta + \gamma)}{3\delta(\gamma + \delta)^2}, & b &= \alpha_1 \frac{1 + \gamma\delta}{3\delta(\gamma + \delta)}, \\ c &= \beta\alpha_2, & d &= \beta(1 - \alpha_2). \end{aligned} \quad (1.2)$$

These formulas lead to the relation

$$(\delta + \gamma)a + b + c + d = S(\gamma, \delta), \quad S(\gamma, \delta) := \frac{1 + \gamma\delta}{3\delta(\gamma + \delta)}. \quad (1.3)$$

The case $\gamma = 0, \delta = 1$ corresponds to the Boussinesq systems for surface water waves analyzed by Bona, Chen, and Saut in [17, 18]. In that case β should be taken equal

to $\frac{1}{2}(1 - \theta^2)$ in the notation of [17, 18], where $0 \leq \theta \leq 1$ defines a parametrization of the depth variable $z = -1 + \theta$, ζ is the displacement of the surface elevation of the wave over the rest position $z = 0$, and the horizontal velocity at the free surface would be given by \mathbf{v} . The variable \mathbf{v}_β represents now the horizontal velocity at depth $z = -1 + \theta$.

In [21] (see also [62]), several asymptotic models for internal waves in different physical regimes are derived, and the consistency of the corresponding full Euler equations with them is established in a rigorous manner. The physical regimes are defined in terms of the scaling parameters

$$\epsilon = \frac{a}{d_1}, \quad \mu = \frac{d_1^2}{\lambda^2}, \quad (1.4)$$

and δ , where a and λ denote a typical amplitude and wavelength of the interface wave, respectively. The parameters (1.4) are defined with respect to the upper layer; similar ones, ϵ_2 and μ_2 , can be defined with respect to the lower layer. Then the system (1.1) is valid in the so-called Boussinesq/Boussinesq (B/B) regime; this means that the flow is in the Boussinesq regime in both fluid domains, i. e. the physical parameters satisfy the conditions $\delta \sim 1$ and

$$\mu \sim \mu_2 \sim \epsilon \sim \epsilon_2 \ll 1. \quad (1.5)$$

For a review of several other issues concerning the modelling of internal waves in the B/B and the other asymptotic regimes defined in [21] we refer the reader to the notes of Saut, [62]. We would also like to mention that Nguyen and Dias derived in [58] a B/B system and extended it to the case of higher-power nonlinear terms. In [39] Duchêne considered free-surface and rigid-lid B/B systems and studied their one-way KdV approximations.

The present study is focused on the one-dimensional version of (1.1), which is written in unscaled, dimensionless variables, for $x \in \mathbb{R}, t \geq 0$, as

$$\begin{aligned} (1 - b\partial_{xx})\zeta_t + \frac{1}{\gamma + \delta}\partial_x v_\beta + \left(\frac{\delta^2 - \gamma}{(\delta + \gamma)^2}\right)\partial_x(\zeta v_\beta) + a\partial_{xxx}v_\beta &= 0, \\ (1 - d\partial_{xx})(v_\beta)_t + (1 - \gamma)\partial_x\zeta + \left(\frac{\delta^2 - \gamma}{2(\delta + \gamma)^2}\right)\partial_x v_\beta^2 + (1 - \gamma)c\partial_{xxx}\zeta &= 0. \end{aligned} \quad (1.6)$$

with $v_\beta = (1 - \beta\partial_{xx})^{-1}u$.

In section 2 of the paper at hand we present an alternative to that of [21] derivation of the family of systems (1.6). We study the linear and nonlinear well-posedness of the B/B systems for various values of the coefficients a, b, c, d , based on the analogous theory valid for the Boussinesq systems for surface waves presented in [17, 18]. We identify seven classes of B/B systems that are linearly well posed with coefficients relevant to the internal wave problem and whose initial-value problems are nonlinearly, in general locally in time, well-posed in appropriate pairs of Sobolev spaces. In the rest of the paper we consider in detail the numerical approximation of these classes of systems and study the existence and numerical construction of their solitary-wave solutions. We also present a numerical study of various issues of stability and interactions of the solitary waves.

Specifically, in section 3 we discretize in space the periodic initial-value problem (ivp) for these systems using the spectral Fourier-Galerkin method and prove L^2 error estimates for the ensuing semidiscrete approximations. These estimates remain

of course valid for the analogous surface-wave Boussinesq systems (take $\gamma = 0, \delta = 1$ in (1.6)).

In recent years there have appeared several papers with rigorous error estimates for numerical methods for surface-wave Boussinesq systems. For example, in [10, 11, 9, 36, 37, 38] one may find error analyses of Galerkin-finite element semidiscretizations for various initial-boundary-value problems (ibvp's) for several Boussinesq systems in one and two space dimensions. The papers [10] and [9] also contain error estimates of temporal discretizations of the semidiscrete problems effected with high-order accurate, explicit Runge-Kutta (RK) time-stepping schemes. In [68] Xavier *et al.* analyze spectral methods of collocation type, coupled with the explicit, 'classical', fourth-order accurate RK scheme for time-stepping for the surface-wave Boussinesq systems corresponding to the classes of the cases (i) and (v), see section 2 in the sequel.

In section 4 we consider the existence and numerical approximation of solitary-wave solutions of the systems (1.6). We apply several techniques for proving existence of such waves, namely Normal Form Theory, [46, 44], valid for solitary-wave speeds close to the limiting value $c_{\gamma,\delta} = \sqrt{(1-\gamma)/(\delta+\gamma)}$, and Toland's theory, [66], Concentration-Compactness theory, [54], and Positive Operator theory, [14], that predict existence of solitary waves also at larger speeds (relative to $c_{\gamma,\delta}$). We construct in several cases of interest classical and generalized solitary-wave profiles by solving numerically the second-order nonlinear ordinary differential equation (ode) systems satisfied by the solitary waves. The ode systems are discretized by a spectral method and the resulting nonlinear systems of algebraic equations are numerically solved by the iterative Petviashvili scheme, [61, 60], accelerated by the Minimal Polynomial extrapolation (MPE) algorithm, [63, 64, 65, 3].

In section 5 we present a computational study of several issues associated with the stability and the dynamics of classical and generalized solitary waves of B/B systems with parameters belonging in the 'generic' class (ii) of section 2. We note that a computational study of solitary waves has been carried out in [58] by a spectral-RK scheme, among others, for a B/B system resembling those in the class (vi); classical solitary waves are constructed and their overtaking and head-on collisions are simulated. In [39] the author used a Crank-Nicolson finite difference-relaxation scheme in order to compare the evolution of solutions of B/B systems with that of the solutions of their associated KdV one-way approximations. In section 5 of the paper at hand, the ode ivp's resulting from the spectral semidiscretizations of the ivp's for some of the B/B systems (1.6) are discretized in time by a three-stage, fourth-order accurate diagonally implicit RK method of composition type, [69, 42]. This scheme is effective for nonlinear dispersive wave problems and was analyzed recently in the case of the KdV equation and other related models in [31]. With this fully discrete method in hand we study computationally the temporal evolutions emanating from small and larger perturbations of initial classical and generalized solitary waves. We also investigate overtaking and head-on collisions of solitary waves and the resolution of initial profiles into sequences of solitary waves. We close the paper with a section of concluding remarks.

In the paper we denote the inner product, resp. norm, on $L^2 = L^2(0, 1)$ by (\cdot, \cdot) , $\|\cdot\|$, resp. For real $\mu \geq 0$ we denote the L^2 -based periodic Sobolev spaces on $[0, 1]$

by H^μ ; for $g \in H^\mu$ its H^μ norm will be given by

$$\|g\|_\mu = \left(\sum_{k \in \mathbb{Z}} (1+k^2)^\mu |\widehat{g}(k)|^2 \right)^{1/2},$$

where $\widehat{g}(k)$ is the k th Fourier coefficient of g . We let $|\cdot|_\infty$ resp. $\|\cdot\|_{j,\infty}$ be the norm on L^∞ , resp. $W^{j,\infty}$, on $(0,1)$, where for $1 \leq p \leq \infty$ $W^{\mu,p} = W^{\mu,p}(0,1)$ is the Sobolev space of periodic functions on $(0,1)$ of order μ , whose generalized derivatives are in L^p .

2. DERIVATION AND WELL-POSEDNESS

In this section we present a derivation of the systems (1.6) which is more classical than that of [21]. We also review results of linear and nonlinear well-posedness of the systems (1.6) based on the analogous theory of [17, 18] valid for surface-wave Boussinesq systems. Finally, we note some invariant functionals of the solutions of these systems.

2.1. Alternative derivation. The derivation of (1.1) (and (1.6)) made in [21] is based on the introduction of two nonlocal operators linking the velocity potentials associated with the two layers at the interface, and the reformulation of the Euler system for internal waves in terms of them, [70]. Then the combination of the assumptions of the Boussinesq regime in both fluids and suitable asymptotic expansions of these nonlocal operators lead to (1.1) and its 1D version (1.6).

An alternative derivation for (1.6) with $a = b = c = 0, d = \beta = S(\gamma, \delta)$ was made in [40] using asymptotic expansions of the velocity potentials associated with the upper and lower fluid layers at the interface (cf. [17] for the case of surface waves). Here, we summarize this procedure and derive the general (a, b, c, d) -system (1.6) from it. If we take into account the assumptions on the B/B regime, expressed in terms of the parameters (1.4) due to the conditions (1.5), the alternative strategy leads, cf. [40], to the scaled system

$$\begin{aligned} \zeta_t + \frac{1}{\delta + \gamma} \partial_x (1 + \beta \epsilon \partial_{xx}) u + \epsilon \kappa_{\gamma, \delta} \partial_x (\zeta u) &= O(\epsilon^2), \\ u_t + (1 - \gamma) \zeta_x + \frac{\epsilon}{2} \kappa_{\gamma, \delta} \partial_x (u^2) &= O(\epsilon^2), \end{aligned} \quad (2.1)$$

in which we took $\epsilon = \mu$, where

$$\kappa_{\gamma, \delta} = \frac{\delta^2 - \gamma}{(\delta + \gamma)^2}, \quad (2.2)$$

and $v_\beta = (1 - \beta \epsilon \partial_{xx})^{-1} u$. From (2.1), the system (1.6) with $a = b = c = 0, d = \beta = S(\gamma, \delta)$ is obtained formally if we note that if $v_\beta = (I - \beta \epsilon \partial_{xx})^{-1} u$ then $v_\beta = (1 + \beta \epsilon \partial_{xx}) u + O(\epsilon^2)$ and drop the $O(\epsilon^2)$ terms. The resulting system is of the form

$$\begin{aligned} \zeta_t + \frac{1}{\gamma + \delta} \partial_x v_\beta + \epsilon \kappa_{\gamma, \delta} \partial_x (\zeta v_\beta) &= O(\epsilon^2), \\ (1 - \beta \epsilon \partial_{xx}) (v_\beta)_t + (1 - \gamma) \partial_x \zeta + \frac{\epsilon}{2} \kappa_{\gamma, \delta} \partial_x v_\beta^2 &= O(\epsilon^2). \end{aligned} \quad (2.3)$$

From (2.3) we may obtain the (a, b, c, d) -system (1.6) by using the BBM trick, [15, 21], i. e. the observation that the first equation in (2.3) implies that

$$\zeta_t = -\frac{1}{\gamma + \delta}u_x + O(\epsilon).$$

From the second equation of (2.3) we also have

$$\partial_t v_\beta = -(1 - \gamma)\zeta_x + O(\epsilon).$$

Thus, introducing the modelling parameters $\alpha_1 \geq 0, \alpha_2 \leq 1$, substituting the expression

$$u_x = (1 - \alpha_1)u_x - \alpha_1(\delta + \gamma)\zeta_t + O(\epsilon),$$

in the third-order derivative term in the first equation of (2.1) and using

$$\partial_t v_\beta = (1 - \alpha_2)\partial_t v_\beta - \alpha_2(1 - \gamma)\zeta_x + O(\epsilon),$$

in the third-order derivative term of the second equation in (2.3), we obtain, using the definition of the parameters a, b, c, d given in (1.2), that

$$\begin{aligned} (1 - b\epsilon\partial_{xx})\zeta_t + \frac{1}{\gamma + \delta}\partial_x v_\beta + \epsilon\kappa_{\gamma,\delta}\partial_x(\zeta v_\beta) + a\epsilon\partial_{xxx}v_\beta &= O(\epsilon^2), \\ (1 - d\epsilon\partial_{xx})\partial_t v_\beta + (1 - \gamma)\partial_x\zeta + \frac{\epsilon}{2}\kappa_{\gamma,\delta}\partial_x v_\beta^2 + (1 - \gamma)\epsilon c\partial_{xxx}\zeta &= O(\epsilon^2). \end{aligned} \quad (2.4)$$

Dropping the $O(\epsilon^2)$ terms, we see that the system (2.4) is the scaled version of (1.6).

Another form of the system (1.6) is related to the property of the Galilean symmetry present in the Euler system for internal waves. The techniques introduced in [41] yields the system

$$\begin{aligned} (1 - b\partial_{xx})\zeta_t + \frac{1}{\gamma + \delta}\partial_x v_\beta + \left(\frac{\delta^2 - \gamma}{(\delta + \gamma)^2}\right)\partial_x(\zeta v_\beta) + a\partial_{xxx}v_\beta \\ - b\kappa_{\gamma,\delta}v_\beta\partial_{xxx}\zeta &= 0, \\ (1 - d\partial_{xx})(v_\beta)_t + (1 - \gamma)\partial_x\zeta + \left(\frac{\delta^2 - \gamma}{2(\delta + \gamma)^2}\right)\partial_x v_\beta^2 + (1 - \gamma)c\partial_{xxx}\zeta \\ - d\kappa_{\gamma,\delta}v_\beta\partial_{xxx}v_\beta &= 0, \end{aligned} \quad (2.5)$$

which can be shown to be invariant under the Galilean transformation

$$x \mapsto x - \kappa_{\gamma,\delta}Ct, \quad t \mapsto t, \quad \zeta \mapsto \zeta, \quad v_\beta \mapsto v_\beta + C,$$

for $C \in \mathbb{R}$. Compared to (1.6), the new terms in (2.5), given by $-b\kappa_{\gamma,\delta}v_\beta\partial_{xxx}\zeta$ and $-d\kappa_{\gamma,\delta}v_\beta\partial_{xxx}v_\beta$, are in scaled variables of $O(\epsilon^2)$. In this sense, the Euler system for internal waves will lose the consistency with (2.5) in the sense specified in Theorem 3 of [21] for the system (1.6). Note also that, since the new terms are nonlinear, (2.5) and (1.6) share the same linear well-posedness theory.

2.2. Well-posedness theory. The associated to (1.6) linearized system, written in terms of ζ and $u = (I - \beta\partial_{xx})v_\beta$ is

$$\begin{aligned} (1 - b\partial_{xx})\zeta_t + \frac{1}{\gamma + \delta}\partial_x(I - \beta\partial_{xx})^{-1}u + a(1 - \beta\partial_{xx})^{-1}\partial_{xxx}u &= 0, \\ (1 - d\partial_{xx})(1 - \beta\partial_{xx})^{-1}u_t + (1 - \gamma)\partial_x\zeta + (1 - \gamma)c\partial_{xxx}\zeta &= 0. \end{aligned} \quad (2.6)$$

The Fourier transform leads to the system

$$\frac{d}{dt} \begin{pmatrix} \widehat{\zeta}(k, t) \\ \widehat{u}(k, t) \end{pmatrix} + (ik)A(k) \begin{pmatrix} \widehat{\zeta}(k, t) \\ \widehat{u}(k, t) \end{pmatrix} = 0, \quad (2.7)$$

where $k \in \mathbb{R}, t \geq 0$, a circumflex denotes the Fourier transform, and

$$A(k) = \begin{pmatrix} 0 & \omega_1(k) \\ \omega_2(k) & 0 \end{pmatrix},$$

where

$$\omega_1(k) = \frac{\left(\frac{1}{\delta+\gamma} - ak^2\right)}{(1+bk^2)(1+\beta k^2)}, \quad \omega_2(k) = \frac{(1-\gamma)(1-ck^2)(1+\beta k^2)}{1+dk^2}.$$

The study of (2.6) (or (2.7)) can be done in a similar way to that of [17]. If

$$\omega_1(k)\omega_2(k) = \frac{\left(\frac{1}{\delta+\gamma} - ak^2\right)(1-\gamma)(1-ck^2)}{(1+bk^2)(1+dk^2)} \geq 0,$$

then the ivp for the linearized system (2.7) is well posed if the matrix

$$e^{-ikA(k)t} = \begin{pmatrix} \cos(k\sigma(k)t) & -i\frac{\omega_1(k)}{\sigma(k)} \sin(k\sigma(k)t) \\ -i\frac{\omega_2(k)}{\sigma(k)} \sin(k\sigma(k)t) & \cos(k\sigma(k)t) \end{pmatrix},$$

where $\sigma = \sqrt{\omega_1\omega_2}$, has elements which are bounded for bounded intervals of k . This holds when ω_1/ω_2 has neither poles nor zeros on the real axis. Since

$$\frac{\omega_1(k)}{\omega_2(k)} = \frac{\left(\frac{1}{\delta+\gamma} - ak^2\right)(1+dk^2)}{(1+\beta k^2)^2(1-\gamma)(1-ck^2)(1+bk^2)},$$

and $\beta \geq 0, 0 < \gamma < 1$ and $\delta > 0$, this is equivalent to ask that the rational function

$$\frac{\left(\frac{1}{\delta+\gamma} - ak^2\right)(1+dk^2)}{(1-ck^2)(1+bk^2)},$$

have no poles nor zeros for $k \in \mathbb{R}$. This leads to the three ‘admissible’ cases,

- (C1) $a, c \leq 0, b, d \geq 0$.
- (C2) $b, d \geq 0, c = a(\delta + \gamma) > 0$.
- (C3) $b = d < 0, c = a(\delta + \gamma) > 0$.

We note that

$$\alpha_1 = \frac{3\delta(\delta + \gamma)}{1 + \gamma\delta}b, \quad \beta = c + d, \quad \alpha_2 = \frac{c}{c + d},$$

and observe that (C3) does not satisfy the hypotheses $\alpha_2 \leq 1, \alpha_1 \geq 0$, while (C2) requires $0 < \alpha_1 < 1, 0 < \alpha_2 \leq 1, \beta > 0$. In the present paper only the case (C1) will be considered.

If we recall that the order of $\sigma(k)$ is the integer l such that

$$\sigma(k) \approx |k|^l, \quad |k| \rightarrow \infty,$$

then Theorem 3.2 of [17] can be applied to prove that if $m_1 = \max\{0, -l\}, m_2 = \max\{0, l\}$ then the ivp for the linear system (2.6) is well posed for (ζ, u) in $H^{s+m_1} \times H^{s+m_2}$ for any $s \geq 0$. For example, when $\beta > 0$ and $s = 0$, in the case (C1) we have:

- $a = c = 0, b, d > 0$. In this case (2.6) is well posed in $H^2 \times L^2$.

- $b, d > 0, a = 0, c < 0$; then (2.6) is well posed in $H^1 \times L^2$.
- $b = d = 0, a, c < 0$; then (2.6) is well posed in $L^2 \times H^2$.

As already mentioned, the case $\beta = 0$ leads to conditions for the linear well-posedness for Boussinesq systems for surface waves, [17].

Remark 2.1. *It is to be noted that not all cases described by the set $a, c \leq 0, b, d \geq 0$ are relevant for the internal wave problem, due to the restrictions on the physical parameters γ, δ and the modelling parameters $\alpha_1, \alpha_2, \beta$ that determine a, b, c , and d , cf. (1.2)-(1.3). Specifically, the case $a = 0, c < 0, b > 0, d = 0$ should be excluded since $d = 0$ implies either $\beta = 0$ or $\alpha_2 = 1$ and in either case $c < 0$ cannot hold. Arguing similarly we may see that all cases with $b = d = 0, a, c \leq 0$ are not valid for internal waves. In addition, note that several other cases hold, under easily checked conditions between the parameters. (For example, if two of the four parameters are zero, then (1.3) implies an affine relation between the other two.)*

As far as local in time well-posedness of the full nonlinear system is concerned, the analysis made in [18] for the case of surface waves can also be used here. (This was confirmed in [7].) Let us consider the systems corresponding to those cases among the set of parameters $b, d \geq 0, a, c \leq 0$ that are relevant for internal waves. In each case of the following list, we mention the corresponding theorem of [18] that applies. All the results concern existence, uniqueness, and regularity locally in t of the corresponding solution in the appropriate pairs of Sobolev spaces shown.

- Case (i): $b, d > 0, a = c = 0$ (systems of ‘BBM-BBM’ type; Theorem 2.1, $H^s \times H^s, s \geq 0$).
- Case (ii): $b, d > 0, a, c < 0$ (‘generic’ case; Theorem 2.5, $H^s \times H^s, s \geq 0$).
- Case (iii): $b = 0, d > 0, a, c < 0$ (Theorem 3.5, $H^s \times H^{s+1}, s \geq 1$).
- Case (iv): $b = 0, d > 0, a = c = 0$ (‘classical’ Boussinesq system; Theorem 3.3, $H^s \times H^{s+1}, s \geq 1$, conditional global existence; see also [40]), or $b > 0, d = 0, a = c = 0$ (analogous theory).
- Case (v): $b, d > 0, a = 0, c < 0$ (Bona-Smith system; Theorem 2.6, $H^{s+1} \times H^s, s \geq 0$, conditional global existence), or $b, d > 0, a < 0, c = 0$ (analogous theory).
- Case (vi): $b = 0, d > 0, a < 0, c = 0$ (Theorem 3.1, $H^s \times H^{s+2}, s \geq 1$).
- Case (vii): $b > 0, d = 0, a < 0, c = 0$ (Theorem 3.9, $H^s \times H^s, s \geq 2$) or $b = 0, d > 0, a = 0, c < 0$ (analogous theory).

Note that slightly sharper regularity results were achieved in [7] for some of these cases.

2.3. Conserved quantities. It is not hard to show that the linear functionals

$$M_1(\zeta) = \int_{-\infty}^{\infty} \zeta dx, \quad M_2(v_\beta) = \int_{-\infty}^{\infty} v_\beta dx = \int_{-\infty}^{\infty} (1 - \beta \partial_{xx})^{-1} u dx.$$

are invariant quantities during the evolution of solutions of (1.6). When $b = d$ (cf. the surface wave case, [18]) we have the conserved functionals

$$I(\zeta, u) = \int_{-\infty}^{\infty} (\zeta v_\beta + b \partial_x \zeta \partial_x v_\beta) dx, \quad (2.8)$$

$$H(\zeta, u) = \int_{-\infty}^{\infty} \left(\frac{(1-\gamma)}{2} \zeta^2 + \frac{1}{2(\delta+\gamma)} v_\beta^2 - a(\partial_x v_\beta)^2 - (1-\gamma)c(\partial_x \zeta)^2 + \frac{\delta^2 - \gamma}{2(\delta+\gamma)^2} \zeta v_\beta^2 \right) dx, \quad (2.9)$$

(where $v_\beta = (1 - \beta \partial_{xx})^{-1} u$) with the Hamiltonian structure for (1.6) given by

$$\frac{d}{dt} \begin{pmatrix} \zeta \\ u \end{pmatrix} = J \frac{\delta H}{\delta(\zeta, u)}, \quad (2.10)$$

$$J = -\partial_x (1 - \beta \partial_{xx})^{-1} \begin{pmatrix} (1 - b \partial_{xx}) & 0 \\ 0 & (1 - d \partial_{xx}) \end{pmatrix} \begin{pmatrix} 0 & -1 \\ 1 & 0 \end{pmatrix},$$

where $\delta H / \delta(\zeta, u)$ stands for the variational derivative with respect to the variables (ζ, u) . All these conservation laws as well as the Hamiltonian structure hold in suitable function spaces.

3. ERROR ESTIMATES FOR A SPECTRAL SEMIDISCRETIZATION OF THE PERIODIC INITIAL-VALUE PROBLEM

We consider the periodic initial-value problem (ivp) for the one-dimensional system (1.6) on the spatial interval $[0, 1]$. In order to simplify notation we denote $v_\beta = u$, $\lambda = \kappa_{\gamma, \delta} = \frac{\delta^2 - \gamma}{(\delta + \gamma)^2}$, $\kappa_1 = \frac{1}{\delta + \gamma}$, $\kappa_2 = 1 - \gamma$. (Thus κ_1 and κ_2 are positive constants.) We also let c' denote the constant $(1 - \gamma)c$ multiplying the term $\partial_{xxx} \zeta$ in the second pde of (1.6); this does not change the sign of the original c . Thus, given $u_0(x)$, $\zeta_0(x)$, 1-periodic real functions, we seek for $0 \leq t \leq T$, $\zeta(x, t)$, $u(x, t)$, 1-periodic in x , satisfying, for $0 \leq x \leq 1$, $0 \leq t \leq T$

$$\begin{aligned} \zeta_t + \kappa_1 u_x + \lambda (\zeta u)_x + a u_{xxx} - b \zeta_{xxt} &= 0, \\ u_t + \kappa_2 \zeta_x + \lambda u u_x + c' \zeta_{xxx} - d u_{xxt} &= 0, \end{aligned} \quad (3.1)$$

with

$$\zeta(x, 0) = \zeta_0(x), \quad u(x, 0) = u_0(x), \quad 0 \leq x \leq 1. \quad (3.2)$$

In the sequel we assume that the ivp (3.1)-(3.2) has a unique solution which is smooth enough for the purposes of error estimation.

We will discretize the ivp (3.1)-(3.2) in space by a spectral Fourier Galerkin method. To this end we let $N \geq 1$ be an integer and define the finite dimensional space S_N as

$$S_N = \text{span}\{e^{ikx}, k \in \mathbb{Z}, -N \leq k \leq N\}.$$

Let $P = P_N$ denote the L^2 -projection operator onto S_N given explicitly for $v \in L^2$ by

$$Pv = \sum_{|k| \leq N} \hat{v}(k) e^{ikx},$$

where $\widehat{v}(k)$ is the k th Fourier coefficient of v . It is obvious that P commutes with ∂_x . Moreover, given integers $0 \leq j \leq \mu$, there exists a constant C independent of N , such that for any $v \in H^\mu$, $\mu \geq 1$,

$$\|v - Pv\|_j \leq CN^{j-\mu}\|v\|_\mu, \quad (3.3)$$

$$|v - Pv|_\infty \leq CN^{1/2-\mu}\|v\|_\mu. \quad (3.4)$$

In addition, the following inverse inequalities hold in S_N : Given $0 \leq j \leq \mu$, there exists a constant C independent of N , such that for any $\psi \in S_N$

$$\|\psi\|_\mu \leq CN^{\mu-j}\|\psi\|_j, \quad \|\psi\|_{\mu,\infty} \leq CN^{1/2+\mu-j}\|\psi\|_j. \quad (3.5)$$

In what follows, as is customary, we will denote constants independent of N by C .

The spectral Galerkin semidiscretization of the ivp (3.1)-(3.2) is defined as follows. Let $T > 0$. We seek real-valued $\zeta_N, u_N : [0, T] \rightarrow S_N$ satisfying for $0 \leq t \leq T$ and $\forall \varphi, \chi \in S_N$

$$(\zeta_{Nt}, \varphi) + \kappa_1(u_{Nx}, \varphi) + \lambda((\zeta_N u_N)_x, \varphi) + a(u_{Nxxx}, \varphi) - b(\zeta_{Nxt}, \varphi) = 0, \quad (3.6)$$

$$(u_{Nt}, \chi) + \kappa_2(u_{Nx}, \chi) + \lambda(u_N u_{Nx}, \chi) + c'(\zeta_{Nxx}, \chi) - d(u_{Nxt}, \chi) = 0, \quad (3.7)$$

and for $t = 0$

$$\zeta_N(0) = P\zeta_0, \quad u_N(0) = Pu_0. \quad (3.8)$$

The ode ivp (3.6)-(3.8) has a unique solution locally in time and has the Fourier implementation

$$\begin{aligned} (1 + bk^2)\widehat{\zeta}_{N,t} + ik\kappa_1\widehat{u}_N + ik\lambda\widehat{\zeta_N u_N} - ik^3 a\widehat{u}_N &= 0, \\ (1 + dk^2)\widehat{u}_{N,t} + ik\kappa_2\widehat{\zeta}_N + \frac{ik}{2}\lambda\widehat{u_N^2} - ik^3 c'\widehat{\zeta}_N &= 0, \end{aligned} \quad (3.9)$$

where $\widehat{\zeta}_N = \widehat{\zeta}_N(k, t)$, $\widehat{u}_N = \widehat{u}_N(k, t)$, $-N \leq k \leq N$, $t \geq 0$ are the Fourier coefficients of ζ_N, u_N with initial values $\widehat{\zeta}_N(k, 0) = \widehat{\zeta}_0(k)$, $\widehat{u}_N(k, 0) = \widehat{u}_0(k)$.

In order to estimate the error of the semidiscretization let $\theta = \zeta_N - P\zeta$, $\rho = P\zeta - \zeta$, so that $\zeta_N - \zeta = \theta + \rho$, and $\xi = u_N - Pu$, $\sigma = Pu - u$, so that $u_N - u = \xi + \sigma$. Then, subtracting the first pde in (3.1) from (3.6) we obtain, while the solution of (3.6)-(3.8) exists and for all $\varphi \in S_N$

$$(\theta_t, \varphi) + \kappa_1(\xi_x, \varphi) + a(\xi_{xxx}, \varphi) - b(\theta_{xt}, \varphi) = -\lambda((\zeta_N u_N)_x, \varphi) + \lambda((\zeta u)_x, \varphi).$$

Therefore for $\varphi \in S_N$

$$(\theta_t, \varphi) + a(\xi_{xxx}, \varphi) - b(\theta_{xt}, \varphi) = -\kappa_1(\xi_x, \varphi) - (A_x, \varphi), \quad (3.10)$$

where

$$A = \lambda(\zeta_N u_N - \zeta u) = \lambda((\zeta + \theta + \rho)(u + \xi + \sigma) - \zeta u),$$

i. e.

$$A = \lambda(u\rho + \zeta\sigma + u\theta + \zeta\xi + \sigma\theta + \rho\xi + \rho\sigma + \theta\xi). \quad (3.11)$$

Subtracting the second pde in (3.1) from (3.7) we get for $\chi \in S_N$

$$(\xi_t, \chi) + \kappa_2(\theta_x, \chi) + c'(\theta_{xxx}, \chi) - d(\xi_{xt}, \chi) = -\lambda(u_N u_{Nx}, \chi) + \lambda(uu_x, \chi).$$

Therefore, for $\chi \in S_N$

$$(\xi_t, \chi) + c'(\theta_{xxx}, \chi) - d(\xi_{xt}, \chi) = -\kappa_2(\theta_x, \chi) - (B_x, \chi), \quad (3.12)$$

where

$$B = \lambda \left(u\sigma + u\xi + \sigma\xi + \frac{1}{2}(\sigma^2 + \xi^2) \right). \quad (3.13)$$

Using the error equations (3.10)-(3.13) we proceed now to derive error estimates for the semidiscrete schemes (3.6)-(3.8).

For the purpose of the error analysis, we consider the same seven cases of nonlinearly well posed systems identified in section 2.2. For simplicity, in the cases (iv), (v) and (vii) the following systems will be analyzed; the others are similar:

- Case (iv): ‘Classical Boussinesq’ case: $b = 0, d > 0, a = c = 0$.
- Case (v): ‘Bona-Smith’ systems: $b, d > 0, a = 0, c < 0$.
- Case (vii): $b > 0, d = 0, a < 0, c = 0$.

As mentioned in the Introduction, the systems of cases (i) (BBM-BBM) and (v) (‘Bona-Smith’) have been discretized by a collocation spectral method in space analyzed by Xavier et al., [68], in the case of surface waves. The error estimates obtained in [68] are similar to those that we obtain below for the spectral Galerkin method in these cases but we include the proofs as our techniques are somewhat different.

In all propositions below we assume for simplicity that $\zeta, u \in C^1(0, T, H^\mu)$, $\mu \geq 1$, and specify in each case the least integer μ needed for the validity of the error estimates. In all cases it is clear that ζ_N, u_N satisfy (3.6)-(3.8) at least locally in t ; part of the proof is checking that they exist uniquely and satisfy (3.6)-(3.7) up to $t = T$.

Proposition 3.1. *Let a, b, c, d as in case (i). If $\mu \geq 1$ then*

$$\max_{0 \leq t \leq T} (\|\zeta_N - \zeta\| + \|u_N - u\|) \leq CN^{-\mu}. \quad (3.14)$$

Proof. While the semidiscrete solution ζ_N, u_N exists, putting $\varphi = \theta$ in (3.10), $\chi = \xi$ in (3.12), using integration by parts and adding the resulting equations give

$$\begin{aligned} \frac{1}{2} \frac{d}{dt} (\|\theta\|^2 + \|\xi\|^2 + b\|\theta_x\|^2 + d\|\xi_x\|^2) &= \kappa_1(\xi, \theta_x) + \kappa_2(\theta, \xi_x) \\ &+ (A, \theta_x) + (B, \xi_x). \end{aligned} \quad (3.15)$$

We estimate as follows the various terms in the right-hand side of (3.15). First

$$|(\xi, \theta_x)| \leq \|\xi\| \|\theta_x\| \leq \frac{1}{2} (\|\xi\|^2 + \|\theta_x\|^2). \quad (3.16)$$

For the various terms of (A, θ_x) we first see, using (3.3),

$$|(u\rho, \theta_x)| \leq |u|_\infty \|\rho\| \|\theta_x\| \leq C (N^{-2\mu} + \|\theta_x\|^2). \quad (3.17)$$

Similarly,

$$|(\zeta\sigma, \theta_x)| \leq |\zeta|_\infty \|\sigma\| \|\theta_x\| \leq C (N^{-2\mu} + \|\theta_x\|^2). \quad (3.18)$$

Now

$$|(u\theta, \theta_x)| \leq |u|_\infty \|\theta\| \|\theta_x\| \leq C \|\theta\|_1^2, \quad (3.19)$$

$$|(\zeta\xi, \theta_x)| \leq |\zeta|_\infty \|\xi\| \|\theta_x\| \leq C (\|\xi\|^2 + \|\theta_x\|^2). \quad (3.20)$$

Using (3.4) we see that $|\sigma|_\infty \leq C$ and therefore

$$|(\sigma\theta, \theta_x)| \leq |\sigma|_\infty \|\theta\| \|\theta_x\| \leq C \|\theta\|_1^2. \quad (3.21)$$

Similarly,

$$|(\rho\xi, \theta_x)| \leq |\rho|_\infty \|\xi\| \|\theta_x\| \leq C(\|\xi\|^2 + \|\theta_x\|^2). \quad (3.22)$$

$$|(\rho\sigma, \theta_x)| \leq |\rho|_\infty \|\sigma\| \|\theta_x\| \leq C(N^{-2\mu} + \|\theta_x\|^2). \quad (3.23)$$

Since $\theta(0) = 0$, using continuity, let $t_N, 0 < t_N \leq T$, be the maximal time for which the solution of (3.6)-(3.8) exists and satisfies

$$\|\theta\|_\infty \leq 1, \quad 0 \leq t \leq t_N. \quad (3.24)$$

Then for $0 \leq t \leq t_N$

$$|(\theta\xi, \theta_x)| \leq \|\theta\|_\infty \|\xi\| \|\theta_x\| \leq \|\xi\| \|\theta_x\| \leq \frac{1}{2}(\|\xi\|^2 + \|\theta_x\|^2). \quad (3.25)$$

From (3.17)-(3.25) we have therefore for $0 \leq t \leq t_N$ that

$$|(A, \theta_x)| \leq C(N^{-2\mu} + \|\xi\|^2 + \|\theta\|_1^2). \quad (3.26)$$

For the rest of the terms on the right-hand side of (3.15) we first note that

$$|(\theta, \xi_x)| \leq \|\theta\| \|\xi_x\| \leq \frac{1}{2}(\|\theta\|^2 + \|\xi_x\|^2). \quad (3.27)$$

For the (B, ξ_x) terms, in view of (3.13) we have the following estimates. Note that by (3.3)

$$|(u\sigma, \theta_x)| \leq |u|_\infty \|\sigma\| \|\theta_x\| \leq C(N^{-2\mu} + \|\theta_x\|^2). \quad (3.28)$$

In addition,

$$|(u\xi, \xi_x)| \leq |u|_\infty \|\xi\| \|\xi_x\| \leq C\|\xi\|_1^2. \quad (3.29)$$

By (3.4)

$$|(\sigma\xi, \xi_x)| \leq |\sigma|_\infty \|\xi\| \|\xi_x\| \leq C\|\xi\|_1^2. \quad (3.30)$$

By (3.3), (3.4)

$$\frac{1}{2}(\sigma^2, \xi_x) \leq \frac{1}{2}|\sigma|_\infty \|\sigma\| \|\xi_x\| \leq C(N^{-2\mu} + \|\xi_x\|^2). \quad (3.31)$$

And finally, by periodicity,

$$\frac{1}{2}(\xi^2, \xi_x) = 0. \quad (3.32)$$

We conclude from (3.28)-(3.32) that, as long as the semidiscrete solution exists,

$$|(B, \xi_x)| \leq C(N^{-2\mu} + \|\theta\|^2 + \|\xi\|_1^2). \quad (3.33)$$

Hence, since $b, d > 0$ we get from (3.15), (3.16), (3.26), (3.27), (3.33) that

$$\frac{d}{dt} (\|\theta\|_1^2 + \|\xi\|_1^2) \leq C(N^{-2\mu} + \|\theta\|_1^2 + \|\xi\|_1^2), \quad 0 \leq t \leq t_N.$$

Hence, by Gronwall's lemma and (3.8) we conclude that for $0 \leq t \leq t_N$ and for some constant $C = C(T)$ there holds

$$\|\theta\|_1 + \|\xi\|_1 \leq CN^{-\mu}. \quad (3.34)$$

Therefore, since $\|\theta\|_\infty \leq C\|\theta\|_1$ by Sobolev's theorem, we conclude by (3.34) and our hypothesis on μ that (for N sufficiently large) t_N was not maximal in (3.24). Arguing in the customary way we see that t_N may be taken equal to T , and (3.34) holds for $0 \leq t \leq T$. By (3.3) we conclude that (3.14) holds, so that ζ_N, u_N satisfy optimal-order error estimates in L^2 , where by 'optimal-order' in the context of

spectral methods we mean that the semidiscrete approximations satisfy estimates like (3.3) if $\zeta, u \in H^\mu$. \square

Proposition 3.2. *Let a, b, c, d as in case (ii). If $\mu \geq 1$ then*

$$\max_{0 \leq t \leq T} (\|\zeta_N - \zeta\| + \|u_N - u\|) \leq CN^{-\mu}.$$

Proof. While the semidiscrete solution ζ_N, u_N exists, putting $\varphi = \theta$ in (3.10), $\chi = \xi$ in (3.12) we obtain, using integration by parts, that

$$\frac{1}{2} \frac{d}{dt} (\|\theta\|^2 + b\|\theta_x\|^2) - a(\xi_{xx}, \theta_x) = \kappa_1(\xi, \theta_x) + (A, \theta_x). \quad (3.35)$$

$$\frac{1}{2} \frac{d}{dt} (\|\xi\|^2 + d\|\xi_x\|^2) + c'(\theta_x, \xi_{xx}) = \kappa_2(\theta, \xi_x) + (B, \xi_x). \quad (3.36)$$

Multiplying (3.35) by $-c'$ and (3.36) by $-a$ and adding the resulting equations we get

$$\begin{aligned} \frac{1}{2} \frac{d}{dt} (|c'|\|\theta\|^2 + |a|\|\xi\|^2 + b|c'|\|\theta_x\|^2 + d|a|\|\xi_x\|^2) &= -c' \kappa_1(\xi, \theta_x) \\ -c'(A, \theta_x) - a\kappa_2(\theta, \xi_x) - a(B, \xi_x). \end{aligned}$$

The rest of the proof proceeds exactly along the lines of that of Proposition 3.1. \square

Proposition 3.3. *Let a, b, c, d as in case (iii). If $\mu > 3/2$ then*

$$\max_{0 \leq t \leq T} (\|\zeta_N - \zeta\| + \|u_N - u\|_1) \leq CN^{1-\mu}. \quad (3.37)$$

Proof. While the semidiscrete solution ζ_N, u_N exists, putting $\varphi = \theta$ in (3.10), $\chi = \xi$ in (3.12) we obtain, using integration by parts, that

$$\frac{1}{2} \frac{d}{dt} \|\theta\|^2 - a(\xi_{xx}, \theta_x) = -\kappa_1(\xi_x, \theta) - (A_x, \theta), \quad (3.38)$$

$$\frac{1}{2} \frac{d}{dt} (\|\xi\|^2 + d\|\xi_x\|^2) + c'(\theta_x, \xi_{xx}) = \kappa_2(\theta, \xi_x) + (B, \xi_x). \quad (3.39)$$

Multiplying (3.38) by $-c'$ and (3.39) by $-a$ and adding the resulting equations gives

$$\begin{aligned} \frac{1}{2} \frac{d}{dt} (|c'|\|\theta\|^2 + |a|\|\xi\|^2 + d|a|\|\xi_x\|^2) &= c' \kappa_1(\xi_x, \theta) + c'(A_x, \theta) \\ -a\kappa_2(\theta, \xi_x) - a(B, \xi_x). \end{aligned} \quad (3.40)$$

We estimate the terms of the right-hand side of the above. Obviously,

$$|(\xi_x, \theta)| \leq \|\xi_x\| \|\theta\| \leq \frac{1}{2} (\|\theta\|^2 + \|\xi_x\|^2). \quad (3.41)$$

For the terms of (A_x, θ) , using (3.11) and (3.3) and the fact that H^1 is an algebra, we have

$$|((u\rho)_x, \theta)| \leq \|u\rho\|_1 \|\theta\| \leq C\|u\|_1 \|\rho\|_1 \|\theta\| \leq C \left(N^{2(1-\mu)} + \|\theta\|^2 \right).$$

Similarly,

$$|((\zeta\sigma)_x, \theta)| \leq C \left(N^{2(1-\mu)} + \|\theta\|^2 \right). \quad (3.42)$$

Using integration by parts we have

$$|((u\theta)_x, \theta)| = \left| \frac{1}{2} (u_x \theta, \theta) \right| \leq C \|u_x\|_\infty \|\theta\|^2 \leq C \|\theta\|^2. \quad (3.43)$$

Also

$$|((\zeta\xi)_x, \theta)| \leq C\|\zeta\|_1\|\xi\|_1\|\theta\| \leq C(\|\xi\|_1^2 + \|\theta\|^2). \quad (3.44)$$

Using integration by parts and (3.4) and our hypothesis on μ

$$|(\sigma\theta)_x, \theta) = \frac{1}{2}|(\sigma_x\theta, \theta)| \leq C|\sigma_x|_\infty\|\theta\|^2 \leq C\|\theta\|^2. \quad (3.45)$$

By (3.3)

$$|(\rho\xi)_x, \theta) \leq C\|\rho\|_1\|\xi\|_1\|\theta\| \leq C(\|\xi\|_1^2 + \|\theta\|^2). \quad (3.46)$$

By (3.3), (3.4), and our hypothesis on μ

$$\begin{aligned} |(\rho\sigma)_x, \theta) &\leq |\rho|_\infty|\sigma_x|\|\theta\| + |\sigma|_\infty|\rho_x|\|\theta\| \\ &\leq CN^{\frac{3}{2}-2\mu}\|\theta\| \leq CN^{-\mu}\|\theta\| \\ &\leq C(N^{-2\mu} + \|\theta\|^2). \end{aligned} \quad (3.47)$$

Now, since $\theta(0) = 0$, using continuity, let t_N , $0 < t_N \leq T$, be the maximal value of t for which the solution of (3.6)-(3.8) exists and satisfies

$$\|\theta\|_\infty \leq 1, \quad 0 \leq t \leq t_N. \quad (3.48)$$

By (3.48) we have for $0 \leq t \leq t_N$, using integration by parts

$$\begin{aligned} |(\theta\xi)_x, \theta) &= \frac{1}{2}|(\xi_x\theta, \theta)| \leq C|\theta|_\infty\|\theta\|\|\xi_x\| \\ &\leq C(\|\theta\|^2 + \|\xi_x\|^2). \end{aligned} \quad (3.49)$$

We conclude from (3.42)-(3.49) that

$$|(A_x, \theta)| \leq C\left(N^{2(1-\mu)} + \|\theta\|^2 + \|\xi\|_1^2\right), \quad 0 \leq t \leq t_N. \quad (3.50)$$

We estimate now (θ, ξ_x) and the terms of (B, ξ_x) exactly as in (3.27)-(3.32), and conclude that as long as the semidiscrete approximation exists it holds that

$$|(\theta, \xi_x)| + |(B, \xi_x)| \leq C(N^{-2\mu} + \|\theta\|^2 + \|\xi\|_1^2). \quad (3.51)$$

Therefore, by (3.40), (3.41), (3.50), (3.51), since $c', a, d \neq 0$ we see that for $0 \leq t \leq t_N$

$$\frac{1}{2}\frac{d}{dt}(\|\theta\|^2 + \|\xi\|_1^2) \leq C\left(N^{2(1-\mu)} + \|\theta\|^2 + \|\xi\|_1^2\right).$$

By Gronwall's lemma and (3.8) we see that for $0 \leq t \leq t_N$ and a constant $C(T)$ there holds

$$\|\theta\| + \|\xi\|_1 \leq C(T)N^{1-\mu}. \quad (3.52)$$

Therefore, since $|\theta|_\infty \leq CN^{1/2}\|\theta\|$ by (3.5), and using (3.52) and the assumption that $\mu > 3/2$, we see that t_N was not maximal in (3.48) if N was sufficiently large. We conclude that (3.52) holds up to $t = T$ which implies that

$$\max_{0 \leq t \leq T} (\|\zeta_N - \zeta\| + \|u_N - u\|_1) \leq CN^{1-\mu},$$

i. e. that the conclusion of the proposition holds. Note that this implies that u_N is optimally close to u in H^1 but ζ_N suboptimally so to ζ in L^2 . \square

Proposition 3.4. *Let a, b, c, d as in case (iv), and with no loss of generality suppose that $b = 0, d > 0, a = c = 0$. If $\mu > 3/2$ then*

$$\max_{0 \leq t \leq T} (\|\zeta_N - \zeta\| + \|u_N - u\|_1) \leq CN^{1-\mu}.$$

Proof. While the semidiscrete solution ζ_N, u_N exists, putting $\varphi = \theta$ in (3.10), $\chi = \xi$ in (3.12), and using integration by parts, then adding the resulting equations yields

$$\frac{1}{2} \frac{d}{dt} (\|\theta\|^2 + \|\xi\|^2 + d\|\xi_x\|^2) = -\kappa_1(\xi_x, \theta) - (A_x, \theta) + \kappa_2(\theta, \xi_x) + (B, \xi_x).$$

We estimate now the terms of (A_x, θ) and (B, ξ_x) exactly as in Proposition 3.3. The conclusion follows. \square

Proposition 3.5. *Let a, b, c, d as in case (v), and with no loss of generality suppose that $b > 0, d > 0, a = 0, c < 0$. If $\mu \geq 1$ then*

$$\max_{0 \leq t \leq T} (\|\zeta_N - \zeta\| + \|u_N - u\|) \leq CN^{-\mu}.$$

Proof. We write (3.10) for $a = 0$ as

$$\theta_t - b\theta_{xxt} = -\kappa_1\xi_x - PA_x,$$

i. e. as

$$(1 - b\partial_x^2)\theta_t = -\kappa_1\xi_x - PA_x. \quad (3.53)$$

For a constant $\kappa > 0$ let \mathcal{T}_κ denote the operator $\mathcal{T}_\kappa = (I - \kappa\partial_x^2)^{-1}$ which is well defined in H^s for any $s \in \mathbb{R}$. Using its Fourier representation we see, for any $f \in H^{j-2}$, that $\mathcal{T}_\kappa f \in H^j$ and that

$$\|\mathcal{T}_\kappa f\|_j \leq C_k \|f\|_{j-2}, \quad j \in \mathbb{R}, \quad (3.54)$$

where C_k is a constant depending on κ . (In the sequel we will only use the property that for $f \in L^2$, $\|f\|_{-j} \leq \|f\|, j \geq 0$, for the negative norms.)

Using this notation we write (3.53) as

$$\theta_t = -\kappa_1 \mathcal{T}_b \xi_x - \mathcal{T}_b P A_x.$$

Therefore, since ∂_x commutes with \mathcal{T}_b and P , (3.54) gives

$$\|\theta_t\|_1 \leq |\kappa_1| \|\mathcal{T}_b \xi_x\|_1 + \|\mathcal{T}_b P A_x\|_1 \leq C (\|\xi\| + \|A\|). \quad (3.55)$$

From the definition of A , cf. (3.11), we see that

$$\begin{aligned} \|A\| &\leq C (|u|_\infty \|\rho\| + |\zeta|_\infty \|\sigma\| + |u|_\infty \|\theta\| + |\zeta|_\infty \|\xi\| \\ &\quad + |\sigma|_\infty \|\theta\| + |\rho|_\infty \|\xi\| + |\rho|_\infty \|\sigma\| + \|\theta\| \|\xi\|_\infty). \end{aligned} \quad (3.56)$$

Since $\xi(0) = 0$, using continuity, let $t_N \in (0, T]$ denote the maximal time for which the solution of the semidiscrete ivp exists and satisfies

$$\|\xi\|_\infty \leq 1, \quad 0 \leq t \leq t_N. \quad (3.57)$$

Therefore, from (3.56), using the fact that $\mu \geq 1$, Sobolev's inequality, (3.3), and (3.4), we obtain, in view of (3.57), that

$$\|A\| \leq C (N^{-\mu} + \|\theta\| + \|\xi\|), \quad 0 \leq t \leq t_N. \quad (3.58)$$

Hence, from (3.55) and (3.58) we get

$$\|\theta_t\|_1 \leq C (N^{-\mu} + \|\theta\| + \|\xi\|), \quad 0 \leq t \leq t_N.$$

We write now (3.12) as

$$(1 - d\partial_x^2)\xi_t = -c'\theta_{xxx} - \kappa_2\theta_x - PB_x,$$

i. e. as

$$\xi_t = -c'\mathcal{T}_d\theta_{xxx} - \kappa_2\mathcal{T}_d\theta_x - \mathcal{T}_dPB_x,$$

from which, using (3.54), we get

$$\begin{aligned} \|\xi_t\| &\leq |c'| \|\mathcal{T}_d\theta_{xxx}\| + |\kappa_2| \|\mathcal{T}_d\theta_x\| + \|\mathcal{T}_dPB_x\| \\ &\leq C(\|\theta\|_1 + \|\theta\| + \|B\|) \leq C(\|\theta\|_1 + \|B\|). \end{aligned} \quad (3.59)$$

From (3.13) we see that

$$\|B\| \leq C(|u|_\infty \|\sigma\| + |u|_\infty \|\xi\| + |\sigma|_\infty \|\xi\| + |\sigma|_\infty \|\sigma\| + |\xi|_\infty \|\xi\|).$$

Therefore, since $\mu \geq 1$, from (3.3) and (3.4), we have, in view of (3.57), that

$$\|B\| \leq C(N^{-\mu} + \|\xi\|), \quad 0 \leq t \leq t_N. \quad (3.60)$$

Therefore, by (3.59) and (3.60) it follows that

$$\|\theta_t\|_1 + \|\xi_t\| \leq C(N^{-\mu} + \|\theta\|_1 + \|\xi\|), \quad 0 \leq t \leq t_N. \quad (3.61)$$

where C does not depend on t_N . From (3.8) we infer that $\theta = \int_0^t \theta_\tau d\tau$, $\xi = \int_0^t \xi_\tau d\tau$. Hence, by (3.61) we have, for $0 \leq t \leq t_N$

$$\begin{aligned} \|\theta\|_1 + \|\xi\| &\leq \int_0^t (\|\theta_\tau\|_1 + \|\xi_\tau\|) d\tau \\ &\leq C \int_0^t (N^{-\mu} + \|\theta\|_1 + \|\xi\|) d\tau \\ &\leq C \int_0^t (\|\theta\|_1 + \|\xi\|) d\tau + CTN^{-\mu}. \end{aligned}$$

Using Gronwall's lemma in integral form gives that for some $C = C(T)$

$$\|\theta\|_1 + \|\xi\| \leq CN^{-\mu}, \quad 0 \leq t \leq t_N. \quad (3.62)$$

From this we observe, since $\mu \geq 1$, that for $0 \leq t \leq t_N$ $|\xi|_\infty \leq 1$ if N is sufficiently large, and therefore that t_N was not maximal in (3.57). We may then take $t_N = T$ and conclude from (3.62) that

$$\|\theta\|_1 + \|\xi\| \leq CN^{-\mu}, \quad 0 \leq t \leq T.$$

Therefore, the conclusion of the proposition holds. It implies that ζ_N and u_N satisfy optimal-order L^2 -error estimates. \square

Proposition 3.6. *Let a, b, c, d as in case (vi) and $\mu > 3/2$. Then*

$$\max_{0 \leq t \leq T} (\|\zeta_N - \zeta\| + \|u_N - u\|_1) \leq CN^{1-\mu}.$$

Proof. Motivated by an *a priori* estimate for this system in Theorem 3.1 of [18], and putting $\varphi = \theta$ in (3.10) and using integration by parts we get, while the semidiscrete approximation exists

$$\frac{1}{2} \frac{d}{dt} \|\theta\|^2 = -\kappa_1(\xi_x, \theta) - (A_x, \theta) + a(\xi_{xx}, \theta_x). \quad (3.63)$$

Now putting $\chi = \xi + a\xi_{xx}$ in (3.12) and using integration by parts, we get, while the semidiscrete approximation exists,

$$\begin{aligned} \frac{1}{2} \frac{d}{dt} (|\xi|^2 + (|a| + d)\|\xi_x\|^2 + |a|d\|\xi_{xx}\|^2) &= -\kappa_2(\theta_x, \xi) - a\kappa_2(\theta_x, \xi_{xx}) \\ &\quad - (B_x, \xi + a\xi_{xx}). \end{aligned} \quad (3.64)$$

In order to eliminate the term (ξ_{xx}, θ_x) from (3.63) and (3.64) we multiply (3.63) by $\kappa_2 > 0$ and add the resulting equation to (3.64). In this way we get

$$\begin{aligned} \frac{1}{2} \frac{d}{dt} (\kappa_2\|\theta\|^2 + \|\xi\|^2 + (|a| + d)\|\xi_x\|^2 + |a|d\|\xi_{xx}\|^2) &= -\kappa_1\kappa_2(\xi_x, \theta) - \kappa_2(A_x, \theta) \\ &\quad - (B_x, \xi + a\xi_{xx}) \\ &\quad - \kappa_2(\theta_x, \xi). \end{aligned} \quad (3.65)$$

We now estimate the right-hand side of (3.65). The terms (ξ_x, θ) , (A_x, θ) are estimated as in the proof of Proposition 3.3. Assuming that t_N is the maximal time in $(0, T]$ for which the semidiscrete approximation exists and satisfies, in view of (3.8),

$$|\theta|_\infty \leq 1, \quad 0 \leq t \leq t_N, \quad (3.66)$$

we see, as in (3.41) and (3.50), that for $0 \leq t \leq t_N$

$$|(\xi_x, \theta)| + |(A_x, \theta)| \leq C \left(N^{2(1-\mu)} + \|\theta\|^2 + \|\xi\|_1^2 \right). \quad (3.67)$$

Examining the rest of the terms in the right-hand side of (3.65) we first note that

$$|(\theta_x, \xi)| = |(\theta, \xi_x)| \leq \frac{1}{2} (\|\theta\|^2 + \|\xi_x\|^2). \quad (3.68)$$

In the last term of the right-hand side of (3.65) the inner product with ξ is easily estimated by integrating by parts and arguing as in (3.28)-(3.32). This gives

$$|(B_x, \xi)| = |(B, \xi_x)| \leq C(N^{-2\mu} + \|\xi\|_1^2). \quad (3.69)$$

We now estimate the terms in the inner product (B_x, ξ_{xx}) . We have, since H^1 is an algebra, using (3.3) and our hypothesis on μ , that

$$|((u\sigma)_x, \xi_{xx})| \leq C\|u\|_1\|\sigma\|_1\|\xi_{xx}\| \leq C(N^{2(1-\mu)} + \|\xi_{xx}\|^2). \quad (3.70)$$

$$|((u\xi)_x, \xi_{xx})| \leq C\|u\|_1\|\xi\|_1\|\xi_{xx}\| \leq C\|\xi\|_2^2. \quad (3.71)$$

$$|((\sigma\xi)_x, \xi_{xx})| \leq C\|\sigma\|_1\|\xi\|_1\|\xi_{xx}\| \leq C\|\xi\|_2^2. \quad (3.72)$$

Since $\mu > 3/2$ we have by (3.3), (3.4)

$$\begin{aligned} |((\sigma^2)_x, \xi_{xx})| &\leq C\|\sigma\|_\infty\|\sigma\|_1\|\xi_{xx}\| \leq CN^{\frac{3}{2}-2\mu}\|\xi_{xx}\| \\ &\leq CN^{-\mu}\|\xi_{xx}\| \leq C(N^{-2\mu} + \|\xi_{xx}\|^2). \end{aligned} \quad (3.73)$$

Finally, assuming that t_N in (3.66) is small enough so that in addition to (3.66) we have

$$|\xi|_\infty \leq 1, \quad 0 \leq t \leq t_N, \quad (3.74)$$

we obtain for $0 \leq t \leq t_N$

$$|((\xi^2)_x, \xi_{xx})| \leq 2|\xi|_\infty\|\xi_x\|\|\xi_{xx}\| \leq C\|\xi\|_2^2. \quad (3.75)$$

From (3.65), (3.67)-(3.73) and (3.75), since $\kappa_2, d > 0$ we obtain

$$\frac{d}{dt} (\|\theta\|^2 + \|\xi\|_2^2) \leq C(N^{2(1-\mu)} + \|\theta\|^2 + \|\xi\|_2^2), \quad 0 \leq t \leq t_N,$$

where the constant C does not depend on t_N . By Gronwall's lemma then, for $0 \leq t \leq t_N$

$$\|\theta\| + \|\xi\|_2 \leq C_T N^{1-\mu}. \quad (3.76)$$

Since by (3.5) $|\theta|_\infty \leq CN^{1/2}\|\theta\|$, and since $|\xi|_\infty \leq C\|\xi\|_1$ by Sobolev's theorem, we see that (3.76) implies, in view of our assumption on μ , that t_N in (3.66) and (3.74) is not maximal if N is sufficiently large, and, as usual, can be taken equal to T . We infer that (3.76) holds up to $t = T$ and that the conclusion of the proposition follows, giving an optimal-order H^1 error estimate for u_N and a suboptimal-order one for ζ_N in L^2 . \square

Proposition 3.7. *Let a, b, c, d as in case (vii) and with no loss of generality suppose that $a < 0, b > 0, d = 0, c = 0$. If $\mu > 3/2$, then*

$$\max_{0 \leq t \leq T} (\|\zeta_N - \zeta\| + \|u_N - u\|) \leq CN^{1-\mu}. \quad (3.77)$$

Proof. These systems are of the form

$$\zeta_t + \kappa_1 u_x + \lambda(\zeta u)_x + au_{xxx} - b\zeta_{xxt} = 0, \quad (3.78)$$

$$u_t + \kappa_2 \zeta_x + \lambda u u_x = 0. \quad (3.79)$$

Motivated by an analogous observation in [18], Section 3.3, we write the first pde (3.78) above in the equivalent form

$$\zeta_t - \frac{a}{b} u_x + (\kappa_1 + \frac{a}{b}) \mathcal{T}_b u_x + \lambda \mathcal{T}_b (\zeta u)_x = 0, \quad (3.80)$$

where $\mathcal{T}_b = (I - b\partial_x^2)^{-1}$ was introduced in the proof of Proposition 3.5.

Consequently, we will adopt the following semidiscretization of the system: For all $\varphi, \chi \in S_N$

$$(\zeta_{Nt}, \varphi) - \frac{a}{b} (u_{Nx}, \varphi) + (\kappa_1 + \frac{a}{b}) (\mathcal{T}_b u_{Nx}, \varphi) + \lambda (\mathcal{T}_b (\zeta_N u_N)_x, \varphi) = 0, \quad (3.81)$$

$$(u_{Nt}, \chi) + \kappa_2 (\zeta_{Nx}, \chi) + \lambda (u_N u_{Nx}, \chi) = 0, \quad (3.82)$$

with

$$\zeta_N(0) = P\zeta_0, u_N(0) = Pu_0. \quad (3.83)$$

It is clear that the solution of this ivp exists at least locally in time.

We proceed now to the proof of the error estimate (3.77). While the semidiscrete solution exists, using our usual notation and subtracting the weak form of (3.80) from (3.81) we have for all $\varphi \in S_N$

$$(\theta_t, \varphi) - \frac{a}{b} (\xi_x, \varphi) = -(\kappa_1 + \frac{a}{b}) (\mathcal{T}_b (\xi_x + \sigma_x), \varphi) - \lambda (\mathcal{T}_b A_x, \varphi), \quad (3.84)$$

From the weak form of (3.79) and (3.82) we obtain

$$(\xi_t, \chi) + \kappa_2 (\theta_x, \chi) = -\lambda (B_x, \chi), \quad \forall \chi \in S_N, \quad (3.85)$$

Putting $\varphi = \theta$ in (3.84), $\chi = \xi$ in (3.85) gives

$$\begin{aligned} \frac{1}{2} \frac{d}{dt} \|\theta\|^2 - \frac{a}{b} (\xi_x, \theta) &= -(\kappa_1 + \frac{a}{b}) (\mathcal{T}_b(\xi_x + \sigma_x), \theta) - \lambda (\mathcal{T}_b A_x, \theta), \\ \frac{1}{2} \frac{d}{dt} \|\xi\|^2 - \kappa_2 (\theta, \xi_x) &= -\lambda (B_x, \xi). \end{aligned}$$

Multiplying the first equation above by κ_2 and the second by $-a/b$ and adding we get

$$\begin{aligned} \frac{1}{2} \frac{d}{dt} \left(\kappa_2 \|\theta\|^2 + \frac{|a|}{b} \|\xi\|^2 \right) &= -\kappa_2 (\kappa_1 + \frac{a}{b}) (\mathcal{T}_b(\xi + \sigma)_x, \theta) \\ &\quad - \kappa_2 \lambda (\mathcal{T}_b A_x, \theta) + \frac{a}{b} \lambda (B_x, \xi). \end{aligned} \quad (3.86)$$

For the first two terms in the right-hand side of (3.86) we have, in view of (3.54)

$$|(\mathcal{T}_b(\xi + \sigma)_x, \theta)| \leq \|\mathcal{T}_b(\xi + \sigma)_x\| \|\theta\| \leq C(\|\xi\| + \|\sigma\|) \|\theta\|, \quad (3.87)$$

$$|(\mathcal{T}_b A_x, \theta)| \leq \|\mathcal{T}_b A_x\| \|\theta\| \leq C \|A\| \|\theta\|. \quad (3.88)$$

We bound the right-hand side of (3.87) as usual by

$$(\|\xi\| + \|\sigma\|) \|\theta\| \leq C(N^{-2\mu} + \|\xi\|^2 + \|\theta\|^2). \quad (3.89)$$

In order to bound the right-hand side of (3.88), we argue as in the proof of Proposition 3.5; in particular, consider (3.56). The only difference is in the last term of A , which we now bound by $\|\xi\| \|\theta\|_\infty$. Consequently, let t_N , $0 < t_N \leq T$ be the maximal time for which the semidiscrete approximation exists and is such that

$$\|\theta\|_\infty \leq 1, \quad 0 \leq t \leq t_N. \quad (3.90)$$

We therefore obtain, for $0 \leq t \leq t_N$, that

$$\|A\| \|\theta\| \leq C(N^{-2\mu} + \|\theta\|^2 + \|\xi\|^2). \quad (3.91)$$

We now estimate the last term of the right-hand side of (3.86). Using the definition (3.13) of B , we have, since H^1 is an algebra and in view of (3.3), that

$$|((u\sigma)_x, \xi)| \leq \|u\|_1 \|\sigma\|_1 \|\xi\| \leq C \|\sigma\|_1 \|\xi\| \leq C(N^{2(1-\mu)} + \|\xi\|^2) \quad (3.92)$$

By integrating by parts we see that

$$|((u\xi)_x, \xi)| = \frac{1}{2} |(u_x \xi, \xi)| \leq \frac{1}{2} |u_x|_\infty \|\xi\|^2 \leq C \|\xi\|^2, \quad (3.93)$$

using our hypothesis on μ . Similarly, by (3.4)

$$|((\sigma\xi)_x, \xi)| = \frac{1}{2} |(\sigma_x \xi, \xi)| \leq \frac{1}{2} |\sigma_x|_\infty \|\xi\|^2 \leq C \|\xi\|^2. \quad (3.94)$$

By our hypothesis on μ and (3.3), (3.4)

$$\begin{aligned} |(\sigma\sigma_x, \xi)| &\leq |\sigma|_\infty \|\sigma_x\| \|\xi\| \leq CN^{\frac{1}{2}-\mu} N^{1-\mu} \|\xi\| \\ &\leq CN^{-\mu} \|\xi\| \leq C(N^{-2\mu} + \|\xi\|^2). \end{aligned} \quad (3.95)$$

And finally, by periodicity

$$(\xi \xi_x, \xi) = 0. \quad (3.96)$$

By (3.92)-(3.96) we conclude, as long as the solution of (3.81)-(3.83) exists, that

$$|(B_x, \xi)| \leq C(N^{2(1-\mu)} + \|\xi\|^2). \quad (3.97)$$

Therefore, by (3.86), since $\kappa_2, b > 0$, and using (3.87), (3.89), (3.91), (3.97) we have for $0 \leq t \leq t_N$

$$\frac{d}{dt} (\|\theta\|^2 + \|\xi\|^2) \leq C(N^{2(1-\mu)} + \|\theta\|^2 + \|\xi\|^2).$$

Hence, by Gronwall's lemma, in view of (3.83) we obtain for $0 \leq t \leq t_N$

$$\|\theta\| + \|\xi\| \leq C_T N^{1-\mu}. \quad (3.98)$$

Since $|\theta|_\infty \leq CN^{1/2}\|\theta\| \leq CN^{3/2-\mu}$ by the above, in view of our hypothesis on μ , and provided we take N sufficiently large, we infer that t_N in (3.90) was not maximal; as usual, we may take $t_N = T$. Thus (3.98) holds up to $t = T$, giving (3.77). This inequality implies that ζ_N and u_N satisfy in this case suboptimal L^2 -error estimates. \square

4. SOLITARY WAVES

This section is focused on the existence and numerical generation of solitary-wave solutions of the B/B systems (1.6). We first review the application of several theories of existence and then we illustrate the corresponding results with some examples of numerical generation of the profiles.

4.1. Some existence results. The solitary waves are solutions of (1.6) of the form $\zeta = \zeta(x - c_s t), u = u(x - c_s t)$ that satisfy

$$\partial_x \begin{pmatrix} c_s(1 - b\partial_{xx}) & -\frac{1}{\delta+\gamma} - a\partial_{xx} \\ -(1-\gamma)(1 + c\partial_{xx}) & c_s(1 - d\partial_{xx}) \end{pmatrix} \begin{pmatrix} \zeta \\ v_\beta \end{pmatrix} = \kappa_{\gamma,\delta} \partial_x \begin{pmatrix} \zeta v_\beta \\ \frac{v_\beta^2}{2} \end{pmatrix},$$

where $\kappa_{\gamma,\delta} = \frac{\delta^2 - \gamma}{(\delta + \gamma)^2}$, cf. section 2.1. Classical solitary waves (CSW), for which $\zeta, u \rightarrow 0$ as $|x - c_s t| \rightarrow \infty$, will be solutions of

$$\begin{pmatrix} c_s(1 - b\partial_{xx}) & -\frac{1}{\delta+\gamma} - a\partial_{xx} \\ -(1-\gamma)(1 + c\partial_{xx}) & c_s(1 - d\partial_{xx}) \end{pmatrix} \begin{pmatrix} \zeta \\ v_\beta \end{pmatrix} = \kappa_{\gamma,\delta} \begin{pmatrix} \zeta v_\beta \\ \frac{v_\beta^2}{2} \end{pmatrix}. \quad (4.1)$$

In addition, there exist Generalized solitary waves (GSW), which are not CSW and satisfy (4.1).

4.1.1. Existence via linearization. (The main references in this section are [24, 4, 47, 48, 25, 49].) In the case of small deviations of c_s from the speed of sound the existence of solitary waves can be studied in a similar way to analogous studies in [19, 35] by using Bifurcation theory, [46, 44]. In order to apply this theory to (4.1), we define $c_{\gamma,\delta}$ to be the speed of sound corresponding to (1.6), i. e. as

$$c_{\gamma,\delta} = \sqrt{\frac{1-\gamma}{\delta+\gamma}}, \quad (4.2)$$

Note that if (c_s, ζ, v_β) is a solution of (4.1), then $(-c_s, \zeta, -v_\beta)$ is also a solution (with the same profile but opposite speed). Thus we can assume $c_s > 0$ and define the parameter

$$\tilde{\mu} := \frac{c_s}{c_{\gamma,\delta}} - 1, \quad (4.3)$$

so that $c_s = \tilde{\mu}c_{\gamma,\delta} + 1$. The parameter $\tilde{\mu}$ given by (4.3) is analogous to the parameter μ used in [48] to discuss, via the Normal Form Theory (NFT), the existence of solitary waves for free surface wave propagation on an inviscid fluid layer under

gravity and surface tension effects. In terms of the variables ζ, v_β , (4.1) can be rewritten as a first-order system, depending on $\tilde{\mu}$, for $U = (U_1, U_2, U_3, U_4)^T := (\zeta, \zeta', v_\beta, v'_\beta)^T$, namely as

$$\begin{aligned}
U' &= V(U, \tilde{\mu}) := L(\tilde{\mu})U + R(U, \tilde{\mu}), \tag{4.4} \\
L(\tilde{\mu}) &= \begin{pmatrix} 0 & 1 & 0 & 0 \\ \frac{dc_s^2 + a(1-\gamma)}{D} & 0 & -\frac{c_s}{D} \left(a + \frac{d}{\delta+\gamma} \right) & 0 \\ 0 & 0 & 0 & 1 \\ -\frac{(1-\gamma)c_s(b+c)}{D} & 0 & \frac{1}{D} \left(bc_s^2 + \frac{c(1-\gamma)}{\delta+\gamma} \right) & 0 \end{pmatrix}, \\
R(U, \tilde{\mu}) &= \begin{pmatrix} 0 \\ \frac{1}{D} \frac{\delta^2 - \gamma}{(\delta + \gamma)^2} \left(-dc_s U_1 U_3 + \frac{a}{2} U_3^2 \right) \\ 0 \\ \frac{1}{D} \frac{\delta^2 - \gamma}{(\delta + \gamma)^2} \left(-c(1 - \gamma) U_1 U_3 - \frac{bc_s}{2} U_3^2 \right) \end{pmatrix}, \\
D &= bdc_s^2 - (1 - \gamma)ac = bdc_s^2 - \frac{ac}{\kappa_1} c_{\gamma, \delta}^2. \tag{4.5}
\end{aligned}$$

We assume that the condition (C1) (cf. section 2.2) holds and $D \neq 0$. The system (4.4), (4.5) admits $U = 0$ as fixed point, that is, $V(0, \tilde{\mu}) = 0$. Additionally, the vector field V is reversible, meaning that

$$SV(U, \tilde{\mu}) = -V(SU, \tilde{\mu}),$$

where $S = \text{diag}(1, -1, 1, -1)$. In view of these observations, we see that the study of homoclinic solutions of (4.1) via NFT requires first to analyze the linearization of (4.4) at the origin $U = 0$. The characteristic equation is

$$\lambda^4 - B\lambda^2 + A = 0, \tag{4.6}$$

where

$$A = \frac{c_s^2 - c_{\gamma, \delta}^2}{D}, \quad B = \frac{(b+d)c_s^2 + (c+a/\kappa_1)c_{\gamma, \delta}^2}{D}. \tag{4.7}$$

(No confusion need arise between these A, B and those of section 3.) The structure of the spectrum of $L(\tilde{\mu})$ in (4.4), (4.5) can be studied following the survey [24]. The distribution of the roots of (4.6) in the (B, A) -plane is given in Figure 1, which reproduces the bifurcation diagram, along with the location and the type of the four eigenvalues, shown in Figure 1 of [24]. Thus, the behaviour of the linear dynamics is determined by the four regions separated by the four bifurcation curves

$$\begin{aligned}
C_0 &= \{(B, A)/A = 0, B > 0\}, \\
C_1 &= \{(B, A)/A = 0, B < 0\}, \\
C_2 &= \{(B, A)/A > 0, B = -\sqrt{A}\}, \\
C_3 &= \{(B, A)/A > 0, B = \sqrt{A}\}.
\end{aligned}$$

The Center Manifold Theorems and the theory of reversible bifurcations, [46, 44], can be applied to study the existence of homoclinic orbits in each bifurcation. The reduced Normal Form systems reveal the existence of homoclinic to zero orbits and homoclinic to periodic orbits. The corresponding solutions are CSW's and GSW's, respectively. In addition, periodic and quasi-periodic orbits are identified, [48].

More specifically, we may adapt the discussion of [24] near the bifurcation curves C_0 to C_3 to the case of (4.4), (4.5), using (4.3) as bifurcation parameter. Note first

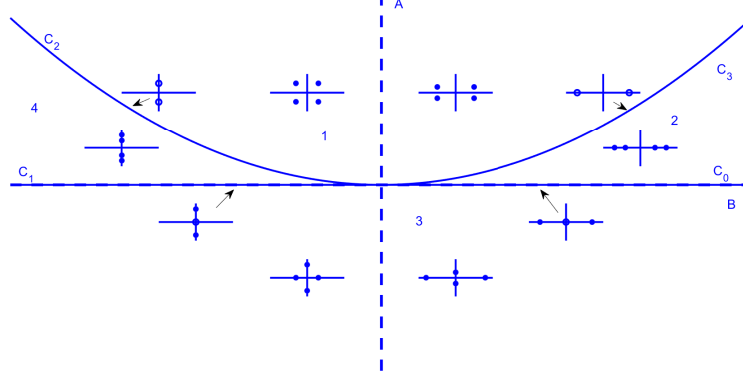


FIGURE 1. Linearization at the origin of (4.4). As in Figure 1 of [24].

that by (4.7), $A = 0$ iff $c_s = c_{\gamma, \delta}$; then $B = S(\gamma, \delta)/(bd - ac/\kappa_1)$, with $S(\gamma, \delta) := \frac{1+\gamma\delta}{3\delta(\delta+\gamma)}$. Therefore, under the hypothesis (C1), the curve C_0 is characterized by the conditions

$$a, c \leq 0, b, d \geq 0, bd - \frac{ac}{\kappa_1} > 0, \tilde{\mu} = 0, \quad (4.8)$$

while the conditions for the curve C_1 are

$$a, c \leq 0, b, d \geq 0, bd - \frac{ac}{\kappa_1} < 0, \tilde{\mu} = 0, \quad (4.9)$$

We now study the information furnished by the Normal Form Theory (NFT) close to each curve C_j , $0 \leq j \leq 3$. In the case of C_0 , the linearization matrix $L(0)$ has two simple eigenvalues equal to

$$\pm \sqrt{\frac{S(\gamma, \delta)}{bd - ac/\kappa_1}}, \quad (4.10)$$

and the zero eigenvalue with geometric multiplicity one and algebraic multiplicity two. As in [48, 24], the main role in describing the dynamics close to C_0 by NFT is played by this two-dimensional center manifold, on which (4.4) is reduced to a nonlinear oscillator system which depends on $\tilde{\mu}$. When $\tilde{\mu}$, A and B are positive, and near C_0 the linear dynamics is given by the spectrum of $L(\tilde{\mu})$ which consists of four real eigenvalues (region 2 in Figure 1). In this case, the normal form system has a unique solution, homoclinic to zero at infinity, symmetric and unique up to spatial translations, ([48], Proposition 3.1), that corresponds to a CSW solution of (4.1).

Remark 4.1. *If $\tilde{\mu}$ is negative, and with similar arguments to those of [48], NFT establishes the existence of a family of periodic solutions of the reduced system (close to C_0) for each $\tilde{\mu}$, unique up to spatial translations. For the case at hand, and due to (4.7), if $\tilde{\mu} < 0$ and $bd - ac/\kappa_1 > 0$, then $D > 0$. Therefore, $A < 0$ and we fall into region 3 of Figure 1. The numerical generation of periodic traveling wave solutions of (4.1) under these conditions will be discussed in section 4.2.*

In the case of C_1 , the spectrum of $L(0)$ consists of zero (with algebraic multiplicity two) and the two simple imaginary eigenvalues given by (4.10) (recall that $bd - ac/\kappa_1 < 0$). The arguments used in [48], Proposition 3.2, apply here and NFT reduces (4.1), on the center manifold, for $\tilde{\mu} \neq 0$ small enough, to a normal form system which admits homoclinic solutions to periodic orbits, that is GSW solutions. Information about the structure of the periodic orbits can also be obtained, cf. [55, 56, 57].

Remark 4.2. *In addition to GSW's, the normal form derived in [48], section 3.2, also reveals the existence of other solutions: periodic, quasi-periodic, and homoclinic to zero solutions (that is, CSW's). This normal form is used in [24] to generalize the result of existence of a homoclinic solution of square hyperbolic secant form (in lowest order of $\tilde{\mu}$) or a pair of hyperbolic secant solutions close to C_1 and corresponding to region 3 of Figure 1. As mentioned in [24], persistence of these solutions under small reversible perturbations of the normal form is not expected.*

The normal form derived in [49] is used in [24] to study the dynamics close to C_2 . Its application to our case reveals the existence of homoclinic to zero solutions (CSW's) with nonmonotone decay for $\tilde{\mu} < 0$ and corresponding to region 1 of Figure 1 (they have a truncated form like $E_1 \operatorname{sech}(E_2 x) e^{i\omega\theta}$, for constants E_1, E_2 and ω related to the coefficients of the normal form, and $\theta \in \mathbb{R}$), and homoclinic solutions to periodic orbits (GSW's) for $\tilde{\mu} > 0$ corresponding to region 4 of Figure 1.

Remark 4.3. *These CSW's with nonmonotone decay require then speeds c_s smaller than the speed of sound $c_{\gamma,\delta}$ (since $\tilde{\mu} < 0$) and are different from the CSW's obtained close to C_0 , which are strictly positive or negative. The generation and stability of these waves will be discussed numerically in sections 4.2 and 5.5, respectively.*

Finally, near C_3 , and according to [24], crossing from the region 2 to region 1 in Figure 1 forms a bifurcation causing the generation of infinity multiplicity of homoclinic orbits. This bifurcation was analyzed for specific problems, [26, 13, 30]. In our case, the numerical computations suggest a similar situation to that of described in [26] (see also section 5.1 of [24] and [4, 25]). In particular, CSW's of nonmonotone decay are numerically generated in section 4.2.

In summary, NFT establishes the existence of CSW solutions of (4.1) for small and positive $c_s^2 - c_{\gamma,\delta}^2$ when (4.8) holds (close to C_0), and GSW solutions for small $c_s^2 - c_{\gamma,\delta}^2$ under the conditions given in (4.9) and close to C_1 . Note that, in the latter case, in view of (1.2), it is not possible to have $a, c < 0, b > 0, d = 0$. Hence, from (4.8) and (4.9), we may distinguish the cases shown in Table 1.

In addition, when $c_s < c_{\gamma,\delta}$, close to C_2 , CSW's of nonmonotone decay are shown to exist. They have also been observed numerically close to C_3 , cf. section 4.2.

Remark 4.4. *In [24] a review is made of existence results of homoclinic orbits using the linearization in each region of Figure 1. In our case, this is beyond the scope of the paper. However, in section 4.2 we will indicate, for each computed solitary wave, the corresponding region, referring to [24] and references therein for more information and possible similarities with other models.*

Table 2 shows the relation between the classification (i)-(vii) of parameter cases for the study of well-posedness in section 2.2 and (A1)-(A6)

Case	Admissible system	Type of solitary wave
(A1)	$a, c < 0, b = 0, d > 0$	GSW
(A2)	$a, c < 0, b, d > 0, \frac{bd}{\delta+\gamma} - ac < 0$	GSW
(A3)	$a, c < 0, b, d > 0, \frac{bd}{\delta+\gamma} - ac > 0$	CSW
(A4)	$a = 0, c < 0, b, d > 0$	CSW
(A5)	$a < 0, c = 0, b, d > 0$	CSW
(A6)	$a = c = 0, b, d > 0$	CSW

TABLE 1. Corresponding admissible system in (1.6) and type of solitary waves and for small and positive $c_s - c_{\gamma,\delta}$, when $D \neq 0$, according to the Normal Form Theory.

$(i) \leftrightarrow (A6)$	$\left. \begin{array}{l} (iv) \\ (vi) \\ (vii) \end{array} \right\} \leftrightarrow D = 0$
$(ii) \leftrightarrow \begin{cases} (A2) \\ (A3) \end{cases}$	
$(iii) \leftrightarrow (A1)$	$(v) \leftrightarrow \begin{cases} (A4) \\ (A5) \end{cases}$

TABLE 2. Relation between the cases (i)-(vii) of section 2.2, and (A1)-(A6) and $D = 0$ for existence of solitary waves according to the Normal Form Theory.

For a particular case of $D = 0$ ('classical Boussinesq' $b = 0, d > 0, a = c = 0$) existence and numerical generation of CSW's are studied in [40], cf. also [8] for the analogous case of surface waves. In other cases where $D = 0$, numerical evidence of existence of CSW's will be presented below.

4.1.2. *Toland's Theory.* For larger deviations $c_s - c_{\gamma,\delta}$ or other conditions on the speed c_s , several general theories may be used to analyze the existence of classical solitary waves: Toland's Theory, [66], Concentration-Compactness Theory, [54], and Positive Operator Theory, [14]. In the first case, and in order to apply the results of [66] to study the existence of CSW's, note that system (4.1) may be written in the form

$$S_1 \mathbf{v}'' + S_2 \mathbf{v} + \nabla g(v_\beta, \zeta) = 0, \quad (4.11)$$

where $\mathbf{v} = (v_\beta, \zeta)^T$ and

$$S_1 = - \begin{pmatrix} \frac{a}{c_s} & b \\ d & \frac{(1-\gamma)c}{c_s} \end{pmatrix}, \quad S_2 = - \begin{pmatrix} \frac{-1}{c_s(\delta+\gamma)} & 1 \\ 1 & -\frac{(1-\gamma)}{c_s} \end{pmatrix}, \quad (4.12)$$

$$g(v_\beta, \zeta) = - \frac{(\delta^2 - \gamma)}{c_s(\delta + \gamma)^2} \frac{\zeta v_\beta^2}{2} = - \frac{\kappa_{\gamma,\delta}}{2c_s} \zeta v_\beta^2,$$

where we recall that $\kappa_{\gamma,\delta}$ is given by (2.2) and $v_\beta = (1 - \beta \partial_{xx})^{-1} u$. Note that the theory of [66] can be applied here in the symmetric case $b = d$, and may be used to give existence results for classical solitary waves for specific systems in terms of c_s, γ and δ or, alternatively, in terms of $c_s, c_{\gamma,\delta}$, cf. (4.2). We recall the general

form of the main result for existence of solitary waves derived in [66], in the form given in [27].

Theorem 4.1. *Let S_1, S_2 be symmetric, $g \in C^2(\mathbb{R}^2)$ such that $g, \nabla g, \nabla^2 g$ are zero at $(0, 0)$. Let Q and f be given for $\mathbf{u} := (u_1, u_2)^T \in \mathbb{R}^2$ by*

$$Q(\mathbf{u}) = \mathbf{u}^T S_1 \mathbf{u}, \quad f(\mathbf{u}) = \mathbf{u}^T S_2 \mathbf{u} + 2g(\mathbf{u}), \quad (4.13)$$

and assume that:

- (I) $\det(S_1) < 0$ and there are two linearly independent vectors $\mathbf{v}_1, \mathbf{v}_2$ such that $Q(\mathbf{v}_1) = Q(\mathbf{v}_2) = 0$.
- (II) There is a closed plane curve \mathcal{F} with $(0, 0) \in \mathcal{F}$ such that
 - (i) $f = 0$ on \mathcal{F} and $\mathcal{F} \setminus \{(0, 0)\} \subset \{\mathbf{u} | Q(\mathbf{u}) < 0\}$.
 - (ii) $f(u_1, u_2) > 0$ in the (nonempty) interior of \mathcal{F} .
 - (iii) $\mathcal{F} \setminus \{(0, 0)\}$ is strictly convex.
 - (iv) $\nabla f(u_1, u_2) = 0$ on $\mathcal{F} \Leftrightarrow (u_1, u_2) = (0, 0)$.

Then there is an orbit $\tilde{\gamma}$ of (4.11) in the $(v_\beta(0), \zeta)$ plane, which is homoclinic to the origin and

- (a) $(v_\beta(0), \zeta(0)) \in \Gamma$ where Γ is the segment of \mathcal{F} including the origin between P_1, P_2 with P_j satisfying

$$\langle \nabla f(P_j), \mathbf{v}_j \rangle = 0, \quad j = 1, 2.$$

- (b) v_β, ζ are even functions on \mathbb{R} .
- (c) $(v_\beta(\xi), \zeta(\xi))$ is in the interior of \mathcal{F} for all $\xi \neq 0$.
- (d) $\tilde{\gamma}$ is monotone.

The application of this theory can be made in a similar way to the case of Boussinesq systems for surface waves, [28]. In our context, from (4.11), (4.12) and assuming $a, c \leq 0, b = d > 0$, we have

$$\begin{aligned} f(v_\beta, \zeta) &= \mathbf{v}^T S_2 \mathbf{v} + 2g(\mathbf{v}) \\ &= \frac{1}{c_s} \left(-\frac{v_\beta^2}{\delta + \gamma} \left(1 + \frac{(\delta^2 - \gamma)}{(\delta + \gamma)} \zeta \right) - (1 - \gamma)\zeta^2 + 2c_s \zeta v_\beta \right). \end{aligned} \quad (4.14)$$

The quadratic form Q defined in (4.13) is indefinite, and its diagonal form (used to identify two linearly independent directions in which Q vanishes) is of the following types:

- (1) If $a < 0$ then

$$Q(U_1, U_2) = -\frac{a}{c_s} U_1^2 + \frac{D}{ac_s} U_2^2,$$

where here $D = b^2 c_s^2 - (1 - \gamma)ac \geq 0$ and

$$U_1 = u_1 + \frac{bc_s}{a} u_2, \quad U_2 = u_2.$$

In this case the two linearly independent directions where $Q = 0$ are given by

$$\begin{aligned} U_2 = \pm \frac{a}{\sqrt{D}} U_1 &\Rightarrow u_2 = \frac{a}{\sqrt{D} - bc_s} u_1, \\ &u_2 = -\frac{a}{\sqrt{D} + bc_s} u_1. \end{aligned}$$

(2) When $a = 0, c < 0$ then

$$Q(U_1, U_2) = -(1 - \gamma) \frac{c}{c_s} U_1^2 + \frac{bc_s}{c(1 - \gamma)} U_2^2,$$

with

$$U_1 = u_1 + \frac{bc_s}{c(1 - \gamma)} u_2, \quad U_2 = u_2.$$

Now $Q = 0$ when

$$\begin{aligned} U_2 = \pm \frac{c(1 - \gamma)}{c_s \sqrt{b}} U_1 &\Rightarrow u_2 = -\frac{c(1 - \gamma)}{c_s \sqrt{b}(1 + \sqrt{b})} u_1 \\ &u_2 = \frac{c(1 - \gamma)}{c_s \sqrt{b}(1 - \sqrt{b})} u_1. \end{aligned}$$

(3) When $a = c = 0$, then $Q(u_1, u_2) = -2bu_1u_2$, and the two independent directions are clearly $u_1 = 0$ and $u_2 = 0$.

As we are investigating existence of classical solitary waves, we will apply Theorem 4.1 for the cases (A3)-(A6) in section 4.1. Note that the condition $\det(S_1) < 0$ in (I) of Theorem 4.1 implies that $D > 0$, where D is given by (4.5). By way of illustration, we consider the simplest case (3). The condition $Q < 0$ (see (II)(i) of Theorem 4.1) implies that u_1, u_2 are taken in the first or the third (v_β, ζ) quadrant. The resulting solitary waves are, respectively, of elevation or of depression type, and this is determined by the sign of $\kappa_{\gamma, \delta}$. Since the linearly independent directions are given in this case by $\mathbf{v}_1 = (1, 0)^T, \mathbf{v}_2 = (0, 1)^T$, the points P_1, P_2 must satisfy

$$f(P_1) = f(P_2) = 0, \quad \frac{\partial f}{\partial u_1}(P_1) = \frac{\partial f}{\partial u_2}(P_2) = 0,$$

which means, following [28]

$$-\kappa_1 u_1^2 - \kappa_{\gamma, \delta} u_1^2 u_2 - \kappa_2 u_2^2 + 2c_s u_1 u_2 = 0, \quad (4.15)$$

$$-\kappa_1 u_1 - \kappa_{\gamma, \delta} u_1 u_2 + c_s u_2 = 0, \quad (4.16)$$

$$-\kappa_{\gamma, \delta} u_1^2 - 2\kappa_2 u_2 + 2c_s u_1 = 0, \quad (4.17)$$

where $\kappa_1 = \frac{1}{\delta + \gamma}$ and $\kappa_2 = 1 - \gamma$ as in section 3. The components of P_1 must satisfy (4.15), (4.16) and those of P_2 (4.15), (4.17). Solving (4.15), (4.16) leads to $u_1 = u_2 = 0$ and

$$u_1 = \frac{c_s^2 - c_{\gamma, \delta}^2}{c_s \kappa_{\gamma, \delta}}, \quad u_2 = \frac{c_s}{\kappa_2} u_1, \quad (4.18)$$

while solving (4.15), (4.17) yields

$$u_1^\pm = 2 \frac{c_s \mp c_{\gamma, \delta}}{\kappa_{\gamma, \delta}}, \quad u_2^\pm = \pm \sqrt{\frac{\kappa_1}{\kappa_2}} u_1^\pm. \quad (4.19)$$

We now discuss the components of P_1 and P_2 by using the requirement that they must be in the first or third (v_β, ζ) quadrant. Assume first that $c_s > 0$. Then u_1 and u_2 in (4.18) have always the same sign, while in the case of (4.19) this holds only for u_1^+ and u_2^+ . Therefore, P_1 has the components given by (4.18), and from (4.19) $P_2 = (u_1^+, u_2^+)$. It is not hard to check that P_1 and P_2 are in the first (v_β, ζ) quadrant when $(c_s - c_{\gamma, \delta})\kappa_{\gamma, \delta} > 0$ and in the third quadrant when $(c_s - c_{\gamma, \delta})\kappa_{\gamma, \delta} < 0$, see Figure 2(a). Then, according to the conclusions of Theorem 4.1, for initial data on $\Gamma = P_1 P_2$, the corresponding classical solitary waves are of

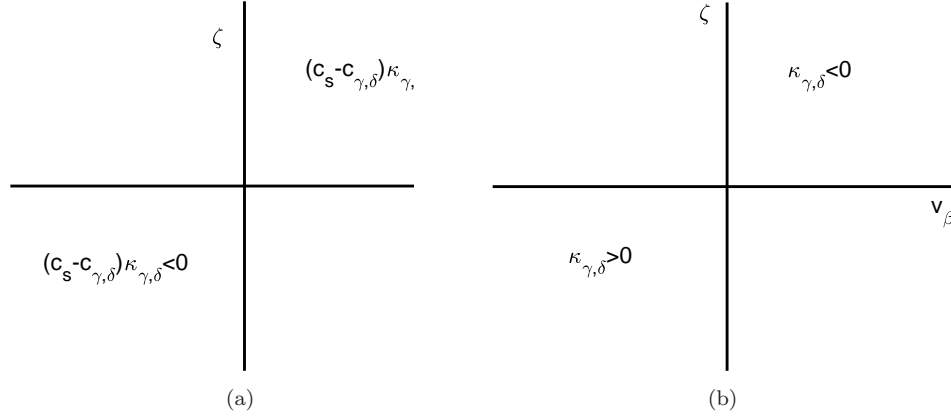


FIGURE 2. Conditions on $c_s - c_{\gamma,\delta}$ and $\kappa_{\gamma,\delta}$ to have P_1 and P_2 in the first or third (v_β, ζ) quadrant. (a) $c_s > 0$; (b) $c_s < 0$.

elevation when $(c_s - c_{\gamma,\delta})\kappa_{\gamma,\delta} > 0$ and of depression when $(c_s - c_{\gamma,\delta})\kappa_{\gamma,\delta} < 0$. The orbit $\tilde{\gamma}$ and the segment Γ for several values of the speed c_s are shown in Figures 3 and 4 respectively.

If we assume that $c_s < 0$, then u_1 and u_2 from (4.18) have always opposite sign. Then necessarily $P_1 = (0, 0)$. The same argument as before leads again to obtain $P_2 = (u_1^+, u_2^+)$, with u_1^+, u_2^+ given by (4.19). Furthermore, in this case $c_s - c_{\gamma,\delta}$ is always negative and the condition for P_2 to be in the first or third (v_β, ζ) quadrant depends only on the sign of $\kappa_{\gamma,\delta}$. For initial data on Γ , the corresponding classical solitary wave is of elevation if $\kappa_{\gamma,\delta} < 0$ and of depression if $\kappa_{\gamma,\delta} > 0$, see Figure 2(b).

Remark 4.5. According to the previous arguments based on Toland's theory, the speed c_s must satisfy, in view of the equation $f = 0$, the speed-amplitude relation

$$\begin{aligned} c_s &= \frac{1}{2\mu} \left(\frac{1}{\delta + \gamma} \left(1 + \frac{(\delta^2 - \gamma)}{(\delta + \gamma)} \zeta(0) \right) + (1 - \gamma)\mu^2 \right) \\ &= \frac{1}{2\mu} (\kappa_1 + \kappa_{\gamma,\delta} \zeta(0) + \kappa_2 \mu^2), \end{aligned} \quad (4.20)$$

where $\mu = \zeta(0)/v_\beta(0)$.

4.1.3. Concentration-Compactness Theory. In the Hamiltonian case ($b = d > 0$) and when $a, c < 0$, another result of existence of CSW's can be obtained from the application of the Concentration-Compactness (C-C) Theory. The method was developed by Lions in [54] and has been used for proving the existence of solitary-wave solutions of a great number of nonlinear dispersive equations, see [67, 2, 23, 53, 1], among other. (A more exhaustive list of references can be found in [5]. For the case of Boussinesq systems for surface wave propagation, see [12].) Here, its application is based on identifying solutions of (4.1) with solutions of minimization problems of the form

$$I_r = \inf \{ E(\zeta, v) : (\zeta, v) \in H^1 \times H^1 / F(\zeta, v) = r \}, \quad (4.21)$$

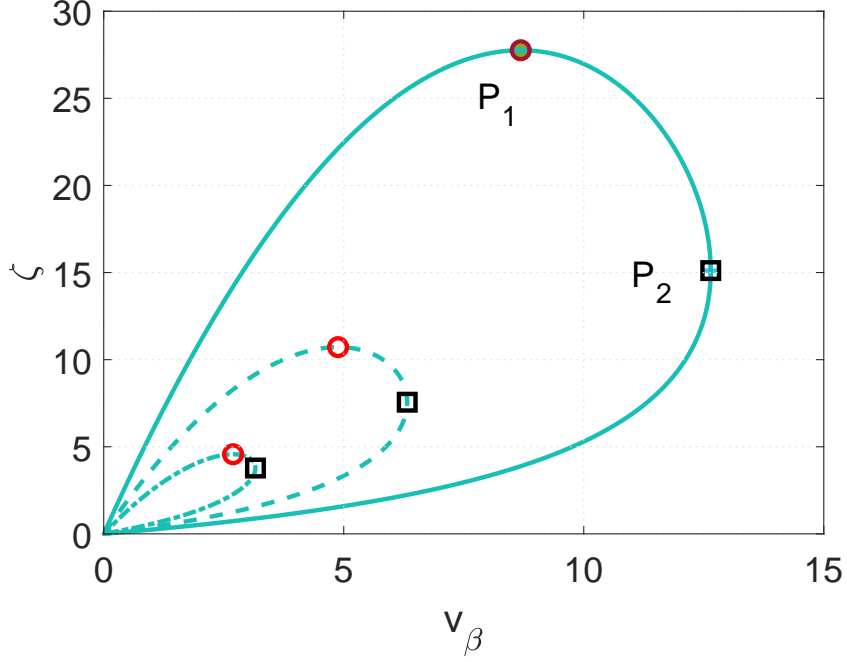


FIGURE 3. Generation of CSW's of elevation (case $(c_s - c_{\delta,\gamma})\kappa_{\gamma,\delta} > 0$). Graphs of orbits for several positive values of $c_s - c_{\delta,\gamma}$. Dashed-dotted line: $c_s - c_{\delta,\gamma} = 0.25$; dashed line: $c_s - c_{\delta,\gamma} = 0.5$; solid line: $c_s - c_{\delta,\gamma} = 1$.

for $r > 0$ where, in the case of the B/B systems at hand,

$$E(\zeta, v) = \int_{-\infty}^{\infty} \left(\frac{\kappa_2}{2} \zeta J_c \zeta + \frac{\kappa_1}{2} v J_a v - c_s \zeta J_b v \right) dx, \quad (4.22)$$

$$F(\zeta, v) = -\frac{\kappa_{\gamma,\delta}}{2} \int_{-\infty}^{\infty} \zeta v^2 dx, \quad (4.23)$$

and

$$J_a = 1 + \frac{a}{\kappa_1} \partial_{xx}, \quad J_b = 1 - b \partial_{xx}, \quad J_c = 1 + c \partial_{xx}. \quad (4.24)$$

Existence of CSW's by means of the C-C Theory has been recently proved in [6] for another class of systems modelling internal wave propagation, specifically belonging to the Boussinesq/Full Dispersion (BFD) regime. The proof of [6] can be adapted to the B/B system (4.1) and we will emphasize here the main steps. The result is based on the following properties of the functional (4.22) (cf. Proposition 2.1 of [6]).

Proposition 4.1. *Assume that $b = d > 0$ and $a, c < 0$. The following properties concerning (4.21)-(4.24) hold:*

(i) $E : H^1 \times H^1 \rightarrow \mathbb{R}$ is well defined and continuous: if $(\zeta, v) \in H^1 \times H^1$ then

$$E(\zeta, v) \leq C \left(\|J_c^{1/2} \zeta\|^2 + \|J_a^{1/2} v\|^2 + \|J_b^{1/2} \zeta\|^2 + \|J_b^{1/2} v\|^2 \right), \quad (4.25)$$

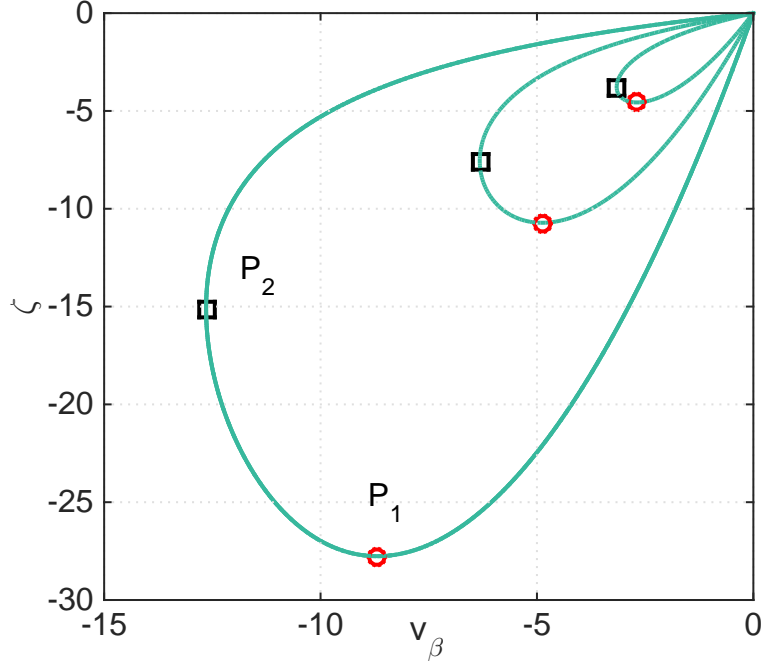


FIGURE 4. Generation of CSW's of depression (case $(c_s - c_{\delta,\gamma})\kappa_{\gamma,\delta} < 0$). Graphs of orbits for several positive values of $c_s - c_{\delta,\gamma}$. Dashed-dotted line: $c_s - c_{\delta,\gamma} = 0.25$; dashed line: $c_s - c_{\delta,\gamma} = 0.5$; solid line: $c_s - c_{\delta,\gamma} = 1$.

for some constant C .

(ii) If

$$|c_s| \leq M := \min\left\{\kappa_2 \frac{|c|}{b}, \frac{|a|}{2b}\right\}, \quad (4.26)$$

then $E(\zeta, v) \geq 0$ and E is coercive:

$$E(\zeta, v) \geq C (\|\zeta\|_1^2 + \|v\|_1^2), \quad (\zeta, v) \in H^1 \times H^1, \quad (4.27)$$

for some constant C depending on $a, b, c, |c_s|, \kappa_1, \kappa_2$.

(iii) $I_r > 0$, all minimizing sequences for I_r are bounded in $H^1 \times H^1$, and for $s \in (0, r)$, I_r satisfies the sub-additivity property

$$I_r < I_s + I_{r-s}. \quad (4.28)$$

Proof. The definition of the operators J_a, J_b and J_c in (4.24) implies that E is well defined in $H^1 \times H^1$ while, from the Cauchy-Schwarz inequality, it is not hard to prove that E satisfies (4.25) and therefore it is continuous.

Let $\langle \cdot, \cdot \rangle$ denote the $L^2(\mathbb{R})$ -inner product. Since J_b is a self-adjoint, positive operator, then from Cauchy-Schwarz inequality we have, for $(\zeta, v) \in H^1 \times H^1$

$$\left| c_s \int_{-\infty}^{\infty} \zeta J_b v dx \right| \leq |c_s| \langle J_b \zeta, \zeta \rangle^{1/2} \langle J_b v, v \rangle^{1/2} \leq \frac{|c_s|}{2} (\langle J_b \zeta, \zeta \rangle + \langle J_b v, v \rangle). \quad (4.29)$$

Note that, using Plancherel Theorem, we get

$$\langle (\kappa_2 J_c - |c_s| J_b) \zeta, \zeta \rangle = \int_{-\infty}^{\infty} p(\xi) |\widehat{\zeta}(\xi)|^2 d\xi, \quad (4.30)$$

where

$$p(\xi) = -(\kappa_2 c + b|c_s|)\xi^2 + \kappa_2 - |c_s|.$$

Since $a, c < 0, b = d > 0$, and using (1.2), we have

$$\frac{|c|}{b} = \frac{-\alpha_2}{1 - \alpha_2} \leq 1, \quad (4.31)$$

Then, under condition (4.26), $p(\xi) \geq 0$ for all $\xi \in \mathbb{R}$, which by (4.30) implies

$$\frac{|c_s|}{2} \langle J_b \zeta, \zeta \rangle \leq \frac{\kappa_2}{2} \langle J_c \zeta, \zeta \rangle. \quad (4.32)$$

Similarly

$$\langle (\kappa_1 J_a - |c_s| J_b) v, v \rangle = \int_{-\infty}^{\infty} q(\xi) |\widehat{v}(\xi)|^2 d\xi,$$

with

$$q(\xi) = -(a + b|c_s|)\xi^2 + \kappa_1 - |c_s|.$$

Since $b = d$, from (1.2)

$$b = \alpha_1 \frac{1 + \gamma\delta}{3\delta(\gamma + \delta)} = \beta(1 - \alpha_2).$$

Then

$$\begin{aligned} a &= \frac{(1 - \alpha_1)(1 + \gamma\delta) - 3\delta\beta(\delta + \gamma)}{3\delta(\gamma + \delta)^2} = (1 - \alpha_1)\kappa_1 \frac{b}{\alpha_1} - \beta\kappa_1 \\ &= \kappa_1 b \left(\frac{1 - \alpha_1}{\alpha_1} - \frac{1}{1 - \alpha_2} \right). \end{aligned}$$

Therefore

$$-\frac{a}{b} = k_1 \left(\frac{\alpha_1 - 1}{\alpha_1} + \frac{1}{1 - \alpha_2} \right), \quad (4.33)$$

where, again from (1.2), and since $b > 0, c < 0$, we have $\alpha_1 > 0, \alpha_2 < 0$. Then

$$\frac{\alpha_1 - 1}{\alpha_1} + \frac{1}{1 - \alpha_2} \leq 2,$$

which, by the hypothesis $a < 0$ and (4.33), leads to

$$\kappa_1 \geq \frac{|a|}{2b}. \quad (4.34)$$

Therefore, (4.34) and (4.26) imply that $q(\xi) \geq 0$ for all $\xi \in \mathbb{R}$, and then, from (4.30), that

$$\frac{|c_s|}{2} \langle J_b v, v \rangle \leq \frac{\kappa_1}{2} \langle J_a v, v \rangle. \quad (4.35)$$

Thus, using (4.29), (4.32) and (4.35), we see that it holds that $E(\zeta, v) \geq 0$ for $(\zeta, v) \in H^1 \times H^1$.

We now prove coercitivity of E . From (4.29) we have

$$E(\zeta, v) \geq \underbrace{\frac{1}{2} \langle (\kappa_2 J_c - |c_s| J_b) \zeta, \zeta \rangle}_I + \underbrace{\frac{1}{2} \langle (\kappa_1 J_a - |c_s| J_b) v, v \rangle}_{II}. \quad (4.36)$$

Note that for $(\zeta, v) \in H^1 \times H^1$, using (4.26) and the fact that $|c|/b \leq 1$, we have

$$\begin{aligned} 2I &= \int_{-\infty}^{\infty} (\kappa_2 \zeta^2 + \kappa_2 |c| \zeta_x^2 - |c_s| \zeta^2 - b |c_s| \zeta_x^2) dx \\ &= \int_{-\infty}^{\infty} \left((\kappa_2 - |c_s|) \zeta^2 + (\kappa_2 \frac{|c|}{b} - |c_s|) b \zeta_x^2 \right) dx \\ &\geq (\kappa_2 \frac{|c|}{b} - |c_s|) \|J_b^{1/2} \zeta\|^2 \geq M \|J_b^{1/2} \zeta\|^2. \end{aligned} \quad (4.37)$$

Similarly, using (4.34) and (4.26), we have

$$\begin{aligned} 2II &= \int_{-\infty}^{\infty} (\kappa_1 v^2 + |a| v_x^2 - |c_s| v^2 - b |c_s| v_x^2) dx \\ &= \int_{-\infty}^{\infty} \left((\kappa_1 - |c_s|) v^2 + (\frac{|a|}{b} - |c_s|) b v_x^2 \right) dx \\ &\geq (\frac{|c|}{2b} - |c_s|) \|J_b^{1/2} v\|^2 \geq M \|J_b^{1/2} v\|^2. \end{aligned} \quad (4.38)$$

Now, since $\|J_b^{1/2} \cdot\|$ is equivalent to $\|\cdot\|_1$, then (4.36), (4.37) and (4.38) imply the existence of a constant $C > 0$ such that (4.27) holds.

Note now that

$$0 < r = F(\zeta, v) \leq \frac{\kappa_{\gamma, \delta}}{2} |v|_{\infty} \|v\| \|\zeta\| \leq C \|(\zeta, v)\|_1^3,$$

for some constant $C > 0$ and where $\|(\zeta, v)\|_1 := (\|\zeta\|_1^2 + \|v\|_1^2)^{1/2}$. Then, using (4.27), we can find a constant C such that

$$r \leq CE(\zeta, v)^{3/2}, \quad (\zeta, v) \in H^1 \times H^1,$$

and therefore

$$E(\zeta, v) \geq \left(\frac{r}{C}\right)^{2/3}, \quad (\zeta, v) \in H^1 \times H^1,$$

which implies $I_r \geq (r/C)^{2/3} > 0$. On the other hand, due to (4.27), it is clear that all minimizing sequences for I_r are bounded for $(\zeta, v) \in H^1 \times H^1$. Finally, the sub-additivity property (4.28) is obtained from the fact that $I_r > 0$ and the property

$$I_{\tau r} = \tau^{2/3} I_r,$$

for all $\tau > 0$, which is a consequence of the homogeneity of E and F (of orders two and three respectively), cf. [6]. \square

At this point we recall the C-C Principle, the main tool of the theory, see Lemma 1.1 of [54].

Lemma 4.1. *Let $\{\rho_k\}_{k \geq 1}$ be a sequence of non-negative functions in $L^1(\mathbb{R})$ such that $\|\rho_k\|_{L^1}$ converges to some $\sigma > 0$. Then there is a subsequence (also denoted by $\{\rho_k\}_{k \geq 1}$) satisfying one of the following three conditions:*

- (a) *Compactness: there exist $y_k \in \mathbb{R}$ such that for any $\epsilon > 0$ there is $R(\epsilon) > 0$ such that for all k*

$$\int_{|x-y_k| \leq R(\epsilon)} \rho_k dx \geq \int_{-\infty}^{\infty} \rho_k dx - \epsilon = L - \epsilon.$$

- (b) *Vanishing: For every $R > 0$*

$$\limsup_{k \rightarrow \infty} \sup_{y \in \mathbb{R}} \int_{|x-y| \leq R} \rho_k dx = 0.$$

- (c) *Dichotomy: there exists $l \in (0, L)$ such that for all $\epsilon > 0$ there are $R, R_k \rightarrow \infty, y_k \in \mathbb{R}$ and k_0 satisfying*

$$\left| \int_{|x-y_k| \leq R} \rho_k dx - l \right| < \epsilon, \quad \left| \int_{R < |x-y_k| \leq R_k} \rho_k dx \right| < \epsilon,$$

for $k > k_0$.

The application of Lemma 4.1 to the existence of solitary waves can be summarized as follows, see e. g. [51, 52, 16] for different examples. One considers $\{\zeta_n, v_n\}_{n \geq 1}$, a minimizing sequence for (4.21), and defines from this a new sequence $\{\rho_n\}_{n \geq 1}$ of non-negative functions in L^1 satisfying the conditions of the lemma; in our case (as in [6]) this is

$$\rho_n(x) = |\zeta_n(x)|^2 + |\zeta'_n(x)|^2 + |v_n(x)|^2 + |v'_n(x)|^2, \quad (4.39)$$

from which, thanks to (iii) of Proposition 4.1, one can find a subsequence $\{\rho_n\}_{n \geq 1}$ such that $\|\rho_n\|_{L^1}$ is convergent. The next step is dismissing the possibility of vanishing and dichotomy for ρ_n ; therefore Lemma 4.1 implies that the compactness property holds.

The final step is: From ρ_n find a subsequence of the translated sequence $\{\zeta_n(x - y_n), v_n(x - y_n)\}_n$ which converges weakly to some $H^1 \times H^1$ function (ζ_0, v_0) and prove that (ζ_0, v_0) solves the variational problem (4.21). A solution (ζ, v) of (4.1) is obtained from (ζ_0, v_0) after some scaling involving the Lagrange multiplier r . The application of all these steps to our system leads to the following result, which should be compared with that of the case of surface waves, [12].

Theorem 4.2. *Let $\delta > 0, \gamma < 1$ and assume that $a, c < 0, b = d > 0$. If (4.26) holds, then the system (1.6) admits a classical solitary wave solution $\zeta = \zeta(x - c_s t), v = v(x - c_s t)$ with $(\zeta, v) \in H^\infty \times H^\infty$. Furthermore, ζ and v decay exponentially as $x \rightarrow \pm\infty$ with*

$$\lim_{x \rightarrow \pm\infty} e^{\sigma_a |x|} v(x) = C_1, \quad (4.40)$$

$$\lim_{x \rightarrow \pm\infty} e^{\sigma_0 |x|} \zeta(x) = C_2, \quad (4.41)$$

with C_1, C_2 constants, $\sigma_a = \sqrt{\kappa_1/|a|}$ and $\sigma_0 \in (0, \sigma_a], \sigma_0 < \sqrt{|c|}$.

Proof. Regularity of the profiles can be proved in a similar way to that of the corresponding result in [6]. On the other hand, it may be worth to explain the details of the proof of the properties of asymptotic decay. In terms of the operators (4.24) the system (4.1) has the form

$$\begin{aligned} -c_s J_b \zeta + \kappa_1 J_a v &= -\kappa_{\gamma, \delta} \zeta v, \\ \kappa_2 J_c \zeta - c_s J_b v &= -\frac{\kappa_{\gamma, \delta}}{2} v^2. \end{aligned} \quad (4.42)$$

The second equation of (4.42) can be written as

$$\kappa_2 \zeta = c_s J_c^{-1} J_b v - \frac{\kappa_{\gamma, \delta}}{2} v^2.$$

Using that $c_{\gamma, \delta}^2 = \kappa_1 \kappa_2$, and substituting into the first equation of (4.42) we get

$$\begin{aligned} c_{\gamma, \delta}^2 J_a v &= G(v) = c_s^2 J_c^{-1} J_b^2 v - c_s \frac{\kappa_{\gamma, \delta}}{2} J_b J_c^{-1}(v^2) \\ &\quad - \kappa_{\gamma, \delta} c_s v J_c^{-1} J_b v + \frac{\kappa_{\gamma, \delta}^2}{2} v J_c^{-1}(v^2). \end{aligned}$$

Therefore

$$v = \frac{1}{c_{\gamma, \delta}^2} J_a^{-1} G(v) = \frac{1}{c_{\gamma, \delta}^2} K_a * G(v),$$

where $\widehat{K}_a(\xi) = \frac{1}{1 + \frac{|a|}{\kappa_1} \xi^2}$, and therefore

$$K_a(x) = \frac{\pi}{2} \sqrt{\frac{\kappa_1}{|a|}} e^{-\sigma_a |x|},$$

where $\sigma_a = \sqrt{\kappa_1 / |a|}$. According to [22], this implies (4.40). Similar arguments to those of [6] can be used to obtain (4.41). \square

Remark 4.6. Note that it is not possible to have $b = d$ in the case (A2) of Table 1. The reason is the following. Assume that $b = d$, that a, b and c satisfy (A2) and let $S(\gamma, \delta)$ be given in (1.3). Then the condition $\frac{bd}{\delta + \gamma} - ac < 0$ gives

$$b^2 < ac(\delta + \gamma) = |a||c|(\delta + \gamma). \quad (4.43)$$

From (1.3), we have

$$b = \frac{1}{2}(S(\gamma, \delta) - a(\delta + \gamma) - c) > 0.$$

Substituting this into (4.43), and since $a, c < 0$, after some computations we obtain

$$S(\gamma, \delta) < -(\sqrt{|c|} - \sqrt{|a|(\delta + \gamma)})^2,$$

which contradicts the fact that $S(\gamma, \delta) > 0$. On the other hand, note that, since $\kappa_2 < 1$ and from (4.31) it holds that $M < 1$. Therefore the inequalities

$$c_{\gamma, \delta} = \sqrt{\kappa_1 \kappa_2} < |c_s| \leq M,$$

imply in particular that $c_{\gamma, \delta} < 1$ and $b^2 \kappa_1 - |a||c| < 0$, that is, a, b and c are in the case (A2) of Table 1. Since we know that this is not possible, Theorem 4.2 applies when $|c_s| < c_{\gamma, \delta}$. This should be compared with Toland's theory, cf. Theorem 4.1, for which this condition was not required.

4.1.4. *Positive Operator theory.* The Positive Operator theory can also be applied as in [16] where some existence results of classical solitary wave solutions of Boussinesq systems for surface waves were derived. In our case, if we take the Fourier transform in (4.1) we obtain

$$\begin{pmatrix} c_s(1 + bk^2) & -\kappa_1 + ak^2 \\ -\kappa_2(1 - ck^2) & c_s(1 + dk^2) \end{pmatrix} \begin{pmatrix} \widehat{\zeta}(k) \\ \widehat{v}_\beta(k) \end{pmatrix} = \kappa_{\gamma, \delta} \begin{pmatrix} \widehat{\zeta v_\beta}(k) \\ \widehat{v_\beta^2/2}(k) \end{pmatrix}. \quad (4.44)$$

System (4.44) is invertible for all $k \in \mathbb{R}$ and for $b, d > 0, a, c \leq 0$ if

$$\Delta(k) = \Delta_0 + \Delta_1 k^2 + \Delta_2 k^4 \neq 0, \quad (4.45)$$

where

$$\begin{aligned} \Delta_0 &= c_s^2 - c_{\gamma, \delta}^2, & \Delta_1 &= (c_s^2(b+d) - c_{\gamma, \delta}^2(-c - \frac{a}{\kappa_1})), \\ \Delta_2 &= c_s^2 bd - c_{\gamma, \delta}^2 \frac{ac}{\kappa_1} = c_s^2 bd - (1-\gamma)ac. \end{aligned}$$

(Note that A is the determinant D given by (4.5).) We assume that $a, c \leq 0, b, d > 0, bd - ac/\kappa_1 > 0$ (case (A3) of Table 1), and $|c_s| > c_{\gamma, \delta}$. Then $\Delta_j > 0, 0 \leq j \leq 2$, and we may write (4.44) in the form

$$\begin{aligned} \widehat{\zeta}(k) &= \frac{\kappa_{\gamma, \delta}}{\Delta(k)} \left(c_s(1 + dk^2) \widehat{\zeta v_\beta}(k) + (\kappa_1 - ak^2) \widehat{v_\beta^2/2}(k) \right) \\ \widehat{v_\beta}(k) &= \frac{\kappa_{\gamma, \delta}}{\Delta(k)} \left(c_s(1 + bk^2) \widehat{v_\beta^2/2}(k) + \kappa_2(1 - ck^2) \widehat{\zeta v_\beta}(k) \right). \end{aligned}$$

As in [16], this leads to an integral form of (4.1)

$$\begin{aligned} \zeta &= k_{12} * (\zeta v_\beta) + \frac{1}{2} k_{22} * (v_\beta^2), \\ v_\beta &= m_{12} * (\zeta v_\beta) + \frac{1}{2} m_{22} * (v_\beta^2), \end{aligned}$$

where the integral kernels are

$$\begin{aligned} k_{12}(x) &= \frac{c_s \kappa_{\gamma, \delta}}{2\Delta_2} \left(\frac{1 - dr_-^2}{r_-(r_+^2 - r_-^2)} e^{-r_-|x|} - \frac{1 - dr_+^2}{r_+(r_+^2 - r_-^2)} e^{-r_+|x|} \right) \\ k_{22}(x) &= \frac{\kappa_{\gamma, \delta}}{2\Delta_2} \left(\frac{\kappa_1 + ar_-^2}{r_-(r_+^2 - r_-^2)} e^{-r_-|x|} - \frac{\kappa_1 + ar_+^2}{r_+(r_+^2 - r_-^2)} e^{-r_+|x|} \right) \\ m_{12}(x) &= \frac{\kappa_{\gamma, \delta}}{2\Delta_2} \left(\frac{\kappa_2(1 + cr_-^2)}{r_-(r_+^2 - r_-^2)} e^{-r_-|x|} - \frac{\kappa_2(1 + cr_+^2)}{r_+(r_+^2 - r_-^2)} e^{-r_+|x|} \right) \\ m_{22}(x) &= \frac{c_s \kappa_{\gamma, \delta}}{2\Delta_2} \left(\frac{1 - br_-^2}{r_-(r_+^2 - r_-^2)} e^{-r_-|x|} - \frac{1 - br_+^2}{r_+(r_+^2 - r_-^2)} e^{-r_+|x|} \right), \end{aligned}$$

with

$$r_\pm^2 = \frac{1}{2\Delta_2} \left(\Delta_1 \pm \sqrt{\Delta_1^2 - 4\Delta_0\Delta_2} \right).$$

Then we have

Theorem 4.3. *Assume that $b, d > 0, a, c \leq 0$, and $bd - ac/\kappa_1 > 0$. If $|c_s| > c_{\gamma, \delta}$, then the system (4.1) admits classical solitary wave solutions of elevation if $\kappa_{\gamma, \delta} > 0$ and of depression if $\kappa_{\gamma, \delta} < 0$.*

Proof. The conclusion follows from the application of the Positive Operator theory as in [16]. When $\kappa_{\gamma, \delta} > 0$, the theory is applied on the cone of continuous real-valued functions (f, g) on \mathbb{R} which are even, positive and non-increasing on $(0, \infty)$, while if $\kappa_{\gamma, \delta} < 0$, the cone consists of continuous real-valued functions on \mathbb{R} which are even, negative and non-decreasing on $(0, \infty)$. \square

Remark 4.7. *Note that when $b = d$, Theorem 4.3 reproduces part of the results of Toland's theory in Theorem 4.1.*

Remark 4.8. *The previous formulas can also be used to estimate the asymptotic decay at infinity of the classical solitary waves. In general, both ζ, v_β should behave as $e^{-r-|x|}$ as $|x| \rightarrow \infty$. In particular, for the cases $b = d > 0, a = 0, c \leq 0$ we may specify r_- in (4.46). If $a = 0, c < 0$ then*

$$\Delta_2 = b^2 c_s^2, \quad \Delta_1 = 2bc_s^2 + cc_{\gamma,\delta}^2, \quad \Delta_0 = c_s^2 - c_{\gamma,\delta}^2,$$

and $\Delta_1^2 - 4\Delta_0\Delta_2 = c^2 c_{\gamma,\delta}^4 + 4b(b+c)c_s^2 c_{\gamma,\delta}^2 > 0$ (since $b+c = \beta > 0$). Therefore

$$\lim_{x \rightarrow \pm\infty} e^{-r-|x|} v(x) = C, \quad r_- = \left(\frac{1}{2\Delta_2} (\Delta_1 - \sqrt{\Delta_1^2 - 4\Delta_0\Delta_2}) \right)^{1/2},$$

and C a constant. The argument used in Theorem 4.2 can be applied here as well to obtain (4.41) for some $\sigma_0 \in (0, r_-], \sigma_0 < \sqrt{|c|}$.

On the other hand, if $a = c = 0$, then

$$r_- = \frac{1}{\sqrt{b}} \sqrt{1 - \frac{c_{\gamma,\delta}}{|c_s|}},$$

and in this case

$$\lim_{x \rightarrow \pm\infty} e^{-r-|x|} v(x) = C_1, \quad \lim_{x \rightarrow \pm\infty} e^{-r-|x|} \zeta(x) = C_2,$$

for some constants C_1, C_2 .

In summary, in addition to the results obtained by the Normal Form Theory, valid for small and positive $c_s - c_{\gamma,\delta}$, and shown in Table 1, the other standard theories contribute to the existence of classical solitary waves as follows:

- Toland's Theory ensures the existence of CSW's when $a, c \leq 0, b = d > 0$ (Theorem 4.1), a condition which intersects with those of the cases (A3) to (A6) of Table 1. The speed and amplitude must satisfy the relation (4.20).
- The C-C Theory establishes the existence of CSW's when $a, c < 0, b = d > 0$, and $bd - ac/\kappa_1 > 0$ (cf. the case (A3) of Table 1), and for speeds satisfying (4.26) and $|c_s| < c_{\gamma,\delta}$, cf. Remark 4.2.
- The Positive Operator Theory proves the existence of CSW's when $b, d > 0, a, c \leq 0$, and $bd - ac/\kappa_1 > 0$, with speeds c_s satisfying $|c_s| > c_{\gamma,\delta}$. The result can also justify the existence of CSW's predicted by NFT in the cases (A3) to (A6) of Table 1.

We finally note that in [40] existence of even, classical solitary waves of the 'classical Boussinesq' system (case (vii) with $b = 0, d > 0, a = c = 0$, for which $D = 0$) is proved for speeds c_s with $|c_s| > c_{\gamma,\delta}$ and for $\delta^2 - \gamma \neq 0$. The waves are of elevation when $\delta^2 - \gamma > 0$ and of depression otherwise. The result is based on phase plane analysis of the system (4.1), which is conservative in this case; see [59] for the case of surface waves.

4.1.5. *Exact solitary wave solutions in 1D.* For particular values of the speed, exact classical solitary waves can be derived by following the arguments used in [27]. If we look for solutions (ζ, v_β) with $v_\beta = B\zeta$ for some constant B , then, substituting into (4.1) we have

$$\begin{aligned} (c_s - \kappa_1 B)\zeta - (bc_s + aB)\zeta'' &= B\kappa_{\gamma,\delta}\zeta^2 \\ (c_s B - \kappa_2)\zeta - (dc_s B + \kappa_2 c)\zeta'' &= \frac{B^2}{2}\kappa_{\gamma,\delta}\zeta^2. \end{aligned} \quad (4.46)$$

The existence of a solution ζ of (4.46) requires then

$$\begin{aligned} 2c_s B - 2\kappa_2 &= c_s B - \kappa_1 B^2 \\ 2dc_s B + 2\kappa_2 c &= bc_s B + aB^2. \end{aligned} \quad (4.47)$$

If we consider (4.47) as a linear system for the variables B^2 and $c_s B$, then we have two possibilities:

- If $b - 2d - a(\delta + \gamma) \neq 0$, then (4.47) has a unique solution from which

$$B^2 = \frac{2\kappa_2(b - 2d - c)}{\kappa_1(b - 2d) - a}, \quad c_s = \frac{1}{B} \frac{2\kappa_2(c\kappa_1 - a)}{\kappa_1(b - 2d) - a}. \quad (4.48)$$

- If $b - 2d - a(\delta + \gamma) = 0$, then (4.47) has infinitely many solutions iff $c = a(\delta + \gamma)$; they satisfy

$$c_s = \frac{2\kappa_2 - \kappa_1 B^2}{B}, \quad (4.49)$$

for $B \neq 0$ arbitrary.

As far as the exact form of the solutions is concerned, differentiating one of the equations of (4.46) and using (4.47) we have

$$\mu_1 \zeta' - \mu_2 \zeta''' = \zeta \zeta', \quad (4.50)$$

where

$$\mu_1 = \frac{\kappa_2 - \kappa_1 B^2}{\kappa_{\gamma, \delta} B^2}, \quad \mu_2 = \frac{(a - b\kappa_1)B^2 + 2b\kappa_2}{2\kappa_{\gamma, \delta} B^2}.$$

Thus, (4.50) admits solutions of square hyperbolic secant form if $\mu_1 \mu_2 > 0$, that is, if

$$(\kappa_2 - \kappa_1 B^2)((a - b\kappa_1)B^2 + 2b\kappa_2) > 0.$$

If this condition is satisfied, then

$$\begin{aligned} \zeta(x, t) &= 3\mu_1 \operatorname{sech}^2 \left(\frac{1}{2} \sqrt{\frac{\mu_1}{\mu_2}} (x - c_s t - x_0) \right), \\ u(x, t) &= B(\zeta(x, t) - \beta \zeta_{xx}(x, t)), \end{aligned} \quad (4.51)$$

with B and c_s given by (4.48) or (4.49), and $x_0 \in \mathbb{R}$ is arbitrary.

4.2. Numerical generation of solitary waves. In this section some classical and generalized solitary wave profiles will be generated numerically. To this end and following a standard procedure, cf. e. g. [32], the system (4.1) is discretized on a long enough interval $(-l, l)$ and with periodic boundary conditions by the Fourier collocation method based on N collocation points given by $x_j = -l + jh$, $j = 0, \dots, N-1$ for an even integer $N \geq 1$ and where $h = 2l/N$. If the vectors $\zeta_h = (\zeta_{h,0}, \dots, \zeta_{h,N-1})^T$ and $v_h = (v_{h,0}, \dots, v_{h,N-1})^T$ denote, respectively, the approximations to the values of ζ and v_β at the x_j , then the discrete system satisfied by ζ_h and v_h has the form

$$S_N \begin{pmatrix} \zeta_h \\ v_h \end{pmatrix} = \kappa_{\gamma, \delta} \begin{pmatrix} \zeta_h \cdot v_h \\ (v_h \cdot \zeta_h)/2 \end{pmatrix}, \quad (4.52)$$

where S_N is the $2N$ -by- $2N$ matrix

$$S_N := \begin{pmatrix} c_s(I_N - bD_N^2) & -(\kappa_1 I_N + aD_N^2) \\ -\kappa_2(I_N + cD_N^2) & c_s(I_N - dD_N^2) \end{pmatrix}, \quad (4.53)$$

with I_N standing for the N -by- N identity matrix and D_N denoting the N -by- N pseudospectral differentiation matrix. The products of the nonlinear terms on the right hand-side of (4.52) are understood in the Hadamard (componentwise) sense. The system (4.52), (4.53) is implemented in the Fourier space, that is, for the discrete Fourier components of ζ_h and v_h , leading to a 2-by-2 system for each component of fixed-point form

$$S(k) \begin{pmatrix} \widehat{\zeta}_h(k) \\ \widehat{v}_h(k) \end{pmatrix} = \kappa_{\gamma,\delta} \begin{pmatrix} \widehat{\zeta}_h \cdot v_h(k) \\ (\widehat{v}_h \cdot \widehat{v}_h)/2(k) \end{pmatrix}, \quad (4.54)$$

where

$$S(k) = \begin{pmatrix} c_s(1 + b\tilde{k}^2) & -(\kappa_1 - a\tilde{k}^2) \\ -\kappa_2(1 - c\tilde{k}^2) & c_s(1 + d\tilde{k}^2) \end{pmatrix}, \quad (4.55)$$

with $\tilde{k} = \pi k/l$, $-N/2 \leq k \leq N/2 - 1$ and $\widehat{\zeta}_h(k), \widehat{v}_h(k)$ denoting, respectively, the k -th discrete Fourier component of ζ_h and v_h .

Assuming that $S(k)$ given by (4.55) is nonsingular for all k , $-N/2 \leq k \leq N/2 - 1$, cf. (4.44), then the system (4.54) is solved iteratively with the Petviashvili scheme, [61, 60],

$$S(k) \begin{pmatrix} \widehat{\zeta}_h^{[\nu+1]}(k) \\ \widehat{v}_h^{[\nu+1]}(k) \end{pmatrix} = m_h^2 \kappa_{\gamma,\delta} \begin{pmatrix} \widehat{\zeta}_h^{[\nu]} \cdot v_h^{[\nu]}(k) \\ ((v_h^{[\nu]}) \cdot v_h^{[\nu]})/2(k) \end{pmatrix}, \quad \nu = 0, 1, \dots, -N/2 \leq k \leq N/2 - 1, \quad (4.56)$$

where m_h is the corresponding stabilizing factor

$$m_h = \left(S_N \begin{pmatrix} \zeta_h^{[\nu]} \\ v_h^{[\nu]} \end{pmatrix}, \begin{pmatrix} \zeta_h^{[\nu]} \\ v_h^{[\nu]} \end{pmatrix} \right)_N / \left(\begin{pmatrix} \zeta_h^{[\nu]} \cdot v_h^{[\nu]} \\ ((v_h^{[\nu]}) \cdot v_h^{[\nu]})/2(k) \end{pmatrix}, \begin{pmatrix} \zeta_h^{[\nu]} \\ v_h^{[\nu]} \end{pmatrix} \right)_N,$$

with $(\cdot, \cdot)_N$ denoting the Euclidean inner product in \mathbb{C}^{2N} . The iterative procedure (4.56) is in some cases accelerated by using vector extrapolation methods, [63, 64, 65]. For the application of these techniques to the Petviashvili's method for traveling wave computations see [3]. The benefits of their use include a reduction in the number of iterations when the Petviashvili's method is convergent, and the transformation of divergent cases into convergent. Once the iteration is completed and approximations ζ_h and v_h are computed, an approximation of $u = (1 - \beta \partial_{xx})v_\beta$ can be obtained as $u_h = (I_N - \beta D_N^2)v_h$.

Some details on the implementation are now given. For the experiments below h varies in a range between 6.25×10^{-2} and 2.5×10^{-1} . In all the computations the approximate profiles for ζ and u and corresponding phase portraits are displayed. The accuracy of the profiles is monitored in two ways. First, the behaviour of the residual error at each iteration

$$RES(\nu) = \left\| S_N \begin{pmatrix} \zeta_h^{[\nu]} \\ v_h^{[\nu]} \end{pmatrix} - \begin{pmatrix} \zeta_h^{[\nu]} \cdot v_h^{[\nu]} \\ ((v_h^{[\nu]}) \cdot v_h^{[\nu]})/2 \end{pmatrix} \right\|, \quad (4.57)$$

where $\|\cdot\|$ denotes the Euclidean norm, is checked and displayed. A second test of accuracy consists of integrating numerically the periodic ivp of (1.6) by some fully discrete scheme, considering the computed profiles as initial condition and monitoring several error indicators during the evolution of the corresponding numerical solution. For the experiments to follow, we use the Fourier pseudospectral

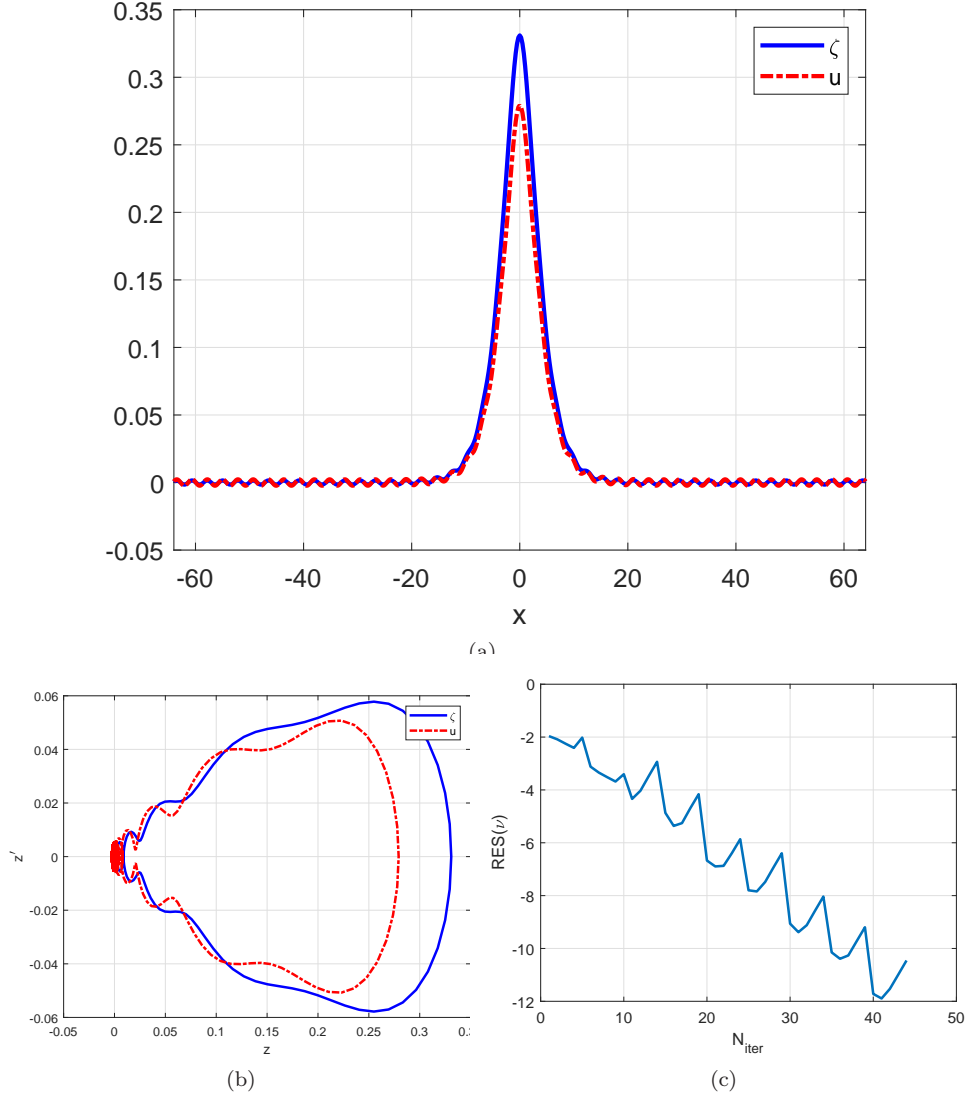


FIGURE 5. GSW generation. Case (A1) with $\delta = 0.9, \gamma = 0.5, c = -1/3, b = 0, d = 1, a = \kappa_1(S(\gamma, \delta) - b - c - d) \approx -0.2022; c_s = c_{\gamma, \delta} + 0.02 \approx 0.6176$. (a) ζ and u profiles; (b) ζ and u phase portraits; (c) Residual error vs. number of iterations (semilog scale).

discretization in space (justified by the analysis of convergence made in section 3), and, as time integrator, we use a fourth-order Runge-Kutta (RK)-composition method based on the Implicit Midpoint Rule. The fully discrete method and the evolution experiments will be described in section 5.

In the rest of the present section we illustrate several cases of numerically generated solitary waves corresponding to the cases (A1)-(A6) of Table 1, to the case

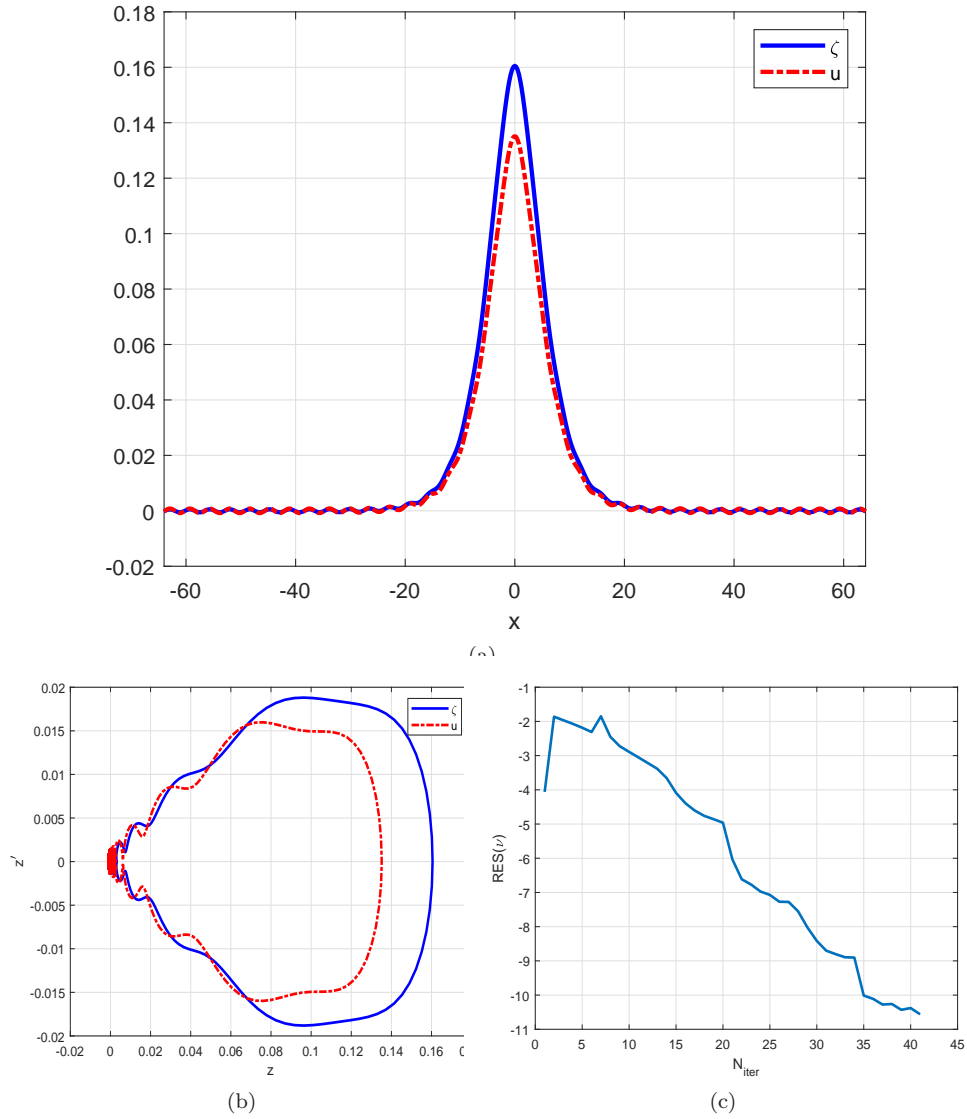


FIGURE 6. GSW generation. Case (A2) with $\delta = 0.9, \gamma = 0.5, a = -1/3, c = -2/3, b = 1/9, d = S - a/\kappa_1 - b - c \approx 1.4058; c_s = c_{\gamma,\delta} + 0.01 \approx 0.6076$. (a) ζ and u profiles; (b) ζ and u phase portraits; (c) Residual error vs. number of iterations (semilog scale).

$D = 0$ and some exceptional cases predicted by NFT. In each one of Figures 5- we present (a) the profiles of the ζ - and u -solitary waves, (b) their phase space diagrams, and (c) a graph of the residual error defined by (4.57) versus the number of iterations required to reach a certain level of residual error down to a minimum value of about 10^{-11} .

We start with two illustrations, in Figures 5 and 6, of GSW's, predicted by NFT (cases (A1) and (A2), respectively, of Table 1). Figure 5 corresponds to the case

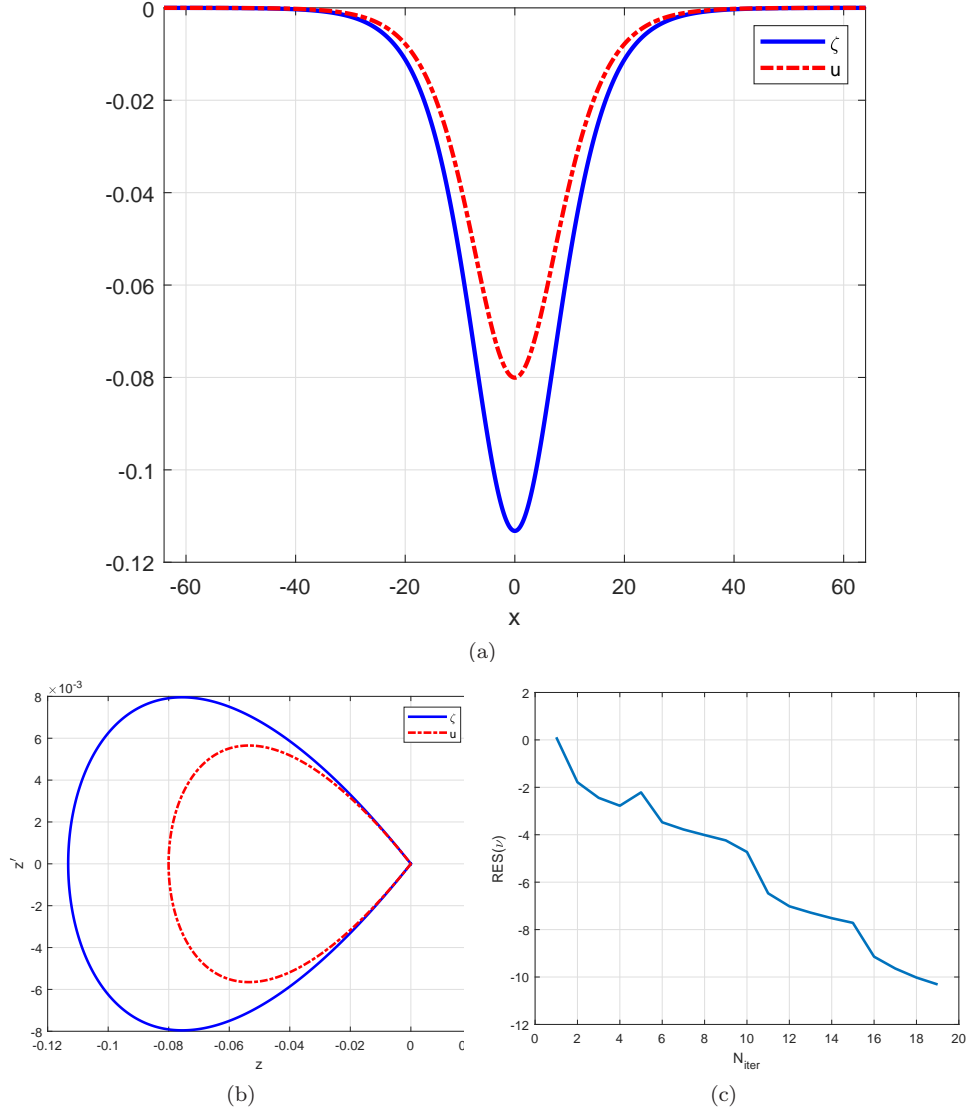


FIGURE 7. CSW generation. Case (A4) with $\delta = \gamma = 0.5, a = 0, c = -1/3, b = 1, d = 1/6; c_s = c_{\gamma, \delta} + 1E - 02$. (a) ζ and u profiles; (b) ζ and u phase portraits; (c) Residual error vs. number of iterations (semilog scale).

(A1) with

$$\delta = \gamma = 0.5, c = -1/3, b = 0, d = 1, a = \kappa_1(S(\gamma, \delta) - b - c - d) \approx -0.2022.$$

The speed is $c_s = c_{\gamma, \delta} + 0.02 \approx 0.6176$. Figure 6 illustrates the case (A2), with

$$\delta = 0.9, \gamma = 0.5, a = -1/3, c = -2/3, b = 1/9, d = S - a/\kappa_1 - b - c \approx 1.4058,$$

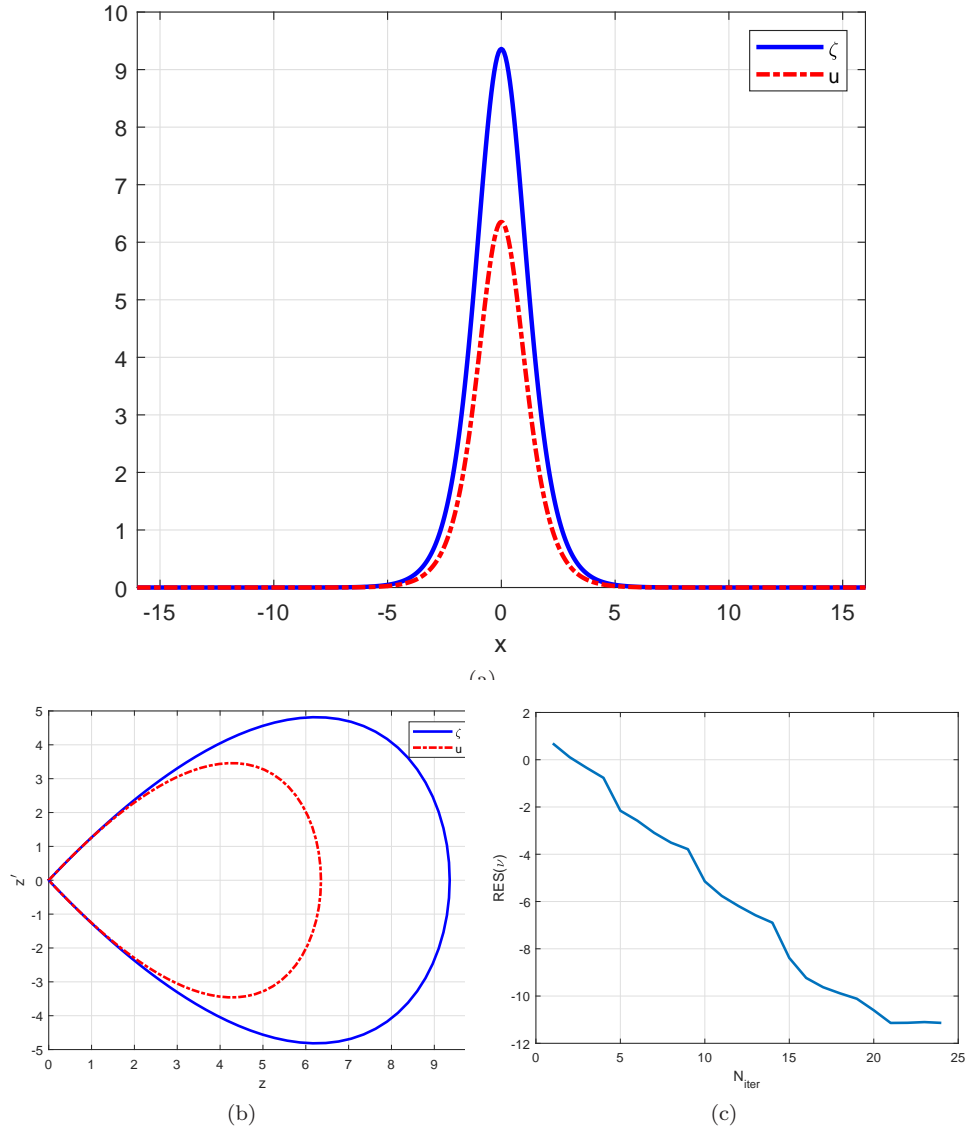


FIGURE 8. CSW generation. Case (A4) with $\delta = 0.9, \gamma = 0.5, a = 0, c = -1/3, b = 1/3, d = -(\delta + \gamma)a - b - c + \frac{1 + \gamma\delta}{3\delta(\gamma + \delta)}$; $c_s = c_{\gamma, \delta} + 0.5$. (a) ζ and u profiles; (b) ζ and u phase portraits; (c) Residual error vs. number of iterations (semilog scale).

and $c_s = c_{\gamma, \delta} + 0.01 \approx 0.6076$. Both are waves of elevation and the corresponding phase portraits show how the profiles are homoclinic to a periodic orbit at infinity. We checked that these homoclinic orbits correspond to region 3 of Figure 1.

We turn now to the numerical generation of CSW's. First we illustrate the cases (A3)-(A6) of Table 1 with examples that are covered by the other three theories considered in section 4.1, namely Toland's Theory, Concentration-Compactness

Theory and Positive Operator Theory. The associated homoclinic orbits correspond to region 2 of the (B, A) -plane in Figure 1.

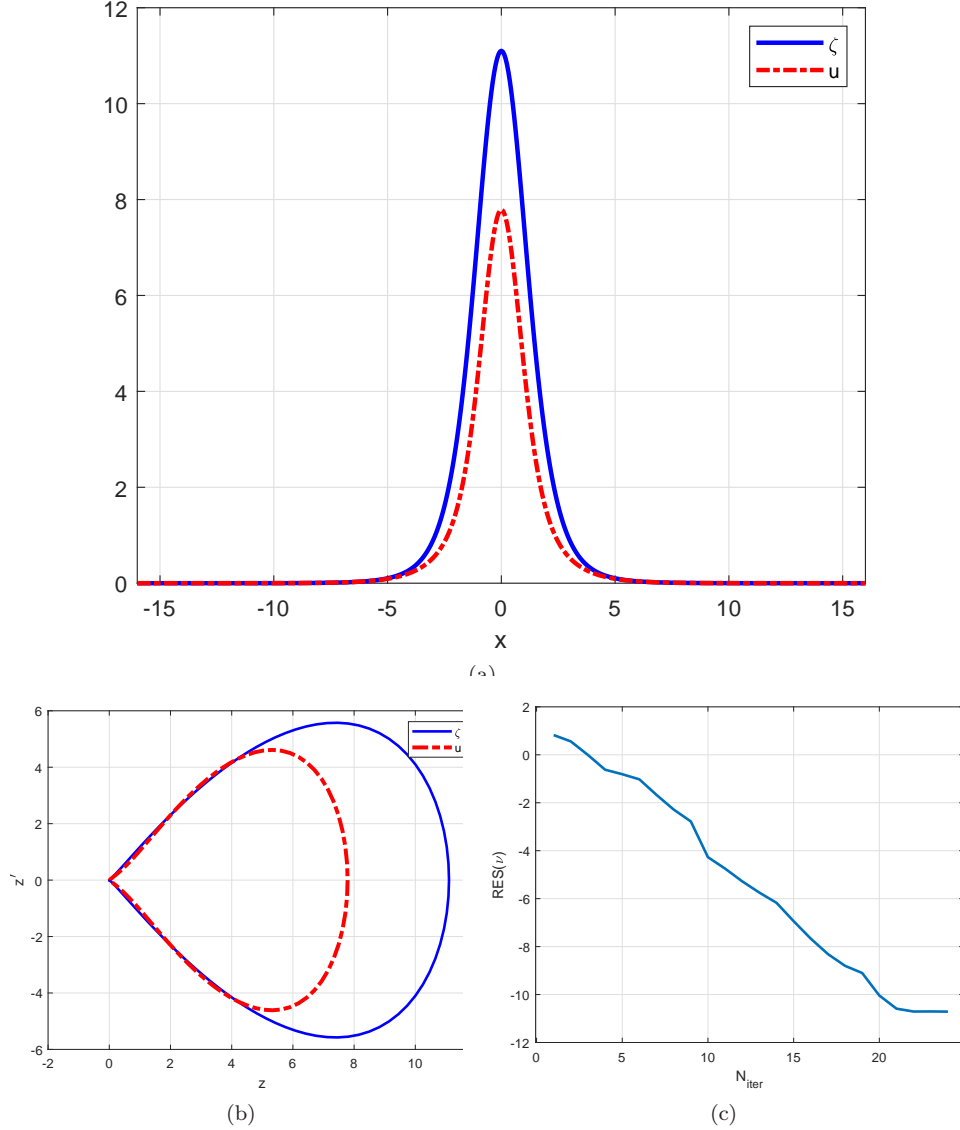


FIGURE 9. CSW generation. Case (A3) with $\delta = 0.9, \gamma = 0.5, a = -1/3, c = -2/3, b = 1/3, d = -(\delta + \gamma)a - b - c + \frac{1+\gamma\delta}{3\delta(\gamma+\delta)} \approx 1.1836; c_s = c_{\gamma,\delta} + 0.5 \approx 1.0976$. (a) ζ and u profiles; (b) ζ and u phase portraits; (c) Residual error vs. number of iterations (semilog scale).

The case (A3) is exemplified in Figures 9 and 10. In Figure 9, we took $\delta = 0.9, \gamma = 0.5, a = -1/3, c = -2/3, b = 1/3, d = -(\delta + \gamma)a - b - c + \frac{1+\gamma\delta}{3\delta(\gamma+\delta)} \approx 1.1836$,

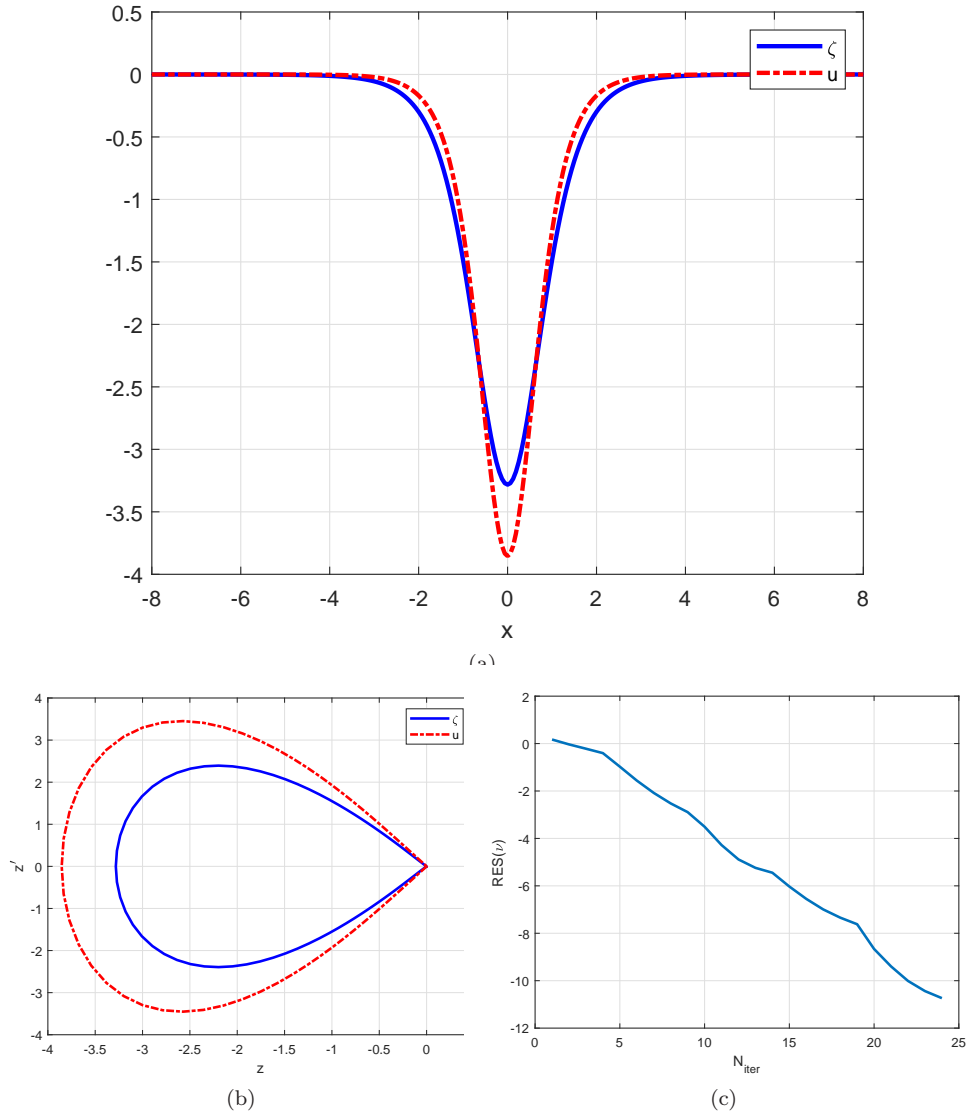


FIGURE 10. CSW generation. Case (A3) with $\delta = 0.9, \gamma = 0.5, a = -1/3, c = -2/3, b = d = \frac{1}{2}(-(\delta + \gamma)a - c + \frac{1+\gamma\delta}{3\delta(\gamma+\delta)}) \approx 0.7585; c_s = c_{\gamma,\delta} - 0.25 \approx 0.3476$. (a) ζ and u profiles; (b) ζ and u phase portraits; (c) Residual error vs. number of iterations (semilog scale).

and $c_s = c_{\gamma,\delta} + 0.5 \approx 1.0976$. The resulting classical solitary wave is of elevation type. It was also checked that $\Delta_j > 0, 0 \leq j \leq 3$, where Δ_j are given by (4.45). Hence this example illustrates Theorem 4.3, i. e. is an application of Positive Operator Theory to (4.1). On the other hand, an application of Theorem 4.2, deduced from the Concentration-Compactness Theory, is illustrated in Figure 10.

In this case, with the same values of δ and γ , a , and c , but different b and d , the computed CSW is of depression type and has speed $c_s = c_{\gamma,\delta} - 0.25 \approx 0.3476$.

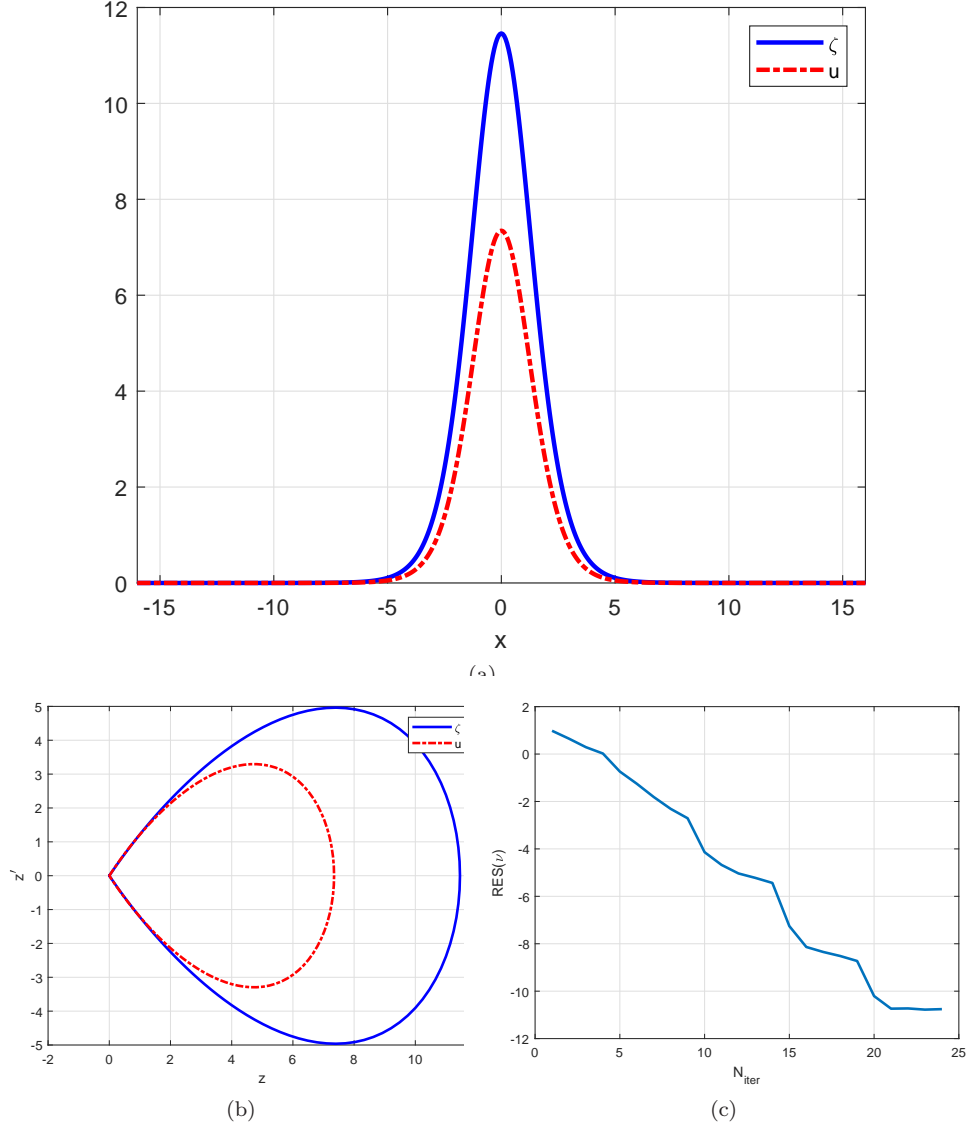


FIGURE 11. CSW generation. Case (A5) with $\delta = 0.9, \gamma = 0.5, a = -2/3, c = 0, b = 1/3, d = -(\delta + \gamma)a - b - c + \frac{1+\gamma\delta}{3\delta(\gamma+\delta)} \approx 0.9836; c_s = c_{\gamma,\delta} + 0.5 \approx 1.0976$. (a) ζ and u profiles; (b) ζ and u phase portraits; (c) Residual error vs. number of iterations (semilog scale).

The case (A5) is illustrated in Figure 11. This example can also be justified by Theorem 4.3.

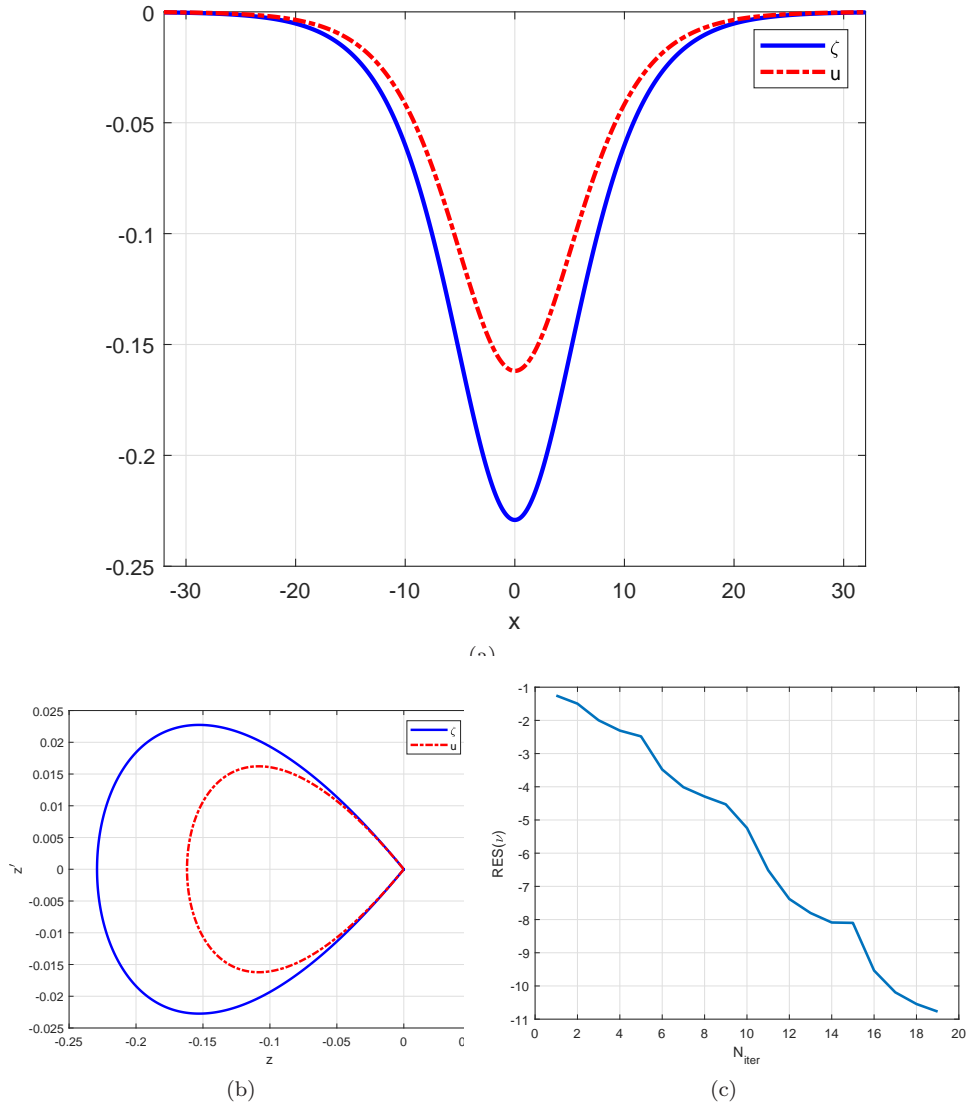


FIGURE 12. CSW generation. Case (A6) with $\delta = \gamma = 0.5, a = 0, c = 0, b = 1/3, d = 1/2; c_s = c_{\gamma, \delta} + 0.01 \approx 0.7171$. (a) ζ and u profiles; (b) ζ and u phase portraits; (c) Residual error vs. number of iterations (semilog scale).

Case (A6) is illustrated by two examples, displayed in Figures 12 and 13. In the case of Figure 12, the speed c_s is quite close to $c_{\gamma, \delta}$ and the example is explained by NFT and Positive Operator Theory. On the other hand, Toland's theory may justify the example of Figure 13, corresponding to a Hamiltonian case of (A6). The numerical experiment is performed using a variant of the Petviashvili method (4.56) as follows. For a fixed speed c_s , each iterate $(v_h^{[v]}, \zeta_h^{[v]})$ of the method is forced to be in the manifold $\{f = 0\}$, where f is given by (4.14). This is accomplished by

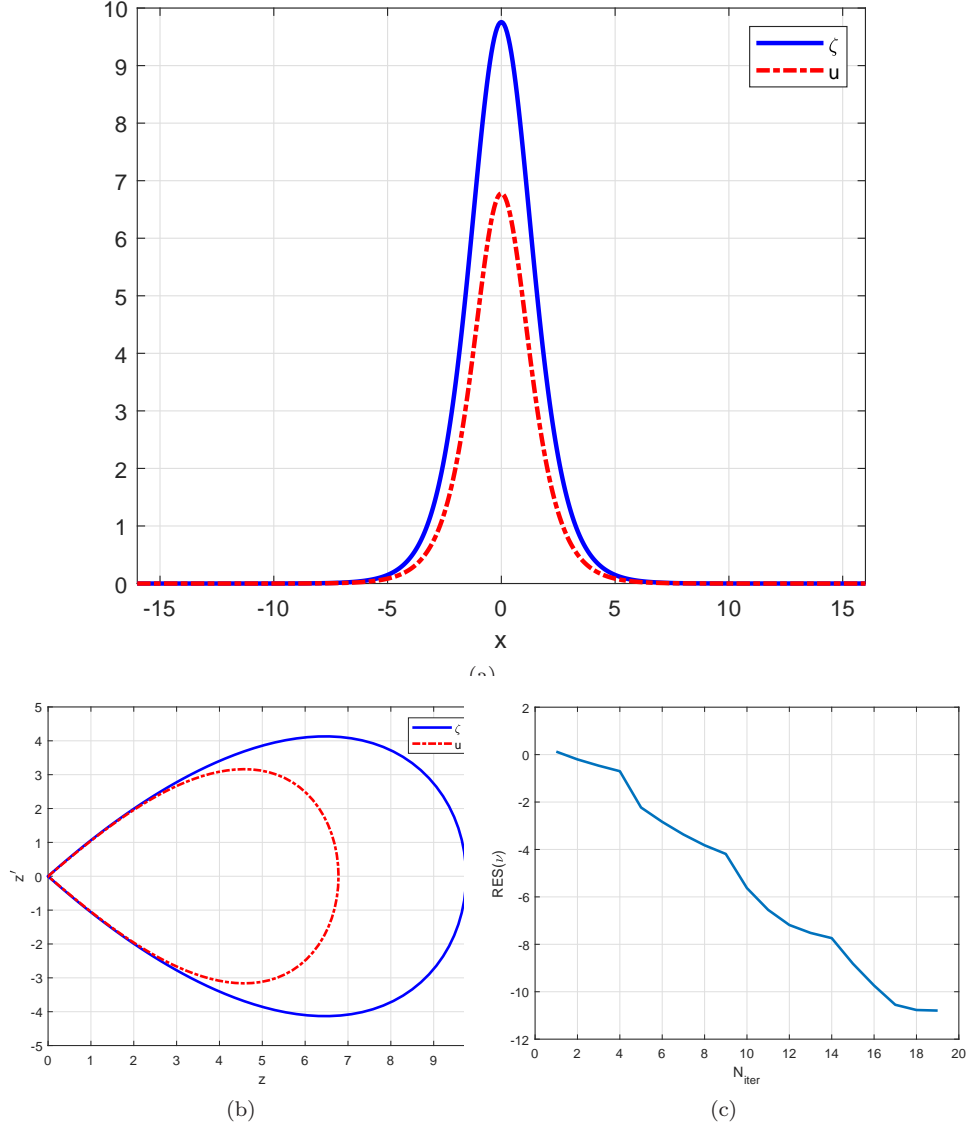


FIGURE 13. CSW generation. Case (A6) with $\delta = 0.9, \gamma = 0.5, a = 0, c = 0, b = d = \frac{1}{2} \frac{1+\gamma\delta}{3\delta(\gamma+\delta)} \approx 0.1918; c_s = c_{\gamma,\delta} + 0.5 \approx 1.0976$. (a) ζ and u profiles; (b) ζ and u phase portraits; (c) Residual error vs. number of iterations (semilog scale).

complementing the Petviashvili iteration with a projection method, implemented in the standard way, [45]. For the particular example of Figure 13, with speed $c_s = c_{\gamma,\delta} + 0.5$, the points P_1 and P_2 of the segment Γ , cf. Theorem 4.1, have the components (approximately)

$$P_1 = (4.8825, 10.7182), P_2 = (6.3226, 7.5569),$$

and the computed solitary wave profile has amplitude $\zeta_{max} \approx 9.7566$ with $v_{max} \approx 5.9357$ and $u_{max} \approx 6.7788$.

Recall that the theories examined in this paper do not consider the case $D = 0$, where D is given by (4.5). However, some numerical experiments in that case suggest existence of classical solitary waves. (Existence of CSW for the particular case of the ‘classical Boussinesq’ system, with $b = 0, d > 0, a = c = 0$, is a special case and is proved e. g. in [40].) By way of illustration Figures 14 and 15 show two CSW’s generated for different combinations of the parameters a, b, c and d leading to $D = 0$, and different speeds.

We complete this numerical study by illustrating the generation of CSW’s with non-monotonic decay and of periodic traveling waves, both predicted by NFT. CSW’s with non-monotonic decay appear in Figures 16 and 17.

Figure 16 corresponds to a homoclinic orbit belonging to the first-quadrant part of region 1 in Figure 1 and corresponding to the values

$$a = -1/9, c = -1/6, b = 0, d = -a/\kappa_1 - c - b + S(\gamma, \delta) \approx 0.7058, \delta = 0.9, \gamma = 0.5,$$

and speed $c_s = c_{\gamma, \delta} - 0.2 \approx 3.9761 \times 10^{-1}$, while the one in Figure 17 belongs to the second quadrant of region 1 and is generated by the parameters

$$a = -1/3, c = -1/3, b = 1/9, d = -a/\kappa_1 - c - b + S(\gamma, \delta) \approx 1.0725, \delta = 0.9, \gamma = 0.5,$$

and speed $c_s = c_{\gamma, \delta} - 0.1 \approx 4.9761 \times 10^{-1}$. (Recall that the generation of these CSW’s requires $c_s < c_{\gamma, \delta}$, cf. section 4.1.)

The numerical generation of periodic traveling wave solutions is illustrated in Figure 18, wherein the values

$$a = c = 0, b = 1/6, d = -a/\kappa_1 - c - b + S(\gamma, \delta) \approx 0.7058, \delta = 0.9, \gamma = 0.5,$$

and speed $c_s = c_{\gamma, \delta} - 0.1 \approx 3.9761 \times 10^{-1}$, are taken. In the spectral analysis of the linearization the corresponding point in the (B, A) -plane is in region 3 of Figure 1.

The last experiment in this section concerns the speed-amplitude relation. Figure 19 displays, in linear and log-log scales and for fixed γ, δ , the amplitude of the computed profiles for ζ, u and v_β as functions of the difference $c_s - c_{\gamma, \delta}$. The results correspond to an experiment with $\delta = 0.9, \gamma = 0.5$ and parameters $a = c = 0, b = d = \frac{1}{2} \frac{1+\gamma\delta}{3\delta(\gamma+\delta)}$ (case (A6) of Table 1 with Hamiltonian structure). Similar experiments were made for different parameters leading to other CSW’s (including those of nonmonotone decay) as well as GSW’s, and the results resemble qualitatively those of this Figure. The three maximum values (for ζ, u and v_β) are increasing functions of $c_s - c_{\gamma, \delta}$, with the amplitude of ζ increasing faster. Figure 19(b), in log-log scale, includes a dotted line of slope 1 for comparison purposes. The representation of the amplitudes as affine functions for small $c_s - c_{\gamma, \delta}$ seems to fit the results (as expected). For larger values of $c_s - c_{\gamma, \delta}$, the slope of the line for the ζ -amplitude is increasing faster while the approximate linear fitting persists longer for the velocity variables.

Remark 4.9. *The study of solitary waves may be completed by studying numerically generations of bi-modal homoclinic orbits in the form of multi-pulses, typically bifurcating from the CSW’s, [25, 24, 4]. An example of these solutions (a positive, two-pulse wave) is shown in section 5.2.*

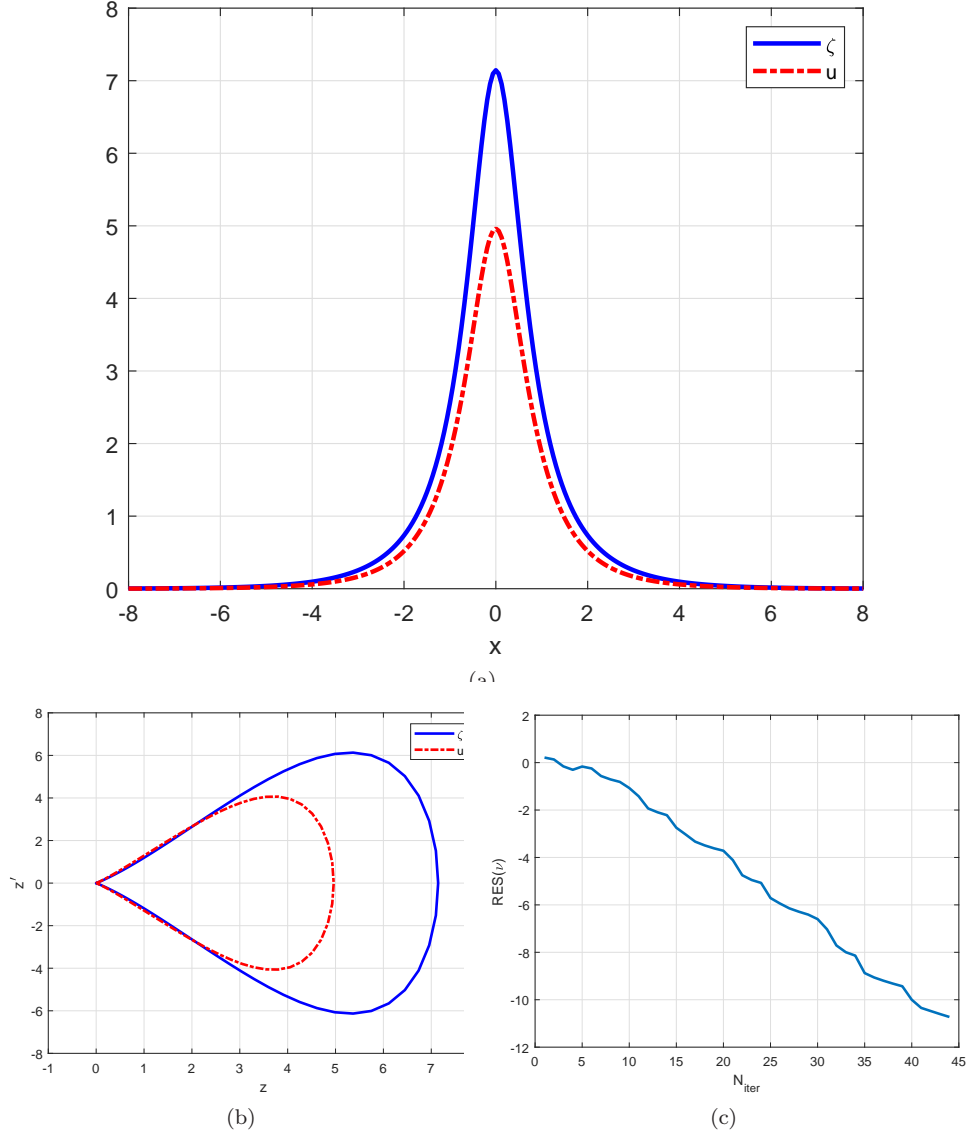


FIGURE 14. CSW generation. Case $D = 0$ with $\delta = 0.9, \gamma = 0.5, a = -1/3, c = 0, b = 0, d = -(\delta + \gamma)a - b - c + \frac{1+\gamma\delta}{3\delta(\gamma+\delta)} \approx 0.8503; c_s = c_{\gamma,\delta} + 0.25 \approx 0.8476$. (a) ζ and u profiles; (b) ζ and u phase portraits; (c) Residual error vs. number of iterations (semilog scale).

5. COMPUTATIONAL STUDY OF SOLITARY WAVE DYNAMICS

In this section we present a computational study of the dynamics of some aspects of solitary waves, both classical and generalized. The *generic case* ($a, c < 0, b, d > 0$) is considered for the experiments. In this case we have the existence of classical

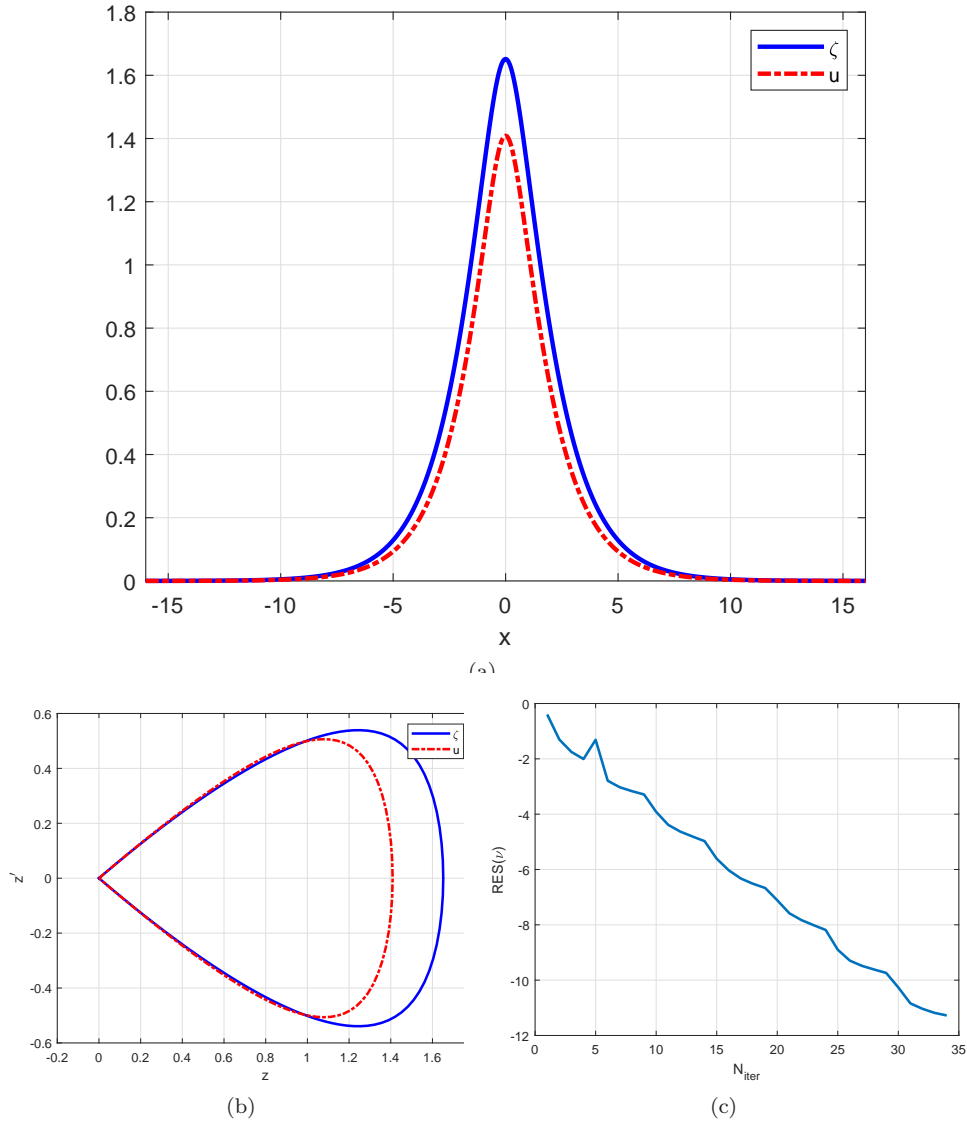


FIGURE 15. CSW generation. Case $D = 0$ with $\delta = 0.9, \gamma = 0.5, a = -2/3, c = 0, d = 0, b = -(\delta + \gamma)a - d - c + \frac{1+\gamma\delta}{3\delta(\gamma+\delta)} \approx 1.3169; c_s = c_{\gamma,\delta} + 0.1 \approx 0.6976$ (a) ζ and u profiles; (b) ζ and u phase portraits; (c) Residual error vs. number of iterations (semilog scale).

solitary waves when $\kappa_1 b d - a c > 0$ (case (A3) of Table 1) and generalized solitary waves when $\kappa_1 b d - a c < 0$ (case (A2) of Table 1).

5.1. Numerical approximation of the periodic ivp for the B/B system.

First we briefly describe the numerical method used for the computational study to follow. We consider the periodic initial-value problem (3.1)-(3.2) on a long

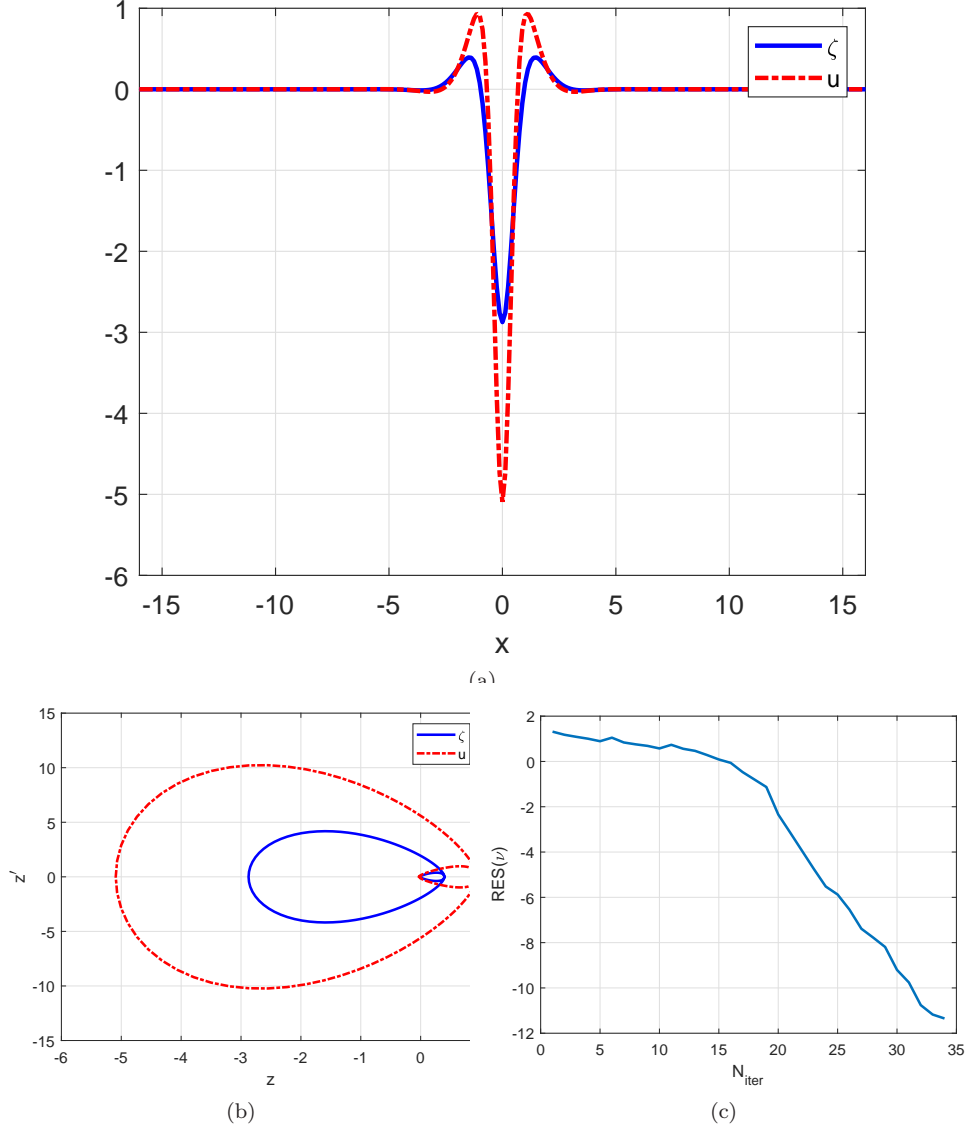


FIGURE 16. CSW generation with $a = -1/9$, $c = -1/6$, $b = 0$, $d = -a/\kappa_1 - c - b + S(\gamma, \delta) \approx 0.7058$, $\delta = 0.9$, $\gamma = 0.5$, and speed $c_s = c_{\gamma, \delta} - 0.2 \approx 3.9761 \times 10^{-1}$ (a) ζ and u profiles; (b) ζ and u phase portraits; (c) Residual error vs. number of iterations (semilog scale).

enough interval $(-L, L)$ and discretize it in space with the spectral Galerkin method introduced in Section 3. After the change from the interval $(0, 1)$ (for which the convergence analysis was made) to $(-L, L)$ is performed, the corresponding system (3.6)-(3.8) is solved in terms of the Fourier coefficients of the semidiscretization, in

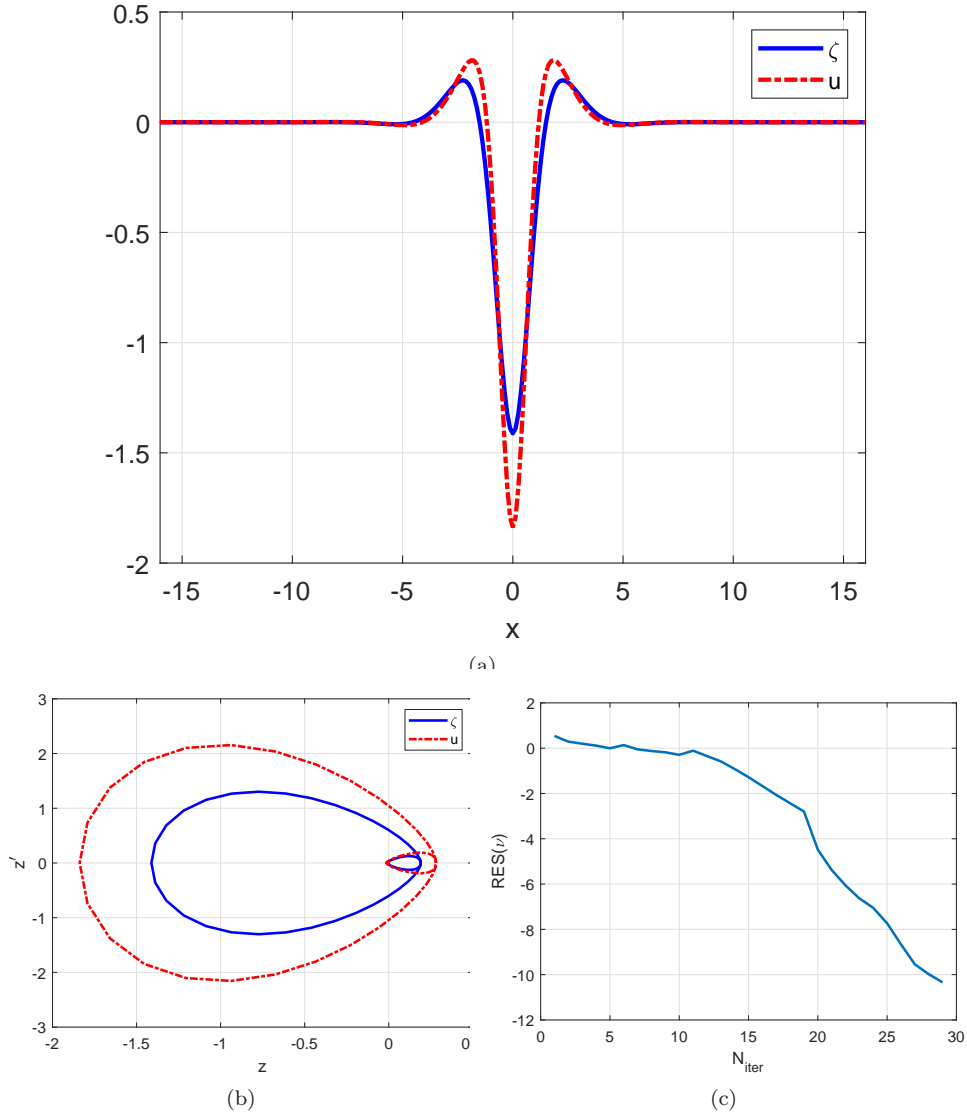


FIGURE 17. CSW generation with $a = -1/3, c = -1/3, b = 1/9, d = -a/\kappa_1 - c - b + S(\gamma, \delta) \approx 1.0725, \delta = 0.9, \gamma = 0.5$, and speed $c_s = c_{\gamma, \delta} - 0.2 \approx 3.9761 \times 10^{-1}$ (a) ζ and u profiles; (b) ζ and u phase portraits; (c) Residual error vs. number of iterations (semilog scale).

analogy to (3.9). This leads to an ode system of the form

$$\frac{d}{dt} \begin{pmatrix} \widehat{\zeta}_N \\ \widehat{u}_N \end{pmatrix} = F \begin{pmatrix} \widehat{\zeta}_N \\ \widehat{u}_N \end{pmatrix}, \tag{5.1}$$

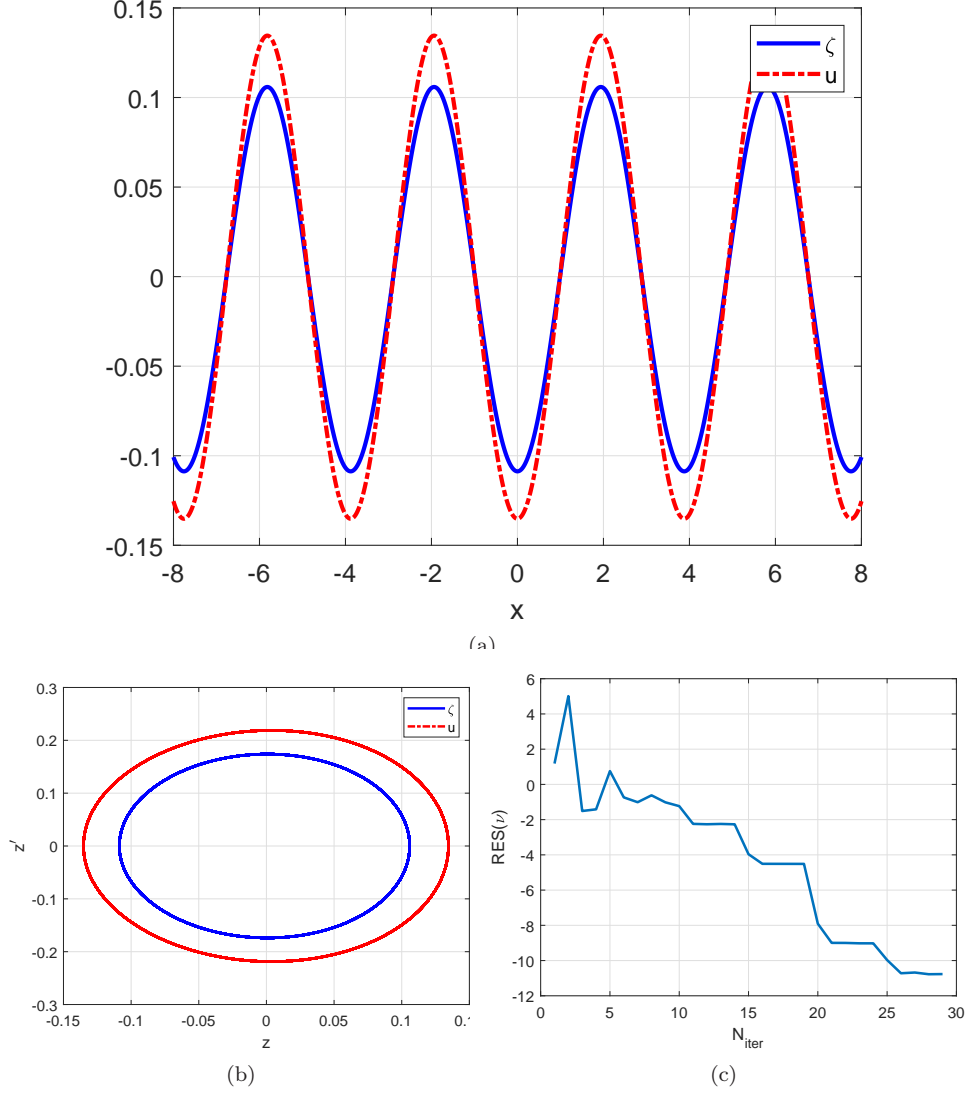


FIGURE 18. PTW generation with $a = c = 0, b = 1/6, d = -a/\kappa_1 - c - b + S(\gamma, \delta) \approx 0.2169, \delta = 0.9, \gamma = 0.5$, and speed $c_s = c_{\gamma, \delta} - 0.2 \approx 3.9761 \times 10^{-1}$ (a) ζ and u profiles; (b) ζ and u phase portraits; (c) Residual error vs. number of iterations (semilog scale).

where for $-N \leq k \leq N, \hat{k} = k\pi/L$

$$F \begin{pmatrix} \widehat{\zeta}_N \\ \widehat{u}_N \end{pmatrix} (\hat{k}) = \begin{pmatrix} \frac{1}{1+b\hat{k}^2} \left(i\hat{k}((- \kappa_1 + a\hat{k}^2)\widehat{u}_N(\hat{k}, t) - \lambda\widehat{\zeta}_N\widehat{u}_N(\hat{k}, t)) \right) \\ \frac{1}{1+d\hat{k}^2} \left(i\hat{k}(-\kappa_2(1 - c\hat{k}^2)\widehat{\zeta}_N(\hat{k}, t) - \frac{\lambda}{2}u_N^2(\hat{k}, t)) \right) \end{pmatrix}, \quad (5.2)$$

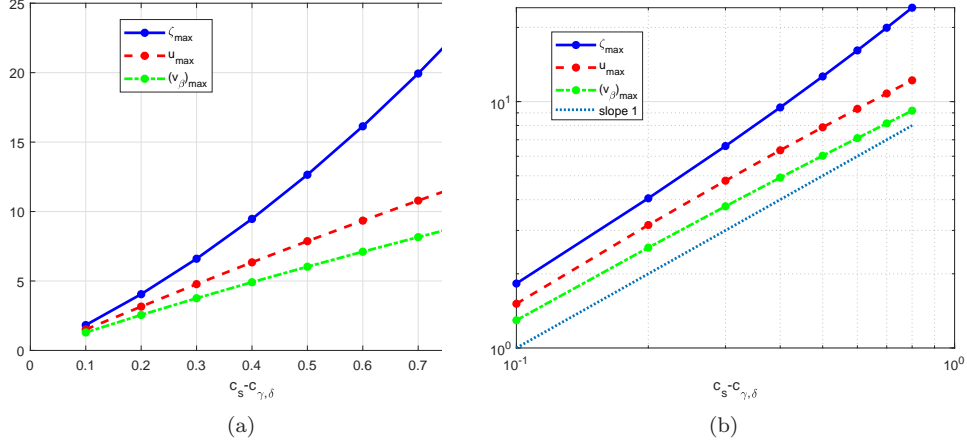


FIGURE 19. Speed-amplitude relation in (a) linear scale and (b) log-log scale. Case (A6) with $\delta = 0.9, \gamma = 0.5, a = 0, c = 0, b = d = \frac{1}{2} \frac{1 + \gamma \delta}{3\delta(\gamma + \delta)}$.

with $\widehat{\zeta}_N(\widehat{k}, 0) = \widehat{\zeta}_0(\widehat{k}), \widehat{u}_N(\widehat{k}, 0) = \widehat{u}_0(\widehat{k})$. The ode system (5.1), (5.2) is then discretized in time with the fourth-order, three-stage RK-composition method based on the implicit midpoint rule (IMR), [69, 45]. The scheme belongs to the family of RK methods with Butcher tableau

$$\left| \begin{array}{c|ccc} & & & \\ & b_1/2 & & \\ & b_1 & b_2/2 & \\ & b_1 & b_2 & \ddots \\ & \vdots & \vdots & \ddots \\ & b_1 & b_2 & \cdots & \cdots & b_s/2 \\ \hline & b_1 & b_2 & \cdots & \cdots & b_s \end{array} \right|, \quad (5.3)$$

in the particular case of $s = 3$ and

$$\begin{aligned} b_1 &= (2 + 2^{1/3} + 2^{-1/3})/3 = \frac{1}{2 - 2^{1/3}} \sim 1.351, \\ b_2 &= 1 - 2b_1 \sim -1.702, \quad b_3 = b_1, \end{aligned} \quad (5.4)$$

The method can be written as a composition of three steps of the IMR with stepsizes $b_1 \Delta t, b_2 \Delta t$ and $b_3 \Delta t$. For a general ode system $\dot{y} = f(y)$ this reads

$$\begin{aligned} y^{n,1} &= y^n + b_1 \Delta t f\left(\frac{y^n + y^{n,1}}{2}\right), \\ y^{n,j} &= y^n + b_j \Delta t f\left(\frac{y^{n,j-1} + y^{n,j}}{2}\right), \quad j = 2, 3, \\ y^{n+1} &= y^{n,3}. \end{aligned}$$

The scheme is fourth-order accurate, symplectic, symmetric and of easy implementation. The full discretization has been analyzed in [31] in the case of spectral semidiscretizations of the periodic ivp for the KdV equation and its efficiency has been checked in computations with other nonlinear dispersive equations, [42, 34].

It has been shown to be L^2 -conservative and convergent under suitable CFL conditions in the case of the KdV. Here, in our experiments with the B/B system (3.1)-(3.2) in the generic case $a, c < 0, b, d > 0$, we also observed that a Courant stability condition of the form $N\Delta t \leq \alpha$ for some $\alpha > 0$ was sufficient to ensure stability and convergence of the fully discrete scheme.

For an integer $M \geq 1$ the corresponding fully discrete approximation at times $t_m = m\Delta t, m = 0, \dots, M$, where $T = M\Delta t$, is computed in the Fourier space with FFT techniques. The computation of initial solitary wave profiles is carried out with the method outlined in Section 4.2.

5.2. Validation of the codes. In this section we present some numerical evidence in order to validate the full discretization introduced in section 5.1 and to complete the study of the accuracy of the numerical procedure to generate approximate solitary wave profiles, developed in section 4.2. The experiments will additionally serve to give confidence to the numerical simulation of stability and interactions of solitary waves to be carried out in sections 5.3 and 5.4.

$N = 2048$				
Δt	ζ -error	Rate	v_β -error	Rate
1/40	1.1028E-05		7.3309E-06	
1/80	6.8977E-07	3.9989	4.5852E-07	3.9989
1/160	4.3076E-08	4.0012	2.8635E-08	4.0011
$N = 4096$				
Δt	ζ -error	Rate	v_β -error	Rate
1/40	1.1028E-05		7.3309E-06	
1/80	6.8977E-07	3.9989	4.5852E-07	3.9989
1/160	4.2945E-08	4.0056	2.8548E-08	4.0055

TABLE 3. L^2 -errors and temporal convergence rates at $T = 100$ with $L = 256$ and $N = 2048$ ($h = 0.25$) and $N = 4096$ ($h = 0.125$).

In a first experiment we check the temporal order of convergence by simulating with the fully discrete scheme the propagation of an exact solitary wave solution of the form (4.51) corresponding to the parameter values

$$\begin{aligned} \delta &= 0.9, \gamma = 0.5, \\ a &= -1/3, c = -2/3, b = d = \frac{1}{2} \left(\frac{a}{\kappa_1} - c + \frac{1 + \gamma\delta}{3\delta(\delta + \gamma)} \right) \approx 0.2918 \end{aligned} \quad (5.5)$$

up to a final time $T = 100$ on an interval $(-L, L)$ with $L = 256$ and periodic boundary conditions. According to (4.48), the speed is $c_s \approx 1.0328$ and the amplitude is $\zeta_{\max} \approx 7.9846$. We made two runs with $N = 2048$ and $N = 4096$ (that is with $h = 2L/N = 0.250$ and 0.125 respectively) and several values of Δt . The normalized L^2 -errors for ζ and v_β at the final time and corresponding temporal convergence rates are displayed in Table 3. The results show the fourth order of convergence of the time discretization and the associated errors in space. Since for the values (5.5) the system (1.6) is Hamiltonian and its solutions are smooth, decaying to zero at infinity, and preserving the quantities (2.8) and (2.9), we may

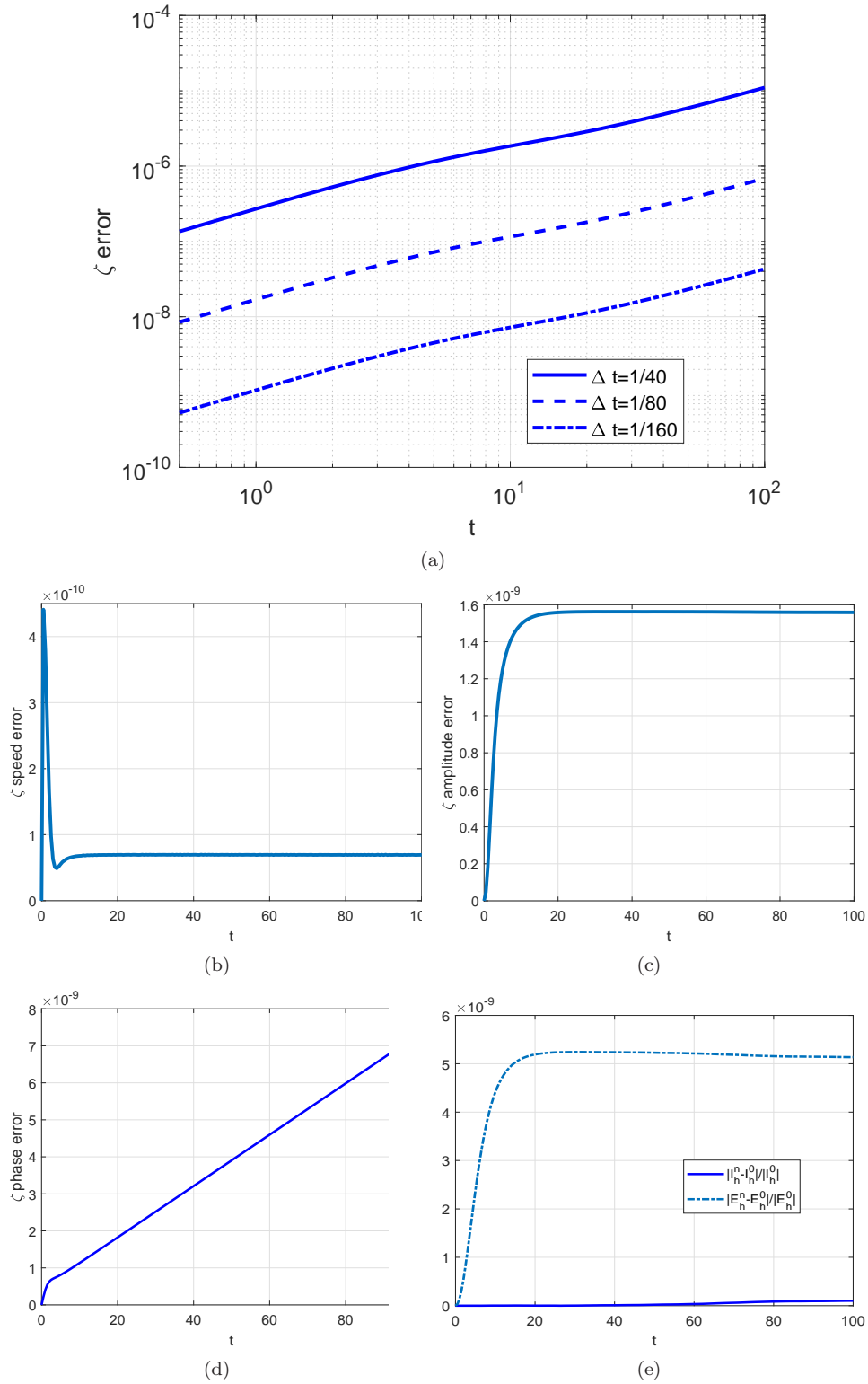


FIGURE 20. Numerical simulation of (1.6) with (5.5) up to $T = 100$ with $N = 4096$. (a) Normalized L^2 -error for ζ vs. time in log-log scale; (b) ζ speed error vs. time; (c) ζ amplitude error vs. time; (d) ζ phase error vs. time; (e) Errors of (5.6) and (5.7) vs. time (semilog scale). In (b)-(e) the errors are normalized and $\Delta t = 1/160$ is taken.

study the ability of the numerical solution to conserve the corresponding discrete versions of the invariants, given by

$$I_h(U, V) = h \sum_{j=0}^{N-1} (U_j V_j + b(D_N U)_j (D_N V)_j), \quad (5.6)$$

$$E_h(u, V) = h \sum_{j=0}^{N-1} \left(\frac{\kappa_2}{2} U_j^2 + \frac{\kappa_1}{2} V_j^2 - a(D_N V)_j^2 - \kappa_2 c (D_N U)_j^2 + \frac{\kappa_{\gamma, \delta}}{2} U_j V_j^2 \right), \quad (5.7)$$

for $U = (U_0, \dots, U_{N-1})$, $V = (V_0, \dots, V_{N-1})$ and D_N standing for the pseudospectral differentiation matrix of order N , cf. section 4.2. If I_h^n, E_h^n denote, respectively, the values of (5.6) and (5.7) of the numerical solution at time $t_n = n\Delta t$, we obtain the evolution of the normalized errors $|(I_h^n - I_h^0)/I_h^0|, |(E_h^n - E_h^0)/E_h^0|$ shown in Figure 20(e) for $\Delta t = 1/160$. It shows the preservation of the two quantities up to the final time $T = 100$ with a normalized error of 1.0198×10^{-10} and 5.1366×10^{-9} respectively. Due to the form of the bilinear invariant (2.8), we have almost exact in time conservation of the discrete H^1 -norm, defined by the pseudospectral differentiation of the numerical solution.

In addition, Figure 20(a) shows, in log-log scale, the evolution of the normalized ζ errors in L^2 norm as function of time for $N = 4096$ and several values of Δt . (The experiment with $N = 2048$ was also made, with similar results.) The slopes of the lines suggest approximately linear growth in time of the errors, as expected, [43]. A source of this behaviour is due to the evolution of the error with respect to some parameters of the solitary waves. For the case at hand this is illustrated by Figures 20(b)-(d) showing, for $N = 4096, \Delta t = 1/160$, the relative errors in speed, amplitude, and the error in phase, respectively, of the numerical approximation of ζ as functions of time. These errors are computed in a standard way, as in e. g. [33]. The results show the preservation of speed and amplitude (up to an error at $t = 100$ of about 6.9340×10^{-11} and 1.5584×10^{-9} respectively) and a linear growth of the phase error.

In a second experiment we took the values

$$\delta = 0.9, \gamma = 0.5, a = c = 0, b = d = \frac{1}{2} \left(\frac{1 + \gamma\delta}{3\delta(\delta + \gamma)} \right) \approx 0.1918, \quad (5.8)$$

and taking as initial profile a superposition of two hyperbolic secant square profiles of amplitudes equal to 1 and centered at $x = \pm 20$, we ran the iteration (4.56). The method converges to the profile shown in Figure 21(a), which has the form of a symmetric two-pulse solitary wave (cf. Remark 4.9). The accuracy of the iteration is first suggested by the convergence to practically zero of the residual error shown in Figure 21(c). Both pulses have a computed amplitude of about 1.6055 and the two-pulse wave travels with a speed of 6.9761×10^{-1} .

In addition, we took this computed two-pulse as initial condition of the fully discrete method and monitored the evolution of the numerical solution up to a final time $T = 400$ with several values of the discretization parameters h (or N) and Δt . The profiles at several times generated with $\Delta t = 1/160$ and $N = 2048, 4096$, are shown in Figure 22; they coincide within graph thickness.

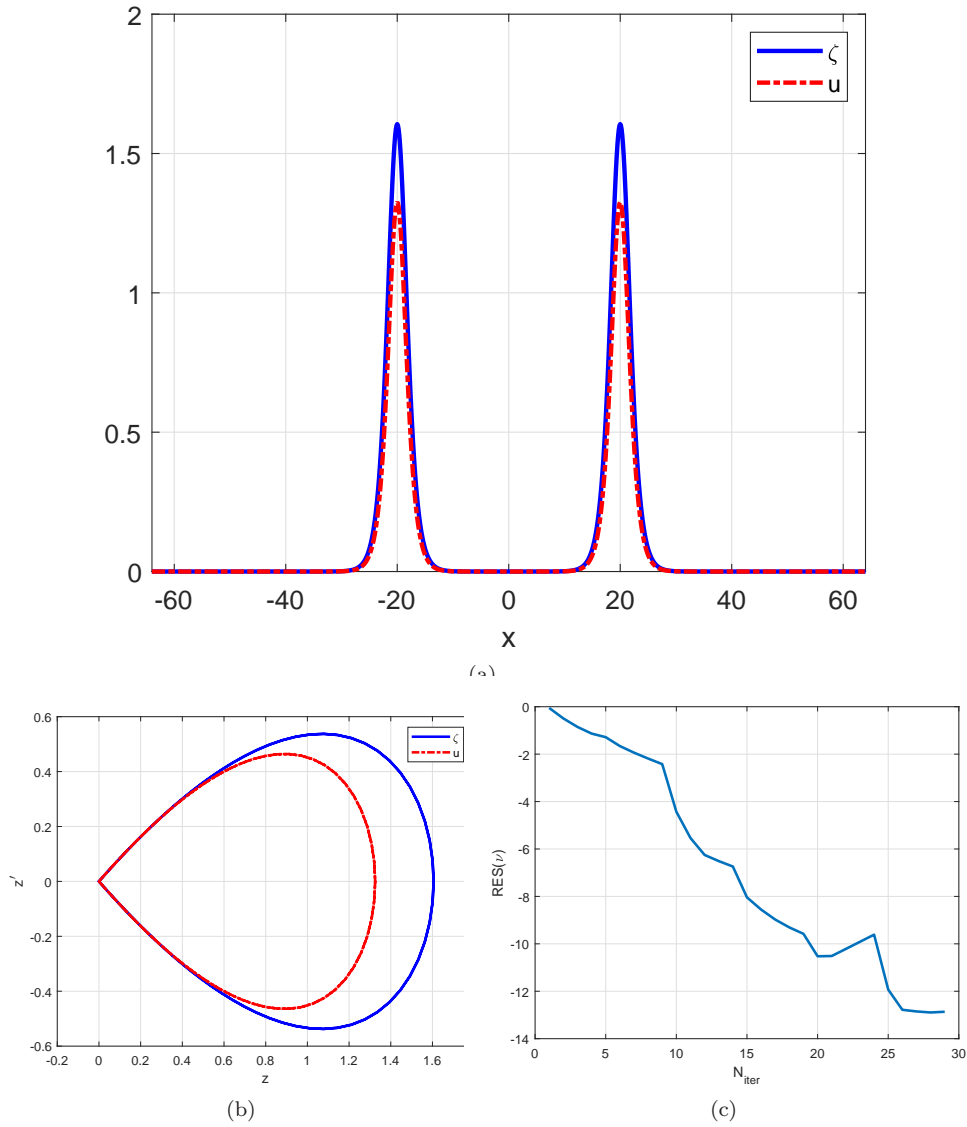


FIGURE 21. Two-pulse solitary wave generated numerically with parameters given by (5.8). (a) ζ and u profiles; (b) ζ and u phase portraits; (c) Residual error vs. number of iterations (semilog scale).

A third experiment for checking the accuracy of the codes concerns the simulation of a generalized solitary wave. Taking the values $L = 256$, and

$$\delta = 0.9, \gamma = 0.5, a = c = -1/3, b = 0, d = -\frac{a}{\kappa_1} - c + \frac{1 + \gamma\delta}{3\delta(\delta + \gamma)} \approx 1.1836, \quad (5.9)$$

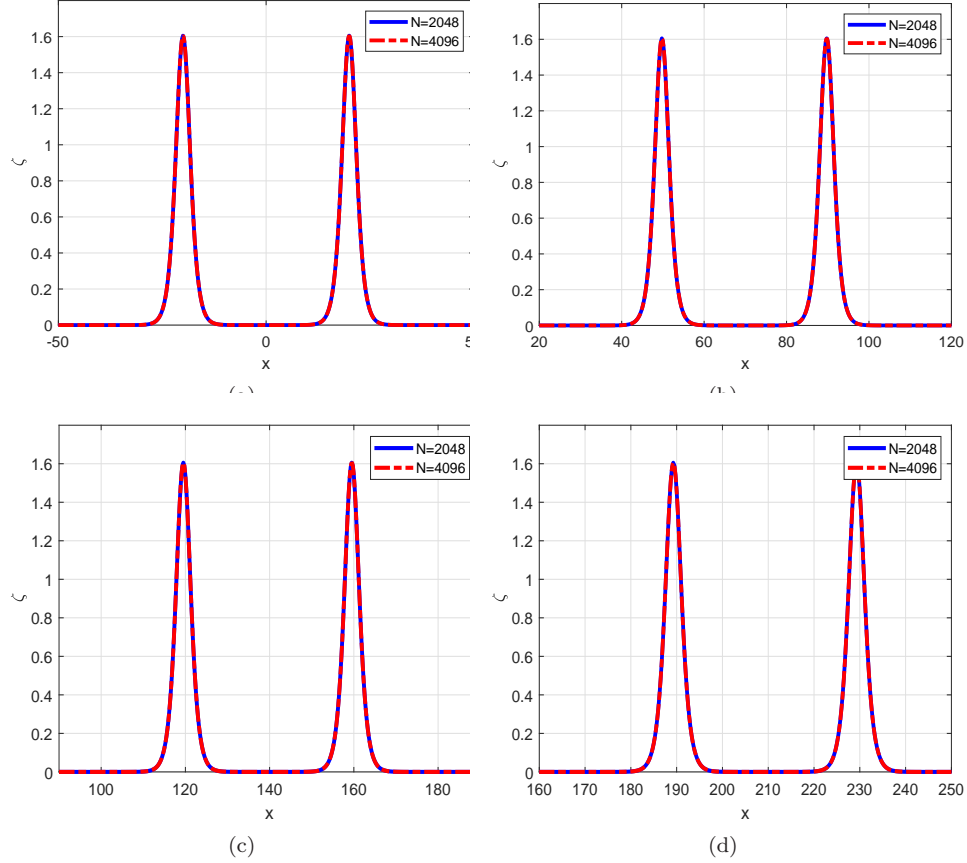


FIGURE 22. Simulation of (1.6) with (5.8) up to $T = 400$ with $\Delta t = 1/160$. Approximation of $\zeta(x, t)$ at (a) $t = 0$; (b) $t = 100$; (c) $t = 200$; (d) $t = 300$.

and the GSW profile generated by the iteration (4.56) as initial condition for the fully discrete scheme, the evolution of the resulting numerical approximation is observed in the following experiments. Figure 23 shows the numerical approximation of ζ at several time instances with $N = 2048$ and $\Delta t = 1/160$, confirming the preservation of the permanent form of the wave as it evolves. (The amplitude of computed initial GSW profile is $\zeta_{max} \approx 1.5764 \times 10^{-1}$ and the profile was generated with speed $c_s = c_{\gamma, \delta} + 0.01 \approx 6.0761 \times 10^{-1}$.) The profiles obtained with $N = 4096$ were also computed and they coincide with the corresponding ones obtained for $N = 2048$ within the graph thickness. Figure 24 is a magnification of Figure 23 and shows the structure of the ripples in more detail.

The accuracy of the computations is also confirmed by monitoring the evolution of amplitude and speed errors, shown in Figure 25. Observe that this case is not Hamiltonian and the quantities (2.8), (2.9) are not preserved by the solution. The L^2 norm of the numerical solution for $N = 2048, 4096$, evaluated at several time instances is shown in Table 4. This is preserved up to twelve significant digits, and

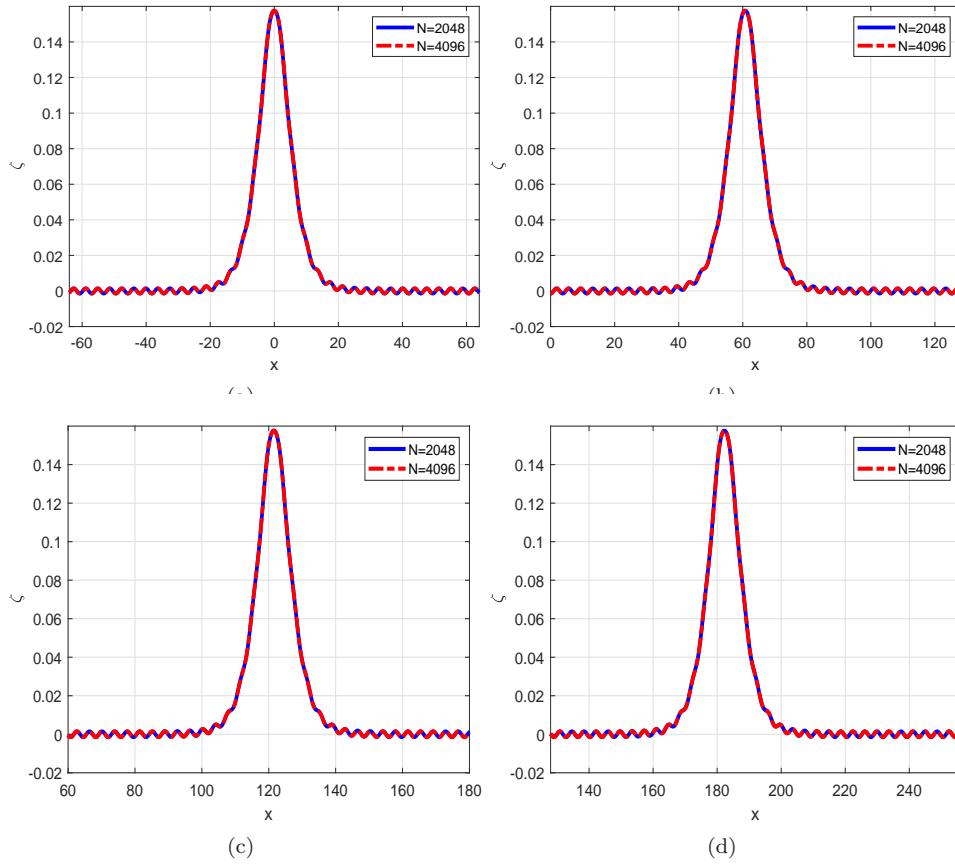


FIGURE 23. Simulation of (1.6) with (5.9) up to $T = 400$ with $\Delta t = 1/160$. Approximation of $\zeta(x, t)$ at (a) $t = 0$; (b) $t = 100$; (c) $t = 200$; (d) $t = 300$.

is equal to $4.5789161770 \times 10^{-1}$, this furnishes more evidence of the accuracy of the computations.

t	$N = 2048$	$N = 4096$
$t = 0$	$4.578916177071256e - 01$	$4.578916177063826e - 01$
$t = 100$	$4.578916177071556e - 01$	$4.578916177064732e - 01$
$t = 200$	$4.578916177072831e - 01$	$4.578916177066413e - 01$
$t = 300$	$4.578916177073125e - 01$	$4.578916177067275e - 01$
$t = 400$	$4.578916177075660e - 01$	$4.578916177070251e - 01$

TABLE 4. Simulation of (1.6) from a GSW (Figure 23) up to $T = 400$ with $\Delta = 1/160$. L^2 norm of ζ component.

5.3. CSW dynamics. Numerical experiments. In this section we present some numerical experiments on the dynamics of CSW's in the generic case ($a, c < 0, b, d >$

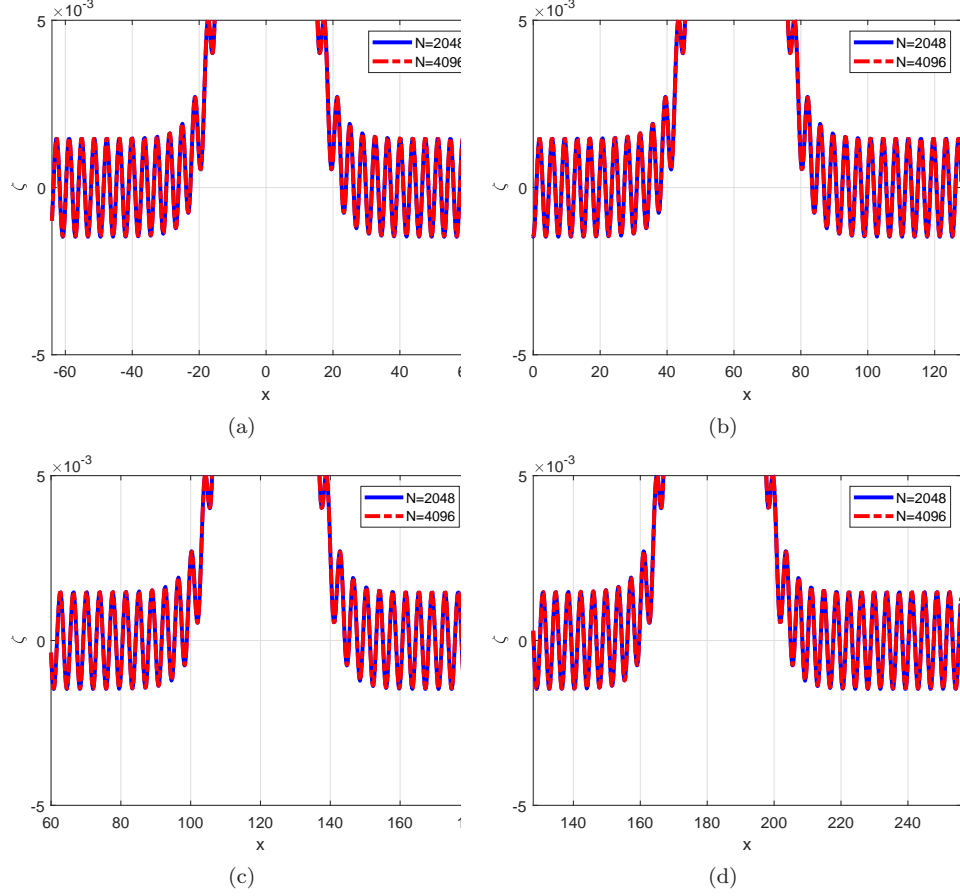


FIGURE 24. Magnification of Figure 23 near the base of the main pulse. Approximation of $\zeta(x, t)$ at (a) $t = 0$; (b) $t = 100$; (c) $t = 200$; (d) $t = 300$.

0) and $\kappa_1 b d - a c > 0$ (case (A3)). The experiments concern the evolution of small and larger perturbations of CSW's, as well as head-on and overtaking collisions of CSW's. For simplicity, only the results for the ζ -component ζ^N will be shown.

5.3.1. *Small perturbations of a CSW.* In order to illustrate the evolution of a perturbed CSW in this generic case, we take the specific values

$$\begin{aligned} \gamma &= 0.5, \delta = 0.9, a = -1/3, c = -2/3, b = 1/3, \\ d &= -\frac{a}{\kappa_1} - b - c + \frac{1 + \gamma\delta}{3\delta(\gamma + \delta)} \approx 1.1836. \end{aligned} \quad (5.10)$$

A typical experiment consists of generating a corresponding approximate CSW profile (ζ_s^N, u_s^N) for these values (here with specific data $L = 256, N = 4096, c_s = c_{\gamma, \delta} + 0.1 \approx 0.6976$, starting from a sech^2 -initial profile), taking a perturbation

$$\zeta^N(0) = A\zeta_s^N, \quad u^N(0) = Au_s^N, \quad (5.11)$$

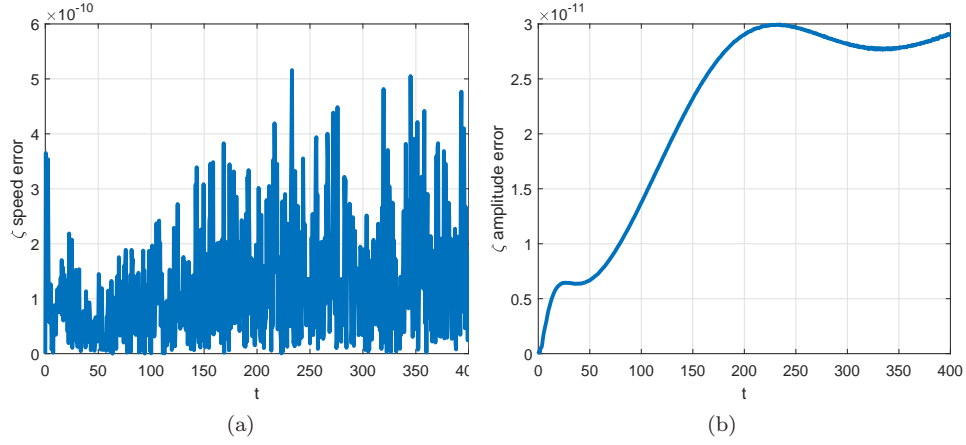


FIGURE 25. Simulation of (1.6) with (5.9) up to $T = 400$ with $\Delta t = 1/160$ and $N = 4096$. (a) Normalized ζ speed error vs. time; (b) Normalized ζ amplitude error vs. time.

with A constant as initial condition and monitoring the resulting numerical solution up to some final time T , which was taken in the experiments to be up to $T = 800$. The time step was $\Delta t = 6.25 \times 10^{-3}$. For $A = 1.1$ the results are given in Figures 26-28. Figure 26 shows the evolution of the numerical approximation at several time instances. In this small perturbation case, a new CSW emerges, with some small-amplitude tail of dispersive nature following the main wave and shown in detail in Figure 26(d).

The structure of these tails emerges when we analyze the behaviour of small-amplitude solutions of the linearized system associated to (1.6) in a frame $y = x - c_s t$ moving with the speed c_s of the CSW, given by

$$(1 - b\partial_{yy})(\partial_t - c_s\partial_y)\zeta + \kappa_1\partial_y J_a v_\beta = 0, \quad (5.12)$$

$$(1 - d\partial_{yy})(\partial_t - c_s\partial_y)v_\beta + \kappa_2\partial_y J_c \zeta = 0, \quad (5.13)$$

where J_a, J_c are given by (4.24). Applying the operator $(1 - d\partial_{yy})(\partial_t - c_s\partial_y)$ to (5.12) and using (5.13) we obtain the high-order wave equation

$$(1 - d\partial_{yy})(1 - b\partial_{yy})(\partial_t - c_s\partial_y)^2\zeta - \kappa_1\kappa_2\partial_y^2 J_a J_c \zeta = 0. \quad (5.14)$$

Plane wave solutions $\zeta(y, t) = e^{i(ky - \omega(k)t)}$ of (5.14) satisfy the linear dispersion relation

$$\omega(k) = \omega_\pm(k) = -kc_s \pm c_{\gamma,\delta} k \phi(k^2),$$

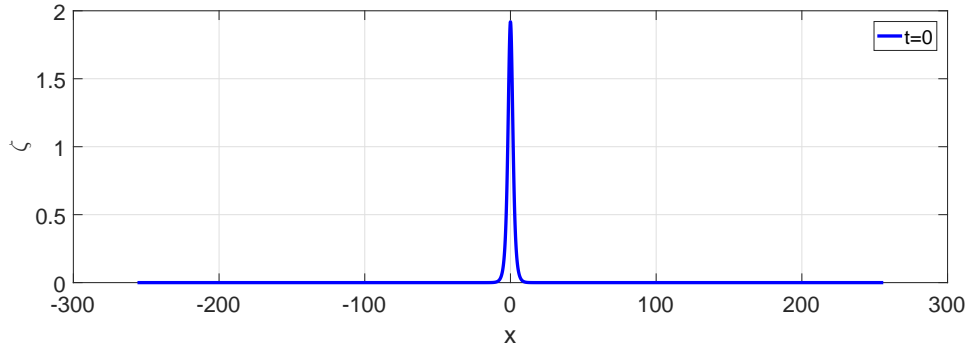
where $\phi : [0, \infty) \rightarrow \mathbb{R}$ is the function

$$\phi(x) = \sqrt{\frac{(1 - \tilde{a}x)(1 - cx)}{(1 + bx)(1 + dx)}}, \quad \tilde{a} = \frac{a}{\kappa_1}.$$

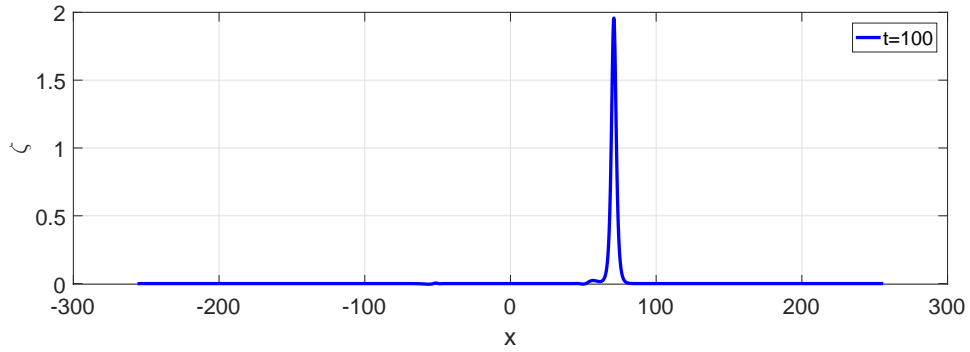
This leads to a local phase speed (relative to the speed of the CSW)

$$v_\pm(k) = -c_s \pm c_{\gamma,\delta} \phi(k^2). \quad (5.15)$$

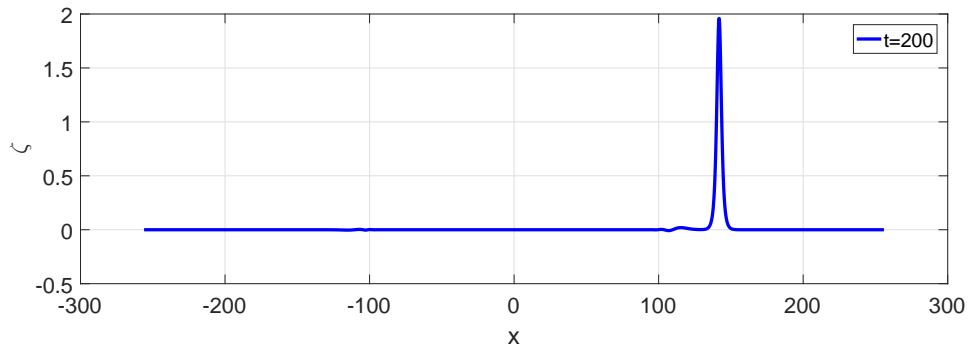
Some properties of the function ϕ can explain the behaviour of (5.15). These are:



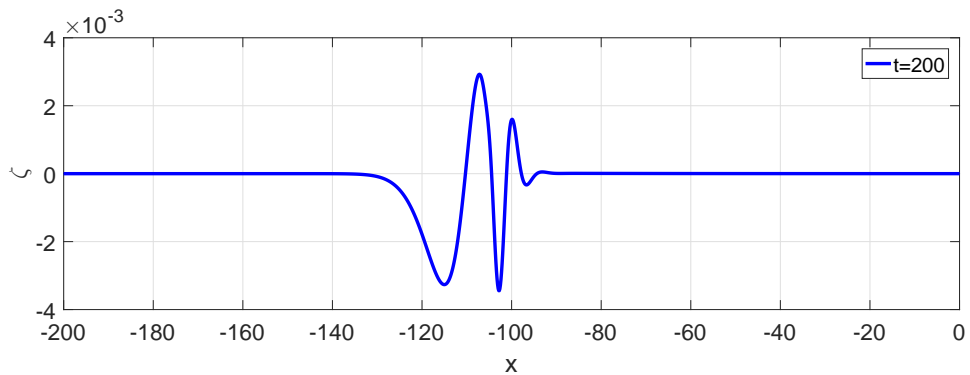
(a)



(b)



(c)



(d)

FIGURE 26. Evolution of a CSW perturbed by a small factor. Case (A3) with (5.10), (5.11) $A = 1.1$, $c_s = c_{\gamma,\delta} + 0.1$. (a)-(c) ζ component of the numerical solution; (d) Magnification of (c) between $x = -200$ and $x = 0$.

- (1) $\phi(x) \geq 0, x \geq 0, \phi(0) = 1$.
 (2) From the condition $\kappa_1 bd - ac > 0$, characterizing (A3), we have

$$\lim_{x \rightarrow \infty} \phi(x) = \phi_* := \sqrt{\frac{ac}{\kappa_1 bd}} < 1.$$

- (3) Let

$$\begin{aligned} p_1 &= \tilde{a}c(b+d) + bd(\tilde{a}+c), \\ p_2 &= 2(\tilde{a}c - bd) < 0 \text{ (cf. (A3))}, \\ p_3 &= \frac{1 + \gamma\delta}{3\delta(\gamma + \delta)} > 0. \end{aligned} \quad (5.16)$$

Then

$$\phi'(x) = \frac{P(x)}{2\phi(x)(1+bx)^2(1+dx)^2}, \quad P(x) = p_1x^2 + p_2x - p_3. \quad (5.17)$$

Therefore, the monotonicity of ϕ depends on the polynomial $P(x)$, in particular on the sign of p_1 . Let $\Delta = p_2^2 + 4p_1p_3$ be the discriminant of the equation $P(x) = 0$. Then we have the cases:

- (i) $p_1 < 0$. In this case $\Delta \leq 0$. Then $P(x)$ has the same sign for all $x \geq 0$. Since $P(0) = -p_3 < 0$, then $P(x) < 0, x \geq 0$. Therefore, $\phi(x)$ is decreasing for $x \geq 0$. On the other hand, when $\Delta = 0$ then $P(x)$ has a double root at $x = x_* = -p_2/2 > 0$, where $P(x)$ attains a minimum.

Thus:

- (1) If $0 \leq x \leq x_*$, then $\phi(x)$ is decreasing with $1 > \phi(x) \geq \phi(x_*)$.
 - (2) If $x_* \leq x$, then $\phi(x)$ is increasing with $\phi(x_*) \leq \phi(x) \leq \phi_* < 1$.
- (ii) $p_1 = 0$. In this case $P(x) = p_2x - p_3$ has only the root $x = p_3/p_2 < 0$ and therefore $\phi(x)$ is decreasing for $x > 0$ with $0 \leq \phi(x) \leq \phi(0) = 1$.
- (iii) $p_1 > 0$. This implies $\Delta > 0$ and the existence of two simple roots of $P(x)$, one positive $x_* = \frac{1}{2}(-p_2 + \sqrt{\Delta})$ and one negative. The behaviour is then similar to the case $\Delta = 0$ in (i), that is
- (1) If $0 \leq x \leq x_*$, then $\phi(x)$ is decreasing with $1 > \phi(x) \geq \phi(x_*)$.
 - (2) If $x_* \leq x$, then $\phi(x)$ is increasing with $\phi(x_*) \leq \phi(x) \leq \phi_* < 1$.

The form of ϕ for the example at hand is given in Figure 27.

With all these properties we have

$$-c_s - c_{\gamma,\delta} < v_-(k) < -c_s < v_+(k) < -c_s + c_{\gamma,\delta}.$$

If we assume $c_s > c_{\gamma,\delta}$, then we conclude that plane wave components of the dispersive tail, traveling to the right or to the left, trail the solitary wave with an absolute phase speed satisfying $v_+(k) + c_s < c_{\gamma,\delta}$ and $|v_-(k) + c_s| < c_{\gamma,\delta}$. Furthermore, components with smaller k (long wavelength) are faster than those with larger k (short wavelength).

For the group velocities we have

$$\omega'_\pm(k) = -c_s \pm c_{\gamma,\delta}\psi(k^2),$$

where $\psi : [0, \infty) \rightarrow \mathbb{R}$ is the function

$$\psi(x) = 2x\phi'(x) + \phi(x), \quad (5.18)$$

Figure 27(b) shows this function when the coefficients of the system are given by (5.10). The behaviour in this case seems to be similar to that of ϕ . Different values of the parameters (always in the generic case and with the condition $\kappa_1 bd - ac > 0$)

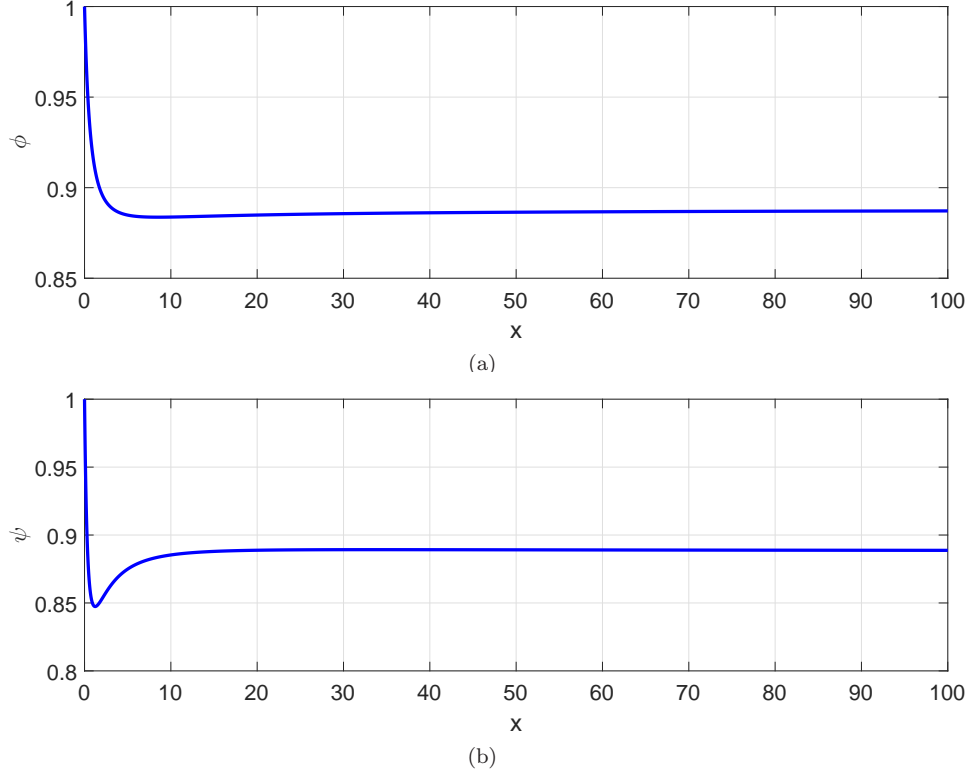


FIGURE 27. Form of the functions (a) $\phi(x)$ and (b) $\psi(x)$ for the values (5.10).

seem to suggest that this is a typical form, with the existence of a minimum, to the left of which $0 \leq \psi(x) \leq 1$ and after which ψ grows up to

$$\lim_{x \rightarrow \infty} \psi(x) = \phi_* := \sqrt{\frac{ac}{\kappa_1 bd}} < 1.$$

Under these conditions, we would have

$$-c_s - c_{\gamma,\delta} < \omega'_-(k) < -c_s < \omega'_+(k) < -c_s + c_{\gamma,\delta}.$$

If we assume $c_s > c_{\gamma,\delta}$ again, this would imply the existence of two dispersive groups, one traveling to the left and one to the right following the solitary wave, with group velocity smaller than c_s with $|\omega'_\pm(k) + c_s| < c_{\gamma,\delta}$. In Figure 26(c) a first tail, close to the main wave is observed, while a second wave packet of smaller amplitude appears in the magnified Figure 26(d). At $t = 200$, this wavelet is traveling to the left with effective support in $[-130, -90]$ (cf. [33] for a similar wavelet in some cases of surface waves).

Finally, Figures 28(a) and 28(b) show, respectively, the evolution of the amplitude and speed of the ζ component of the numerical approximation of the main pulse for the system with parameters given by (5.10). In this example, the emerging solitary wave is faster and larger than the perturbed initial profile.

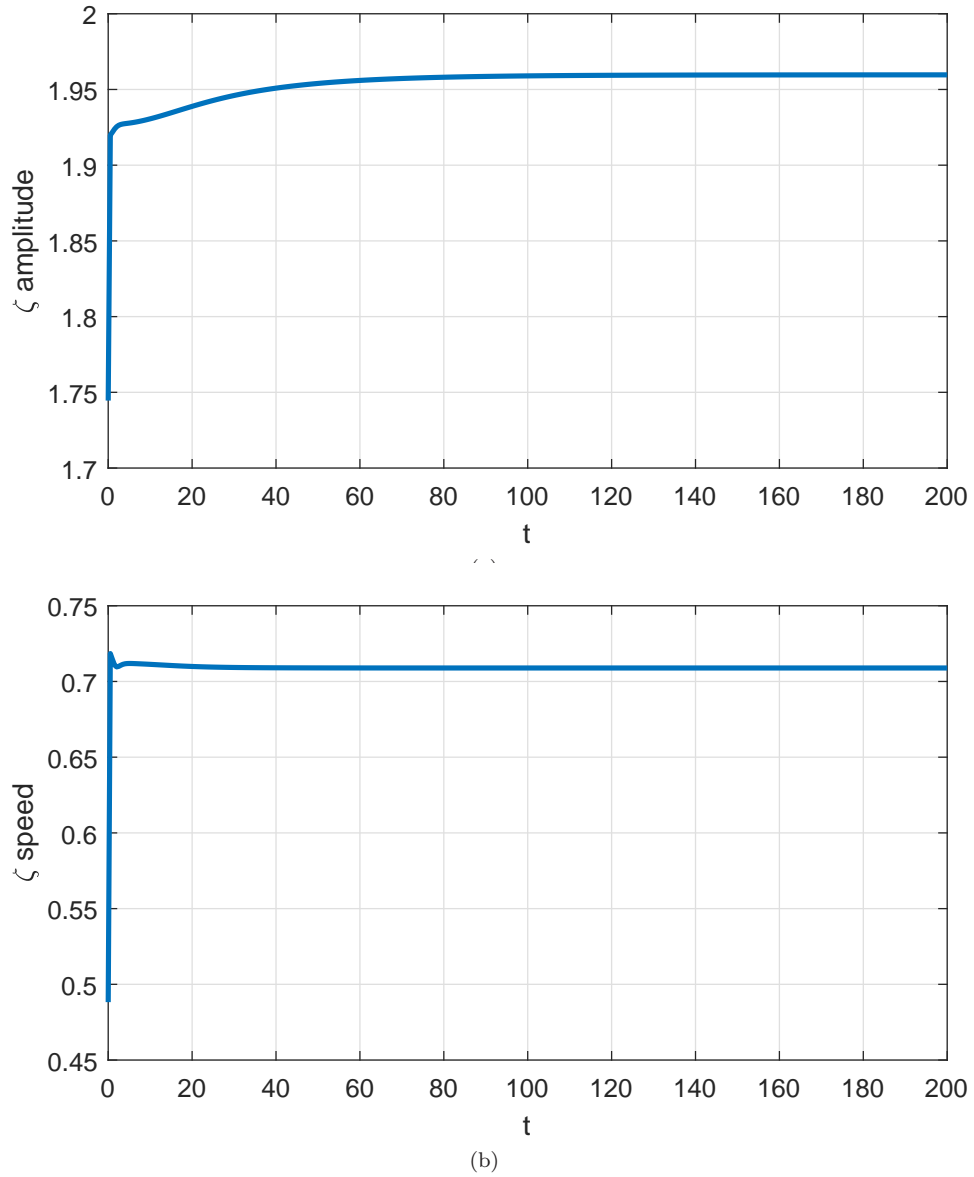


FIGURE 28. Evolution of a CSW perturbed by a small amount. Case (A3) with (5.10), (5.11) $A = 1.1$, $c_s = c_{\gamma,\delta} + 0.1$. Evolution of amplitude (a) and speed (b) of the ζ component of the main pulse.

Remark 5.1. A similar study can also be applied to the rest of the cases (A4)-(A6) of Table 1. Thus, in the cases (A4) and (A5), we have $p_1 < 0$, while in the case (A6), $p_1 = 0$. Then, analogous results to those of the generic case (A3) of CSW's hold.

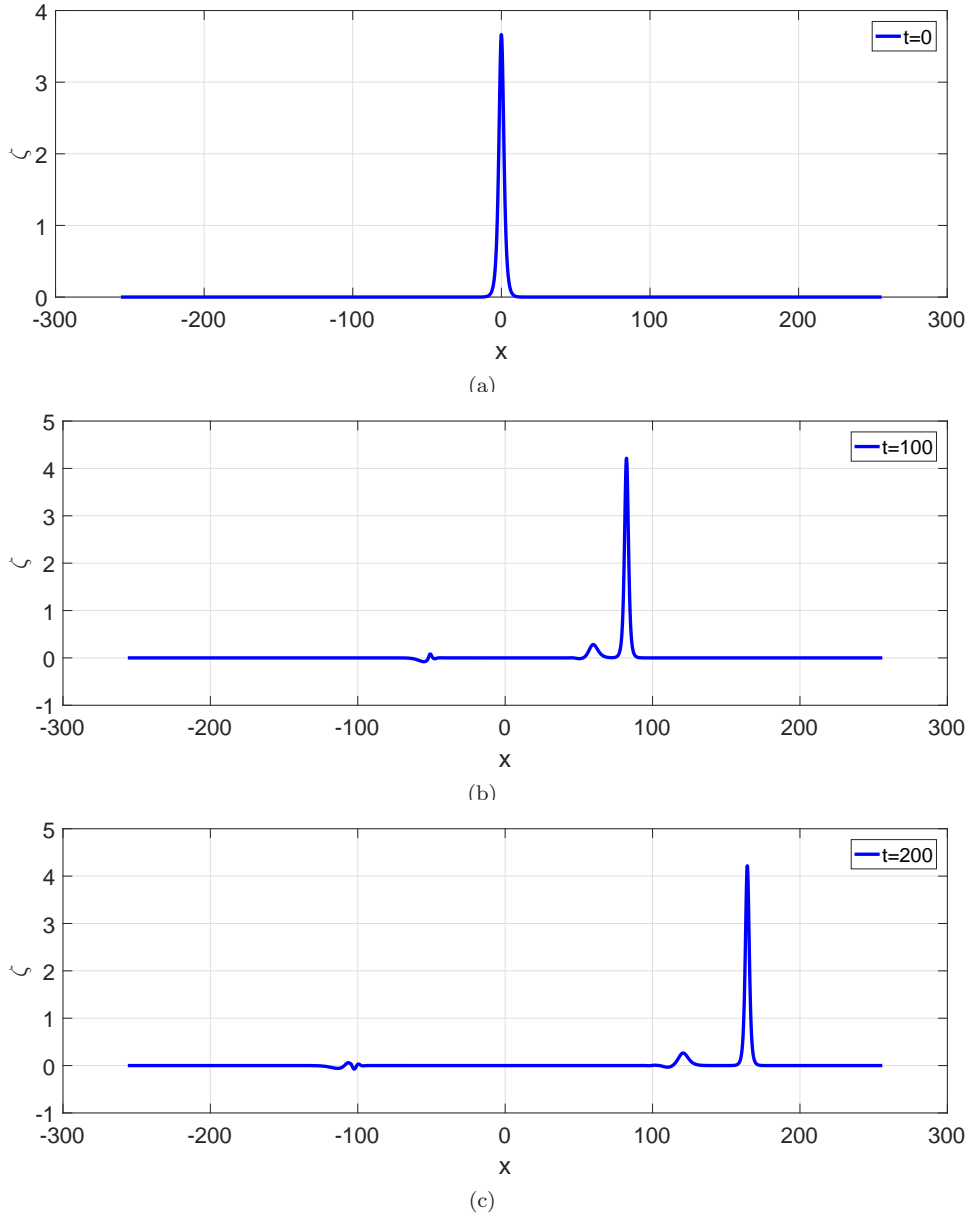


FIGURE 29. Evolution of a perturbed CSW. Case (A3) with (5.10), (5.11) $A = 2.1$, $c_s = c_{\gamma,\delta} + 0.1$. (a)-(c) ζ component of the numerical solution.

5.3.2. *Larger perturbation of a CSW.* Increasing the value of the perturbation parameter A leads, in our example, to the generation of another solitary wave; no instability was observed. Figures 29-31 illustrate the experiment with $A = 2.1$. The evolution of the numerical approximation (see Figure 29) shows, in addition

to the generation of a dominant, emerging solitary wave, (a bit taller than that of the perturbed initial data, cf. Figure 31), the formation of two other structures.

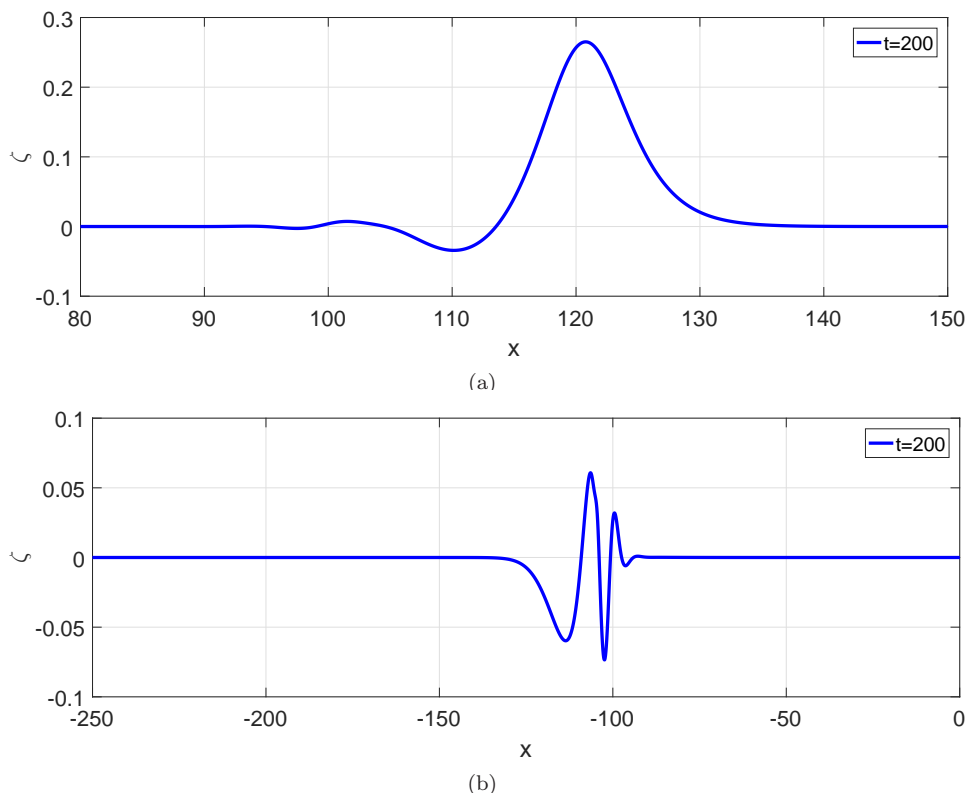


FIGURE 30. Evolution of a perturbed CSW. Case (A3) with (5.10), (5.11) $A = 2.1, c_s = c_{\gamma, \delta} + 0.1$. (a) First structure of the ζ component of the numerical solution; (b) Second structure.

Immediately behind the main wave, a nonlinear wave of solitary-wave type seems to be forming, along with a dispersive tail trailing it, as Figure 30(a) reveals. The nature of the second structure on the left (see the magnification in Figure 30(b)) is not so clear. Apparently, the wave should contain some dispersive component (as in the experiment with small perturbations in the previous section) but its persistence during the evolution may suggest the existence of something that does not disperse strongly. Similar conclusions hold from the experiments (not shown here) with $A = 3.1$. This behaviour also suggests, as the structure seems to be moving to the left, the formation of a wavelet, or a superposition of them, such as observed in Boussinesq systems for surface waves, see e. g. [10]. Nevertheless, the possibility of the formation of a CSW with nonmonotone decay is not to be discarded.

These observations persist when the value of A is taken to be larger. In order to illustrate this, we show the analogous experiment corresponding to $A = 6.1$, in Figures 32-33. For this larger perturbation, the initial perturbed wave gives rise to a main solitary-wave pulse and seems to exhibit a sort of stronger resolution property,

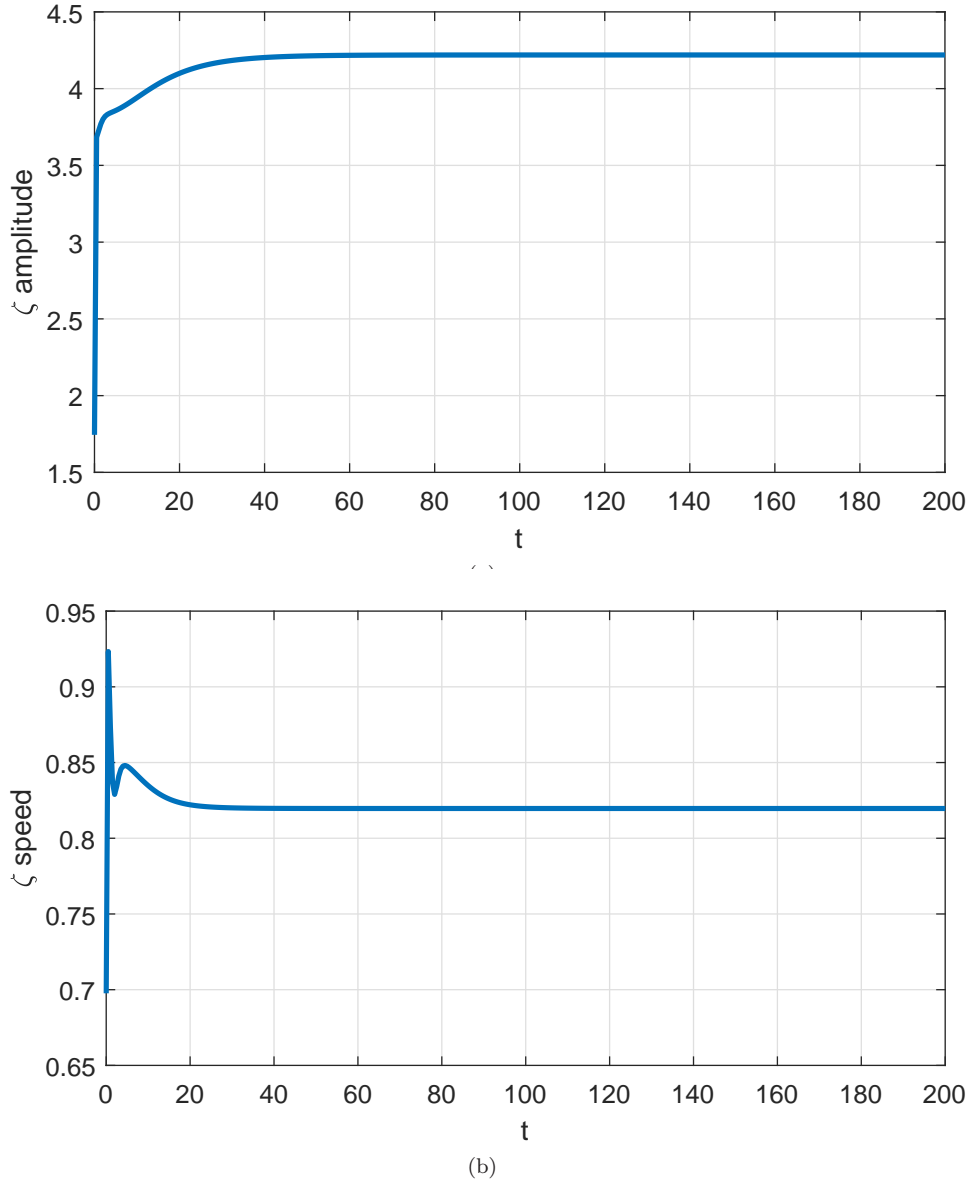


FIGURE 31. Evolution of a perturbed CSW. Case (A3) with (5.10), (5.11) $A = 2.1, c_s = c_{\gamma,\delta} + 0.1$. Evolution of amplitude (a) and speed (b) of the ζ component of the numerical solution.

with a solitary wave of elevation forming behind the main wave, see Figure 33(a). As for the second structure, the possible formation of a CSW of depression with nonmonotone decay is more clearly observed (Figure 33(b)) than in the previous experiment.

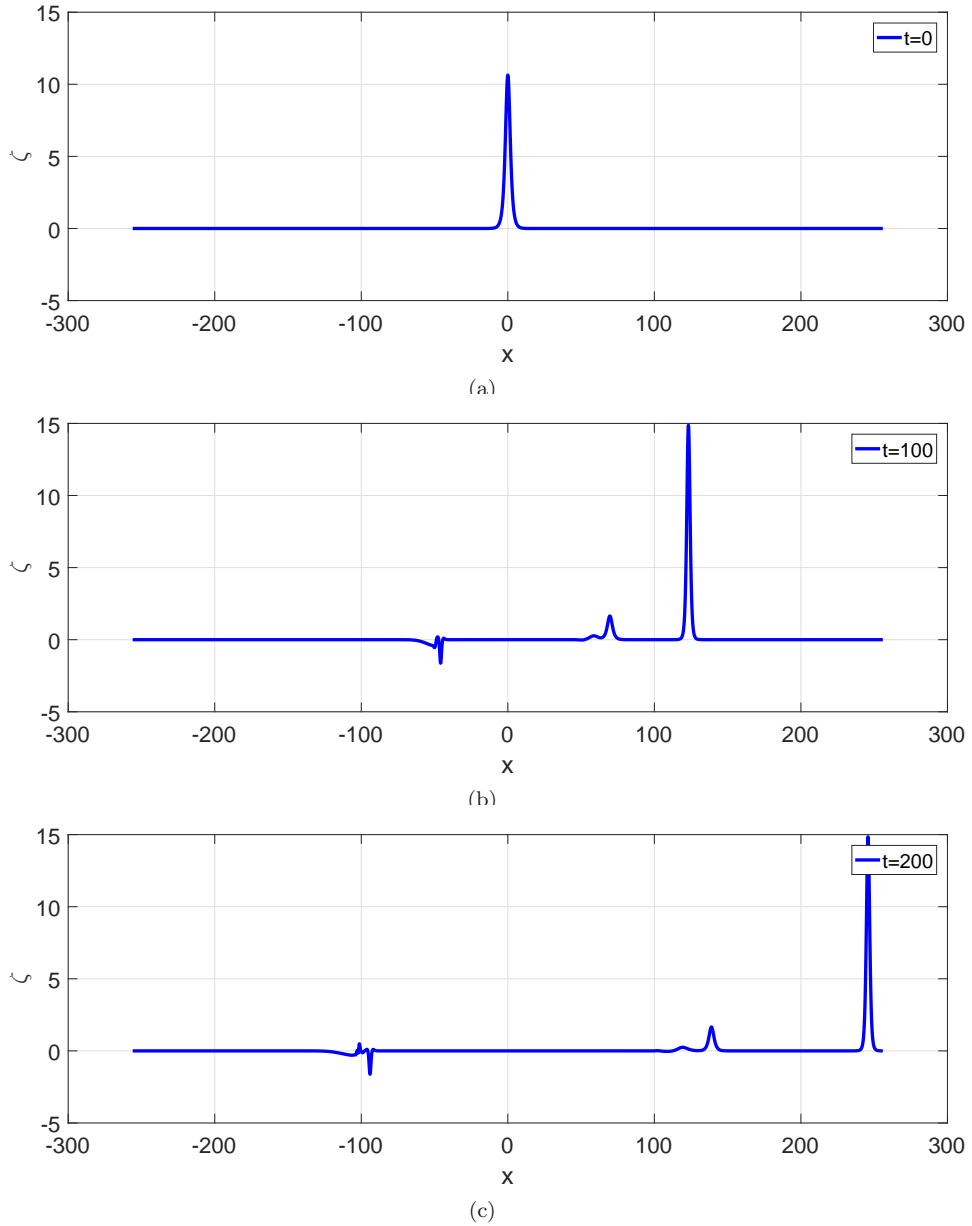


FIGURE 32. Evolution of a perturbed CSW. Case (A3) with (5.10), (5.11) $A = 6.1, c_s = c_{\gamma,\delta} + 0.1$. (a)-(c) ζ component of the numerical solution.

5.3.3. *Overtaking collisions.* Overtaking collisions are illustrated in the following experiment. With the same values of the parameters given by (5.10), we generate two approximate CSW profiles with speed $c_s^{(1)} = c_{\gamma,\delta} + 0.5 \approx 1.0976$ centered at $x_0^{(1)} = 0$, and speed $c_s^{(2)} = c_{\gamma,\delta} + 0.2 \approx 0.7976$ centered at $x_0^{(2)} = 20$, respectively.

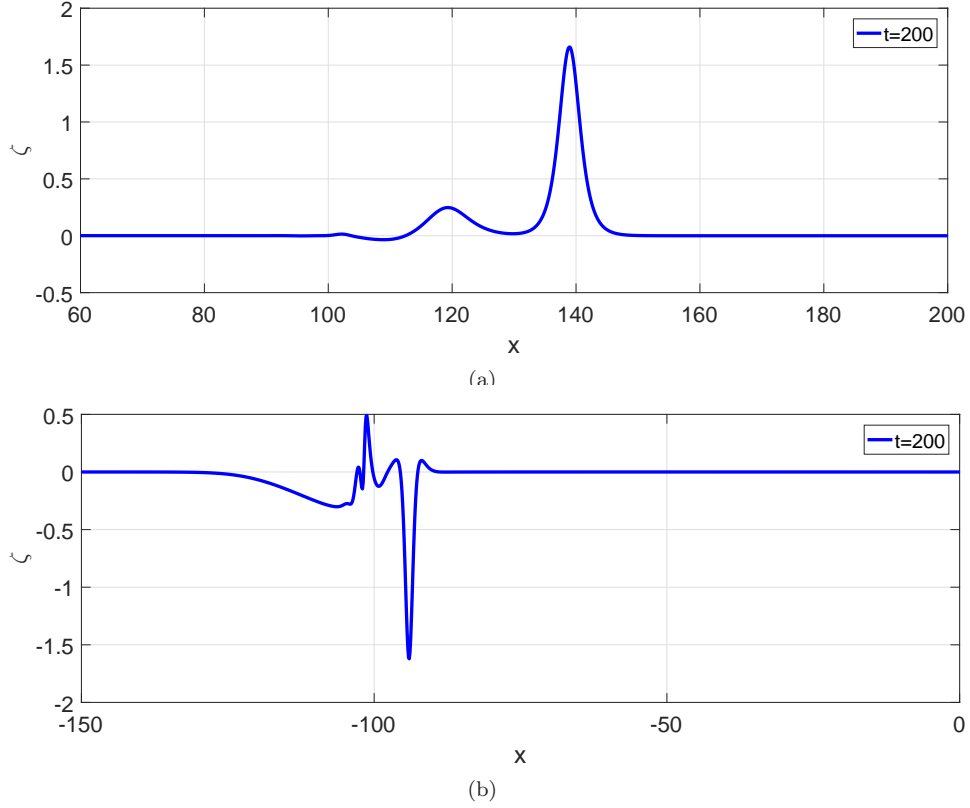


FIGURE 33. Evolution of a perturbed CSW. Case (A3) with (5.10), (5.11) $A = 6.1$, $c_s = c_{\gamma,\delta} + 0.1$. (a) First structure of the ζ component of the numerical solution; (b) Second structure.

The superposition of these profiles is taken as initial condition for the numerical method. The ensuing evolution is shown in Figure 34, while Figure 35 shows a magnified version.

The experiment shows that after the one-way collision, two solitary waves emerge. The amplitude of the larger one, compared to that of the corresponding wave before the collision, has decreased slightly; the relative difference is of 9.7×10^{-6} . In the case of the second, smaller solitary wave, the comparison shows an increase of the amplitude after the collision, which in relative terms is about 2.0×10^{-6} . The effect in the corresponding speeds is qualitatively similar to the experimental speed-amplitude relation developed in section 4, as the taller wave reduces slightly its speed after the collision, while that of the shorter one is increasing. The evolution of the errors of amplitude and speed of the tall solitary wave is displayed in Figure 36.

Additional features of this inelastic interaction are shown in Figure 35 and in magnification in Figure 37. Behind the shorter emerging wave a small dispersive tail is generated (Figures 37(b),(d),(f)), while a second, wavelet-type structure is observed to have formed and to be traveling to the left (Figures 37(a),(c),(e)).

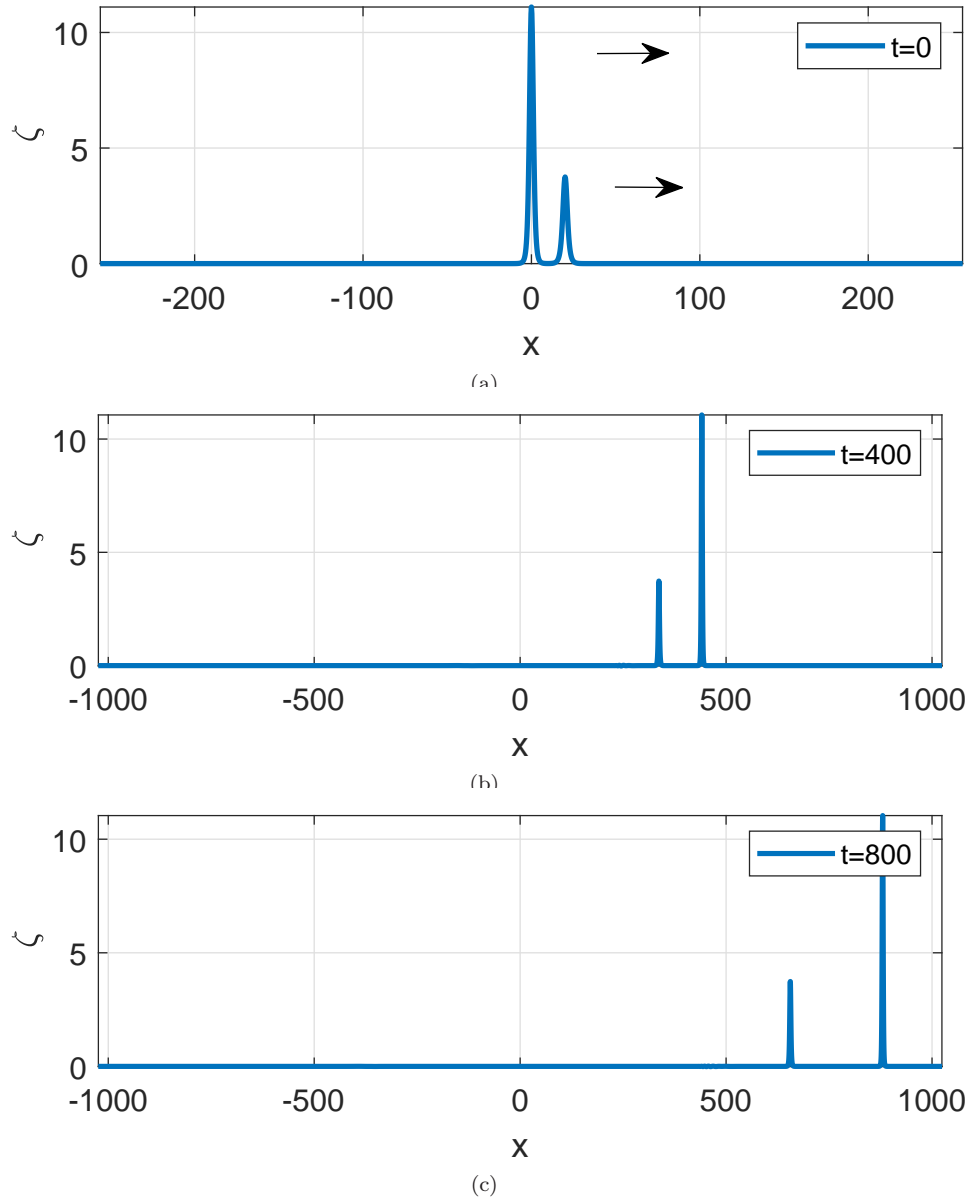
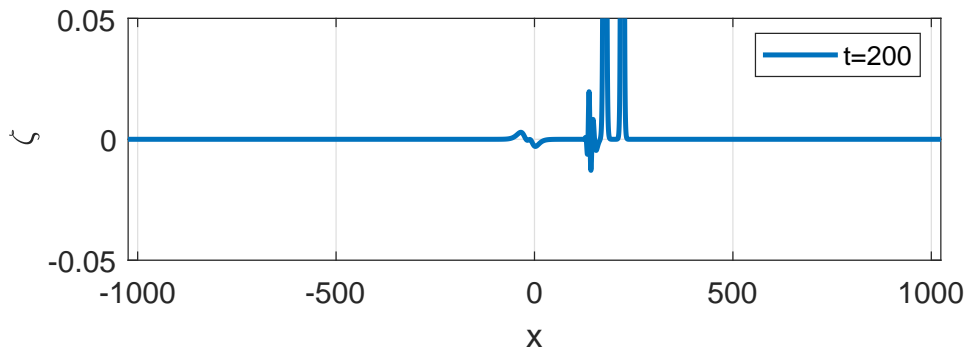
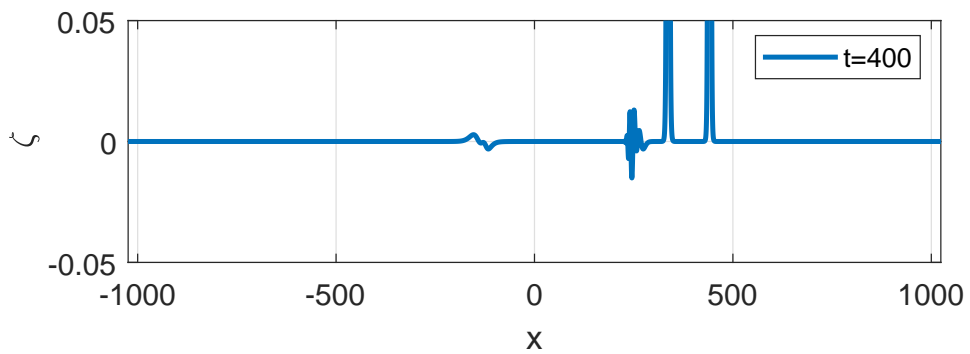


FIGURE 34. Overtaking collision of CSW's. (a)-(c) ζ component of the numerical approximation.

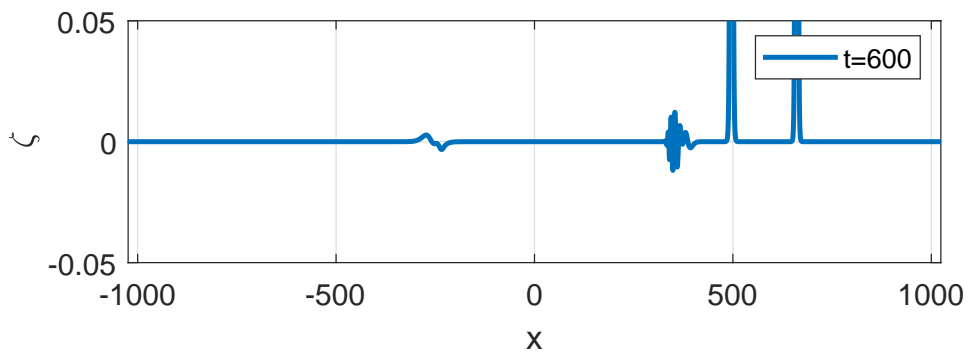
5.3.4. *Head-on collisions.* Two experiments on head-on collisions are reported here. With the same values of the parameters as in (5.10), in the first experiment we follow the evolution of the superposition of two approximate CSW-profiles of equal heights, initially centered at $x = \pm 20$, with opposite speeds of absolute values equal to $c_s = c_{\gamma,\delta} + 0.5 \approx 1.0976$, the waves undergo a symmetric head-on collision, shown in Figures 38 and 39.



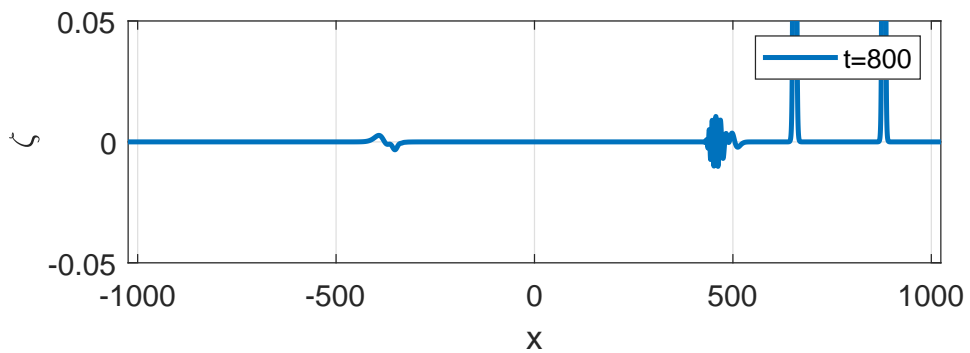
(a)



(b)



(c)



(d)

FIGURE 35. Overtaking collision of CSW's. Magnifications of the numerical solution of Figure 34.

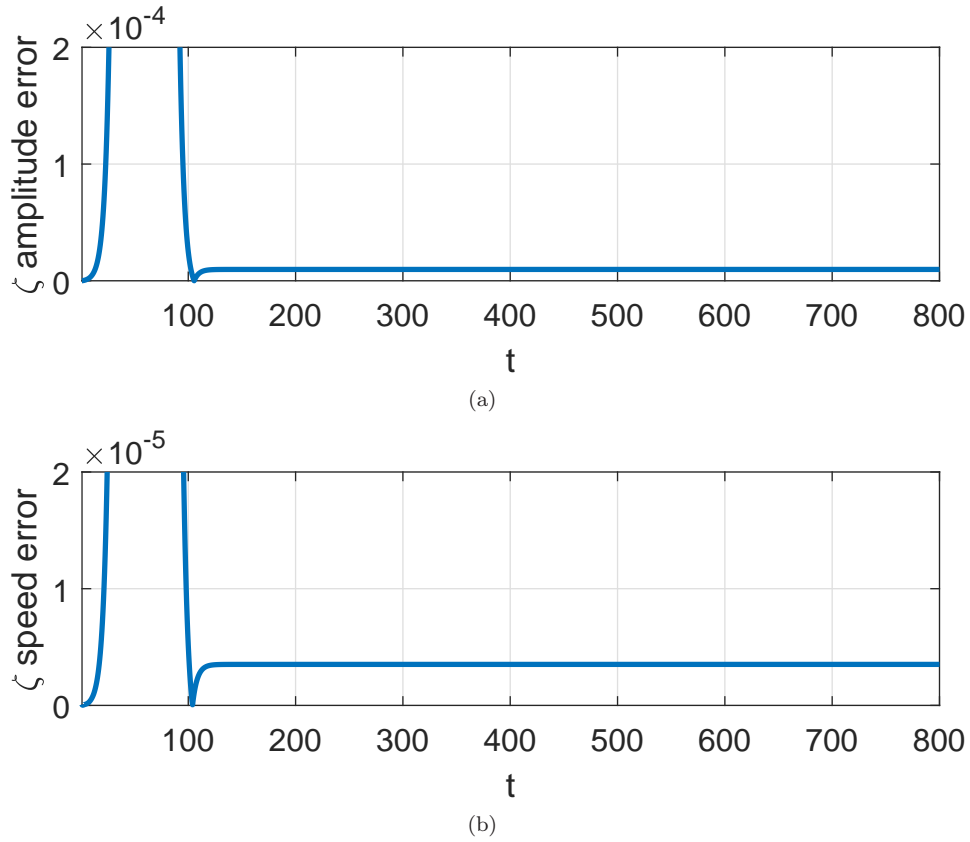


FIGURE 36. Overtaking collision of CSW's. Evolution of amplitude (a) and speed (b) errors of the tall emerging solitary wave (ζ component of the numerical solution).

The outcome of the collision is symmetric as well. After the interaction, there emerge two solitary waves and structures traveling behind them, similar to ones already observed in other experiments. In this case, the amplitude of the emerging right-traveling CSW is smaller than that of the initial one with a relative difference of about 1.8×10^{-3} . The emerging waves are also slightly slower than the initial ones, with a relative decrease of 6.4×10^{-4} in their speeds.

The structures behind the solitary waves, shown in more detail in Figures 40 and 41, are of bigger size than those of the previous experiment of overtaking collision, but seem to be again of dispersive and nonlinear type. The form of the nonlinear structure, however, is not yet clear from Figure 41.

The second experiment concerns a non-symmetric head-on collision. Here the initial condition is a superposition of two approximate CSW profiles, one with amplitude 11.101, speed $c_s^{(1)} = c_{\gamma,\delta} + 0.5 \approx 1.0976$ (traveling to the right) and centered at $x = -20$, and a second one with amplitude 4.8324, absolute value of speed equal to $c_s^{(2)} = c_{\gamma,\delta} + 0.25 \approx 0.8476$ traveling to the left and centered at $x = 20$. The evolution at several time instances of the corresponding numerical approximation

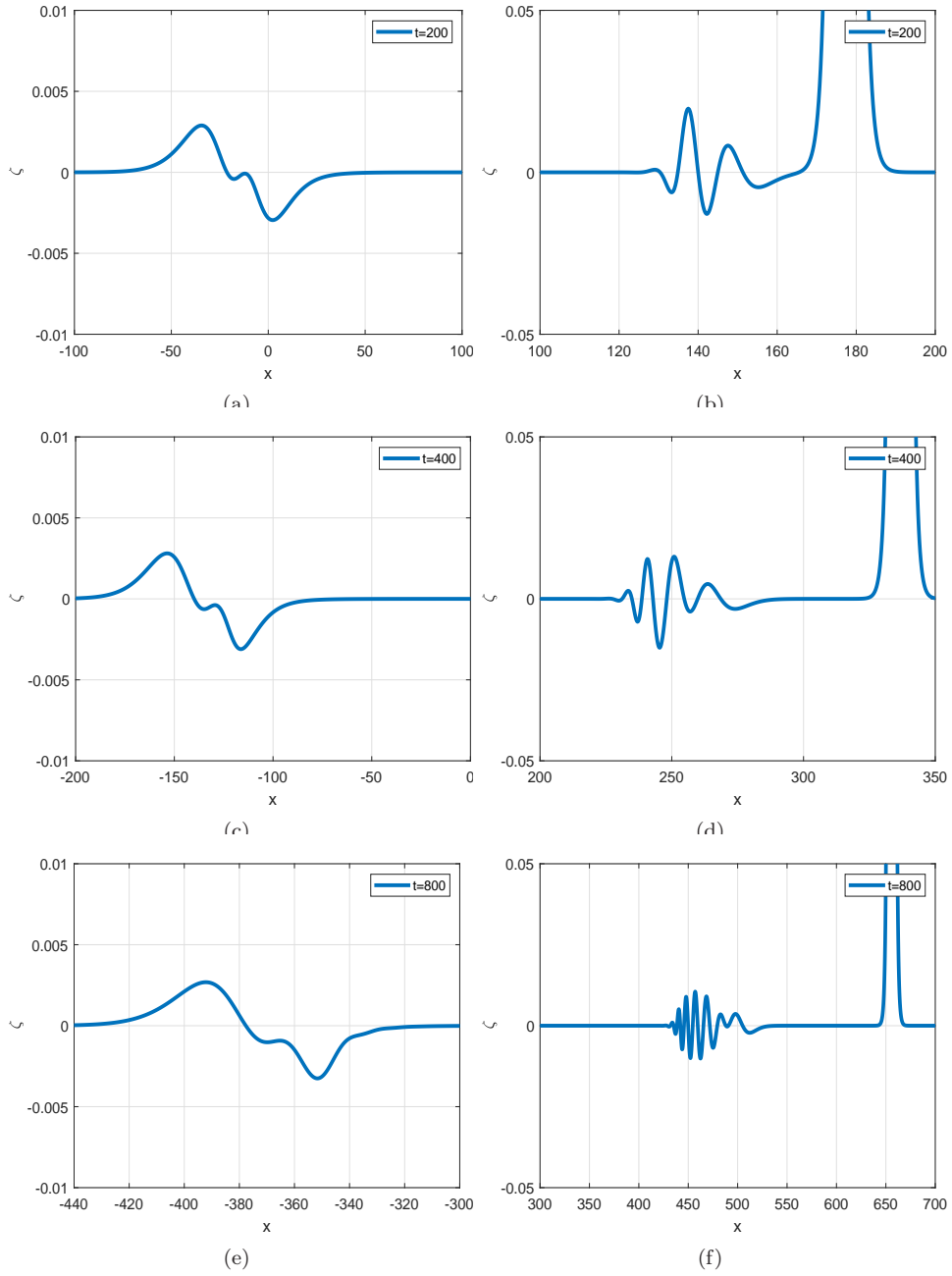


FIGURE 37. Overtaking collision of CSW's. Magnifications of the numerical solution of Figure 35.

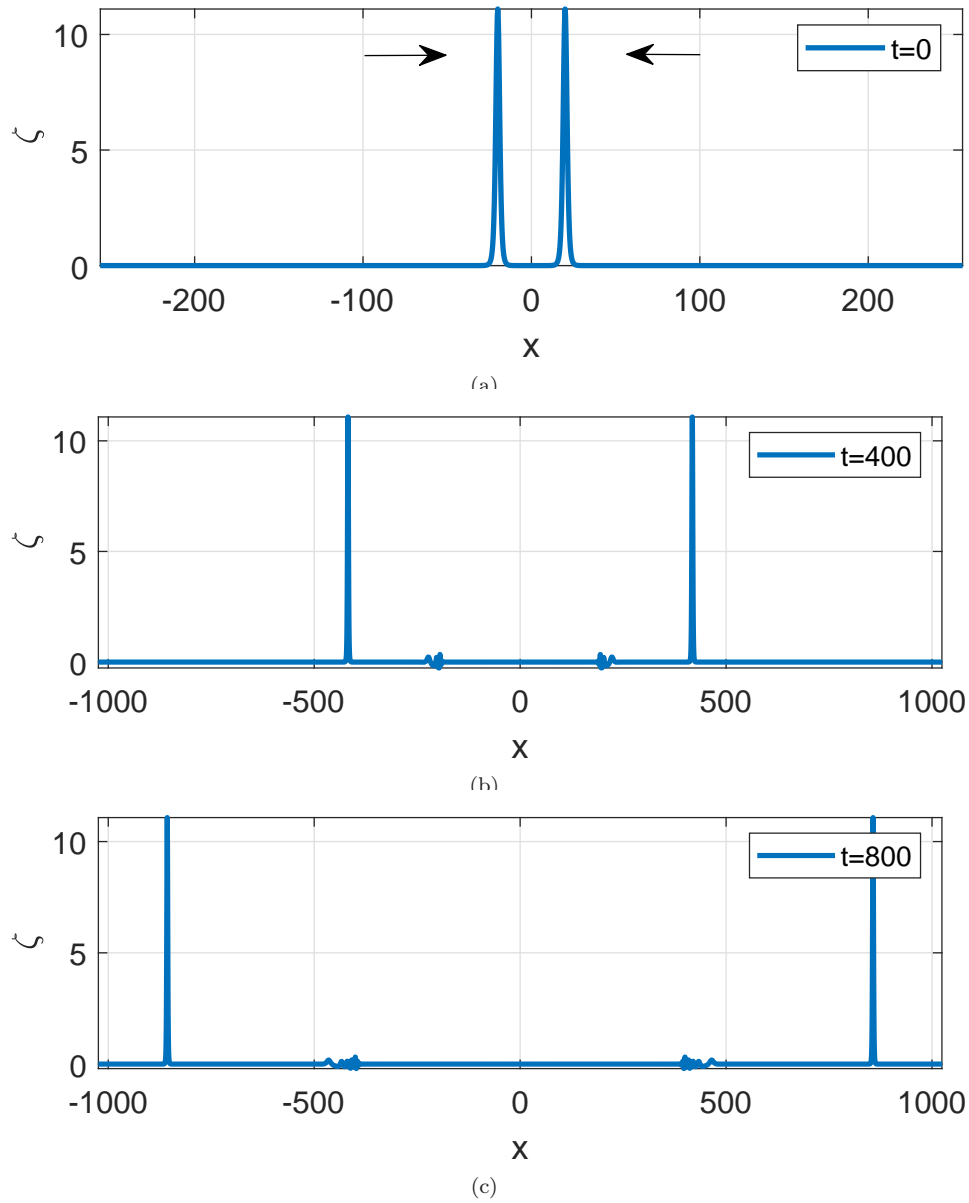


FIGURE 38. Symmetric head-on collision of CSW's. (a)-(c) ζ component of the numerical approximation.

of ζ is shown in Figures 42 and 43. After the non-symmetric interaction, the taller emerging CSW has smaller amplitude than before the collision (with a relative difference of about 6.3×10^{-4} , see Figure 46(a)) but the amplitude of the shorter emerging CSW has decreased more (about 5.2×10^{-3}). (Consequently, the emerging CSW's are slower than their corresponding counterparts before the collision, cf. Figure 46(b)). The tails trailing the emerging waves are not symmetric either

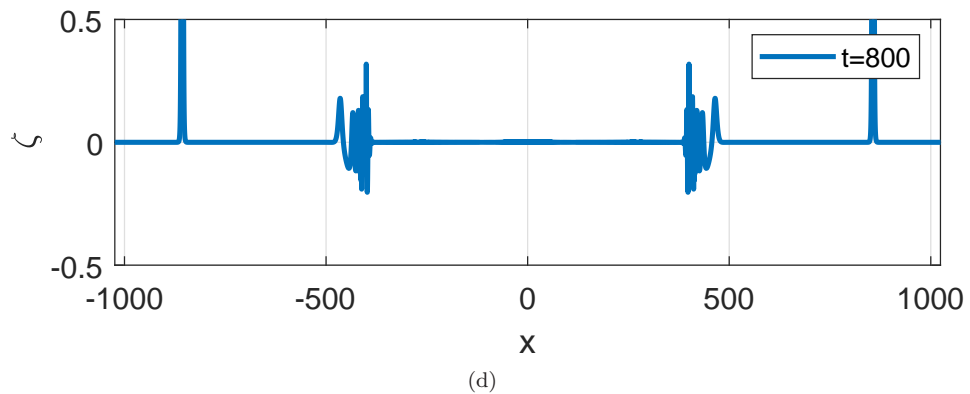
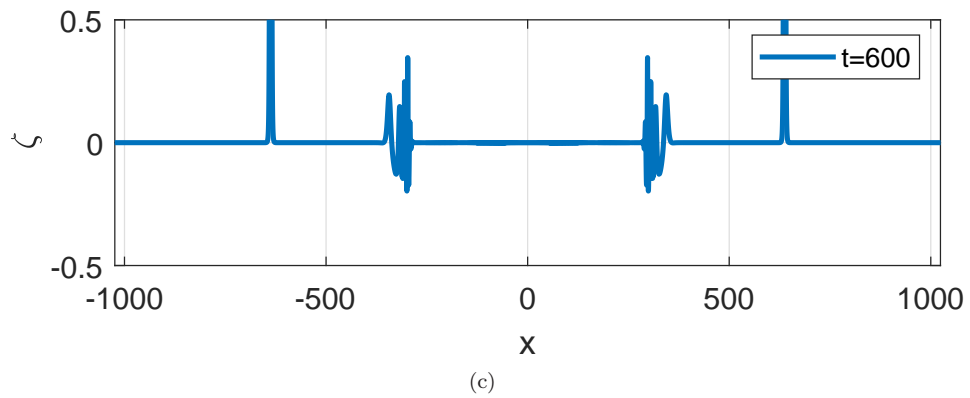
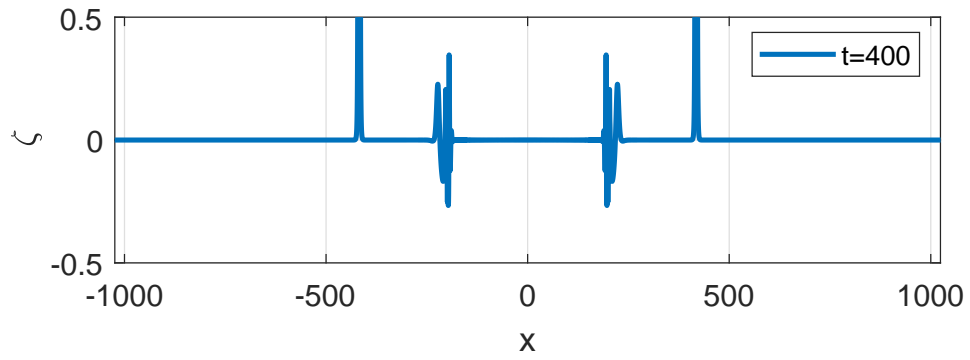
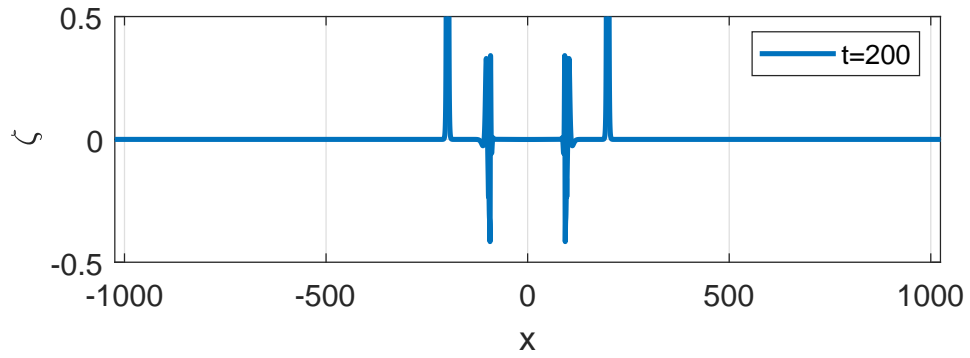


FIGURE 39. Symmetric head-on collision of CSW's. Magnifications of the numerical solution of Figure 38.

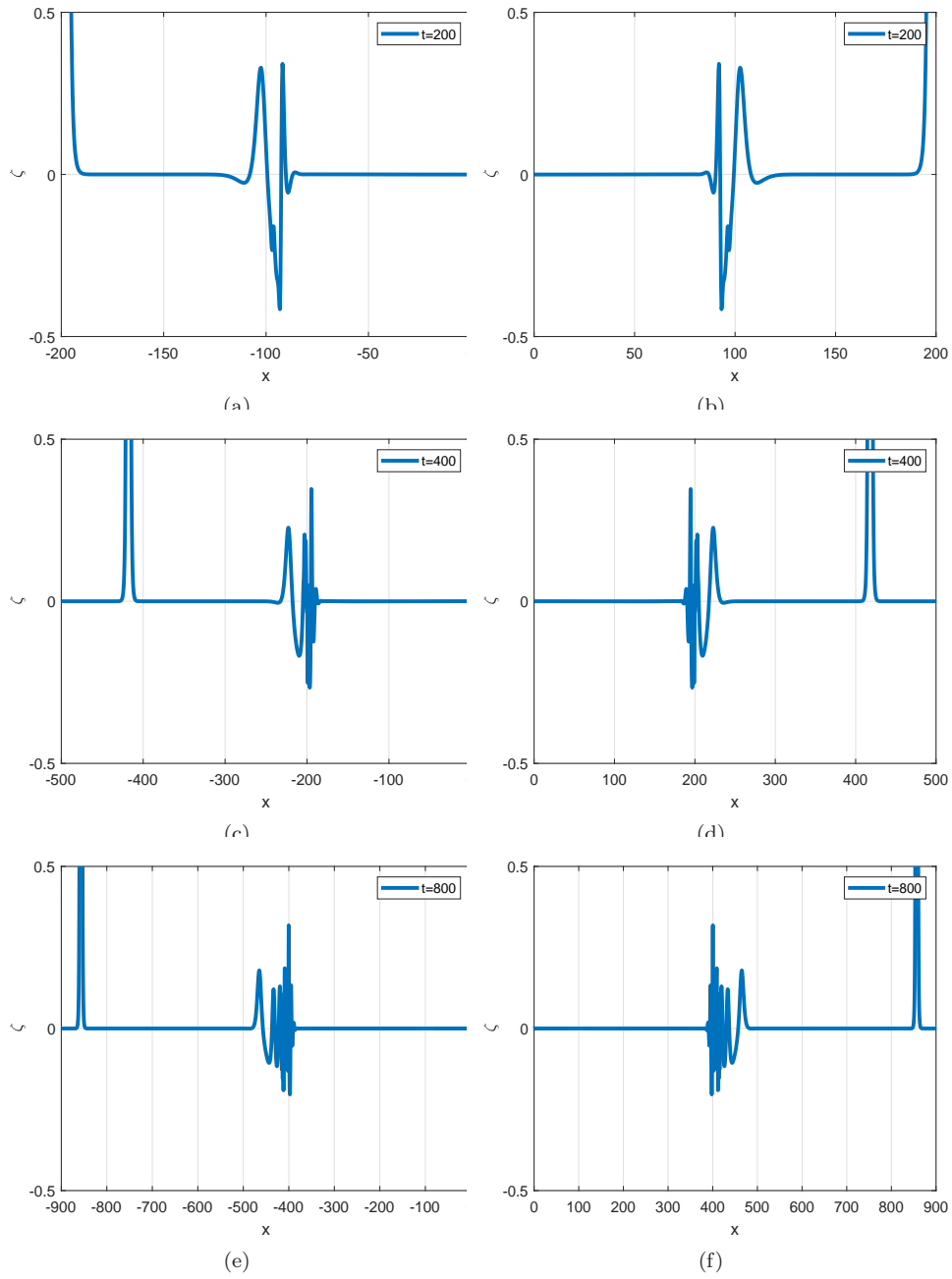


FIGURE 40. Symmetric head-on collision of CSW's. Magnifications of the numerical solution of Figure 39.

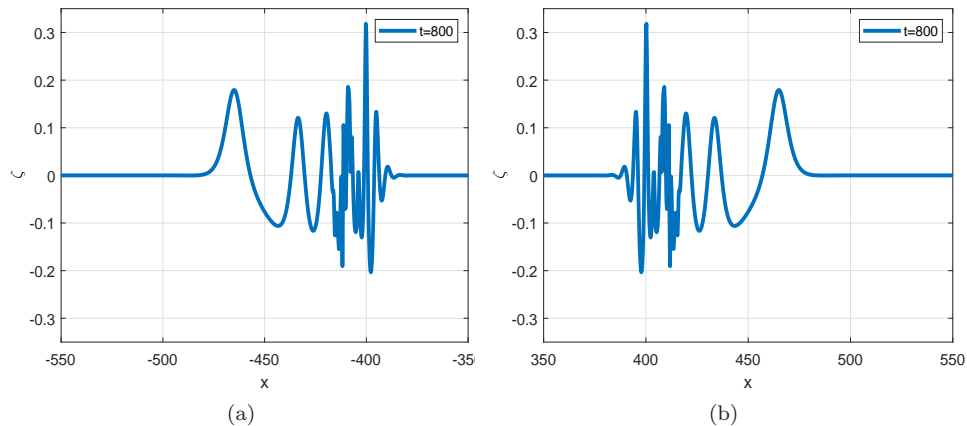


FIGURE 41. Symmetric head-on collision of CSW's. Magnifications of the numerical solution of Figure 40(c).

and they seem to have a similar structure to those of the symmetric head-on collision shown in Figure 38: A wavelet-type form in front and a strong dispersive component behind. This is shown in Figures 44 and 45. For a comparison with the symmetric case see Figure 47.

5.3.5. Resolution property. In addition to the evidence of generation of more than one CSW observed in the evolution of initial profiles with larger perturbations in section 5.3.2, the resolution into solitary waves also appears in the evolution of other types of initial conditions. This is illustrated in Figures 48 and 49, which represent the temporal behaviour of the ζ -component of the numerical solution emerging from an initial Gaussian pulse $\zeta(x, 0) = Ae^{-\tau x^2}$, $u(x, 0) = \zeta(x, 0)$, with $A = 2$, $\tau = 0.01$. In this example, a train of solitary waves of elevation is formed, followed by a left-traveling dispersive structure, see Figure 50. The evolution of the maximum of the ζ -component of the numerical solution is shown in Figure 51(a). It stabilizes to around 4.1790, which is the amplitude of the leading solitary wave profile of the train. The speed, computed from the point where the maximum is attained, cf. [33], is shown in Figure 51(a), and is about 8.1779×10^{-1} .

5.4. GSW dynamics. Numerical experiments. In this section we illustrate some aspects of the dynamics of GSW's in the generic case (A2). As in the previous section, the experiments are concerned with perturbations and collisions of GSW's.

5.4.1. Perturbations of GSW. We consider the parameters

$$\begin{aligned} \gamma &= 0.5, \delta = \frac{\gamma + \sqrt{\gamma^2 + 8}}{2} \approx 1.6861, \\ c &= -1/6, b = 1/9, d = 4/3, a = \kappa_1(1/6 - b - c - d) \approx -0.5083, \end{aligned} \quad (5.19)$$

and generate the corresponding approximate GSW, with amplitude 4.5728×10^{-2} and speed 4.8824×10^{-1} . (The values of γ and δ in (5.19) are taken appropriately to ensure that the parameters a, b, c and d satisfy the conditions in (A2) in Table

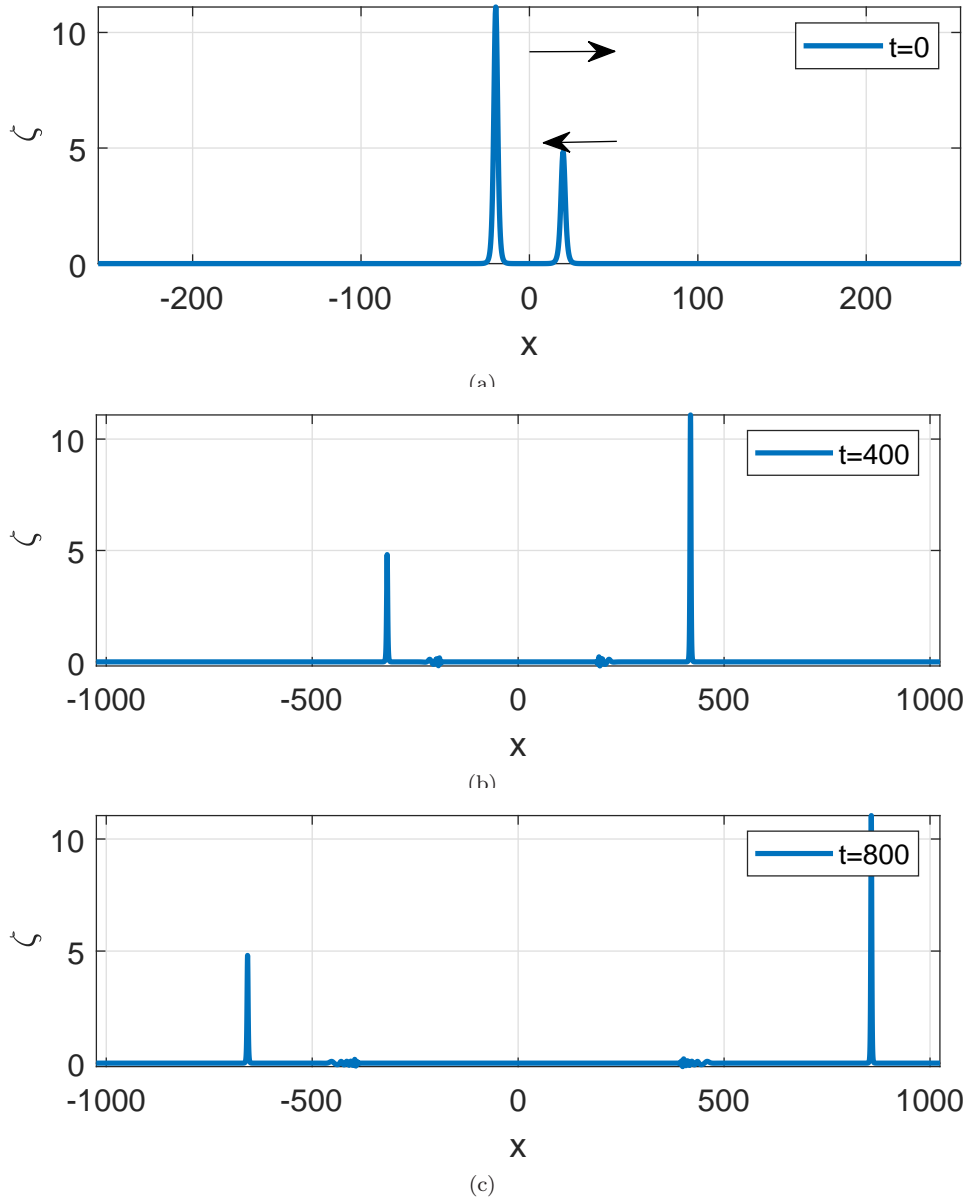


FIGURE 42. Non-symmetric head-on collision of CSW's. (a)-(c) ζ component of the numerical approximation.

1.) The first experiment consists of perturbing the two components (ζ_s^N, u_s^N) of the GSW with the same quantity $A = 1.01$, i. e. considering

$$\zeta_s^N(0) = A\zeta_s^N, u_s^N(0) = Au_s^N, \tag{5.20}$$

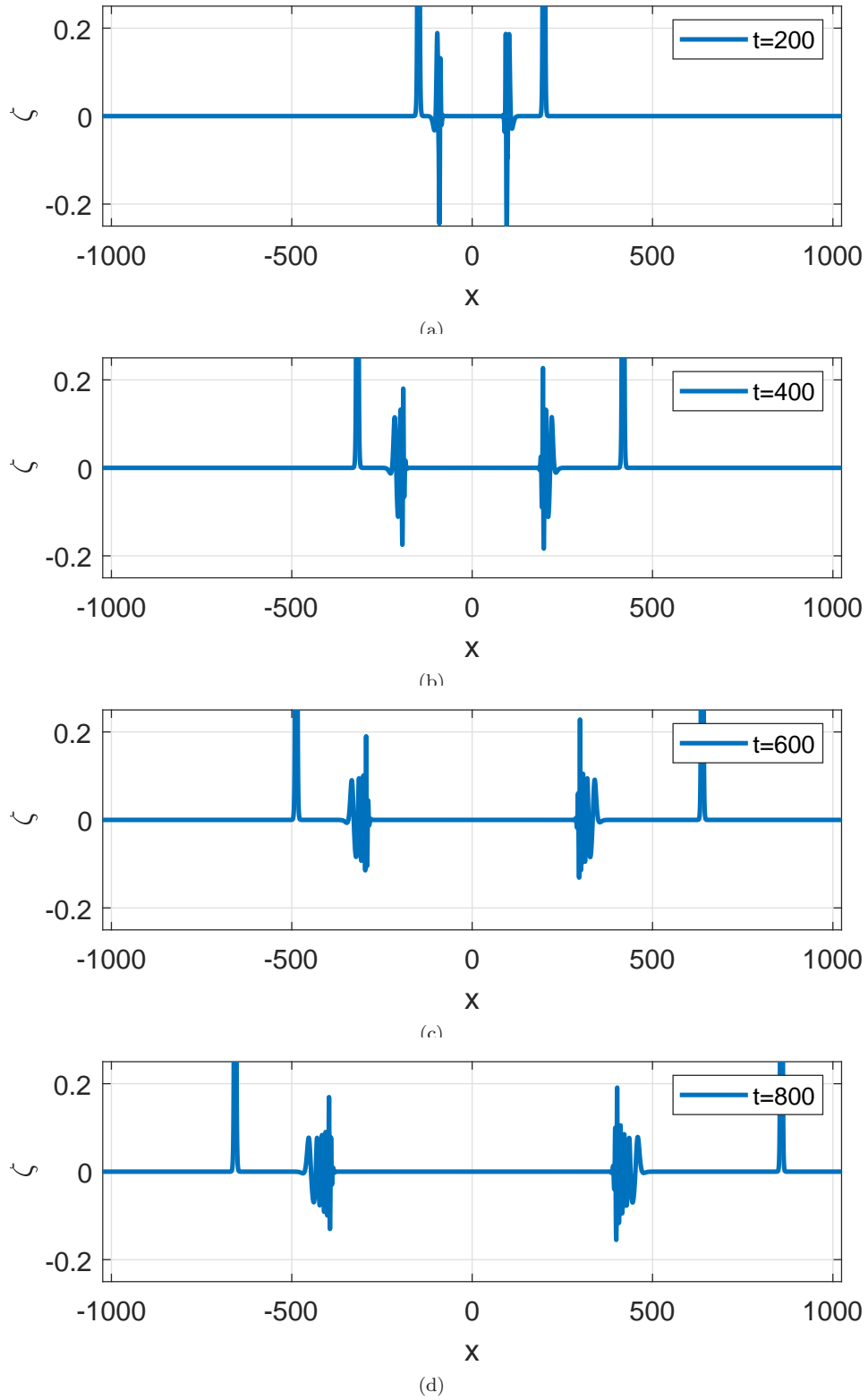


FIGURE 43. Non-symmetric head-on collision of CSW's. Magnifications of the numerical solution of Figure 42.

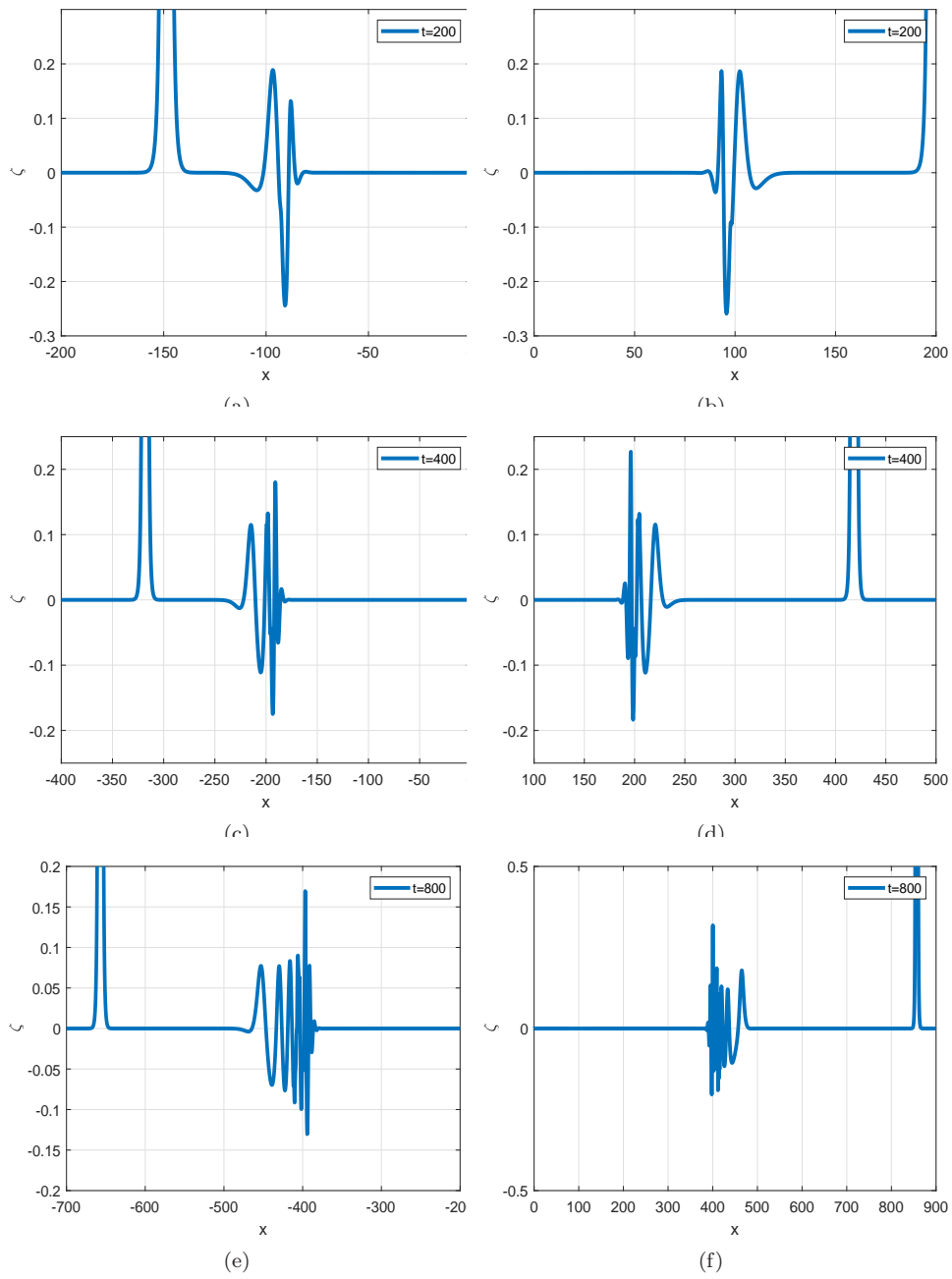


FIGURE 44. Non-symmetric head-on collision of CSW's. Magnifications of the numerical solution of Figure 43.

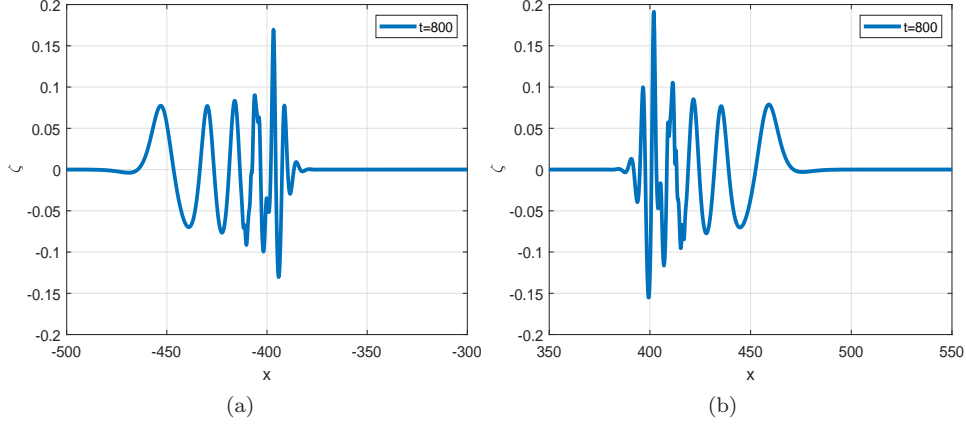


FIGURE 45. Non-symmetric head-on collision of CSW's. Magnifications of the numerical solution of Figure 44(e),(f).

as initial condition of the numerical method and monitoring the evolution of the corresponding numerical solution. This is shown in Figure 52. This small perturbation of the GSW generates a new GSW.

The evolution of the amplitude and speed of the emerging wave, shown in Figures 53(a),(b), suggests that its parameters stabilize at slightly larger values than those of the initial condition. Specifically, the amplitude of the perturbed initial GSW is of about 4.612×10^{-2} and that of emerging GSW is between 4.61×10^{-2} and 4.62×10^{-2} . In the case of the speed, the relative difference is about 3.26×10^{-4} . The structure of the ripples appears to be the same. Since we expect that the small perturbation will generate some sort of dispersion, for this experiment these are apparently of very small size and are probably hidden in the ripples.

The study of the structure of dispersive tails via the linearized system (5.12), (5.13), made in section 5.3 for the generic case (A3) of classical solitary waves can be adapted to the generic case (A2) for generalized solitary waves. Now we have $p_2 > 0$ in (5.16) and the cases (i)-(iii) are as follows:

- (i) $p_1 < 0$. Compared to the analogous case in section 5.3, the only change occurs when $\Delta = 0$. Then $P(x)$ has a double root at $x = x_* = -p_2/2 < 0$; therefore, $\phi(x)$ is decreasing for $x \geq 0$.
- (ii) $p_1 = 0$. Here $P(x)$ has only one root $x = x_* = p_3/p_2 > 0$ and therefore:
 - (1) If $0 \leq x \leq x_*$, then $\phi(x)$ is decreasing with $1 > \phi(x) \geq \phi(x_*)$.
 - (2) If $x_* \leq x$, then $\phi(x)$ is increasing with $\phi(x_*) \leq \phi(x) \leq \phi_* < 1$.
- (iii) $p_1 > 0$. Then $\Delta > 0$ and P has two simple roots, one positive and one negative. The same behaviour as in section 5.3 follows.

On the other hand, the case (A1) is different. Now we have

$$\phi(x) = \sqrt{\frac{(1 - \tilde{a}x)(1 - cx)}{1 + dx}}, \quad \tilde{a} = \frac{a}{\kappa_1}, \quad x \geq 0,$$

and $p_1 = \tilde{a}cd > 0$ in (5.16). The case (iii) of section 5.3 applies but note that now $\phi(x) \rightarrow +\infty$ as $x \rightarrow +\infty$ (see Figure 54(a)). Therefore $\phi(x) > 1$ for large enough

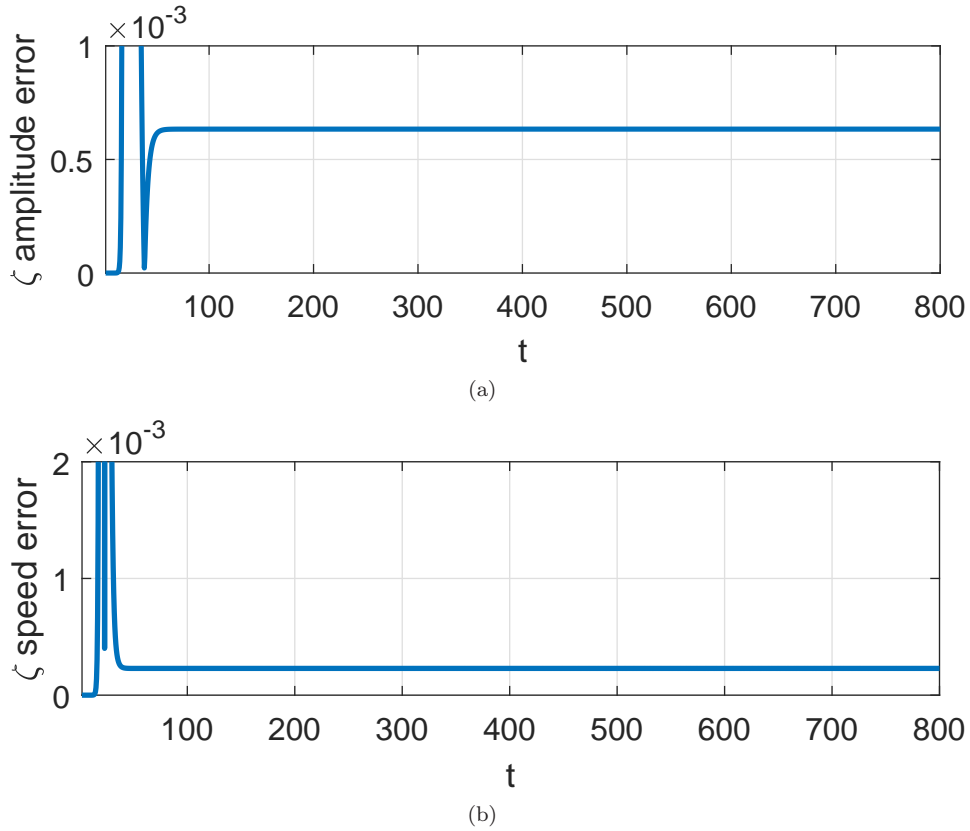


FIGURE 46. Non-symmetric head-on collision of CSW's. Evolution of amplitude (a), and speed (b) errors of the right-traveling emerging solitary wave (ζ component of the numerical approximation); cf. Figure 42.

$x > 0$. This means that for sufficiently large $|k|$ and from (5.15) we have

$$-c_s - c_{\gamma,\delta} < v_-(k) < -c_s < v_+(k),$$

and $v_+(k) > -c_s + c_{\gamma,\delta}$. This implies the existence of plane wave components of small amplitude traveling to the right and in front of the GSW. Similarly, the formation of two dispersive groups, one traveling to the left behind the solitary wave and one to the right in front of it, is suggested by the form of the function ψ , given by (5.18), for the case (A1), and displayed in Figure 54(b).

The range of the size of the perturbations from which the GSW evolves in a stable way seem to be smaller than those for CSW. Figures 53(c),(d) show the evolution of amplitude and speed, respectively, of the numerical solution from a perturbed GSW with (5.19), (5.20) and $A = 1.1$. Note that by $t = 800$ the parameters have not stabilized.

As the perturbation parameter A grows, new phenomena in the dynamics appear. Figures 55 and 56 show the evolution of the numerical solution generated from an initial GSW profile of the system with parameters given by (5.19) multiplied by

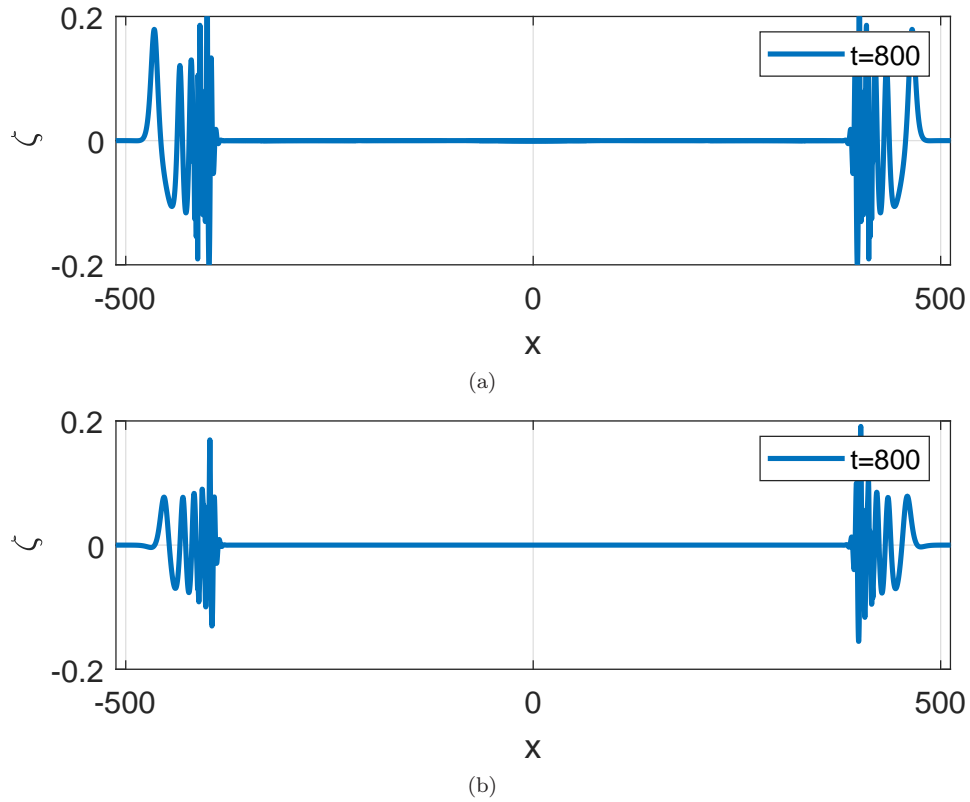


FIGURE 47. Symmetric vs. non-symmetric head-on collisions of CSW's. (a) Magnification of Figure 39(d); (b) Magnification of Figure 43(d).

a perturbation factor $A = 4.1$ as in (5.20). The experiment suggests (cf. Figure 56) that the perturbed initial GSW evolves into a new GSW, although by the final time of simulation ($t = 800$), Figure 58 shows that the amplitude and speed do not seem to have completely stabilized. Behind the main wave, similar structures to those observed in the case of large perturbations of CSW's (cf. Figures 29 and 30) seem to be generated, superimposed on the ripples. They are observed in Figures 57(a),(b). By $t = 400$, some perturbation tails have formed in front of the main emerging wave, see Figure 57(c). This fact and the behaviour of the amplitude and speed of the main pulse observed in Figure 58 suggest a possible instability.

5.4.2. Resolution. In order to study the resolution property in systems with generalized solitary wave solutions, we consider again the values of the parameters given by (5.19) and use, as initial condition, the same Gaussian pulse as that considered in section 5.3 for CSW's, of the form $\zeta(x, 0) = Ae^{-\tau x^2}$, with $A = 2$, $\tau = 0.01$, and $u(x, 0) = \zeta(x, 0)$. The evolution of the numerical approximation is illustrated in Figure 59.

The behaviour of the approximation of ζ may be compared with that of the CSW case (Figures 48-50). Now, the Gaussian profile seems to evolve into a train

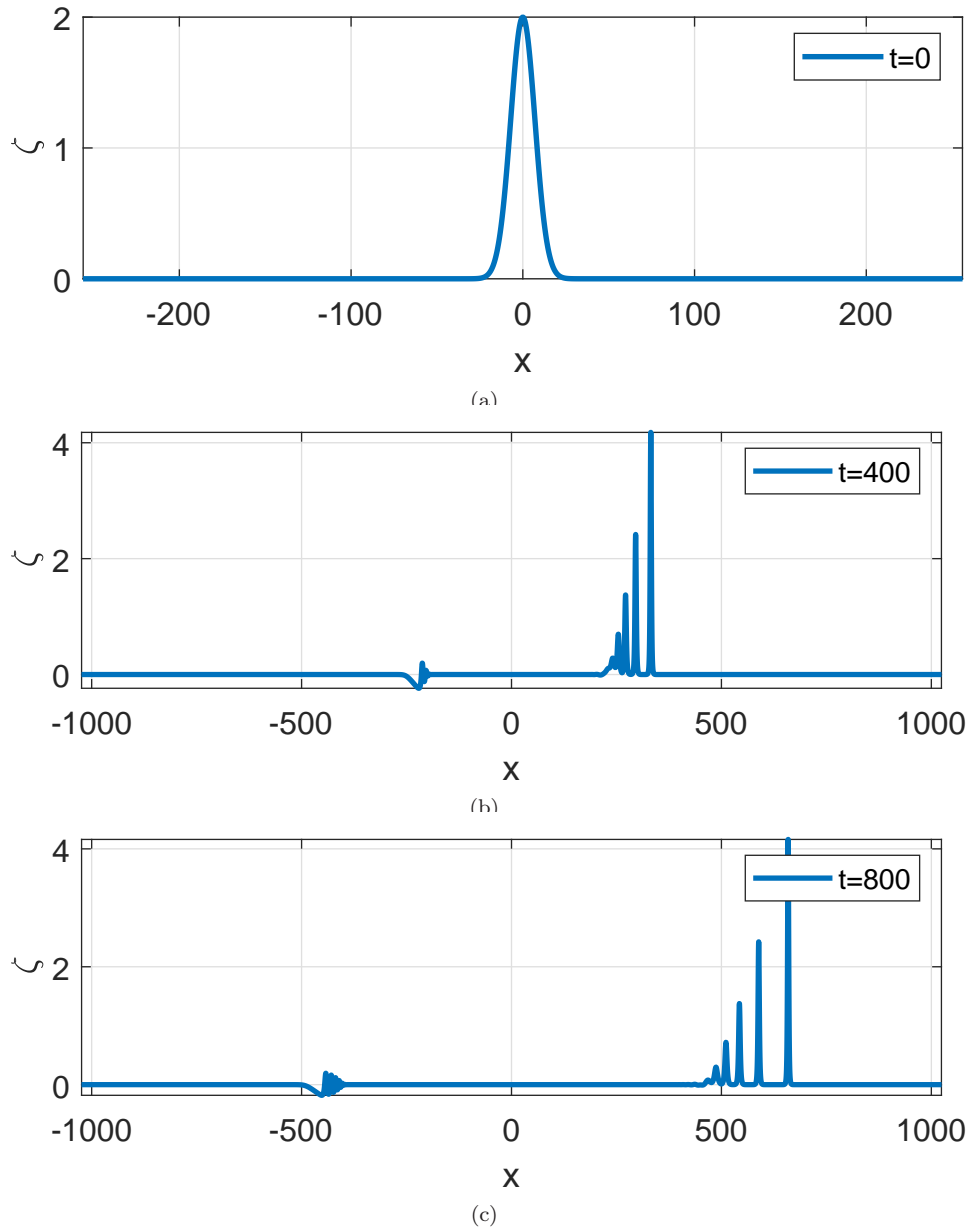


FIGURE 48. Resolution property. Initial Gaussian pulse $\zeta(x, 0) = Ae^{-\tau x^2}$, $u(x, 0) = \zeta(x, 0)$, with $A = 2$, $\tau = 0.01$. Case (A3). (a)-(c) ζ component of the numerical solution.

of solitary waves of elevation, followed by some structures of different form. They are displayed in more detail in Figure 60. Figure 60(a) is a magnification of the tail formed just behind the solitary wave train and Figure 60(b) is a detail of the solution between two solitary waves. Some dispersive pulses are radiated in front

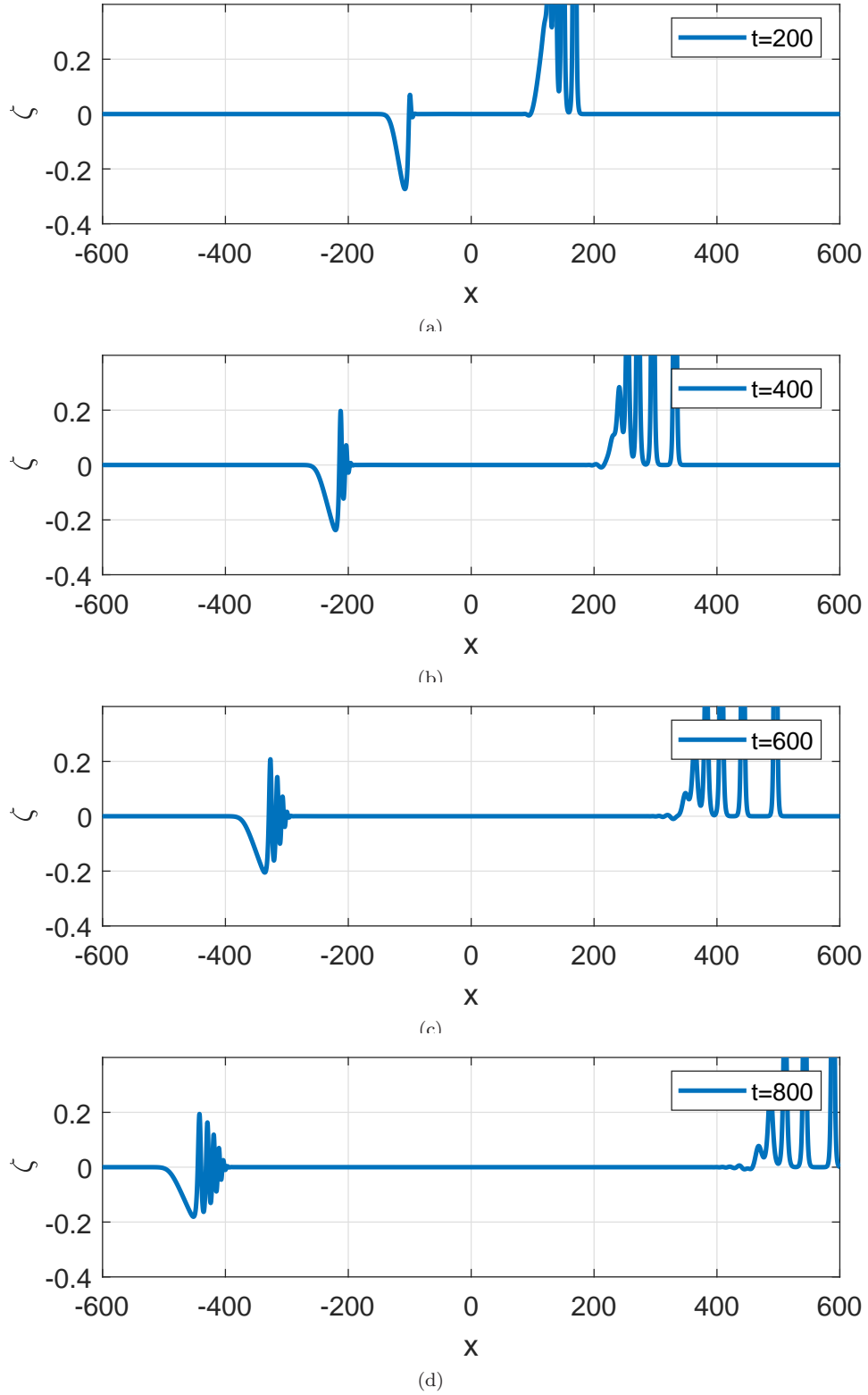


FIGURE 49. Resolution property. Initial Gaussian pulse $\zeta(x, 0) = Ae^{-\tau x^2}$, $u(x, 0) = \zeta(x, 0)$, with $A = 2$, $\tau = 0.01$. Case (A3). (a)-(c) ζ component of the numerical solution (magnified).

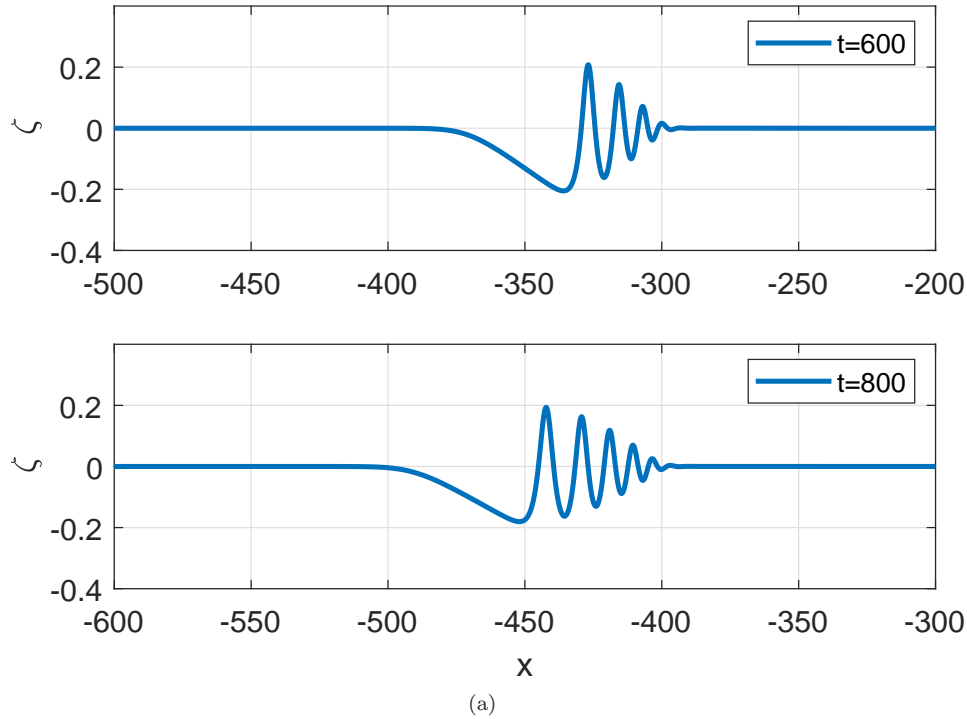


FIGURE 50. Resolution property. Initial Gaussian pulse $\zeta(x, 0) = Ae^{-\tau x^2}$, $u(x, 0) = \zeta(x, 0)$, with $A = 2$, $\tau = 0.01$. Case (A3). ζ component of the numerical solution at (a) $t = 600$; (b) $t = 800$.

of each profile. These are also observed behind the wave train of solitary waves, see Figure 60(c). A third structure, magnified in Figure 60(d), seems to consist of a train of classical solitary waves with non-monotonic decay and a dispersive tail.

5.4.3. Head-on collisions. The interactions of GSW's are illustrated with experiments of head-on collisions. The first experiment shown in the sequel is concerned with a symmetric head-on collision of GSW's. For the system with parameters given by (5.19), a superposition of approximate GSW profiles with absolute values of the speed $c_s = c_{\gamma, \delta} + 10^{-2} \approx 4.8824 \times 10^{-1}$, traveling to the right and to the left and centered at $x_0 = -20$ and $x_0 = 20$ respectively, is taken as initial condition, and the simulation of the evolution is represented in Figures 61 and 62. The initial amplitudes are about 4.5654×10^{-2} .

The temporal interval of collision lasts approximately from $t = 30$ to $t = 50$; thereafter two symmetric GSW's emerge. The evolution of the amplitude of the ζ component of the numerical solution is shown in Figure 65(a). This seems to stabilize in a value around 4.62×10^{-2} , so the emerging waves are taller (and hence faster), and the relative difference in amplitude is about 1.2×10^{-2} . By comparing Figure 62(a) with Figures 62(b) and (c), we note that after the collision the amplitude of the ripples is larger.

In order to illustrate the dynamics of non-symmetric head-on collisions, we consider, for the system with parameters given by (5.19), the evolution of an initial

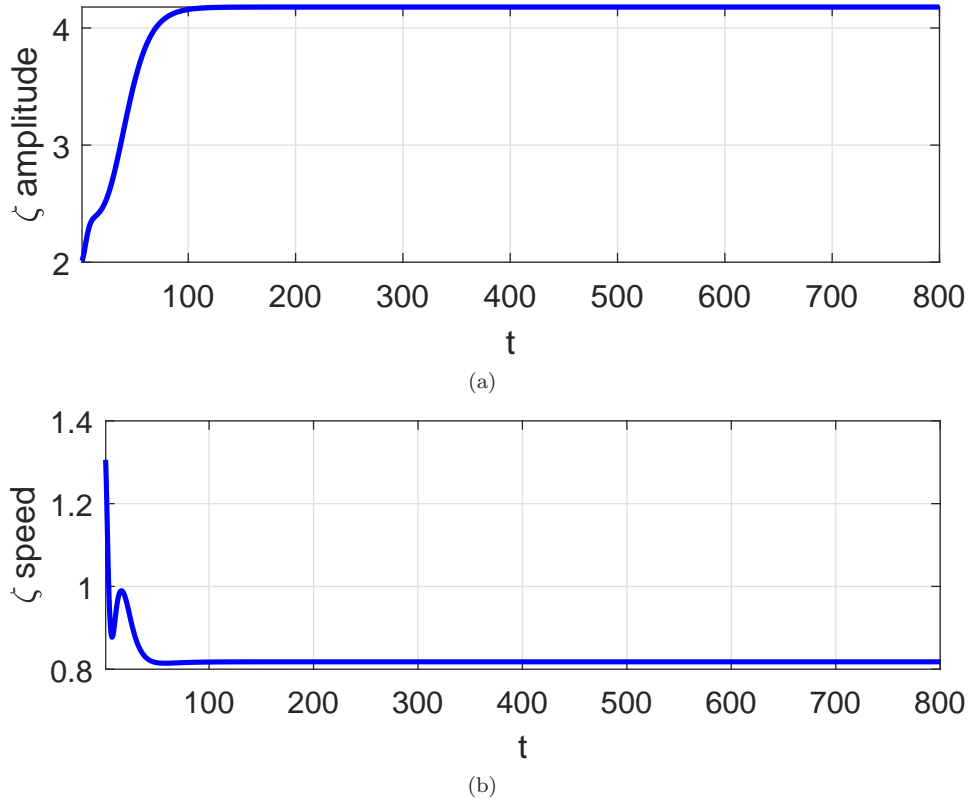


FIGURE 51. Resolution property. Initial Gaussian pulse $\zeta(x, 0) = Ae^{-\tau x^2}$, $u(x, 0) = \zeta(x, 0)$, with $A = 2$, $\tau = 0.01$. Case (A3). Evolution of amplitude (a) and speed (b) of the taller emerging solitary wave in the ζ -component of the numerical solution; cf. Figure 48.

profile consisting of a superposition of two approximate GSW's with absolute values of speeds $c_s^{(1)} = c_{\gamma, \delta} + 0.01$, centered at $x_0^{(1)} = -20$ and traveling to the right, and $c_s^{(2)} = c_{\gamma, \delta} + 0.005$, centered at $x_0^{(1)} = 20$ and traveling to the left. The results are shown in Figures 63 and 64.

Similar effects to those of the symmetric collision case are observed. Note from Figure 64 that in this case the ripples generated after the collision do not increase in amplitude, with respect to those before the interaction, in a significant way, at least in comparison with the symmetric case, cf. Figure 62.

The corresponding evolution of the amplitudes in both experiments of head-on collisions is shown in Figure 65. In the nonsymmetric case, the emerging taller wave increases in amplitude with a relative increase of 2.1×10^{-2} .

5.5. Dynamics of classical solitary wave solutions with non monotone decay. In this section we present some experiments concerning the dynamics of CSW solutions of (1.6) with non monotone decay, whose existence was justified by an application of the Normal Form Theory in section 4.1, and for speeds smaller than the corresponding speed of sound. For simplicity we focus on the behaviour

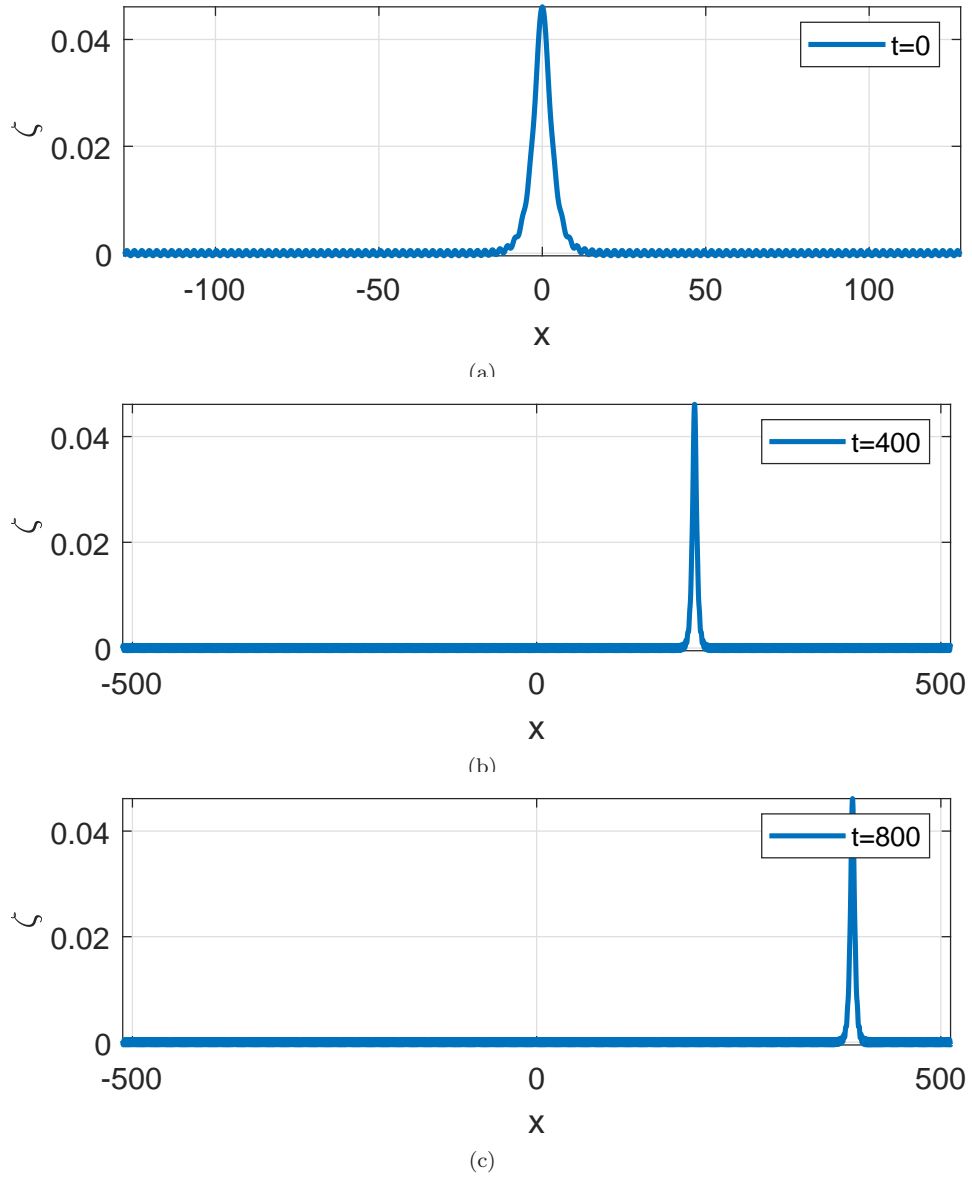
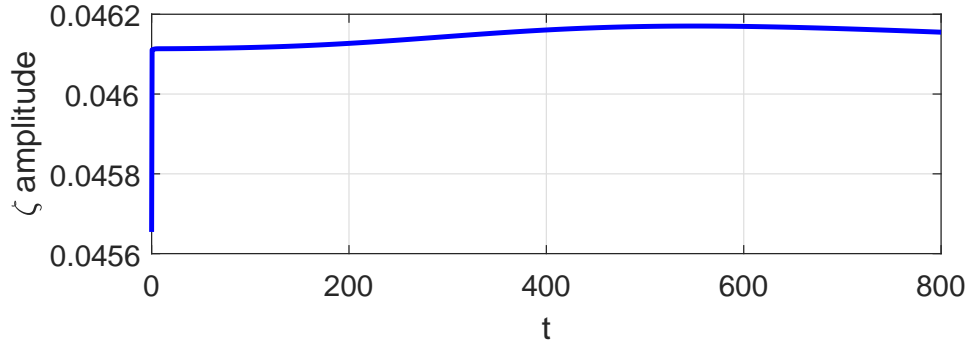


FIGURE 52. Small perturbation of a GSW. Case (A2) with (5.19), (5.20) with $A = 1.01$. (a) Perturbed GSW profile; (b), (c) ζ component of the numerical solution.

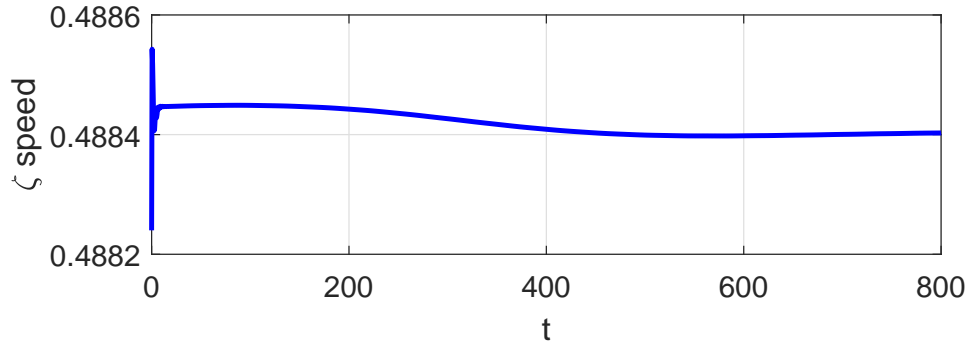
under small and large perturbations of the type (5.20) as those used in sections 5.3 and 5.4.

We consider the numerical profile obtained in section 4.2 from the parameters

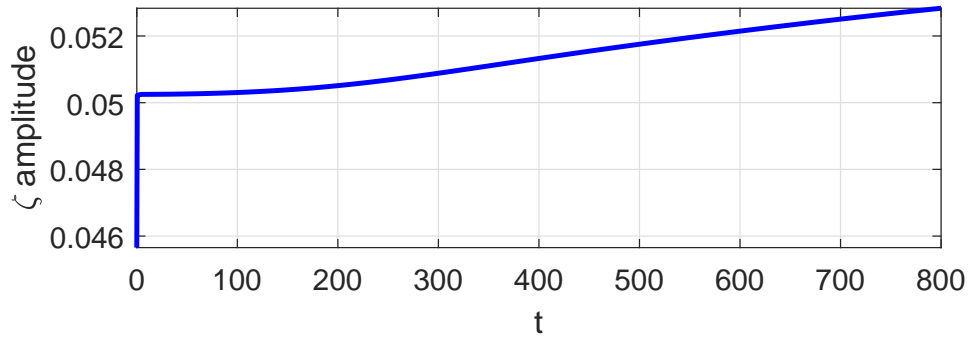
$$\begin{aligned} \gamma &= 0.5, \delta = 0.9, \\ a &= -1/9, b = 0, c = -1/6, d = S(\gamma, \delta) - \frac{a}{\kappa_1} - b - c \approx 0.7058. \end{aligned} \quad (5.21)$$



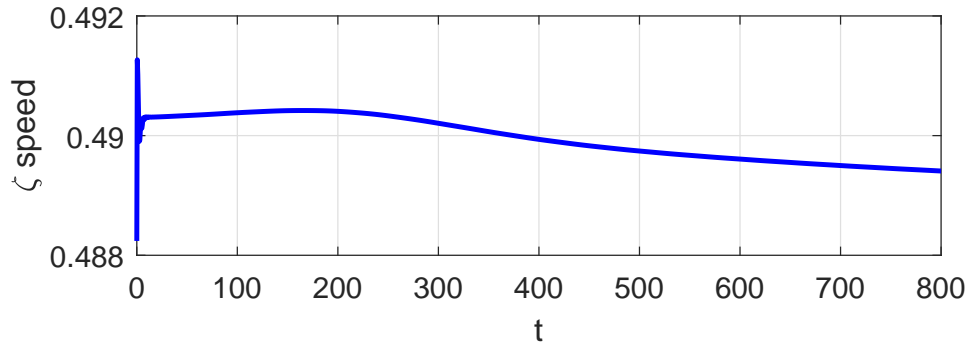
(a)



(b)



(c)



(d)

FIGURE 53. Small perturbation of a GSW. Case (A2) with (5.19), (5.20). Evolution of amplitude and speed of the tallest emerging solitary wave (ζ component of the numerical solution); (a), (b) $A = 1.01$; (c), (d) $A = 1.1$.

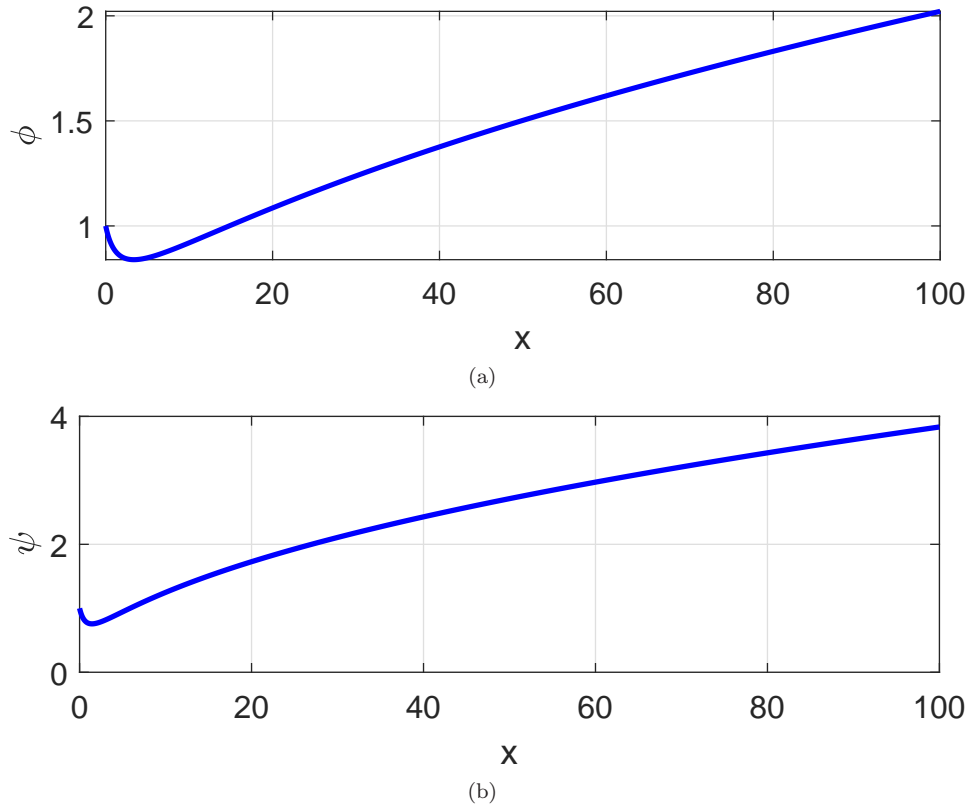


FIGURE 54. Form of the functions (a) $\phi(x)$ and (b) $\psi(x)$ for the case (A1).

The ζ component has a maximum negative excursion of about -2.8740 and the speed is $c_s = c_{\gamma,\delta} - 0.2 \approx 0.3976$. The ζ_h and v_h components are perturbed in amplitude with a perturbation factor $A = 1.1$. The perturbed wave $(A\zeta_h, Av_h)$ is taken as initial condition of the numerical method to approximate (1.6) with $L = 1024$, and the evolution of the resulting numerical approximation is monitored up to $t = 800$ and shown in Figure 66.

During the evolution, a new solitary wave of the same type is formed. Compared to the initial perturbed wave, whose maximum negative excursion was approximately -3.1614 , the emerging wave dips to about -3.1376 . The wave is slower, with a speed around 0.3832 , see Figure 69.

Behind and in front of the emerging solitary wave, some other small structures form. They are observed in the magnification of Figure 66 given by Figure 67, and displayed in more detail in Figure 68.

The main character of these small-amplitude waves seems to be dispersive. The generation of dispersive oscillations in front of the emerging solitary wave can be justified from the study of small-amplitude solutions of the linearized system (5.12), (5.13). In this case we have a linear dispersion relation of the form

$$\omega(k) = \omega_{\pm}(k) = -kc_s \pm c_{\gamma,\delta}k\phi(k^2),$$

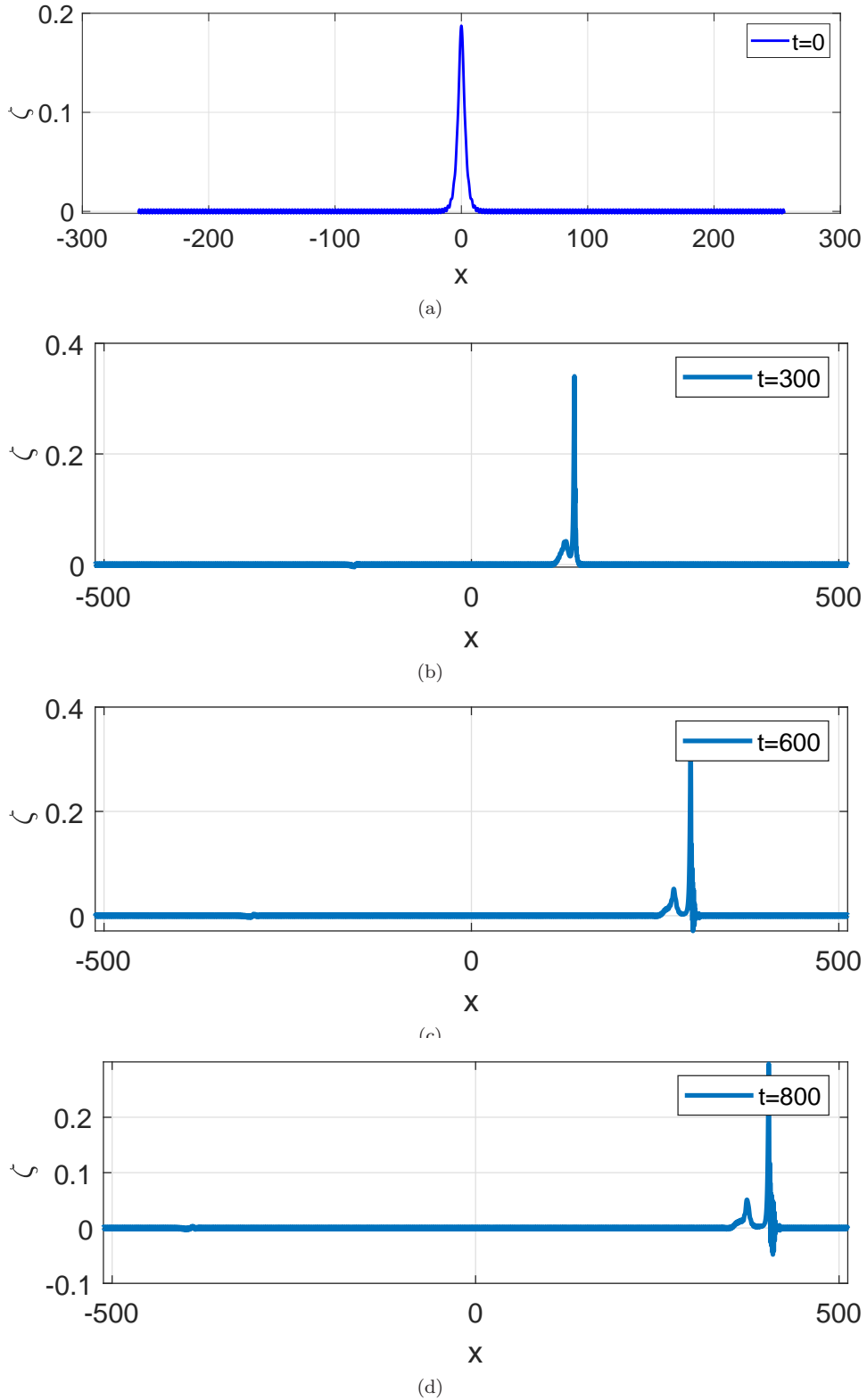


FIGURE 55. Large perturbation of a GSW. Case (A2) with (5.19), (5.20) with $A = 4.1$. (a) Perturbed GSW profile; (b), (c) ζ component of the numerical solution.

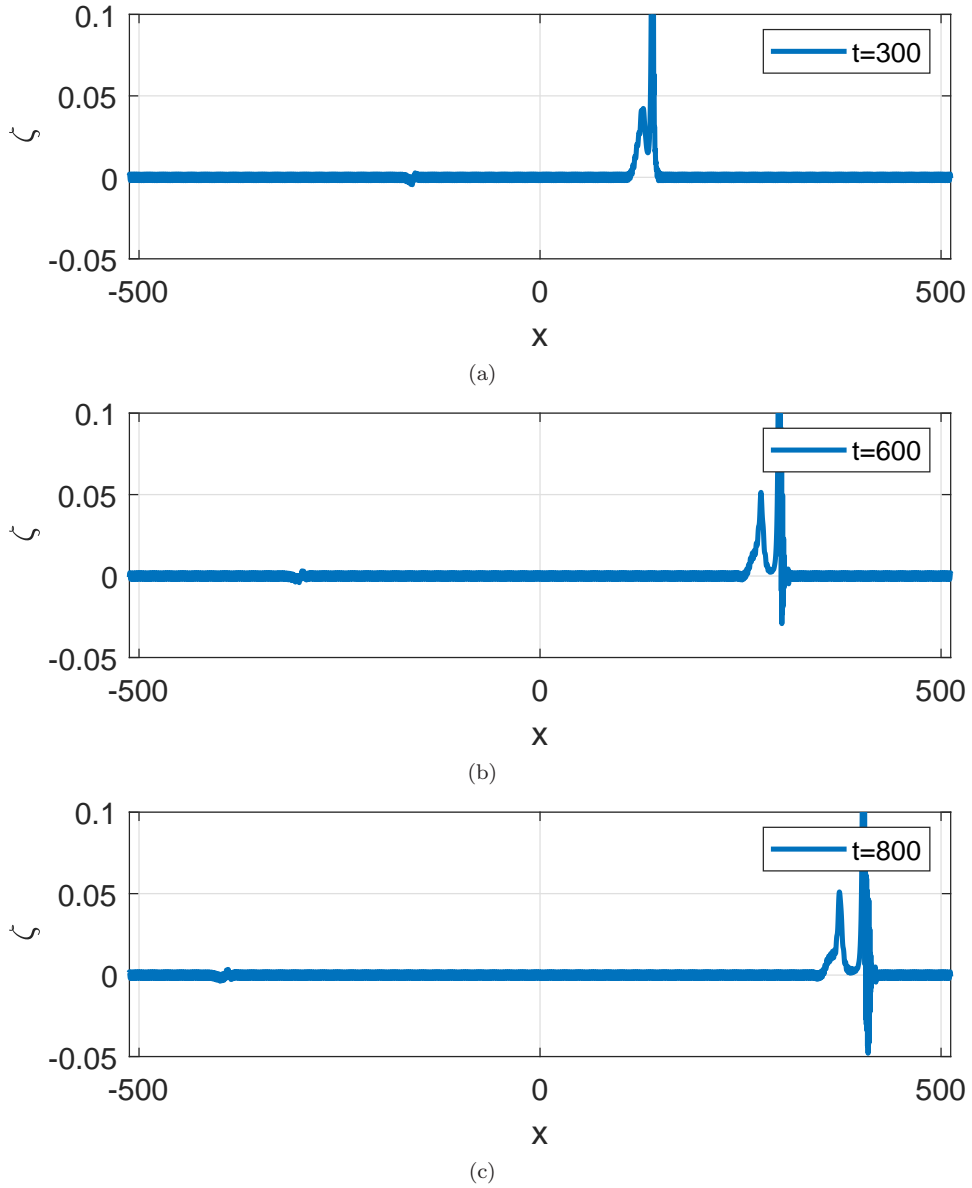
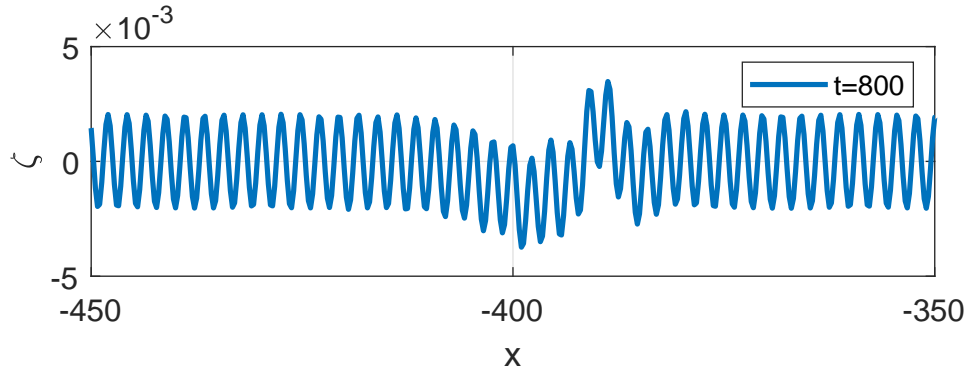


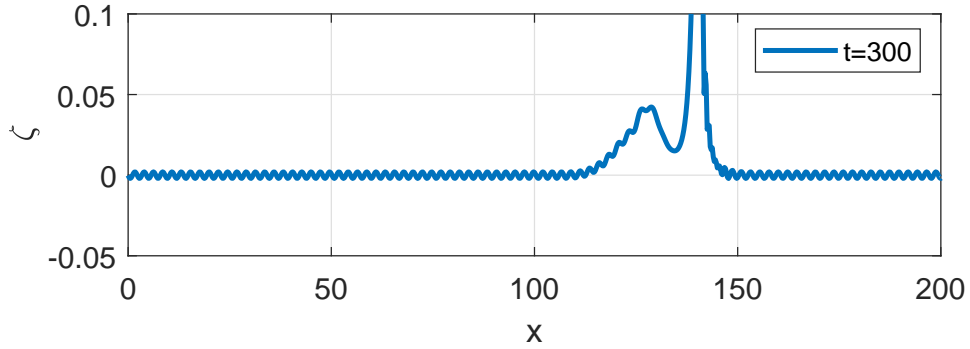
FIGURE 56. Large perturbation of a GSW. Case (A2) with (5.19), (5.20) with $A = 4.1$. Magnification of Figures 55(b)-(d).

where $\phi : [0, \infty) \rightarrow \mathbb{R}$ is the function

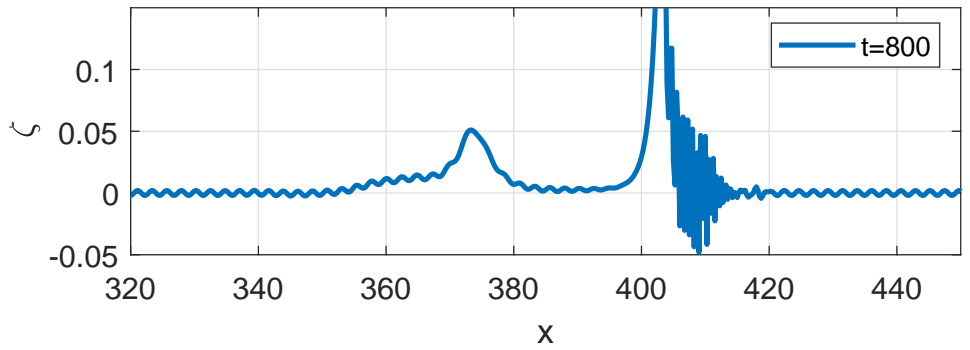
$$\phi(x) = \sqrt{\frac{(1 - \tilde{a}x)(1 - cx)}{1 + dx}}, \quad \tilde{a} = \frac{a}{\kappa_1},$$



(a)



(b)



(c)

FIGURE 57. Large perturbation of a GSW. Case (A2) with (5.19), (5.20) with $A = 4.1$. (a), (c) Magnifications of Figure 55(d); (b) Magnifications of Figure 55(b).

with a, c, d given by (5.21). The local phase speed (relative to the speed of the CSW) is therefore

$$v_{\pm}(k) = -c_s \pm c_{\gamma, \delta} \phi(k^2).$$

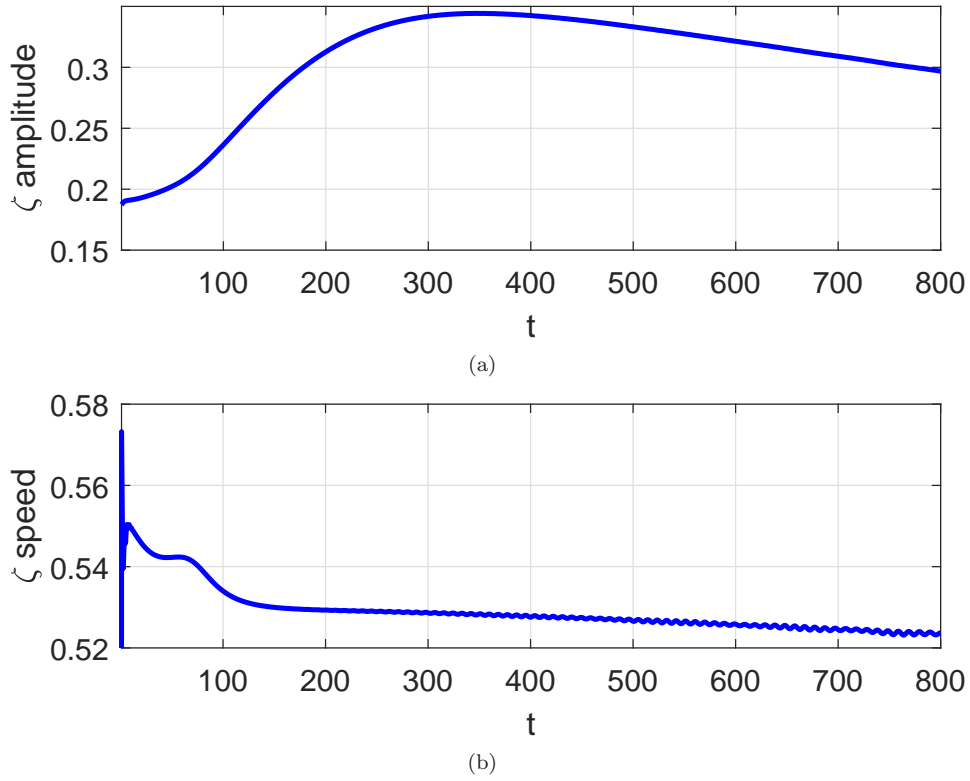


FIGURE 58. Large perturbation of a GSW. Case (A2) with (5.19), (5.20) with $A = 4.1$. Evolution of amplitude (a) and speed (b) of the taller emerging wave (ζ component of the numerical solution).

An analysis of ϕ similar to that made in section 5.4 for the case (A1) shows that the function ϕ has the form displayed in Figure 54(a): It is decreasing up to some x^* and increasing for $x \geq x^*$ with $\phi(x) \rightarrow +\infty$ as $x \rightarrow \infty$. As in section 5.4, this means that for large $|k|$

$$v_+(k) > -c_s + c_{\gamma,\delta},$$

and most of the components of the dispersive tail travel to the right and in front of the solitary wave. Similarly, for the group velocities

$$\omega'_\pm(k) = -c_s \pm c_{\gamma,\delta}\psi(k^2),$$

where $\psi : [0, \infty) \rightarrow \mathbb{R}$, given by (5.18), has the form shown in Figure 54(b), and therefore, for $|k|$ large enough

$$\omega'_+(k) \geq -c_s + c_{\gamma,\delta} > 0.$$

Hence one dispersive group travels to the right and in front of the solitary wave.

We reproduce now the analogous experiment with $A = 2.1$ in (5.20), and the results are shown in Figures 70-73. As the perturbation factor A grows, the size of both tails also grows. In addition, Figures 71 and 72 suggest the formation of nonlinear structures, in the form of wavelets and perhaps some very small CSW's with non monotone decay. (These two structure were conjectured in Figure 68.)

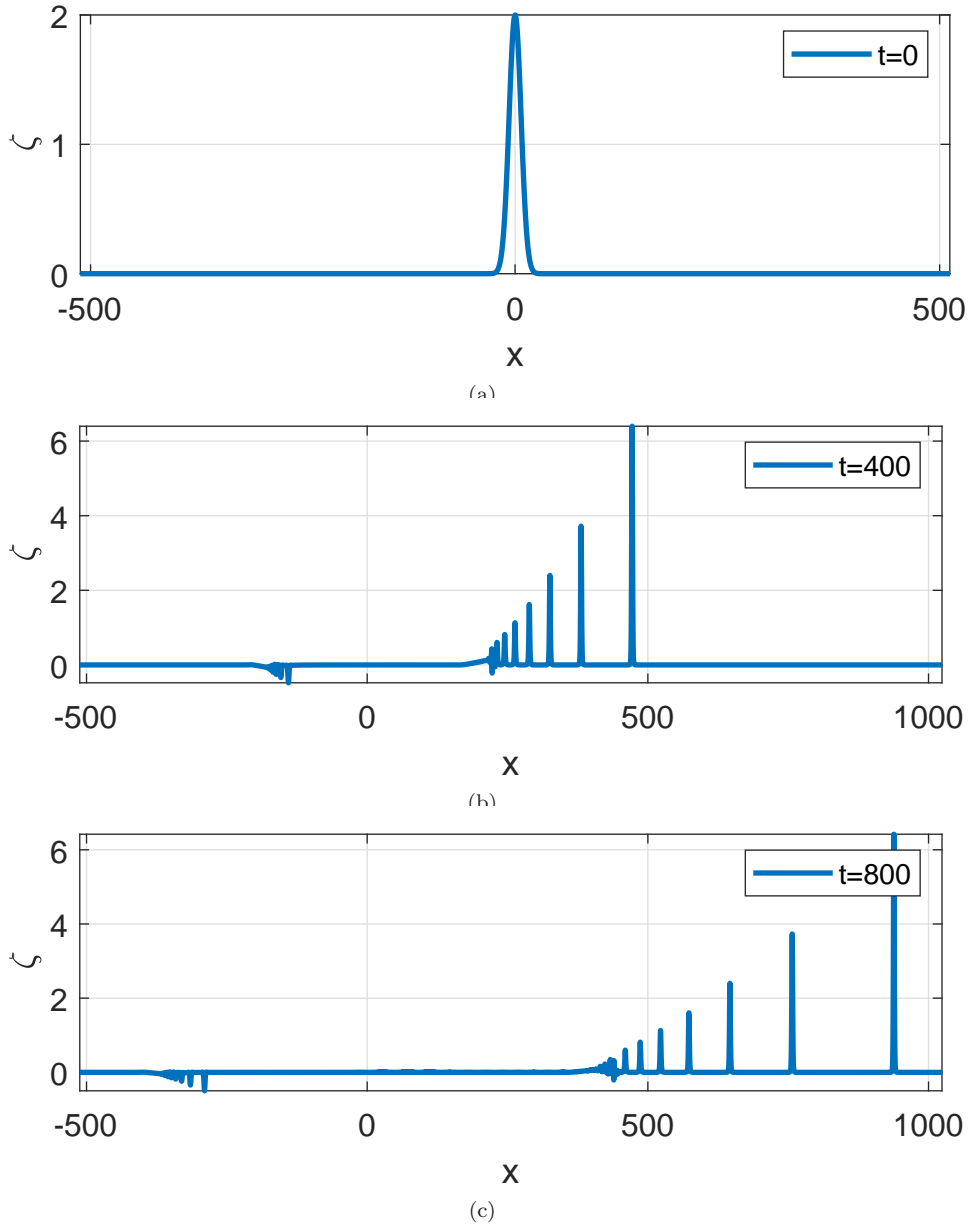
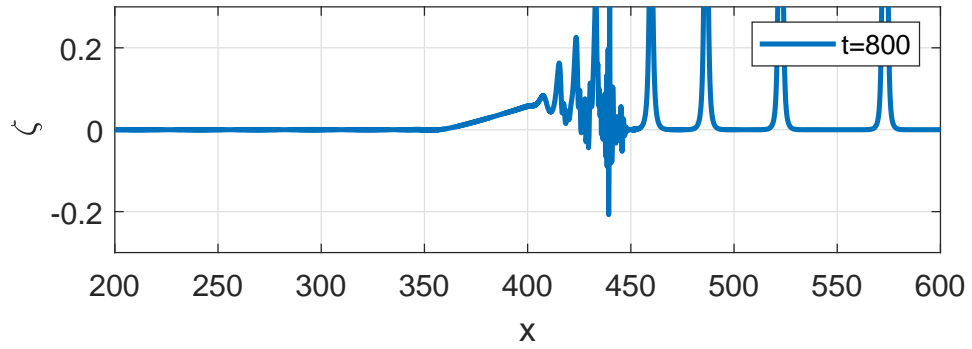
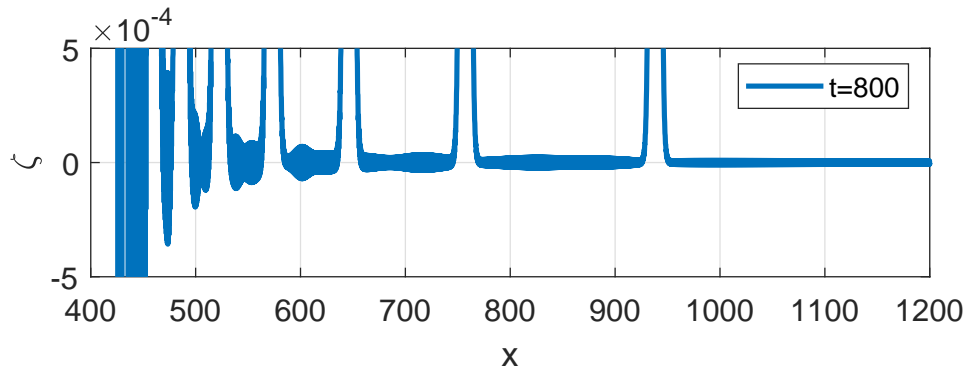


FIGURE 59. Resolution property. Case (A2) with (5.19), and a Gaussian pulse $\zeta(x, 0) = u(x, 0) = Ae^{-\tau x^2}$, with $A = 2, \tau = 0.01$, as initial condition. ζ component of the numerical solution.

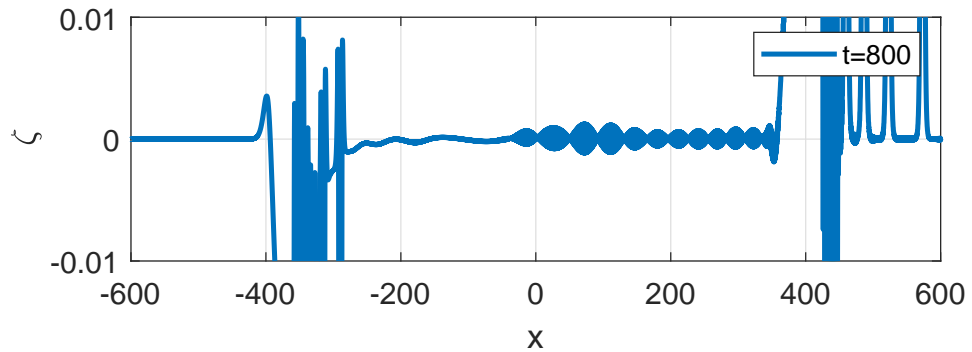
The emerging solitary wave is shorter (its maximum negative excursion is approximately -5.233 , compared to -6.035 for the initial perturbed wave) and slower (the speed is now about 0.237).



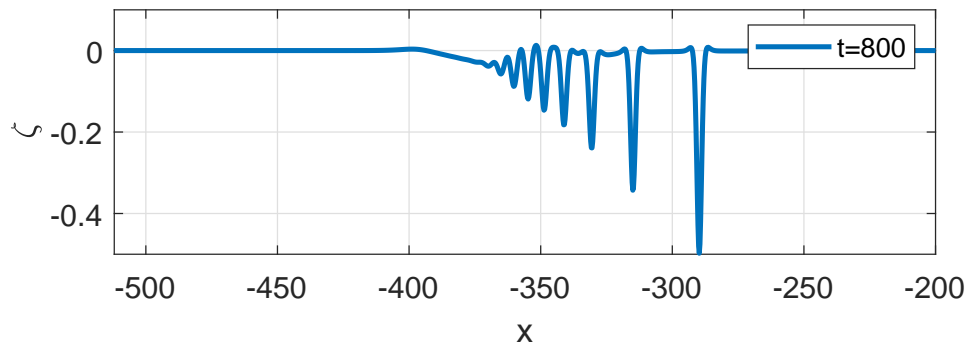
(a)



(b)



(c)



(d)

FIGURE 60. Resolution property. Case (A2) with (5.19), and a Gaussian pulse $\zeta(x, 0) = u(x, 0) = Ae^{-\tau x^2}$, with $A = 2, \tau = 0.01$, as initial condition. Several structures of the ζ component of the numerical solution at $t = 800$.

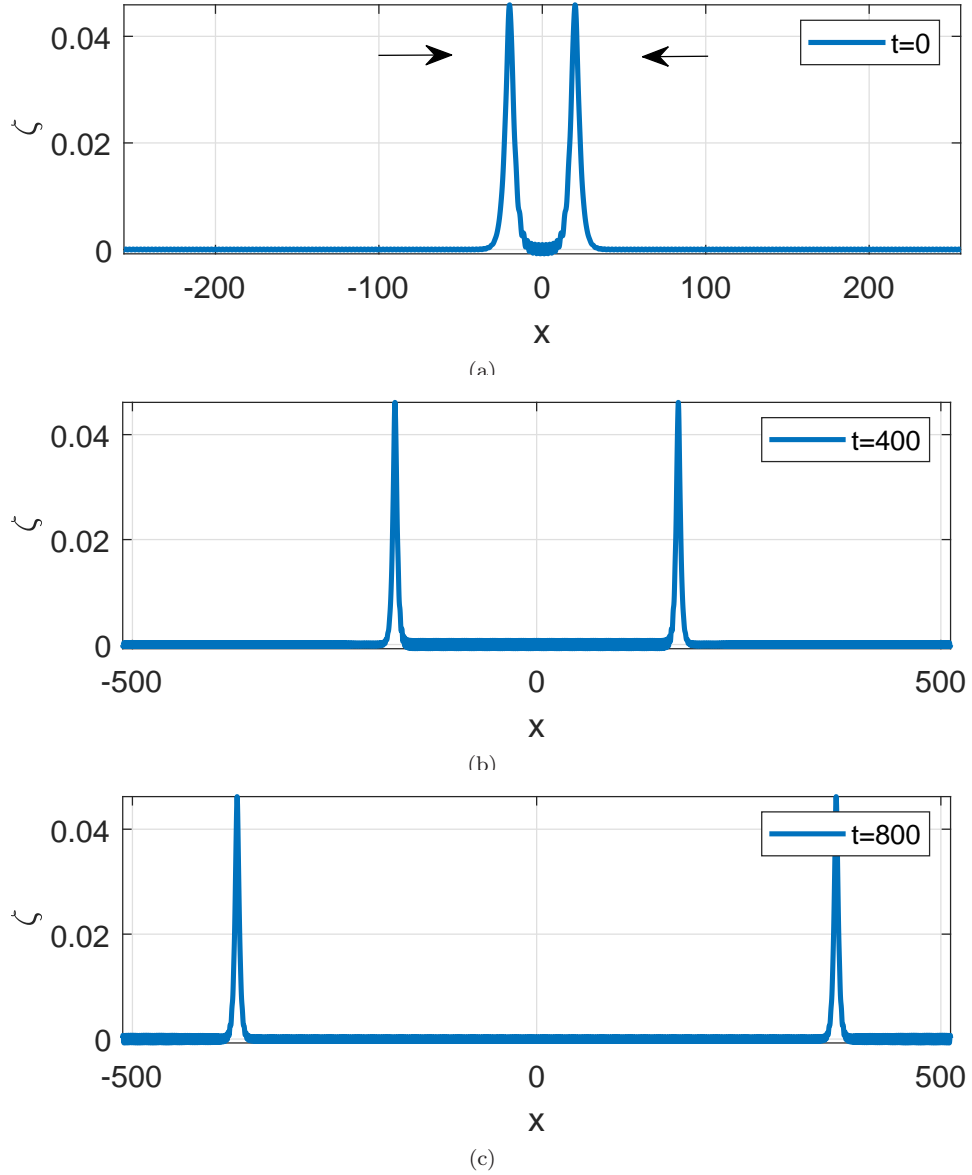


FIGURE 61. Symmetric head-on collision of GSW's. Case (A2) with (5.19). ζ component of the numerical solution.

6. CONCLUDING REMARKS

The present paper is concerned with the three-parameter family of internal-wave Boussinesq/Boussinesq (B/B) systems (1.6). They model the bi-directional propagation of internal waves along the interface of a two-layer system of fluids under a rigid-lid assumption for the upper layer and over a rigid bottom bounding the lower layer below. The systems were derived in [21] under the hypothesis

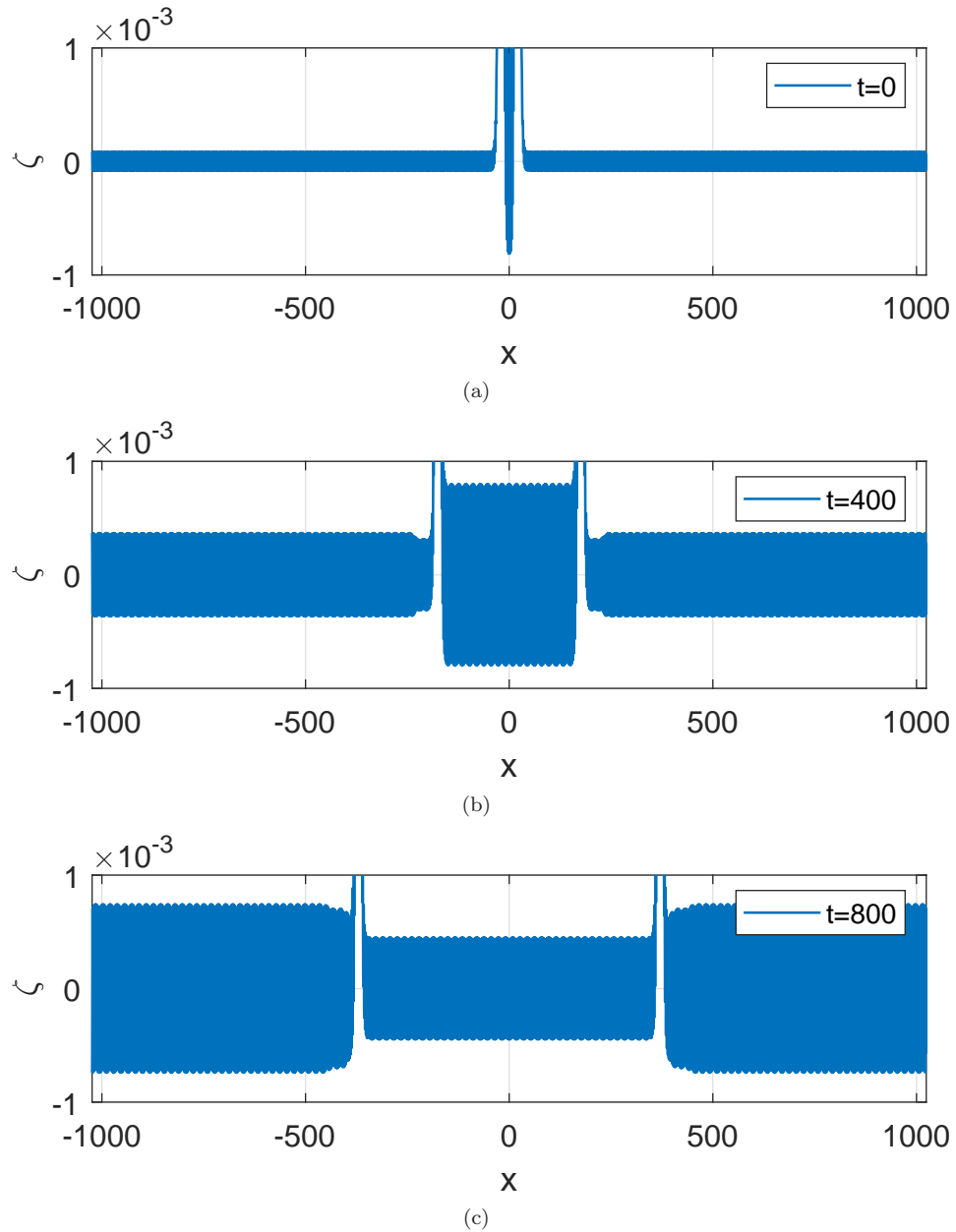


FIGURE 62. Symmetric head-on collision of GSW's. Case (A2) with (5.19). ζ component of the numerical solution. Magnifications of Figure 61.

that the flow is in the Boussinesq regime in both layers and are described by four parameters, a, b, c, d , three of them independent, like those corresponding to surface wave propagation, [17, 18].

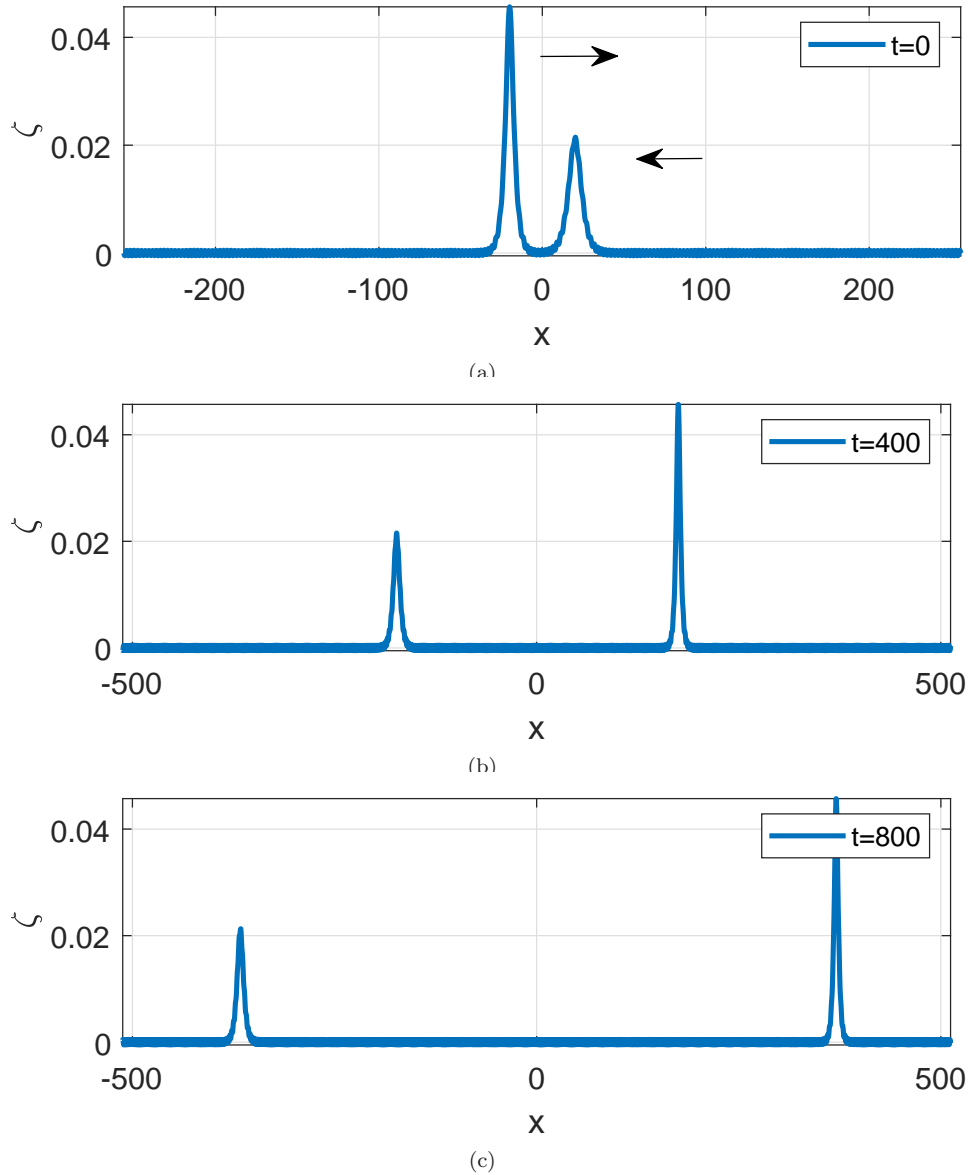


FIGURE 63. Non-symmetric head-on collision of GSW's. Case (A2) with (5.19). ζ component of the numerical solution.

In Section 2 several theoretical aspects of this family of systems are discussed. We first present an alternative derivation, cf. [17, 40], based on asymptotic expansions of the velocity potential associated to the fluid layers without using nonlocal operators as in [21]. Then the theory developed in [17] for the case of surface waves is used to review linear and nonlinear well-posedness of the internal-wave systems. Specifically, the B/B systems are linearly well-posed when $a, c \leq 0, b, d \geq 0$. As for local (and in some cases conditionally global) nonlinear well-posedness, an analysis

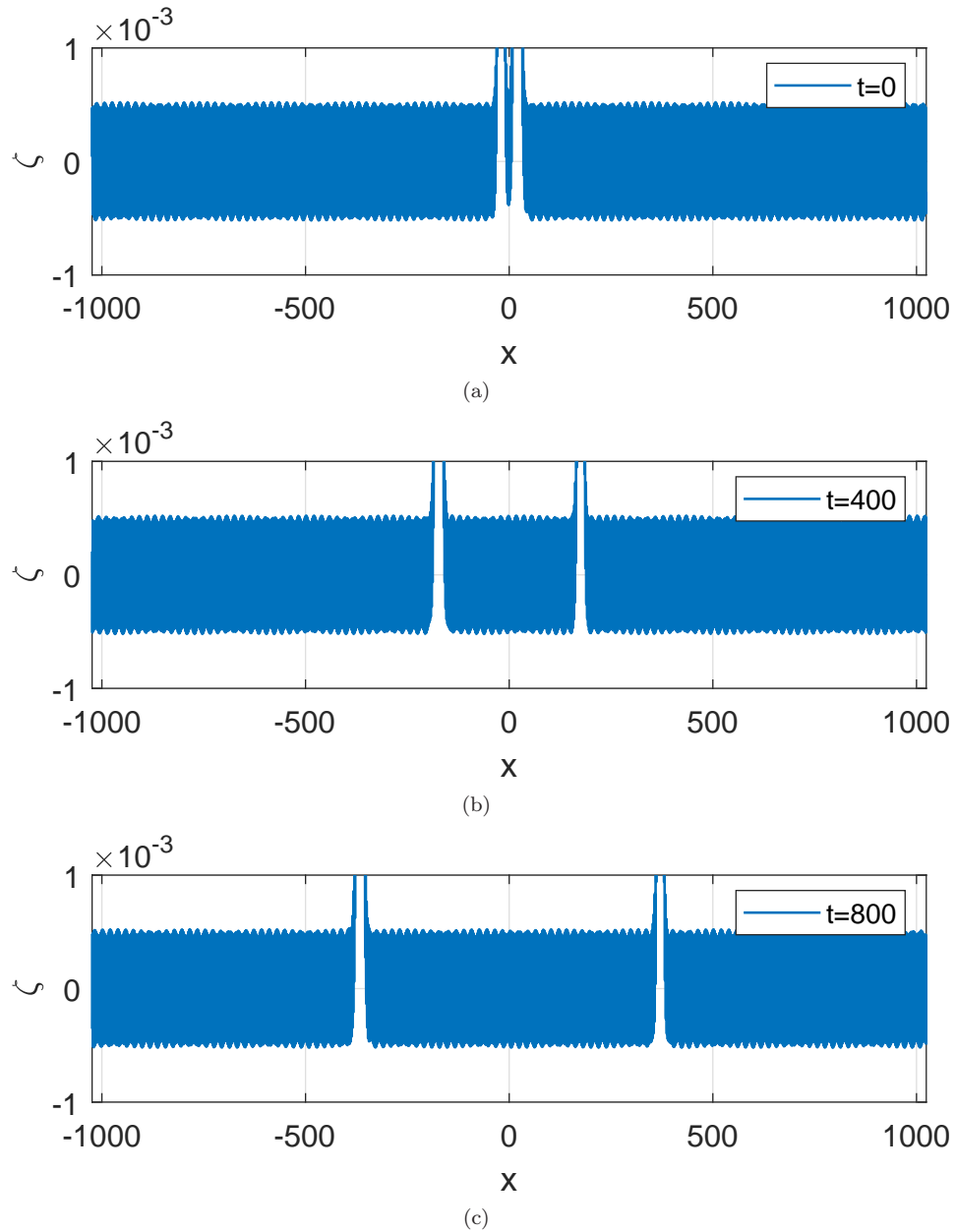


FIGURE 64. Non-symmetric head-on collision of GSW's. Case (A2) with (5.19). ζ component of the numerical solution. Magnifications of Figure 63.

similar to the one in [18] establishes seven types of systems, depending on the parameters a, b, c, d , in corresponding Sobolev spaces where existence, uniqueness and regularity locally in time of solutions hold. They correspond to the cases (i)-(vii)

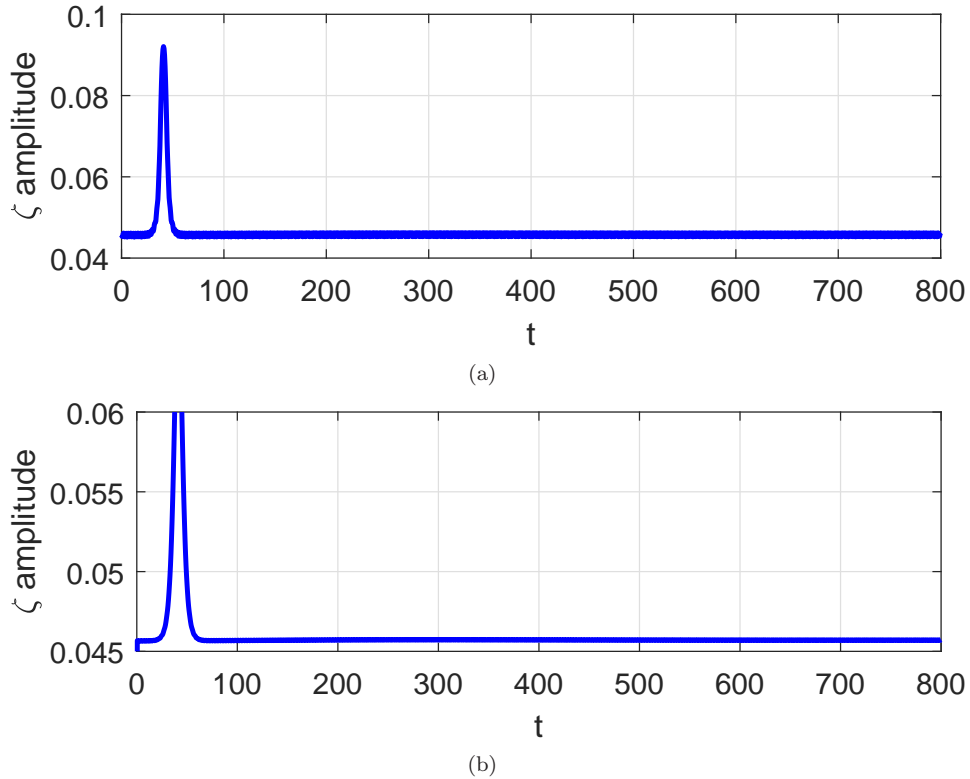


FIGURE 65. Head-on collisions of GSW's. Case (A2) with (5.19). Evolution of amplitude: (a) Symmetric case; (b) Non-symmetric case (tallest emerging wave).

in section 2.2. When $b = d$ these systems admit a Hamiltonian structure, and the Hamiltonian and other conserved quantities are derived in section 2.3.

Section 3 is devoted to the error analysis of the spectral semidiscretization for approximating the periodic ivp for the B/B systems. Error estimates for the semidiscrete schemes are derived for each case (i)-(vii) of nonlinearly well posed systems obtained in section 2.

In sections 4 and 5 we study solitary-wave solutions of the B/B systems. Section 4 is concerned with the existence and numerical generation of this type of solutions. In the first part, section 4.1, we apply standard theories such as Normal Form Theory (NFT), [46, 44], Toland's Theory, [66], Concentration-Compactness Theory (CCT), [54], and Positive Operator Theory (POT), [14], in order to derive existence results. If we make use of the linearization of the system for the solitary waves (4.1), written as a first-order system (4.3), at the origin, NFT allows us to establish the existence of classical solitary waves (CSW's) and generalized solitary waves (GSW's), in two 'generic' cases (cf. Table 1), respectively:

- $a, c \leq 0, b, d \geq 0, bd - ac/\kappa_1 > 0$ (CSW),
- $a, c \leq 0, b, d \geq 0, bd - ac/\kappa_1 < 0$ (GSW),

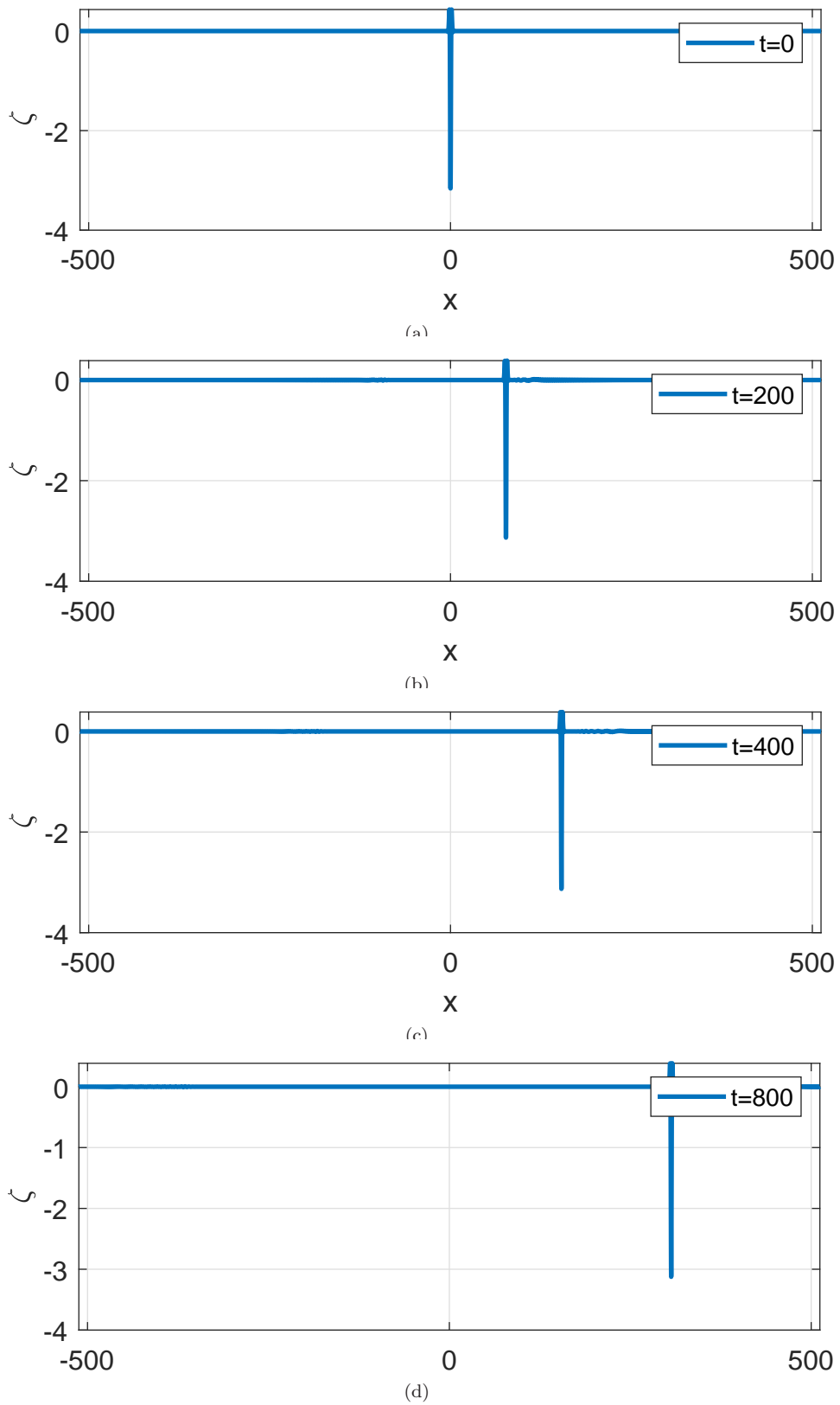


FIGURE 66. Small perturbation of a CSW with nonmonotone decay. $A = 1.1$, ζ component of the numerical solution.

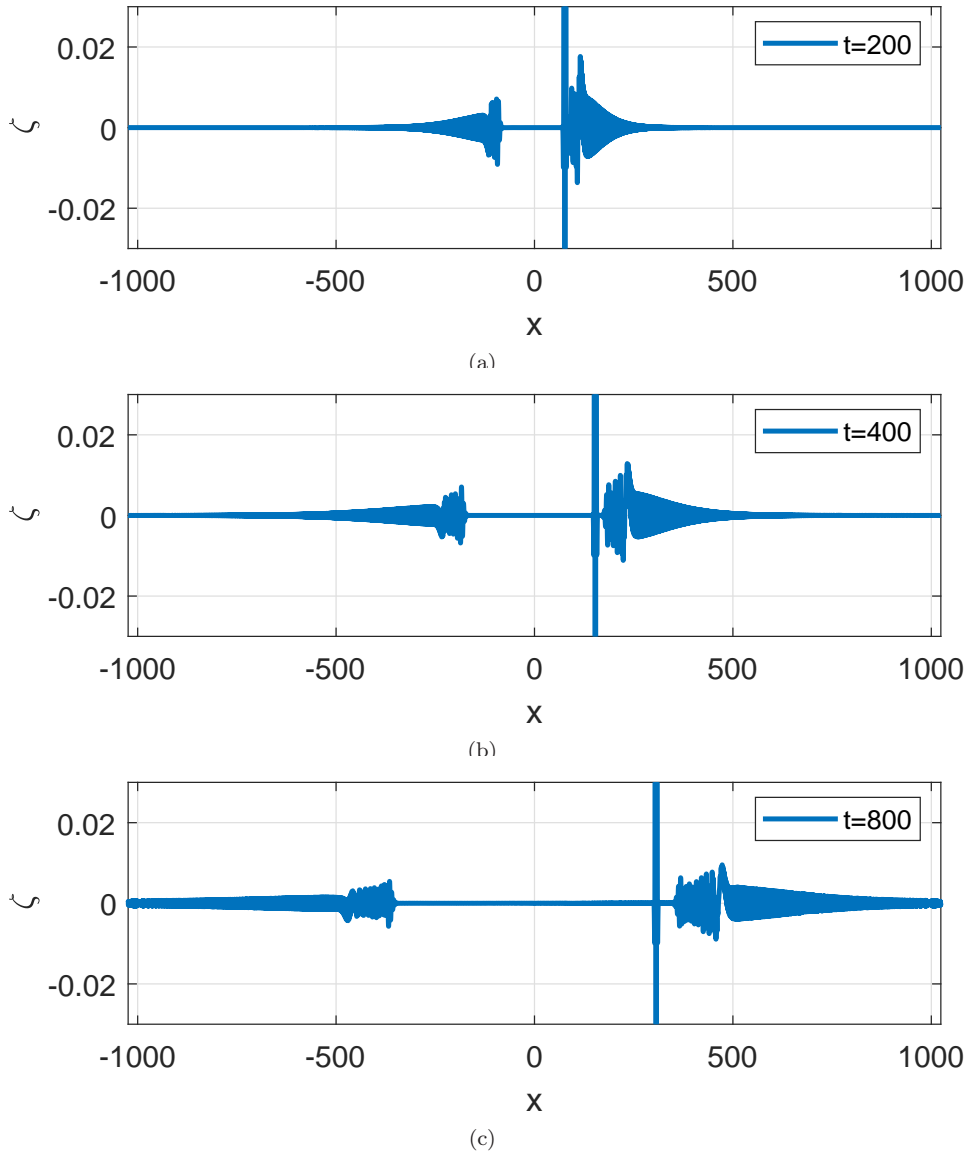


FIGURE 67. Small perturbation of a CSW with nonmonotone decay. $A = 1.1$. ζ component of the numerical solution. Magnifications of Figure 66.

where $\kappa_1 = 1/(\delta + \gamma)$, with δ and γ denoting, respectively, the depth and density ratios of the two-layer system of fluids. Existence of such solitary waves is ensured by the NFT when the magnitude of the speed c_s is greater than but close to the limiting value $c_{\gamma,\delta} = \sqrt{(1-\gamma)/(\delta+\gamma)}$ (speed of sound). In addition, NFT also predicts periodic solutions close to the region of generation of CSW's, as well as classical solitary waves with non monotone decay for speeds c_s satisfying $|c_s| < c_{\gamma,\delta}$.

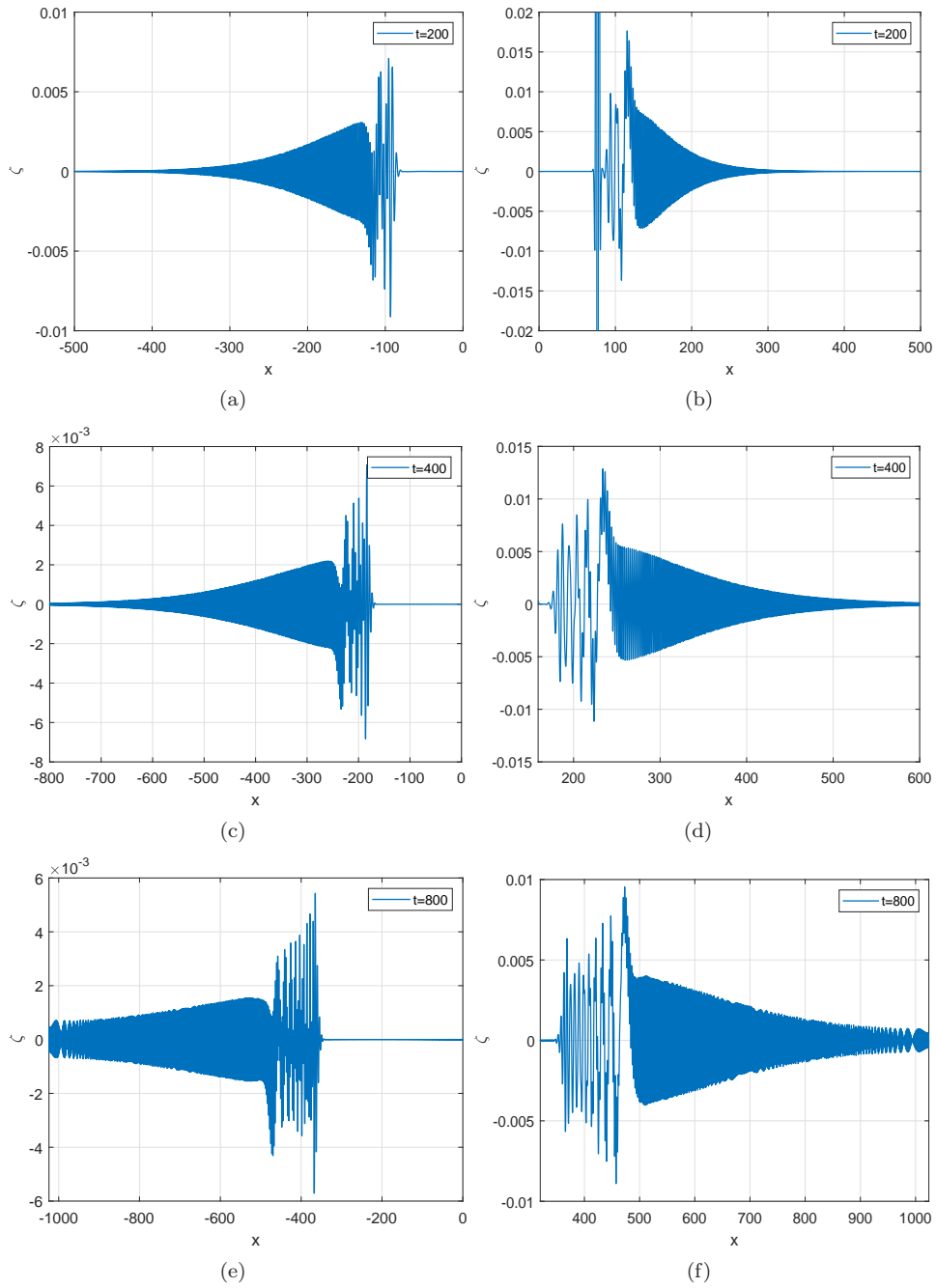


FIGURE 68. Small perturbation of a CSW with nonmonotone decay. $A = 1.1$. ζ component of the numerical solution. Magnifications of Figure 67.

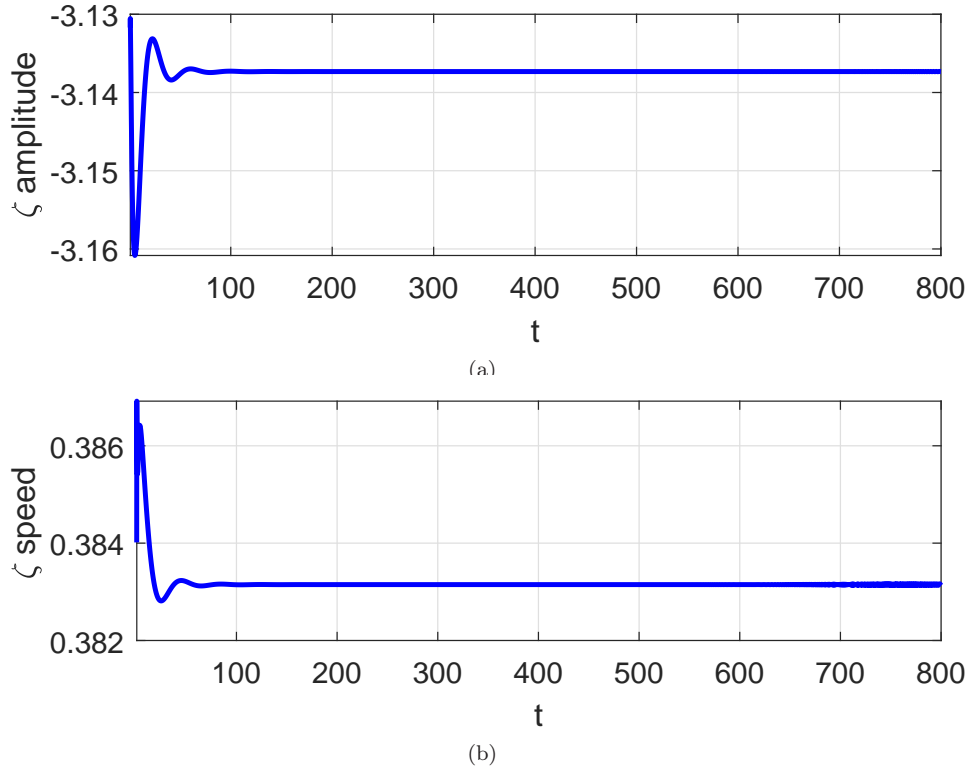


FIGURE 69. Small perturbation of a CSW with nonmonotone decay. $A = 1.1$. Evolution of maximum negative excursion (a) and speed (b) of the emerging solitary wave.

The rest of the theories contribute more results for the existence of CSW's of speeds not necessarily close to $c_{\gamma,\delta}$. Thus:

- When $a, c \leq 0, b = d > 0$ (Hamiltonian case), Toland's theory ensures the existence of classical solitary waves. A specific speed-amplitude relation of the form (4.20) holds.
- When $a, c < 0, b = d > 0$, CCT establishes the existence of CSW's for speeds c_s satisfying a bound of the form (4.26) and $|c_s| < c_{\gamma,\delta}$.
- The application of POT proves the existence of CSW's when $b, d > 0, a, c \leq 0$, and $bd - ac/\kappa_1 > 0$, with speeds c_s satisfying $|c_s| > c_{\gamma,\delta}$.

For particular values of c_s , some exact formulas of CSW's of sech^2 type may be obtained by using similar arguments to those of [27] valid in the case of surface waves.

These existence results are illustrated in section 4.2, where CSW and GSW solutions are numerically generated. The numerical procedure consists of discretizing the system (4.1) of ode's satisfied by the solitary wave profiles, on a long enough interval with periodic boundary conditions, by the Fourier collocation method. In the Fourier space, the differential equation systems for the profiles become algebraic systems, which are iteratively solved by the Petviashvili's scheme, [61], accelerated

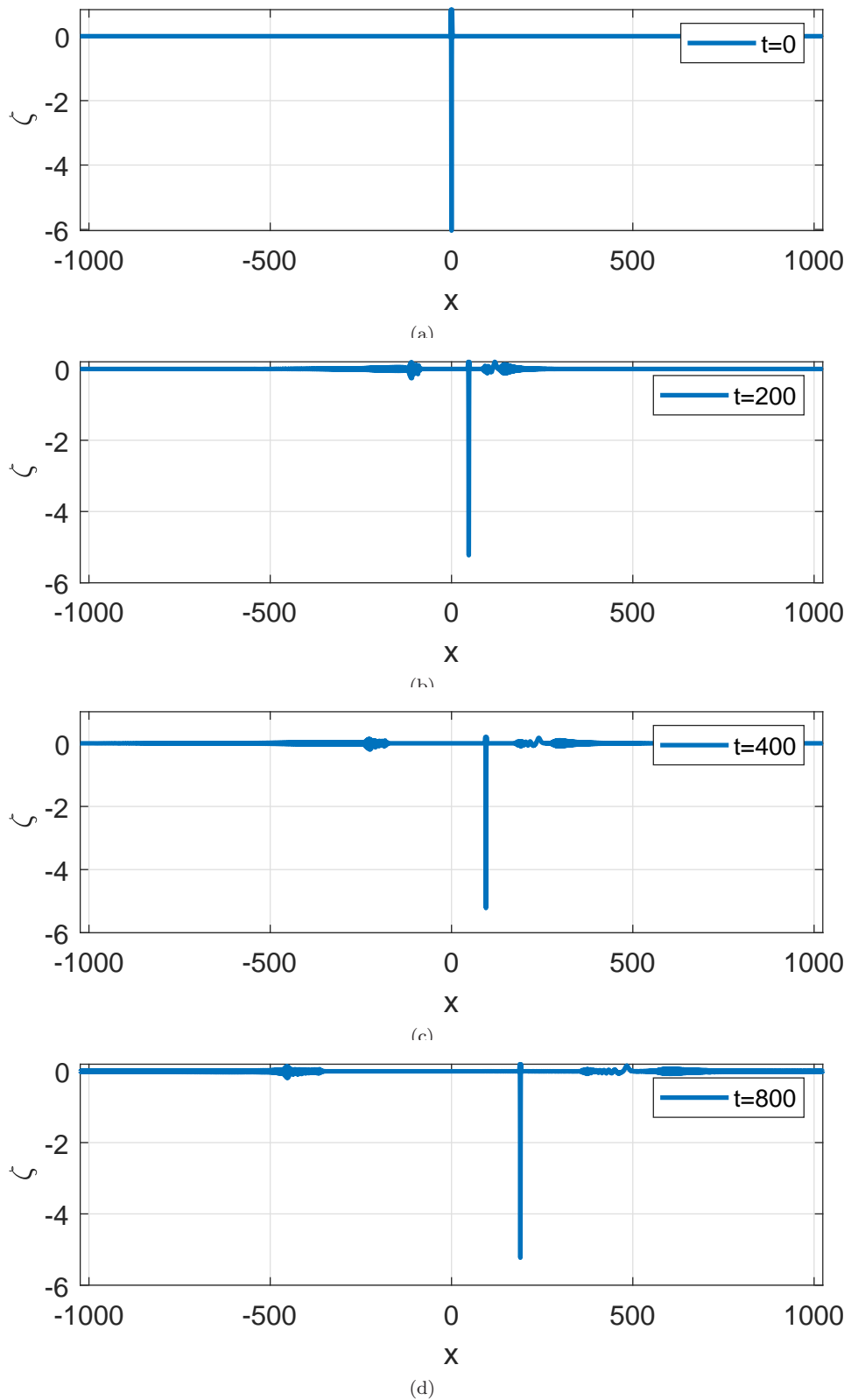


FIGURE 70. Perturbation of a CSW with nonmonotone decay.
 $A = 2.1$. ζ component of the numerical solution.

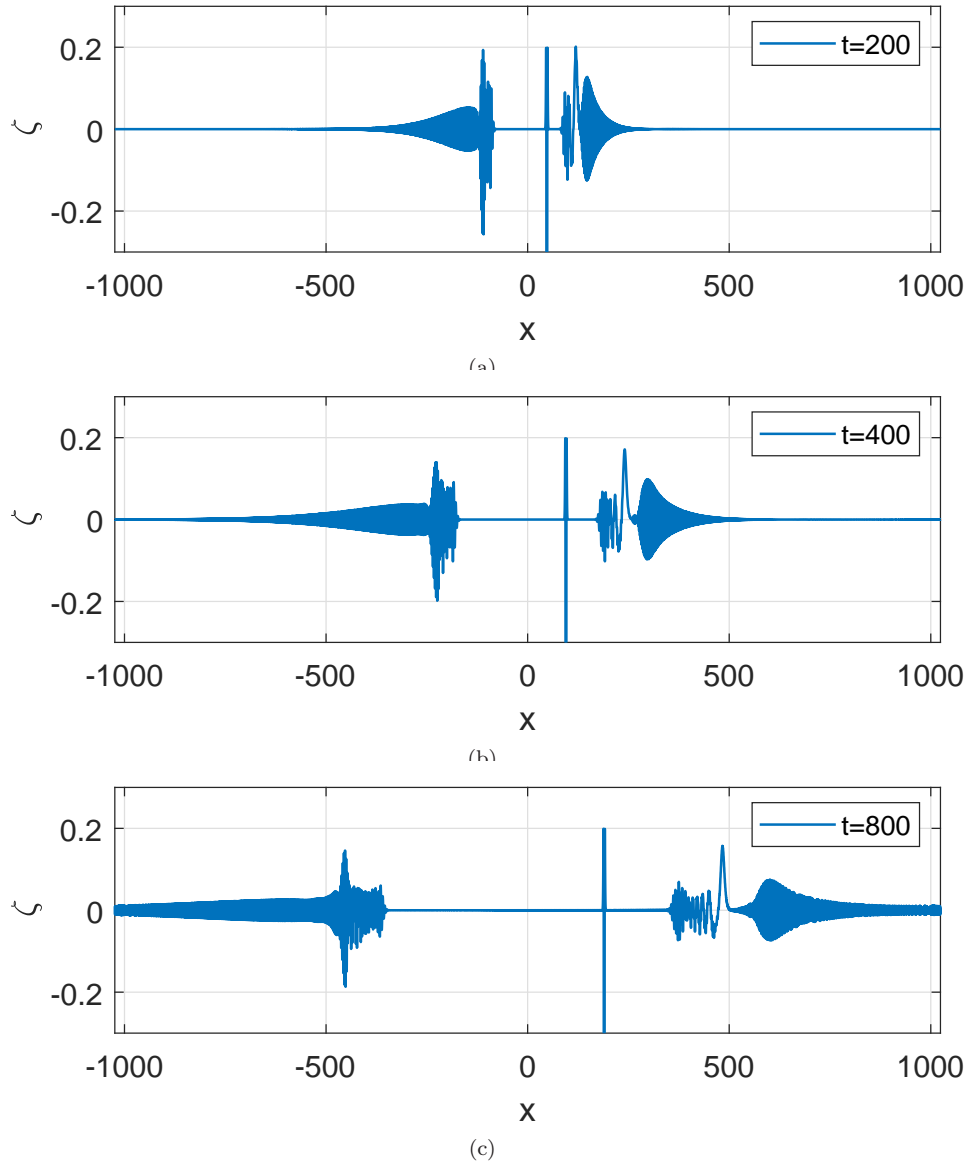


FIGURE 71. Perturbation of a CSW with nonmonotone decay. $A = 2.1$. ζ component of the numerical solution. Magnifications of Figure 70.

with vector extrapolation techniques, [63]. Each case is illustrated by exhibiting the approximate solitary wave profiles (ζ and v_β components), the corresponding phase portraits, and the decrease of the residual error with the number of iterations in order to check the convergence of the iteration. It is worth mentioning that, in order to illustrate the results of Toland's Theory, the iterative method is modified by projection techniques so that the speed-amplitude relation (4.20) is satisfied up

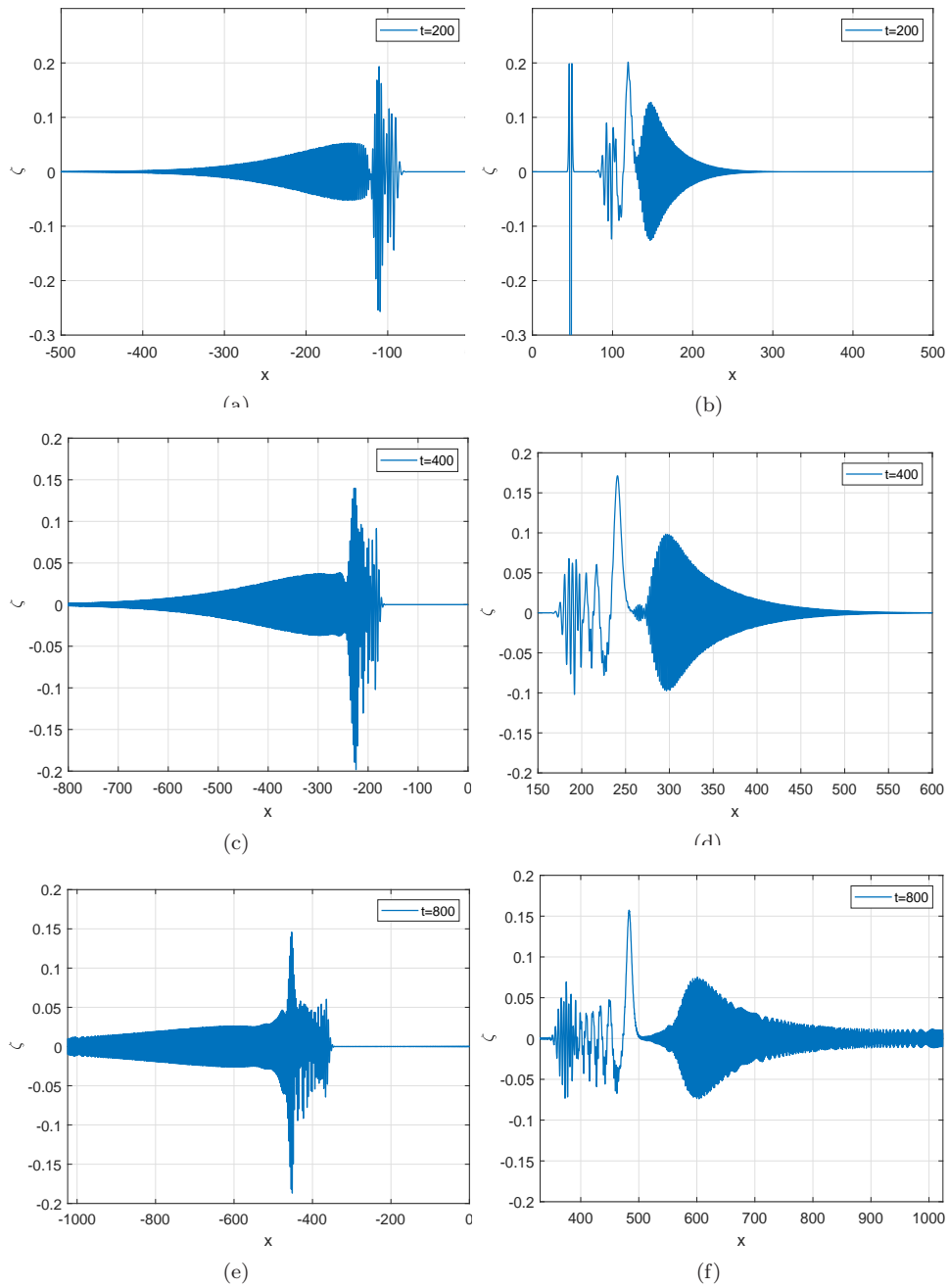


FIGURE 72. Perturbation of a CSW with nonmonotone decay. $A = 2.1$. ζ component of the numerical solution. Magnifications of Figure 71.

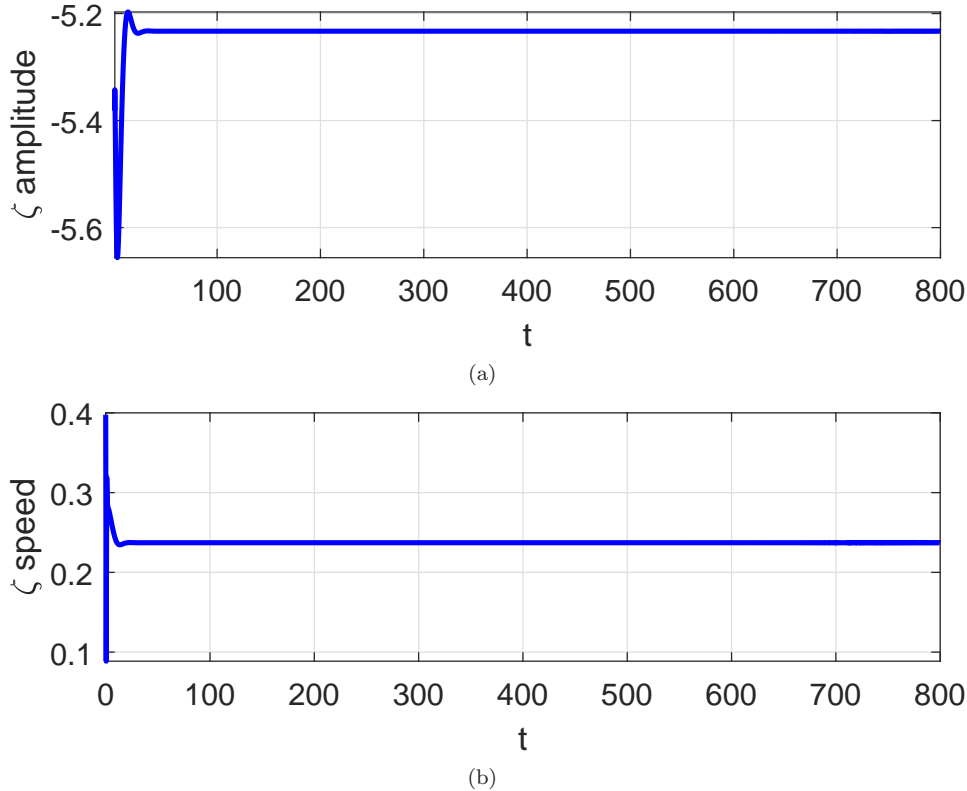


FIGURE 73. Perturbation of a CSW with nonmonotone decay. $A = 2.1$. Evolution of maximum negative excursion (a) and speed (b) of the emerging solitary wave.

to machine accuracy. In addition, numerical experiments suggest that in all cases, and for both CSW's and GSW's, the amplitude is an increasing function of the speed difference $c_s - c_{\gamma,\delta}$.

In section 5 we make a computational study on some aspects of the dynamics of classical and generalized solitary-wave solutions of the B/B systems by solving numerically the periodic ivp on a long enough interval. The numerical method used for these evolution simulations is a spectral Fourier discretization in space coupled with an implicit fourth-order RK-composition method based on the implicit midpoint rule as time integrator. The choice of the spatial discretization is justified by the error estimates in section 3, while the time integrator has been analyzed in [31] in the case of spectral discretizations of the periodic ivp for the KdV equation and shown to be computationally efficient when used in other nonlinear dispersive equations as well, [42, 34]. The resulting full discretization is computationally validated in section 5.2, where several numerical experiments are performed to check its accuracy, as well as the accuracy of the numerical solitary waves as traveling waves.

Section 5.3 is devoted to a computational study of the dynamics of CSW solutions which are strictly positive or negative. The experiments are made for the generic

case $a, c < 0, b, d > 0, bd - ac/\kappa_1 > 0$ and are concerned with the ensuing evolution from small and large perturbations of CSW's, from superpositions of CSW's (in order to study overtaking and head-on collisions), and from Gaussian pulses, in order to study resolution into solitary waves. Some of the main conclusions of this study are reported here:

- Under small initial perturbations, the solution evolves into a modified CSW with small dispersive tails following the main wave. The generation and structure of these tails are justified by an analysis of small-amplitude solutions of the associated linearized system in a reference frame moving with the speed of the solitary wave. In the case of these strictly positive or negative classical solitary waves, the results predict the formation of two types of dispersive oscillation groups, trailing the solitary wave and traveling in opposite directions.
- Increasing the size of the perturbation of the initial solitary wave may lead to the generation of additional stable, nonlinear structures. They may consist of smaller CSW's, CSW's of non monotone decay or others of wavelet type.
- The collisions are, as expected, inelastic. In both cases (overtaking and head-on collisions), two CSW's emerge; the effects of the inelastic interactions include the generation of tails of dispersive nature and nonlinear structures of the same type as those already mentioned.
- The evolution ensuing from initial Gaussian pulses shows resolution into a train of CSW's, leaving a small structure behind which seems to be dispersive.

In section 5.4 we perform a corresponding computational study of the dynamics of GSW's. To this end, the experiments are in the generic case $a, c < 0, b, d > 0, bd - ac/\kappa_1 < 0$ and are of the same type as those in the study of section 5.3. The main conclusions are:

- The experiments with small perturbations of GSW's suggest that the question of stability of these waves is more intricate, in the sense that the formation of emerging, stable GSW's seems to require smaller initial perturbations and takes longer time than in the case of CSW's. In some examples the dispersive tails are hard to observe, as they are hidden in the ripples of the structure being of much smaller size.
- The experiments with larger perturbations of an initial GSW show the formation of nonlinear structures of similar type to those observed in the case of CSW's, but overimposed on the ripples. In addition, larger ripples along with dispersive tails form in front of an emerging GSW, a fact that surely affects its stability.
- The experiments show the evolution, from initial Gaussian pulses, of a train of solitary-wave type pulses traveling to the right. Ripples are formed between each pair of consecutive pulses, mixed somehow with dispersive tails. These dispersive groups are also observed behind the train. Finally, a second train of solitary-wave pulses is formed, traveling to the left, consisting of nonmonotonically decaying solitary waves; thus each wave of this train should have speed less than the limiting value $c_{\gamma,\delta}$.
- The main effect observed in the experiments of overtaking and head-on collisions of GSW's is the formation of two emerging GSW's with ripples of

different size, larger, in general, than those of the initial GSW's. Dispersive structures seem now to be smaller and are superimposed on the emerging ripples.

The existence of nonmonotonically decaying classical solitary waves, established in section 4.1 and numerically generated in section 4.2, as well as their role in the dynamics of other solitary waves, observed in the experiments of sections 5.3 and 5.4, motivate the numerical experiments of section 5.5, devoted to a computational study of the behaviour of these waves under small and large perturbations. The experiments suggest persistence and stability of these waves. From small perturbations, a new solitary wave of the same type is formed. The analysis of small-amplitude plane wave solutions of the linearized system in a reference moving with the speed of the solitary wave, shows now that the main part of the dispersive oscillations travels to the right in front of the solitary wave, with the rest traveling to the left, behind it. When the perturbation factor grows, the formation of a new solitary wave with nonmonotone decay is observed, and now the dispersive tails seems to be accompanied by the generation of small nonlinear structures, in the form of wavelets or nonmonotone CSW's.

ACKNOWLEDGEMENTS

Vassilios Dougalis and Angel Duran would like to acknowledge travel support, that made possible this collaboration, from the Institute of Mathematics (IMUVA) of the University of Valladolid, and the Institute of Applied and Computational Mathematics of FORTH. Leetha Saridaki was supported by the grant "Innovative Actions in Environmental Research and Development (PErAn)" (MIS5002358), implemented under the "Action for the strategic development of the Research and Technological sector" funded by the Operational Program "Competitiveness, and Innovation" (NSRF 2014-2020) and co-financed by Greece and the EU (European Regional Development Fund). The grant was issued to the Institute of Applied and Computational Mathematics of FORTH.

REFERENCES

- [1] J. P. Albert, J. Angulo, Existence and stability of ground state solutions of a Schrödinger-KdV system, Proc. Royal Soc. Edinburgh Sec. A 133, 5 (2003) 987-1029
- [2] J. Albert, J.L. Bona and J.-C. Saut, Model equations for waves in stratified fluids, Proc. Royal Soc. London A, 453 (1997) 1233-1260.
- [3] J. Alvarez, A. Duran, Petviashvili type methods for traveling wave computations: II. Acceleration with vector extrapolation methods, Math. Comput. Simul., 123 (2016) 19-36.
- [4] C. J. Amick, J. F. Toland, Homoclinic orbits in the dynamic phase-space analogy of an elastic strut, Eur. J. Appl. Math., 3 (1992) 97-114.
- [5] J. Angulo-Pava, *Nonlinear Dispersive Equations. Existence and Stability of Solitary and Periodic Travelling Wave Solutions*, Amer. Math. Soc., Providence, Rhode Island, 2009.
- [6] J. Angulo-Pava, J.-C. Saut, Existence of solitary wave solutions for internal waves in two-layer systems, Quart. Appl. Math. 78 (2020), 75-105.
- [7] C. T. Anh, On the Boussinesq/Full dispersion systems and Boussinesq/Boussinesq systems for internal waves, Nonl. Anal., 72 (2010) 409-429.
- [8] D. C. Antonopoulos, V. A. Dougalis, Numerical solution of the 'classical' Boussinesq system, Math. Comput. Simul., 82 (2012) 984-1007.

- [9] D. C. Antonopoulos, V. A. Dougalis, Error estimates for Galerkin approximations of the ‘classical’ Boussinesq system, *Math. Comp.*, 82 (2013) 680-717.
- [10] D. C. Antonopoulos, V. A. Dougalis, and D. E. Mitsotakis, Numerical solution of Boussinesq systems of the Bona-Smith family, *Appl. Numer. Math.*, 60 (2010), 314-336.
- [11] D. C. Antonopoulos, V. A. Dougalis, and D. E. Mitsotakis, Galerkin approximations of periodic solutions of Boussinesq systems, *Bull. Greek Math. Soc.*, 57 (2010) 13-30.
- [12] E. S. Bao, R. M. Chen, Q. Liu, Existence and symmetry of ground states to the Boussinesq abcd systems, *Arch. Rational Mech. Anal.*, 216 (2015) 569-591.
- [13] L.A. Belyakov, Bifurcation of systems with homoclinic curve of a saddle-focus with saddle quantity zero, *Mat. Zam.*, 36 (1984) 838-843.
- [14] T.B. Benjamin, J.L. Bona, D.K. Bose, Solitary-wave solutions of nonlinear problems, *Philos. Trans. Royal Soc. London A* 331 (1990), 195-244.
- [15] T. B. Benjamin, J. L. Bona, J. J. Mahony, Model equations for long waves in nonlinear dispersive systems, *Philos. Trans. Roy. Soc. London, Ser. A*, 272 (1972) 47-78.
- [16] J. L. Bona, H. Chen, Solitary waves in nonlinear dispersive systems, *Discr. Cont. Dyn. Syst. Series B*, 2(3) (2002) 313-378.
- [17] J. L. Bona, M. Chen, J.-C. Saut, Boussinesq equations and other systems for small-amplitude long waves in nonlinear dispersive media: I. Derivation and linear theory, *J. Nonlin. Sci.* 12 (2002), 283-318.
- [18] J. L. Bona, M. Chen, J.-C. Saut, Boussinesq equations and other systems for small-amplitude long waves in nonlinear dispersive media: II. The nonlinear theory, *Nonlinearity* 17 (2004), 925-952.
- [19] J. L. Bona, V. A. Dougalis, D. E. Mitsotakis, Numerical solution of KdV-KdV systems of Boussinesq equations: I. The numerical scheme and generalized solitary waves, *Math. Comp. Simul.*, 74(2007) 214-228.
- [20] J. L. Bona, V. A. Dougalis, D. E. Mitsotakis, Numerical solution of Boussinesq systems of KdV-KdV type: II. Evolution of radiating solitary waves, *Nonlinearity* 21 (2008) 2825-2848.
- [21] J. L. Bona, D. Lannes, J. C. Saut, Asymptotic models for internal waves, *J. Math. Pures Appl.*, 89 (2008), 538-566.
- [22] J. L. Bona, Y. A. Li, Decay and analyticity of solitary waves, *J. Math. Pures Appl.*, 76 (1997) 377-430.
- [23] A. de Bouard and J.-C. Saut, Solitary waves of generalized Kadomtsev-Petviashvili equations, *Ann. Inst. Henri Poincaré Anal. Non Linéaire* 14 (1997) 211-236.
- [24] A. R. Champneys, Homoclinic orbits in reversible systems and their applications in mechanics, fluids and optics, *Physica D*, 112 (1998) 158-186.
- [25] A. R. Champneys, A. Spence, Hunting for homoclinic orbits in reversible systems: A shooting technique, *Adv. Comput. Math.*, 1(1993) 81-108.
- [26] A.R. Champneys, J.F. Toland, Bifurcation of a plethora of multi-modal homoclinic orbits for autonomous Hamiltonian systems, *Nonlinearity* 6 (1993) 665-772.
- [27] M. Chen, Exact traveling-wave solutions to bi-directional wave equations, *Int. J. Theor. Phys.*, 37(1998) 1547-1567.
- [28] M. Chen, Solitary-wave and multi pulsed traveling-wave solutions of Boussinesq systems, *Applic. Analysis*, 75(2000) 213-240.
- [29] B. Deconinck, J. N. Kutz, Computing spectra of linear operators using the Floquet-Fourier-Hill method, *J. Comput. Phys.*, 219(2006) 296-321.
- [30] R.L. Devaney, Homoclinic orbits in Hamiltonian systems, *J. Diff. Eq.*, 21 (1976) 431-438.
- [31] V. A. Dougalis, A. Durán, A high order fully discrete scheme for the Korteweg-de Vries equation with a time stepping procedure of Runge-Kutta Composition type, to appear. Preprint available at: <http://arxiv.org/abs/2005.12955>.
- [32] V. A. Dougalis, A. Durán, D. E. Mitsotakis, Numerical approximation of solitary waves of the Benjamin equation, *Math. Comp. Simul.*, 127 (2016) 56-79.
- [33] V. A. Dougalis, A. Durán, M. A. López-Marcos, D. E. Mitsotakis, A Numerical Study of the Stability of Solitary Waves of the Bona-Smith Family of Boussinesq Systems, *J. Nonlinear Sci.*, 17 (2007) 569-607.

- [34] V. A. Dougalis, A. Durán, D. E. Mitsotakis, Numerical approximation to Benjamin-type equations. Generation and stability of solitary waves, *Wave Motion*, 85 (2019) 34-56.
- [35] V. A. Dougalis, D. E. Mitsotakis, Theory and Numerical Analysis of Boussinesq systems: A review, in: *Effective Computational Methods in Wave Propagation*, N. A. Kamparis, V. A. Dougalis, J. A. Ekaterinaris (eds.) CRC Press 2008, 63-110.
- [36] V. A. Dougalis, D. E. Mitsotakis, J.-C. Saut, On some Boussinesq systems in two space dimensions: Theory and numerical analysis, *ESAIM: Mathematical Modelling and Numerical Analysis*, 41(2007) 825-854.
- [37] V. A. Dougalis, D. E. Mitsotakis, J.-C. Saut, On initial-boundary-value problems for a Boussinesq system of BBM-BBM type in a plane domain, *J. Discr. Cont. Dyn. Systems*, 23 (2009) 1191-1204.
- [38] V. A. Dougalis, D. E. Mitsotakis, J.-C. Saut, Boussinesq systems of Bona-Smith type on plane domains: Theory and numerical analysis, *J. Sci. Computing*, 44 (2010) 109-135.
- [39] V. Duchêne, Boussinesq-Boussinesq systems for internal waves with a free surface and the KdV approximation, *ESAIM-M2AN* 46 (2012), 145-185.
- [40] A. Durán, On a nonlocal Boussinesq system for internal wave propagation, in *Recent Advances in Differential Equations and Applications*, J. L. García Guirao, J. A. Murillo, F. Periago editors, Springer, 2019.
- [41] A. Durán, D. Dutykh, D. Mitsotakis, On the Galilean invariance of some nonlinear dispersive wave equations, *Stud. Appl. Math.*, 131 (2013) 359-388.
- [42] J. de Frutos, J. M. Sanz-Serna, An easily implementable fourth-order method for the time integration of wave problems, *J. Comput. Phys.*, 103 (1992) 160-168.
- [43] J. de Frutos, J. M. Sanz-Serna, Accuracy and conservation properties in numerical integration: the case of the Korteweg-de Vries equation, *Numer. Math.*, 75 (1997) 421-445.
- [44] M. Haragus, G. Iooss, *Local Bifurcations, Center Manifolds, and Normal Forms in Infinite-Dimensional Dynamical Systems*, Springer London Dordrecht Heidelberg New York, 2011.
- [45] E. Hairer, C. Lubich and G. Wanner, *Geometric Numerical Integration, Structure-Preserving Algorithms for Ordinary Differential Equations*, Springer-Verlag, New York-Heidelberg-Berlin, 2004.
- [46] G. Iooss, M. Adelmeyer, *Topics in Bifurcation Theory and Applications*, 2nd ed., World Scientific, Singapore, 1999.
- [47] G. Iooss, K. Kirchgässner, Bifurcation d'ondes solitaires en presence d'une faible tension superficielle, *C. R. Acad. Sci. Paris, Ser. 1*, 311 (1990) 265-268.
- [48] G. Iooss, K. Kirchgässner, Water waves for small surface tension: an approach via normal form, *Proc. Roy. Soc. Edinburgh A* 112 (1992) 267-200.
- [49] G. Iooss, M.C. Peroueme, Perturbed homoclinic solutions in reversible 1 : 1 resonance vector fields, *J. Diff. Eq.*, 102 (1993) 62-88.
- [50] T Kapitula, N Kutz, B Sandstede, The Evans function for nonlocal equations, *Indiana University Mathematics Journal* 53 (2004) 1095-1126.
- [51] C.E. Kenig, G. Ponce, L. Vega. (1991), Well-posedness of the initial value problem for the Korteweg-de Vries equation, *J. Amer. Math. Soc.* 4, pp. 323-347.
- [52] C.E. Kenig, G. Ponce, L. Vega. (1993), Well-posedness and scattering results for the generalized Korteweg-de Vries equation via contraction principle, *Comm. Pure Appl. Math.* 46, pp. 527-620.
- [53] S. Kichenassamy, Existence of solitary waves for water-wave models, *Nonlinearity* 10 (1997) 133-151.
- [54] P. L. Lions. (1984), The concentration-compactness principle in the calculus of variations. The locally compact case. Part I and Part II. *Ann. Inst. Henri Poincaré Sect A (N.S.)* 1, pp. 109-145 and pp. 223-283.
- [55] E. Lombardi, Homoclinic orbits to small periodic orbits for a class of reversible systems, *Proc. Roy. Soc. Edinburgh A* 126 (1996) 1035-1054.
- [56] E. Lombardi, Homoclinic orbits to exponentially small periodic orbits for a class of reversible systems: Application to water waves, *Arch. Rat. Mech. Anal.* 137 (1997) 227-304.

- [57] E. Lombardi, *Oscillatory Integrals and Phenomena Beyond all Algebraic Orders*, Springer-Verlag, Berlin-Heidelberg, 2000.
- [58] H. Y. Nguyen, F. Dias, A Boussinesq system for two-way propagation of interfacial waves, *Physica D* 237 (2008) 2365-2389.
- [59] R. L. Pego, M. Weinstein, Convective linear stability of solitary waves for Boussinesq equations, *Studies in Appl. Math.*, 99(1997) 311-375.
- [60] D. E. Pelinovsky and Y. A. Stepanyants, Convergence of Petviashvili's iteration method for numerical approximation of stationary solutions of nonlinear wave equations, *SIAM J. Numer. Anal.* 42 (2004) 1110-1127.
- [61] V. I. Petviashvili Equation of an extraordinary soliton, *Soviet J. Plasma Phys.* 2 (1976) 257-258.
- [62] J.-C. Saut, *Asymptotic Models for Surface and Internal Waves*, 29^o Colóquio Brasileiro de Matemática, IMPA, Rio de Janeiro, 2013.
- [63] A. Sidi, *Vector Extrapolation Methods with Applications*, SIAM Philadelphia, 2017.
- [64] A. Sidi, W. F. Ford, D. A. Smith, Acceleration of convergence of vector sequences, *SIAM J. Numer. Anal.*, 23 (1986) 178-196.
- [65] D. A. Smith, W. F. Ford, A. Sidi, Extrapolation methods for vector sequences, *SIAM Rev.*, 29 (1987) 199-233.
- [66] J. F. Toland, Existence of symmetric homoclinic orbits for systems of Euler-Lagrange equations, *A. M. S. Proceedings of Symposia in Pure Mathematics*, 45(2) 1986, 447-459.
- [67] M. I. Weinstein, Existence and dynamic stability of solitary wave solutions of equations arising in long wave propagation, *Comm. PDE*, 12 (1987) 1133-1173.
- [68] J. C. Xavier, M. A. Rincon, D. G. Alfaro Vigo, D. E. Amundsen, Stability analysis for a fully discrete spectral scheme for Boussinesq systems, *Applic. Anal.*, 97 (2018) 610-632.
- [69] H. Yoshida, Construction of higher order symplectic integrators, *Phys. Lett. A* 150 (1990) 262-268.
- [70] V. E. Zakharov, Stability of periodic waves of finite amplitude on the surface of a deep fluid, *J. Appl. Mech.Theor. Phys.*, 2 (1968) 190-194.

MATHEMATICS DEPARTMENT, UNIVERSITY OF ATHENS, 15784 ZOGRAPHOU, GREECE AND INSTITUTE OF APPLIED & COMPUTATIONAL MATHEMATICS, FO.R.T.H., 71110 HERAKLION, GREECE
Email address: `doug@math.uoa.gr`

APPLIED MATHEMATICS DEPARTMENT, UNIVERSITY OF VALLADOLID, 47011 VALLADOLID, SPAIN
Email address: `angel@mac.uva.es`

MATHEMATICS DEPARTMENT, UNIVERSITY OF ATHENS, 15784 ZOGRAPHOU, GREECE AND INSTITUTE OF APPLIED & COMPUTATIONAL MATHEMATICS, FO.R.T.H., 71110 HERAKLION, GREECE
Email address: `leetha.saridaki@gmail.com`